UNIVERSIDAD AUTÓNOMA DE MADRID
FACULTAD DE CIENCIAS
DEPARTAMENTO DE QUÍMICA FÍSICA APLICADA

Bio-Nanohybrid Materials Based on Clays and Phospholipids

Bernd Wicklein

Doctoral Thesis

Consejo Superior de Investigaciones Científicas
Instituto de Ciencia de Materiales de Madrid
Departamento de Nuevas Aquitecturas en Química de Materiales

Madrid, 2011

Supervisors

Professor Eduardo Ruiz Hitzky,

Doctor Pilar Aranda Gallego,

Doctor Margarita Darder Colom,

Group of Porous, Hybrid, and Biohybrid Materials

Materials Science Institute of Madrid, CSIC

"Everything you can imagine is real."

Pablo Picasso

Abstract

by Bernd Wicklein

Bio-nanohybrid materials based on self-assembly of phospholipid molecules on clay minerals afford biomimetic interfaces which can be valuable for non-degradative immobilization of biological species. Their successful implementation in technological applications relies strongly on the preservation of their native conformation which can be compromised by interactions with the supporting host material. Therefore, biointerfaces are prepared from phosphatidylcholine on the surface of the layered clay montmorillonite and the microfibrous mineral sepiolite as well as on a Mg/Al type layered double hydroxide. Sampling of lipid adsorption isotherms allows for the controlled formation of supported lipid mono- and bilayers both on the external surfaces as well as in the intracrystalline space of montmorillonite. Physico-chemical characterization suggests hydrogen bonding and ion-exchange as the principle interaction mechanism. Another type of biointerface inspired from the membrane of erythrocytes is prepared on gold electrodes for the manufacturing of an impedimetric affinity biosensor for Influenza A viruses.

Immobilization of the model enzymes urease and cholesterol oxidase indicates that sepiolite based bio-nanohybrids provide a suitable scaffold for different kinds of enzymes. Assays reveal highest enzymatic activity on the bilayer lipid interface for both enzymes. This has promoted their incorporation in urea biosensors and cholesterol bioreactors. Clay-lipid hybrids are also evaluated for mycotoxin sequestration and demonstrate enhanced retention capacity as compared to alkylammonium organoclays. The bilayer lipid membrane on sepiolite and layered double hydroxide is found to conserve high bioactivity of immobilized Influenza virions and the viral membrane protein hemagglutinin. Especially their thermal stability on these supports is shown to be above standard aluminum hydroxide adjuvants. These findings have prompted *in vivo* studies of immunization in mice demonstrating the high efficacy of sepiolite-lipid biohybrids as Influenza vaccine carrier.

The obtained results in this Dissertation confirmed that biomimetic interfaces can be prepared in a controlled manner on different types of clay minerals. The choice of the specific supports in this work may give rise to substitution of standard supports such as the organoclays in mycotoxin sequestration in animals or aluminum based adjuvants in vaccine formulations. The label-free affinity biosensor shows Influenza subtype selectivity but at the same time is more user-friendly than other selective Influenza biosensors.

Resumen

de Bernd Wicklein

Materiales bio-nanohíbridos basados en el auto-ensamblaje de moléculas de fosfolípidos y minerales de la arcilla proporcionan interfaces biomiméticas que pueden ser valiosas para la inmovilización de forma no-degradatante de especies biológicas. Su posible implementación en aplicaciones tecnológicas se apoya fuertemente en la conservación de su conformación nativa, que puede verse alterada por interacciones con el material de soporte. Dichos biointerfaces se han preparado a partir de fosfatidilcolina que se asocia a las superficies de una arcilla laminar (montmorillonita) y del silicato microfibroso sepiolita, así como a un hidróxido doble laminar de tipo Mg/Al. El estudio de las isotermas de adsorción de lípidos permite la formación controlada de la mono- y la bicapa lipídica soportada, tanto en las superficies externas, como en el espacio intracristalino de la montmorillonita. La caracterización físico-química sugiere enlaces de hidrógeno e intercambio íonico como mecanismos principales de interacción. Otro tipo de biointerface inspirado en la membrana de los eritrocitos se ha preparado sobre electrodos de oro para la fabricación de un biosensor impedimetrico de afinidad para la detection del virus de la gripe.

La inmovilización de los enzimas modélicos ureasa y colesterol oxidasa indica que los bio-nanohíbridos basados en la sepiolita proporcionan una adecuada organización estructural para los diferentes tipos de enzimas. Los ensayos revelan una actividad enzimática mas alta en la membrana de bicapa lípidica para ambos enzimas. Esto ha promovido su incorporación en biosensores de urea y bioreactores de colesterol. Híbridos de lípido-arcilla también han sido evaluados para secuestrar micotoxinas demostrando una capacidad de retención mayor en comparación con organoarcillas convencionales del tipo alquilamonio. La membrana bicapa lipídica soportada en los hidróxidos doble laminares y en la sepiolita permite la conservación de la elevada bioactividad de las particulas virales de la gripe y de la hemaglutinina, proteína de la membrana viral inmovilizada. Especialmente su estabilidad térmica en estos soportes es superior al hidróxido de aluminio empleado como adyuvante estándar. Estos resultados han conducido al estudio de inmunización *in vivo* en ratones demonstrando que los bio-híbridos de sepiolita presentan una alta eficacia como soportes en vacunas de gripe.

Los resultados obtenidos en esta Tesis confirman que las interfaces biomiméticas se pueden preparar de una manera controlada en los diferentes tipos de soporte inorgánico. La

elección de dichos soportes puede aconsejar la sustitución de soportes estandard, como las organoarcillas en el secuestro de micotoxinas o adyuvantes de alúmino en formulaciones de vacunas. El biosensor de afinidad sin marcador muestra selectividad por los subtipos del virus de influenza, pero al mismo tiempo, es más fácil de usar que otros biosensores selectivos a la influenza.

Acknowledgements

This Thesis would not have been possible without the help and guidance of numerous persons. Foremost, I would like to express my deep and sincere gratitude to my supervisor, Professor Eduardo Ruiz-Hitzky, former Head of the Department of New Architectures in Materials Chemistry, Materials Science Institute of Madrid. His wide knowledge and his logical way of thinking have been of great value for me. His understanding, encouraging and guidance have provided a good basis for the present Thesis.

I am deeply grateful to my supervisor, Dr. Pilar Aranda, for her detailed and constructive comments, for her guidance and for the revision of many works.

I wish to express my warm and sincere thanks to my supervisor Dr. Margarita Darder, for her never-ending patience, valuable advices and for her important support throughout this work.

I owe my deepest gratitude to Prof. Miguel Camblor and Dr. Carolina Belver for fruitful discussions and important comments.

I want to express my gratitude to Andrés Valera and Tomás García for their helping hand in all matters of laboratory work and for numerous opportunities to sneak in samples for FE-SEM.

I am indebted to my group members and fellow labmates to support me, namely Alex, Almudena, Ana, Ezzouhra, Francisco, Javier, Regina, and Yorexis.

Furthermore, I would like to thank my office mates Dr. Simone Fratini, Dr. Gladys León, Dr. Marco Leonetti, and Francisco Valdivia-Valero for their good company and atmosphere.

I am grateful to Dr. Pedro Tartaj for letting me use his Zetasizer to conduct the dynamic light scattering measurements and to Dr. Marisa Ferrer for lending me her liposome miniextruder equipment.

It is a pleasure to thank Dr. Gustavo del Real, María Angeles del Burgo, and Dr. María Yuste from the Instituto Nacional de Investigación y Tecnología Agraria y Alimentaria (INIA, Madrid) for a productive and fruitful collaboration during the *Proyecto Intramural de Frontera* (PIF) NANOVIR CSIC project.

Equal gratitude is owed to Dr. César Fernández-Sánchez from the CNM-IMB (CSIC) in Barcelona (Spain) for helpful advices and collaboration in EIS measurements, self-assembly, and providing gold chips and electrodes during the PIF NANOVIR project.

I would like to show my sincere gratitude to Prof. Giora Rytwo for making my research stay at his laboratory at Migal Technological Center (Kiryat Shmona, Israel) so pleasant and for many valuable discussions. Furthermore, I am owing gratitude to Sivan Margalit for the close collaboration.

The financial support of the Comunidad de Madrid by a *Personal Investigador de Apoyo* contract is gratefully acknowledged. This work was supported by the CICYT (MAT2006-03356, MAT2009-09960), the Comunidad Autónoma de Madrid (S-0505/MAT/0027) and the CSIC (PIF08-018) NANOVIR projects.

I want to thank my good friends Matthias, Sebastian, and Solomon from back home for their friendship and the many "skype hours" during my stay abroad.

My special gratitude is due to my family and parents, Franz and Katharina, for their support and never-ending patience.

Lastly, I owe my deepest gratitude and regards to Belén for her encouragement and understanding throughout this period.

To my parents and Belén

Contents

Abstract iii

Resumen iv

Acknowledgements vi

List of Figures xii

List of Tables xvi

Abbreviations xvii

1 Introduction 1
- 1.1 Hybrid and Biohybrid Materials . . . 1
- 1.2 Inorganic Host Materials and Related Biohybrids . . . 4
  - 1.2.1 Clay Minerals and Bio-Organoclays . . . 4
  - 1.2.2 Layered Double Hydroxides and Related Biohybrids . . . 7
- 1.3 Biomimetic Interfaces . . . 9
  - 1.3.1 Self-Assembly . . . 10
  - 1.3.2 Surfactants and Biosurfactants . . . 10
  - 1.3.3 Artificial Lipid Membrane . . . 12
  - 1.3.4 Bio-Nanohybrid Materials Based on Phospholipids . . . 14
- 1.4 Association of Bioactive Species to Lipid - Biohybrid Materials . . . 16
  - 1.4.1 Enzyme Immobilization Mechanism . . . 17
  - 1.4.2 Virus and Antigen Immobilization . . . 18
- 1.5 Objectives of the Dissertation . . . 20

2 Materials and Methods 22
- 2.1 Starting Materials . . . 22
  - 2.1.1 Supports for Lipid-based Biohybrids . . . 22
    - 2.1.1.1 Montmorillonite . . . 22
    - 2.1.1.2 Sepiolite . . . 23
    - 2.1.1.3 Mica . . . 23
  - 2.1.2 Biomolecules: Phosphatidylcholine, Enzymes, Proteins, Influenza Viruses, and Mycotoxins . . . 23

2.1.3 Other Chemicals and Materials . . . 27
2.2 Materials Syntheses . . . 29
2.2.1 Synthesis of Lipid-based Biohybrids . . . 29
2.3 Characterization Methods and Instrumentation . . . 31
2.3.1 Elemental Analysis . . . 31
2.3.2 Thermal Analysis . . . 31
2.3.3 Fourier Transform Infrared Spectroscopy . . . 32
2.3.4 UV-visible Spectroscopy . . . 33
2.3.5 Powder X-ray Diffraction . . . 33
2.3.6 Nuclear Magnetic Resonance . . . 33
2.3.7 Specific Surface Area . . . 34
2.3.8 Electron Microscopy . . . 34
2.3.9 Atomic Force Microscopy . . . 35
2.3.10 X-ray Photoelectron Spectroscopy . . . 36
2.3.11 Electrochemical Instrumentation . . . 37
2.3.12 Dynamic Light Scattering . . . 37
2.3.13 Water Sorption . . . 38
2.3.14 Contact Angle Measurement . . . 39
2.4 Protocols and Applications . . . 39
2.4.1 Immobilization Protocols for Biological Species . . . 39
2.4.2 Quantification and Activity Protocols for Biological Species . . . 40
2.4.3 Enzyme Activity Assays and Preparation of an Urea Biosensor . . . 44
2.4.4 Preparation and Measurements of Influenza Virus Biosensor . . . 47
2.4.5 Cholesterol Bioreactor . . . 49
2.4.6 Mycotoxin Adsorption Study . . . 50

3 Results and Discussion 51
3.1 Synthesis and Characterization of Lipid - Nanohybrids . . . 51
3.1.1 Clay-Lipid Interactions . . . 52
3.1.1.1 Sepiolite-Lipid Adsorption Mechanism . . . 52
3.1.1.2 Montmorillonite-Lipid Intercalation Mechanism . . . 64
3.1.2 Mixed Lipid/Octyl-Galactoside Layers on Sepiolite and Characteristics of Supported Interfaces . . . 75
3.1.3 Mg/Al Layered Double Hydroxide-Lipid Biohybrids . . . 82
3.1.4 Concluding Remarks . . . 88
3.2 Applications of Clay-Lipid Biohybrids for the Immobilization of Enzymes and Mycotoxins . . . 90
3.2.1 Urease and Cholesterol Oxidase Immobilization on Sepiolite Supported Biointerfaces . . . 91
3.2.1.1 Adsorption Processes on Different Biointerfaces . . . 91
3.2.1.2 Immobilization Model Based on Bioactivity and Enzyme Orientation . . . 95
3.2.2 Application of Supported Enzymes as Urea Biosensor and Cholesterol Bioreactor . . . 101
3.2.2.1 Sensing Characteristics of Urea Biosensor . . . 101

3.2.2.2 Cholesterol Bioreactor . . . 103
3.2.3 Clay-Lipid Biohybrids as Adsorbents for Mycotoxins . . . 105
3.2.3.1 Aflatoxin B1 Adsorption and Release Study . . . 105
3.2.3.2 Deoxynivalenol Adsorption Study . . . 107
3.2.4 Concluding Remarks . . . 109
3.3 Lipid Bio-Nanohybrids as Influenza Vaccine Adjuvants . . . 111
3.3.1 Influenza Virus Immobilization on Sepiolite- and Mg/Al LDH-Lipid Hybrids . . . 113
3.3.2 Hemagglutinin Immobilization on Sepiolite- and Mg/Al LDH-Lipid Hybrids . . . 119
3.3.3 Thermal Stability of Immobilized Viral Species . . . 120
3.3.4 Immunization Test with Supported Viral Species . . . 125
3.3.5 Concluding Remarks . . . 125
3.4 Biomimetic Lipid-Based Thin Films . . . 127
3.4.1 Lipid-based Films on Mica . . . 128
3.4.2 Biomimetic Thin Films Applied in Influenza Virus Biosensors . . . 133
3.4.2.1 Characterization of the Self-Assembly Process of 1-Octanethiol / Octyl-Glucoside Hybrid Bilayers on the Gold Surface . 135
3.4.2.2 Sialic Acid Functionalization of the Othiol-OGal Interface 145
3.4.3 Influenza Virus Sensing . . . 148
3.4.3.1 Detection Tests for PR8 Influenza Virus . . . 148
3.4.3.2 Selectivity of Influenza Virus Subtypes . . . 152
3.4.4 Concluding Remarks . . . 155

4 Conclusions **157**

A Synthesis and Characterization of Lipid-Biohybrids **160**

B Immobilization of Enzymes on Clay-Lipid Biohybrids **168**

C Lipid Bio-Nanohybrids as Influenza Vaccine Adjuvant **170**

D Biomimetic Lipid-Based Thin Films **172**

Bibliography **174**

List of Figures

1.1 Schematic representation of the crystal structure of montmorillonite . . . 5
1.2 Schematic representation of the crystal structure of sepiolite 6
1.3 Schematic representation of the crystal structure of a layered double hydroxide 8
1.4 Representation of the molecular structure of phosphatidylcholine and schematics of a bilayer lipid membrane and a liposome 13
1.5 Scheme of intrinsic and extrinsic association of proteins to a lipid bilayer membrane 18
1.6 Scheme of an Influenza virus showing the lipid bilayer membrane together with the core and the membrane proteins hemagglutinin and neuraminidase 19

2.1 Representation of the molecular protein structure of urease (A) and cholesterol oxidase (B) 25
2.2 Representation of the Influenza virus and the protein structure of hemagglutinin 26
2.3 Representation of the molecular structure of aflatoxin B1 (A) and deoxynivalenol (B) 27
2.4 Representation of a Randles equivalent circuit model 37
2.5 UV-Vis spectra and calibration curve of BSA as obtained by the micro-Bradford method 41
2.6 UV-Vis spectra and calibration curve of octyl-glucoside as obtained by the phenol-sulfuric acid method 42
2.7 Cyclic voltammetry of DTNB modified Au electrode confirming the pH sensitivity 45
2.8 Schematics of the three electrode setups used in urease (A) and cholesterol oxidase (B) activity assays 47
2.9 Interdigitated gold electrode used for virus detection 48

3.1 PC adsorption isotherm from ethanol on sepiolite 53
3.2 ζ-Potential of liposomes as function of pH 55
3.3 PC adsorption isotherms on sepiolite from aqueous (A) and ethanol phase (B) 56
3.4 Scheme of PC adsorption on sepiolite from aqueous (A) and ethanol phase (B) 57
3.5 ^{29}Si CP/MAS NMR (A) and FT-IR (B) spectra of neat sepiolite and sepiolite-lipid hybrids 59

3.6 ^{31}P MAS NMR and FT-IR spectra of sepiolite-lipid biohybrids showing the phosphorous nuclei, the phosphatidyl, and ester groups, respectively . 60
3.7 Scheme of the proposed interaction mechanism between PC molecules and the Si-OH group of sepiolite 61
3.8 Water contact angles on cast SEP-PC films 62
3.9 PC adsorption isotherm on Na^+-montmorillonite from methanol 64
3.10 Sodium to silicon ratios in at.% obtained from semi-quantitative EDX measurements as function of PC content 66
3.11 XRD patterns of MMT-PC biohybrids obtained from methanol 67
3.12 PC adsorption isotherms on Na^+-montmorillonite from aqueous (A) and methanol phase (B) 69
3.13 FT-IR spectra of MMT-LUV biohybrids (A) and the normalized intensity of δ_{HOH} as function of the PC concentration (B) 70
3.14 XRD pattern of MMT-LUV biohybrids obtained from liposome adsorption on Na^+-montmorillonite 71
3.15 FT-IR spectra of MMT-LUV biohybrids showing the $\upsilon_{P=O}$ band 72
3.16 PC adsorption from methanol on pre-hydrated Na^+-MMT 73
3.17 Thermogravimetric analysis of pristine Na^+-montmorillonite and a MMT-PC biohybrid 74
3.18 Adsorption isotherm of OGal on SEP-ML-PC from aqueous media. . . . 76
3.19 Schematic of possible OGal layer assemblies on SEP-ML-PC. 77
3.20 Water adsorption isotherms at 25 °C on the surface of bare SEP, SEP-CTA, SEP-ML-PC and SEP-PC-OGal with increasing OGal quantities 79
3.21 XRD pattern of co-precipitated Mg/Al LDH-PC and pristine LDH 83
3.22 TEM images of co-precipitated Mg/Al LDH-PC and pristine Mg/Al LDH 86
3.23 FT-IR spectra of co-precipitated Mg/Al LDH-PC and pristine Mg/Al LDH 87
3.24 Scheme of the proposed Mg/Al LHD-PC formation mechanism 88
3.25 Urease adsorption quantities on bare sepiolite and sepiolite hybrid materials 92
3.26 FT-IR and ^{29}Si MAS NMR spectra of SEP-URE 93
3.27 Potential shift of DTNB as result of pH increase produced by urea oxidation 96
3.28 Calibration and Lineweaver-Burk plots of immobilized COx 98
3.29 Response time, calibration curve and shelf-life time of urease-biosensor . 102
3.30 Interference of urease-biosensor with ascorbic acid 103
3.31 Catalytic activity of COx biocatalyst based on SEP-ML-PC and SEP-BL-PC as function of number of catalytic cycles 104
3.32 Aflatoxin B1 adsorption isotherms from water on lipid modified montmorillonite and sepiolite as well as on reference materials 106
3.33 Deoxynivalenol adsorption from a 5 μg/mL aqueous solution. 108
3.34 PR8/34(H1N1) virus retention on SEP-ML-PC, SEP-BL-PC, and $Al(OH)_3$ gel 114
3.35 TEM micrographs of virus particles immobilized on sepiolite supported PC (A) mono- and (B) bilayer 115
3.36 TEM micrographs of PR8/34(H1N1) virus supported on SEP-BL-PC (A,B) and Mg/Al LDH-PC (C,D) 117
3.37 NA activity assay for PR8/34(H1N1) virus immobilized on SEP-BL-PC and Mg/Al LDH-PC as well as control on $Al(OH)_3$ gel 118

3.38 Quantity of immobilized HA on SEP-BL-PC, Mg/Al LDH-PC, and $Al(OH)_3$ gel . . . 119
3.39 HA titer of immobilized PR8 virus relative to the HA titer of immobilized HA on SEP-BL-PC, Mg/Al LDH-PC, and $Al(OH)_3$ gel . . . 121
3.40 Thermal stability of immobilized H1N1 virus (A) and HA (B) assessed by NA activity and hemagglutination, respectively. The viral species were immobilized on SEP-BL-PC, Mg/Al LDH-PC, and $Al(OH)_3$ gel and compared to the thermal stability of the freely suspended species . . . 122
3.41 FE-SEM images of lyophilized SEP-BL-PC, Mg/Al LDH-PC, and $Al(OH)_3$ gel . . . 123
3.42 Relative NA activity of freely suspended and immobilized H1N2 virus particles on thawed adjuvants after lyophilization. The virus was immobilized on SEP-BL-PC, Mg/Al LDH-PC, and $Al(OH)_3$ gel and compared to the thermal stability of the freely suspended species . . . 124
3.43 AFM images of PC multi- and monolayer supported on mica . . . 129
3.44 XPS survey scans and C1s core level bands from PC multilayer, hydrated PC layer and mixed PC-OGal layers supported on mica . . . 130
3.45 Illustration of lipid layer configurations supported on mica . . . 131
3.46 Schematic of an erythrocyte membrane and mixed Othiol-OGal film presenting sialic acid groups . . . 133
3.47 Scheme of self-assembly approaches for the preparation of mixed Othiol/OGal films . . . 134
3.48 Nyquist plots of hybrid Othiol/OGlu bilayers by sequential and simultaneous self-assembly . . . 136
3.49 Cyclic voltammograms of the bare Au surface and Othiol-OGlu layers . . 138
3.50 Concentration of dissolved OGlu from octanethiolated gold chips which were incubated in 5 mM OGlu for 2, 6, 16, 24, and 72 hours (A) and advancing water contact angle measurements on bare Au surface and octanethiolated gold chips incubated in 5 mM OGlu for 1 and 3 days (B) . 139
3.51 Nyquist plots of thiolated gold electrodes incubated in OGlu for varying durations . . . 140
3.52 Cyclic voltammograms (A) from Othiol desorption of hybrid Othiol-OGlu layers on gold electrodes. Surface coverage (B) of Othiol as function of OGlu incubation time. . . . 141
3.53 Relative R_{ct} (A) and Othiol surface coverage (B) of Au-Othiol-OGlu electrodes as function of the OGlu concentration during incubation . . . 142
3.54 Topographic AFM images of the bare gold surface (A), the Othiol SAM (B), and the Othiol-OGal bilayer (C) as well as a frequency shift image of the bilayer (D) . . . 144
3.55 Scheme of the formation process of a mixed Othiol-OGlu bilayer based on the experimental findings . . . 145
3.56 XPS survey scans and core level bands of C1s, O1s, and N1s photoelectrons from Au-Othiol, Au-Othiol-OGal, and Au-Othiol-OGal-SA . . . 146
3.57 Western Blot image of α-2,3 sialylated gold chips displaying terminal sialic acid moieties after incubation with a H5N9 Influenza virus solution . . . 147
3.58 PR8 virus adsorption from 0.1 μg/ml on sialylated and non-sialylated electrodes (A) and PR8 detection at various concentrations (B) . . . 149

3.59 Topographic AFM images of biosensor surfaces after detection of 0.1 μg/ml PR8 solutions . . . 150
3.60 Reproducibility of PR8 virus detection from a 0.5 μg/ml solution (A) and PR8 virus adsorption kinetics on a virgin α-2,6 sialylated electrode surface (B) . . . 151
3.61 Scheme for selectivity of α-2,6 and α-2,3 sialylated electrodes toward H1N1 and H5N9 Influenza viruses . . . 153
3.62 Nyquist plots of α-2,6 and α-2,3 sialylated electrodes after 45 min incubation in solutions of H1N1 (PR8) and H5N9 virus . . . 154
3.63 Unspecific PRRS virus adsorption from 0.07 μg/ml and detection of active PR8 virus from 0.01 μg/ml. . . . 155

A.1 Adsorption isotherms of PC from methanol and ethanol on sepiolite . . . 160
A.2 Thermal analysis of sepiolite-lipid biohybrid . . . 161
A.3 Particle size distribution of extruded liposomes . . . 163
A.4 Adsorption isotherms of PC from methanol and ethanol on Na^+-MMT . 163
A.5 Thermal analysis of montmorillonite-lipid biohybrid . . . 164
A.6 Adsorption isotherm of PC liposomes on Mg/Al LDH . . . 165
A.7 EDX spectrum of co-precipitated Mg/Al LDH-PC and the derived atomic fraction of the present elements . . . 166
A.8 Particle size distribution of pristine Mg/Al LDH and Mg/Al LDH-lipid obtained from dynamic light scattering . . . 167

B.1 FT-IR spectra of immobilized urease on various interfaces . . . 168
B.2 Activity of COx four weeks after immobilization on SEP-BL-PC and SEP-ML-PC (A) and Lineweaver-Burk plots derived from the conversion data (B) . . . 169

C.1 XRD pattern (A) and TEM micrograph (B) of commercial $Al(OH)_3$ adjuvant 170

D.1 Nyquist plots of an Othiol/OGlu modified gold electrode before and after treatment with sulfuric acid . . . 172
D.2 Response profiles of α-2,6 sialylated electrodes toward PR8 Influenza viruses at 0.05 and 0.075 μg/ml concentration . . . 173

List of Tables

3.1 Langmuir fitting parameters of the PC adsorption isotherm on Na^+-MMT and Gibbs free energy of adsorption 65
3.2 Water adsorption data of sepiolite and sepiolite based hybrid materials. . 80
3.3 Surface characteristics of sepiolite based hybrid materials. 81
3.4 Crystal domain size and particle size of Mg/Al LDH and Mg/Al LDH-PC 85
3.5 Summary of physico-chemical properties of sepiolite supported interfaces 90
3.6 Enzymatic activity and kinetic parameters of immobilized urease 97
3.7 Analytic and kinetic parameters of immobilized COx 98
3.8 Results of Langmuir isotherm fitting of AfB1 adsorption on modified clays. 107
3.9 NA activity assay for free and supported PR8/34(H1N1) virus on SEP-BL-PC and Mg/Al LDH-PC 116
3.10 Dynamic water contact angle values of mica supported lipid films 129
3.11 EIS data from sequential and simultaneous preparation of mixed Oth-iol/OGlu bilayers 136
3.12 EIS data of thiolated gold electrodes incubated in OGlu for varying durations 140

Abbreviations

AA	Ascorbic acid
AfB1	Aflatoxin B1
AFM	Atomic force microscopy
ATR	Attenuated total reflectance
BET	Brunauer-Emmett-Teller
BL	Bilayer
BSA	Bovine serum albumin
CEC	Cation exchange capacity
CHO	Cholesterol
CLO	Cloisite®
CMC	Critical micelle concentration
CMP	Cytidine-5'-monophospho-N-acetylneuraminic acid sodium salt
COx	Cholesterol oxidase
CP NMR	Cross-polarization nuclear magnetic resonance
CTA	Cetyltrimethylammonium
DLS	Dynamic light scattering
DON	Deoxynivalenol
DTG	Differential thermogravimetry
DTNB	5,5'-Dithiobis(2-nitrobenzoic acid)
EIS	Electrochemical impedance spectroscopy
ELISA	Enzyme-linked immunosorbent assay
EtOH	Ethanol
Fla	Flagellin
FT-IR	Fourier transform infrared

HA	Hemagglutinin
iep	Isoelectric point
LDH	Layered double hydroxide
LUV	Large unilamellar vesicle
MAS	Magic angle spinning
MeOH	Methanol
ML	Monolayer
MMT	Montmorillonite
OGal	Octyl-galactoside
OGlu	Octyl-glucoside
Othiol	Octanethiol
PBS	Phosphate buffer saline
PC	Phosphatidylcholine
PL	Phospholipid
PVA	Polyvinyl alcohol
RMS	Root mean square
SA	Sialic acid
SAM	Self-assembled monolayer
SAT	Sialyltransferase
sBLM	Supported bilayer lipid membrane
SBS	Sugar-based surfactant
SEP	Sepiolite
TLC	Thin layer chromatography
URE	Urease
WB	Western blot
XPS	X-ray photoelectron spectroscopy
XRD	X-ray diffraction

Chapter 1

Introduction

1.1 Hybrid and Biohybrid Materials

This Dissertation deals with the preparation and application of a class of materials that is commonly referred to as *biohybrids* (Ruiz-Hitzky et al., 2008b). Owing to the tremendous expansion which this field of Materials Science has experienced over the last two decades, a brief definition of concepts and material classes is considered as expedient.

The combination of organic compounds with inorganic host materials gives rise to the class of *organic-inorganic materials*. One way to prepare these materials is to modify an inorganic solid with organic or organometallic molecules. If this modification occurs at the molecular level, e.g. at the nanoscale, the resultant material is denominated as a *hybrid* (Ruiz-Hitzky, 2004). However, not all organic-inorganic materials should be included in this definition. These are for instance physical mixtures or combinations at the micro- and macroscale.

Organic-inorganic hybrid materials can be subdivided into three types: i) intercalation compounds, ii) organic derivatives of inorganic solids, and iii) sol-gel hybrid materials (Ruiz-Hitzky, 2004). With regard to type i) the term *intercalation* is used in this Thesis exclusively to describe the insertion of organic species into layered inorganic solids. Such solids can be e.g. clay minerals, layered double hydroxides (LDHs), perovskites,

phosphates, or titanates which display an organically modifiable intracrystalline space of several Angström. Organic derivatives of inorganic solids (type ii) can be obtained by grafting reactions of organic groups onto inorganic surfaces which render stable, covalent bonds. Typical anchoring groups on e.g. siliceous host materials are silanol groups (Si-OH). These surface groups can be conveniently esterified with alkanols or brought to reaction with silanes, isocyanates, amines, or epoxy functions. The third type of organic-inorganic materials are sol-gel hybrid materials. Among the brought variety of sol-gel materials organopolysiloxane derived hybrids are probably the most important group (Gill and Ballesteros, 2000a).

Substituting the synthetic organic compounds for biological species originates in the emerge of *biohybrid* materials (Ruiz-Hitzky et al., 2010b). This was an important advance in the development of functional materials as the incorporation of biological molecules conveys diverse functionalities often beyond man-made synthetic systems. Illustrative examples are nanoparticles modified with genetic species for labeling *via* hybridization reactions (Maxwell et al., 2002), association of enzymes to biocompatible solids for biocatalysis (Forano and Prevot, 2008), or immobilization of light-harvesting cell species for artificial photosynthesis (Itoh et al., 2002). A versatile synthesis route for nanostructured biohybrids is the bottom-up approach using well-defined building units (Ruiz-Hitzky et al., 2010b; Ruiz-Hitzky et al., 2011). This approach follows soft-chemistry principles mandatory for many fragile and sensitive biological entities. Representative methods within this route are i) entrapment of e.g. enzymes in sol-gel derived matrices, ii) inclusion of e.g. chlorophyll a in mesoporous silica, iii) encapsulation of e.g. living cells in various rigid or soft matrices, and iv) intercalation of e.g. proteins or polysaccharides in layered host materials (Ruiz-Hitzky et al., 2008b; Ruiz-Hitzky et al., 2010b). A common characteristic of these biohybrids is that the biological guest is in intimate contact with the inorganic host material. Thus, the host-guest components may experience manifold interaction mechanism: electrostatic interactions, hydrogen bonding and water bridges, ion-dipole coordination, proton and electron transfer processes, Van der Waals forces, or covalent bonds (Ruiz-Hitzky et al., 2010b).

The use of biological compounds also provides the possibility to synthesis materials which are structurally and /or functionally a step closer to naturally occurring hybrid materials. In Nature, most hybrid materials belong to the group of *bionanocomposites* (Darder et al., 2007). This subclass of organic-inorganic materials is formed of a combination of two or more compounds with one constituting a continuous bulk phase and the other being the dispersed phase. The continuous phase consists typically of biopolymeric compounds while the dispersed phase are minerals of layered or particulate texture (Darder et al., 2007). Amongst the most prominent examples of natural bionanocomposites are nacre and bone which consist of calcium carbonate/lustrine A and collagen/hydroxyapatite, respectively (Ruiz-Hitzky et al., 2005). Man-made bionanocomposites are designed using the same or similar components as found in Nature. Widely used biopolymers are polysaccharides, polypeptides, proteins, nucleic acids, etc.

Maybe one of the most intriguing features of many biomolecules is their ability to undergo self-assembly into of hierarchical structures. Especially the group of *biosurfactants*, which will be addressed in more detail in Section 1.3.2, shows enormous versatility since they may convey functionalities which convert the resultant materials into structurally and functionally diversified biohybrids (Davis et al., 2003; Vemula and John, 2008). Apart from bulk biohybrids, materials with biological surfaces are of utmost concern to an increasing scientific community. The reason is that in biological systems a great number of reactions, functions and recognition mechanism rely on interfacial properties (Sun et al., 2011). This triggered a considerable effort to mimic these interfaces with the same molecules as in Nature or rebuild them with synthetic molecules based on inspiration from biology. Examples may be artificial cell membranes based on bilayer lipid membranes or superhydrophobic surfaces inspired from the lotus leaf. Meanwhile, a broad variety of supporting structures for these *biointerfaces* has been developed and carefully studied. Depending on the final application of the materials, supports may be metal surfaces for biosensing applications (Ramsden, 1998; Nikolelis et al., 2010), mesoporous and particulate silica-based solids affording large specific surfaces for high-yield bioreactors (Itoh et al., 2002), metal oxide nanoparticles for vectorial drug or gene delivery (Gutierrez et al., 2009), or layered solids such as for instance clay minerals for ion-sensing devices

(Darder et al., 2003). Another example for clay supported biointerfaces is provided by Ruiz-Hitzky and co-workers who prepared sepiolite-xanthan biohybrids inspired by the nasal mucous membrane for the delivery of Influenza A virons in a vaccination study (Ruiz-Hitzky et al., 2009).

The formation of lipid based interfaces on this last group of host materials will be one of the mayor subjects of investigation in this Dissertation. In order to fully appreciate the presented outcomes of this work, the subsequent Section is devoted to the description of clay minerals and specific interaction mechanism in derived biohybrids.

1.2 Inorganic Host Materials and Related Biohybrids

1.2.1 Clay Minerals and Bio-Organoclays

The supporting structure within many biohybrid materials is based on naturally occurring silicate minerals (Ruiz-Hitzky et al., 2008a). Clays are fine-grained silicates with either lamellar or fibrous morphology (Ruiz-Hitzky et al., 2004). Important characteristics of clay minerals related to their application in Materials Science are (Ruiz-Hitzky and Van Meerbeeck, 2006):

- Layered structure with one dimension on the nanometer scale.

- Several types of surfaces comprising external basal (planar) and edge surfaces as well as internal (interlayer) surfaces.

- Ease with which the external and often also the internal surfaces can be modified, e.g. by adsorption, ion exchange, or grafting.

Their unique characteristics such as colloidal behavior, ion-exchange capacity and adsorption properties, together with a general nonhazardous nature and even biocompatibility,

make them suitable as host structures for biological species (Darder et al., 2007). The clays used in this Thesis are the phyllosilicate montmorillonite, belonging to the smectite family, and sepiolite, a microfibrous mineral.

Smectites show important structural and morphological features such as colloidal particle size, high specific surface area, large cation exchange capacity (CEC) and different layer structures. In the case of montmorillonite, a 2:1 layer structure is formed by the repetition of octahedral alumina sheets sandwiched by two tetrahedral silica sheets (Figure 1.1) (Brigatti et al., 2006). Magnesium and other cations can be present in the octahedral layers isomorphically replacing aluminum cations. This results in negatively charged layers which are compensated by hydrated exchangeable alkali and alkaline earth metal cations in the intracrystalline space between two consecutive layers (Ruiz-Hitzky et al., 2004). The general composition of montmorillonite is hence $(M_y^+ \text{ x } n H_2O)(Al_{2-y}^3 Mg_y^{2+})Si_4^{4+}O_{10}(OH)_2$ (Brigatti et al., 2006). Typical cation exchange capacity of montmorillonite is in the 70-100 meq/100g range. A common feature of smectites is their swelling capability by stepwise hydration of these interlayer cations. Furthermore, these cations can easily be exchanged with organic cations and positively charged biomolecules (Szabo et al., 2008).

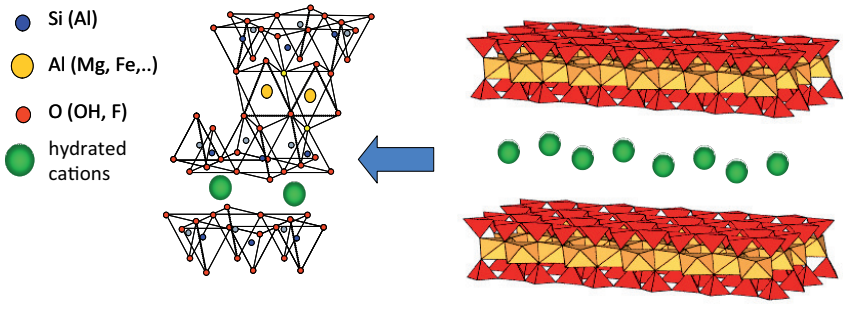

FIGURE 1.1: Schematic representation of the crystal structure of montmorillonite.

Sepiolite is a hydrated magnesium silicate of 2-10 μm particle size and with $Si_{12}O_{30}Mg_8(OH,F)_4(H_2O)_4 \cdot 8\,H_2O$ as the ideal unit cell formula (Brauner and Preisinger, 1956; Santarén et al., 1990; Ruiz-Hitzky, 2001). It is composed of ribbons of a 2:1 phyllosilicate structure with a discontinuous sheet of octahedral magnesium oxide-hydroxide being sandwiched by continuous sheets of silica tetrahedra (Brigatti et al., 2006). These

building blocks form channels and tunnels in the dimension of 1.1 x 0.4 nm which are accessible to water and other small molecules. Sepiolite exhibits free Si-OH silanol groups along the rims of the channels and at the end of the tunnels, respectively. The sepiolite structure possesses a relatively small charge deficit resulting of partial isomorphic substitution and crystal defects that determine a low cation exchange capacity (≈15 meq/100 g) (Ruiz-Hitzky, 2001). The free Si-OH groups on the external surface of the sepiolite fiber represent good anchor points for functionalization of this clay. Si-OH groups are susceptible for interaction with functional groups through grafting methods (Ruiz-Hitzky, 2004) or electrostatically *via* hydrogen bonding (Ruiz-Hitzky et al., 2004). However, there exist more ways to organically modify the sepiolite fiber, as for instance impregnation with organic vapors or solutions for tunnel penetration or entrapment of macromolecules in the microcavities on the fiber surface (Ruiz-Hitzky, 2001).

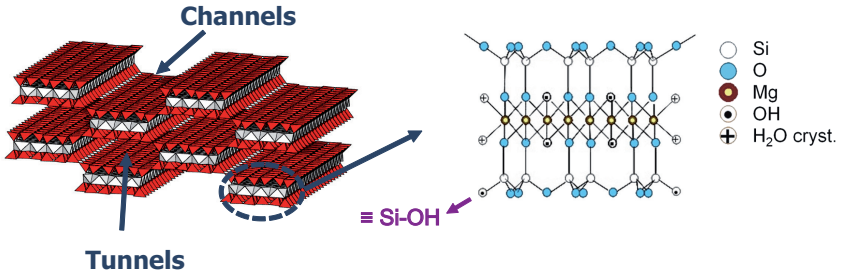

FIGURE 1.2: Schematic representation of the crystal structure of sepiolite.

An important class of materials based on these interactions are organically modified clay minerals, designated as organoclays (Lagaly, 1986; Ruiz-Hitzky and Van Meerbeeck, 2006). These highly stable organophilic clays find a broad range of applications, for instance as rheological additives, gas chromatography stationary phases, contaminant adsorbents or as filler in polymer-clay nanocomposites (Ruiz-Hitzky et al., 2004; Ruiz-Hitzky and Van Meerbeeck, 2006; Ruiz-Hitzky et al., 2010a). Versatile synthesis routes for the preparation of these organoclays are ion-exchange of interlayer cations against organic cations or *in situ* intercalative polymerization of monomers (Ruiz-Hitzky et al., 2007). The intercalation process is in most cases governed by both ionic and van der Waals forces. One of the most commonly applied and well-studied organic modifiers for clay minerals are long-chain quaternary alkylammonium cations (Lagaly, 1986). Ion-exchange

with interlayer cations in smectites may result in various arrangements of densely packed alkylammonium chains, such as monolayers, bilayers or paraffin-type structures while the surrounding silicate framework offers robust accommodation (Lagaly, 1986; Ruiz-Hitzky et al., 2004). In this way, alkylammonium exchanged montmorillonite was used as sequestration agent of mycotoxins (Lemke et al., 2001). However, a severe drawback in the expansion of possible applications toward biological fields is the toxicity and lack of biocompatibility of the quaternary alkylammonium salts. Organo-clays or leached surfactant compounds may inhibit microbial activity and cause other sorts of environmental damage (Abbate et al., 2009; Ruiz-Hitzky et al., 2010a).

Therefore, attempts in enhancing biocompatibility of organophilic clays have been undertaken. Two basic routes can be followed in this pursuit: i) adsorption of biopolymers, ii) assembly of biomolecules which are structurally similar to quaternary alkylammonium salts (Ruiz-Hitzky et al., 2005; Darder et al., 2007). According to route i), a variety of clay-biohybrids has been prepared by incorporation of polysaccharides, proteins, polypeptides, or nucleic acids. Applications are as divers as electrochemical sensors based on montmorillonite-chitosan (Darder et al., 2003) or *green* plastics for food packaging derived from sepiolite-zein bionanocomposites (Alcântara et al., 2011). Route ii) is based on similar adsorption concepts as developed for organic alkylammonium surfacants. It has been shown, that analogous biological compounds can be likewise associated with clay minerals giving rise to the so-called "bio-organoclays". In this way, Undabeytia and co-workers adsorbed phospholipid molecules, which are regarded as biological surfactants, on smectites for controlled herbicide release (Sánchez-Verdejo et al., 2008).

1.2.2 Layered Double Hydroxides and Related Biohybrids

Layered double hydroxides (LDHs), also referred to as "anionic clays", are versatile support materials for the preparation of biohybrids, including entrapment of biological species (Choy et al., 2002; Forano and Prevot, 2008) and biopolymers (Darder et al., 2005a). LDHs display a brucite-like layered structure which consists of stacks of positive $[M^{2+}_{(1-x)}M^{3+}_{x}(OH)_2]^{x+}$ layers where M^{2+} and M^{3+} are metal cations. Edge-shared

$M(OH)_6$ octahedra constitute the layers where trivalent cation substitution causes a positive layer charge (Figure 1.3). The deficit of negative charge is compensated by anions $[A^{n-}]_{x/n}\cdot zH_2O$ in the interlayer region. The resulting crystalline structure is that of the natural mineral hydrotalcite, $Mg_6Al_2(OH)_{16}CO_3\cdot 4H_2O$. A wide range of cations and anions can be combined in the synthesis of LDHs, e.g. Mg^{2+}, Zn^{2+}, Fe^{2+}, or Cu^{2+} as divalent cations and Al^{3+}, Cr^{3+}, Mn^{3+}, or Fe^{3+} as trivalent cations. The selected anions depend on the synthesis procedure and are typically CO_3^{-2}, NO_3^-, Cl^-, or OH^- (Evans and Slade, 2005). The versatility of LDHs as host structure relies on the broad range of chemical composition, the high and adjustable layer charge density and anion exchange capacity.

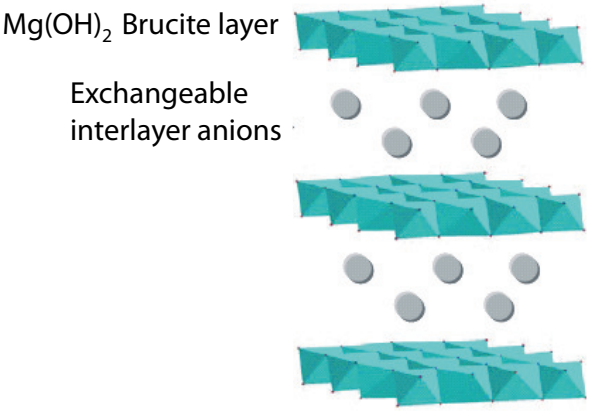

FIGURE 1.3: Schematic representation of the crystal structure of a layered double hydroxide.

In the synthesis of biohybrids based on LDHs exist two broadly followed routes: i) intercalation of an anionic organic compound into the lamellar LDH galleries by anion exchange (Meyn et al., 1990; Moujahid et al., 2002), or ii) co-precipitation of the LDH structure around the biomolecules of interest (Crepaldi et al., 2000; Desigaux et al., 2006; Costantino et al., 2008). But also the reconstruction methodology from so-called layered double oxide (LDO) phases has been applied in some cases to intercalate polymers (Dimotakis and Pinnavaia, 1990).

The second approach is conveniently employed in the encapsulation of biological species such as for instance DNA fragments or enzymes within the framework of *in situ* formed LDH crystals (Desigaux et al., 2006; Forano and Prevot, 2008). LDHs can also act as

support for bioinspired membranes. In this way, following the first route, Begú and co-workers prepared for the first time well-ordered Mg/Al LDH-lipid biohybrids by an exchange reaction with the anionic phospholipid 1,2-dimyristoyl-*sn*-glycero-3-phosphate for the use as drug delivery system (Begú et al., 2009).

1.3 Biomimetic Interfaces

The generic terms *biomimicry* or *biomimetism* appeared for the first time in 1962 (McCulloch, 1962). It referred to the imitation of one form of life by a man-made, artificial form. However, from the mid 1980s on materials scientists interpreted these terms rather as to understand how Nature solves "engineering" problems and how these strategies can help in the preparation of advanced materials for technological applications (Bensaude-Vincent et al., 2002). Glittering examples of such advanced functional materials are superhydrophobic and superadhesive surfaces based on designs that referred to structures in living creatures, such as the lotus leaf and gecko foot (Ruiz-Hitzky et al., 2010b). The concept of biomimetism is very broad. It may comprise the replication of structures, morphologies, or functionalities in natural products by synthetic chemistry routes or following synthesis strategies applied by Nature. Biomineralization is one approach which falls into this latter category (Mann, 1989). And indeed, most synthesis routes taught by Nature are inherently versatile and most importantly of all, are conducted under gentile conditions like ambient temperatures or in aqueous solvents. These conditions are incorporated in laboratory approaches by the so-called *soft chemistry* (chimie douce) (Livage, 1977). Another lesson learnt from Nature is self-assembly. This strategy, by aligning and combining molecules over various length scales to often hierarchical structures, is one of the most versatile ways by which Nature constructs multifunctional materials or interfaces (Sanchez et al., 2005). The implementation of this natural strategy into chemical synthesis to obtain advanced materials is laid out in the following Section.

1.3.1 Self-Assembly

Nature performs self-assembly of higher order structures with the aid of genetically inscribed codes (Bensaude-Vincent et al., 2002). The challenge for chemists is to construct these materials without genetic information. In 1978, Lehn introduced *supramolecular chemistry* as one method to mimic the coding in naturally occurring systems (Lehn, 1978). This strategy is based on molecular recognition due to intermolecular interaction by electrostatics and/or hydrophobic forces which allows for the assembly of suitable molecules and even of preformed building blocks (Ariga et al., 2008). The directing entities in these processes display certain structural and functional features which permit this controlled assembly. Tensioactive molecules (*surfactants*) are frequently employed as directors and templates in the synthesis of precursors of zeolites and other porous materials (Beck et al., 1994; Xu et al., 2007a). Moreover, they can also be used as the constituting compound in self-assembled layers at interfaces. Therefore, self-assembly with biological surfactants (*biosurfactants*) is especially appropriate for the design of biomimetic interfaces (Davis et al., 2003; Angelatos et al., 2006; Becker et al., 2010). The Langmuir-Blodgett technique, layer-by-layer (LbL) adsorption, or molecular assembly into monolayers are methods of special relevance in this context (Ariga et al., 2008). Concerning the solid component of such self-assembled materials, clay minerals have been increasingly incorporated in these processes. Either as building blocks or as host structure for assembled bio-organic layers within their intracrystalline space. Montmorillonite/chitosan building blocks assembled to mimic the nacre structure (Yao et al., 2010) or gelatin helices aligned at the channels of sepiolite fibers (Fernandes et al., 2011) are just two examples of this recent trend in self-assembly.

1.3.2 Surfactants and Biosurfactants

Surfactants are widely used in common applications such as detergents or as dispersants in paints, paper coatings, food, and pharmacy (Jönsson et al., 1997). But also in Materials Science they hold a prominent post, for instance as templates in the synthesis of

mesoporous materials (Beck et al., 1992). The term surfactant abbreviates *surface active agent*. Surfactants are also known as amphiphiles which is derived from the Greek words *amphis* and *philis*, meaning *both* and *love*. This name describes the behavior and structure of a surfactant. It contains a lipophilic (fat-loving) part and a hydrophilic (water-loving) part. These parts are constituted of an apolar tail and a polar headgroup. Surfactants are generally classified by the nature of their headgroup, referring to them as anionic, cationic, nonionic or zwitterionic surfactants. The hydrophobic tail typically consists of hydrocarbons or any other apolar species.

As a consequence of their structure, dissolved surfactants tend to aggregate in order to reduce Gibbs free energy by minimizing the contact with the surrounding media. In aqueous phase, for instance, surfactants form micelles above a critical concentration (CMC) with the hydrophilic headgroups in contact with water and the hydrophobic tails buried inside the aggregate. In bulk solution occur also other divers forms of aggregation, such as spheres (vesicles) or tubes. Especially tubular structures gained great technological importance since the first synthesis of the mesoporous silica MCM-41 which was prepared from surfactant tubes acting as templates (Beck et al., 1992). At interfaces, surfactants are characterized by the tendency to assemble into layers in order to lower the free energy of this phase boundary. This behavior is called *tensioactivity*. At a solid interface, surfactants form self-assembled monolayers (SAMs) by simultaneous interaction with the surface and intermolecular interactions between the tails owing to hydrophobic interactions. Very stable SAMs are obtained from organosulfur compounds that undergo covalent linkage with the supporting solid which is usually gold (Nuzzo et al., 1987; Bain et al., 1989). Also the interfacial modification of clays with surfactants, such as the group of the quarternary alkylammonium compounds, is a broadly explored field as mentioned earlier (Section 1.2.1).

But as pointed out in the previous Section 1.2.1, these compounds, likewise other synthetic surfactants, are known to inflict harm on the environment by being toxic or not being degradable. Furthermore, they might render the hybrid material of which part they are bio-incompatible. Therefore, a new class comprised of biological surfactants has

emerged (Kosaric, 1993). These *biosurfactants* display a similar polar/apolar structure as conventional surfactants, but with the additional quality of more sophisticated functional groups and structural features owing to their biological origin (Lang, 2002). The hydrophilic headgroup is comprised of mono-, oligo-, or polysaccharides, peptides, or proteins. The hydrophobic tail may consist of saturated, unsaturated and hydroxylated fatty acids or fatty alcohols (Lang, 2002). Some groups of naturally occuring biosurfactants are glycolipids, fatty acids, phospholipids and neutral lipids, lipopeptides, and polymeric biosurfactants (Pacwa-Plociniczak et al., 2011). However, there is an increasing contribution of synthetically produced biosurfactants constructed by the combination of biological moieties. In this sense, full peptide surfactants, sugar-based surfactants, or DNA surfactants can be mentioned (Lu et al., 2007; Molina-Bolivar and Carnero Ruiz, 2009). Further advantages besides the structural and functional variability are inherent biocompatibility, biodegradability, and non-hazard (Pacwa-Plociniczak et al., 2011). These are the qualities which make this type of surface-active substance prone to the interest of materials scientists in the construction of advanced and multifuncional biointerfaces.

1.3.3 Artificial Lipid Membrane

Lipid molecules are an important class of biosurfactants and have been employed for many decades in fundamental studies of cell membranes (Eytan, 1982; van Meer et al., 2008). On the other side, solid supported lipid membranes find important technological applications in areas as diverse as membrane mimetic chemistry, amplification of biomolecule recognition, or design of biosensors (Reimhult et al., 2008).

The lipid phosphatidylcholine (PC) is the main constituent of cell membranes. It provides amongst others their structural framework and is crucial in cell metabolism and membrane signal trafficking (van Meer et al., 2008). Two fatty acid chains are connected *via* a glycerol backbone to a zwitterionic headgroup constituting the amphiphilic nature of phosphatidylcholine (Figure 1.4A). The headgroup consists of an anionic phosphate group esterified to a cationic choline group.

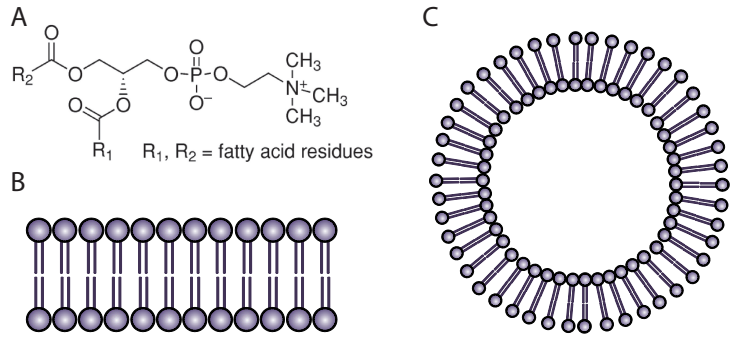

FIGURE 1.4: Representation of the molecular structure of phosphatidylcholine (A) and schematics of a bilayer lipid membrane (B) and the cross-section of a large unilamellar vesicle (LUV), commonly referred to as liposome (C).

Lecithin is a trivial name referring to the entire group of yellow-brownish fatty substances found in animal and plant tissues. Lecithin consists of different classes of phospholipids (PL), triglycerides, fatty acids, cholesterol and proteins. Phospholipids are determined through the headgroup which displays a great diversity and where the choline and phosphatidyl groups constitute the phosphatidylcholine class. Unfortunately, lecithin is often ambiguously used as synonym for phosphatidylcholine. Each PL class comprises lipids of different chain lengths (fatty acid residues) and PC extracted from e.g. egg yolk has a certain fatty acid chain length distribution.

As a result of its amphiphilicity, PC has the ability to form self-assembled structures such as micelles, tubes, vesicles (liposomes), or supported artificial membranes (Menger et al., 2005). The assembled lipid membrane is only a few nanometers thick, consisting of two lipid monolayers which are called leaflets, and held together by hydrophobic interactions (Figure 1.4B). Lipid membranes are furthermore considered as two-dimensional liquid crystals displaying considerable lateral molecule mobility (van Meer et al., 2008). This fluidity allows the embedment of guest species such as proteins and their reorganization within the membrane (Pack et al., 1997).

The self-assembly capacity of lipids has attracted considerable attention over the past decades both from fundamental and technological viewpoints and triggered the development of many lipid systems (Reimhult, 2010; Bally et al., 2010; Chemburu et al., 2010). Freely suspended liposomes (Figure 1.4C), for instance, have attained interest as model

for cell membranes in biochemical and physiological research (Eytan, 1982; Peetla et al., 2009), but also as biomimetic supports for pharmaceutical drug carriers (Puri et al., 2009), gene delivery (Zhang et al., 2010), or immobilizing biological species such as membrane proteins (Steinem and Janshoff, 2010).

However, for many technological applications it is advantageous to immobilize the lipid membrane on a solid support. In the mid 1980s, the McConnell group (Brian and McConnell, 1984; Tamm and McConnell, 1985) introduced for the first time solid supported lipid bilayers, which are well suited to serve as cell membrane mimics (McConnell et al., 1986; Sackmann, 1996; Kam and Boxer, 2003). These initial works triggered the development of a variety of solid-supported membrane systems such as tethered lipid bilayers, polymer-cushioned lipid bilayers, supported vesicular layers, or hybrid bilayers (Plant, 1999; Richter et al., 2006). The most common assembly methods are based on vesicle fusion (Brian and McConnell, 1984) or layer-by-layer deposition using the Langmuir-Blodgett technique (Petty, 1996).

These tailored, supported lipid membranes receive great (bio)technological interest since they provide a biomimetic environment for the gentile association of bioactive species. Immobilization of enzymes and proteins enable the exploration of biosensing devices and biocatalytic processes (Ramsden, 1998; Girard-Egrot et al., 2005).

1.3.4 Bio-Nanohybrid Materials Based on Phospholipids

The efficiency and yield of many technological applications of solid materials depend on their large specific surface area. It may provide, for instance, the possibility to incorporate large quantities of biological species. Catalytic surfaces, sensing systems, or adsorption processes (contaminant removal) can be mentioned in this context. In order to obtain large lipid membrane surfaces, modification of particulate and/or porous materials with lipid molecules could satisfy this demand. Clay minerals and related siliceous materials are especially suited as host structure, owing to their large specific surface area and multiple internal surfaces which provide a robust framework and an "easy to handle" carrier

system for lipid membranes. Another favorable fact are the diverse interaction mechanism between the lipid headgroup and the various adsorption sites on clays. Interaction with silicate surfaces is related to Coulombic interactions between the ionic headgroup and surface charge sites, ion-exchange mechanism, and H-bonding with surface hydroxyl groups or chemisorbed water molecules (Rapuano and Carmona-Ribeiro, 2000; Wiegart et al., 2005; Sahai, 2002).

Based on these mechanism a wide range of lipid-biohybrid materials has been prepared over the past years. For instance, herbicide containing PC vesicles which have been adsorbed on colloidal montmorillonite platelets rendered release agents for agricultural purposes (Sánchez-Verdejo et al., 2008). Also layered double hydroxides proofed to be adequate for the accommodation of bilayer lipid membranes (BLMs) which was achieved by an anion-exchange process (Begú et al., 2009). Related to the fact that silica particles are a precisely controllable colloid system, a lot of work has been dedicated to the immobilization of BLMs on these materials (Rapuano and Carmona-Ribeiro, 2000; Bayerl, 2004; Anderson et al., 2009). These contributions have been important in this Thesis to elucidate interaction mechanism between lipid molecules and clay surfaces since silica materials show chemical similarities with silicate clays with respect to surface groups or interaction with water molecules by the formation of *water bridges* (Bayerl, 2004).

The great majority of synthesis routes for lipid-biohybrid materials follows the three most common methods to produce supported BLMs: i) the Langmuir-Blodgett technique, ii) vesicle deposition, or iii) molecular self-assembly from a lipid solution. All methods have advantages and inconveniences. The Langmuir-Blodgett technique, for instance, is very precise and layer formation is highly controllable, but the process is time consuming and often inapplicable to particulate materials (Petty, 1996). Vesicle deposition allows for efficient bilayer formation on particulate materials of diverse geometries by adsorption of preformed bilayers (Rapuano and Carmona-Ribeiro, 1997), but the preparation of liposomes can be tedious and thus, might face limitations toward up-scaling for industrial processes. Molecular self-assembly of lipid molecules from solution offer a fast and large-scale approach in the synthesis of lipid-hybrid materials. This method is especially

suited for intercalation processes (Wicklein et al., 2010). A drawback, however, is the employment of organic solvents necessary for the dissolution of the lipids and accompanied environmental issues with regard to principles of *green chemistry* (Anastas and Warner, 2000).

1.4 Association of Bioactive Species to Lipid - Biohybrid Materials

Bioactive species such as enzymes, proteins, antigens, or DNA have shown to be invaluable for many biotechnological applications related to their specificity, molecular recognition ability, and fast kinetics. Amongst them, enzymes received special attention as they are a group of proteins with the ability to catalyze specific reactions (Illanes, 2008). This property has been widely exploited in analytic reagents, as biosensors (Girard-Egrot et al., 2005), bioreactors (Illanes, 2008), or in enzymatic fuel cells (Cracknell et al., 2008). Economic reasons demand reusability, long shelf-life time and efficient usage of the applied enzymes.

Immobilization on solid supports is one approach to match these requirements. Numerous strategies have been developed over the past decades. Amongst them, covalent linkage of proteins *via* amine chemistry of the protein amino acid chains renders highly stable complexes with negligible leaching (Colowick et al., 1998). However, this method can convey degradation caused by distortion of the protein structure which would limit the bioactivity and operation time.

As a consequence, softer routes for enzyme immobilization in solid materials have been developed with great success. They include entrapment of biological species by inclusion in porous materials such as mesoporous silica (Oda et al., 2006), layered double hydroxides (Vial et al., 2008), or sol-gel materials (Braun et al., 1990; Gill and Ballesteros, 2000b; Avnir et al., 2006). However, many enzyme-solid complexes may suffer from leaching.

Therefore, a challenge in immobilization of any biological species is to provide sufficient linkages as necessary to prevent leaching but at the same time accommodating these species as gentle as possible. One of the most promising routes to overcome these problems are to immobilize biomolecules in environments as similar as possible to biological systems. An interesting approach herein are bioinspired interfaces. Biomimetic, supported BLMs are ideal host matrices for the maintenance and transduction of enzymatic activity (Nikolelis et al., 1999) and also applicable to antibodies, receptors, virus particles and DNA probe for recognition (Trojanowicz, 2001).

1.4.1 Enzyme Immobilization Mechanism

Enzymes are proteins with catalytic properties which greatly depend on the conformation of their amino acid chains. The active catalytic sites are often buried inside the molecule and only accessible for specific substrate molecules. Therefore, enzymes show molecular recognition and can catalyze a wide range of processes such as hydrolysis, condensation, redox reactions, transfer reactions, or isomerization at high reaction rates (Forano and Prevot, 2008). A crucial aspect in this context is the spatial orientation of immobilized enzymes with respect to the supporting surface. This depends on the immobilization mechanism and on the mobility of the accommodating matrix to provide the possibility for enzymes to assemble into a suitable orientation (Pack et al., 1997).

Related to a similar chemical nature, enzyme and protein immobilization at lipid interfaces goes along the same routes. The immobilization of a protein on a native lipid membrane can be of *intrinsic* or *extrinsic* nature (Stenesh, 1998). The intrinsic (or integral) association is based on the insertion of hydrophobic amino acid side chains or entire protein parts into the lipophilic internal space of the membrane. These side chains are also termed *spikes* in some cases (El Karadaghi et al., 1984). The extrinsic (or peripherical) immobilization can be a transient association of the protein at the outer membrane surface *via* hydrogen bonds, electrostatic, or ionic interactions (Figure 1.5).

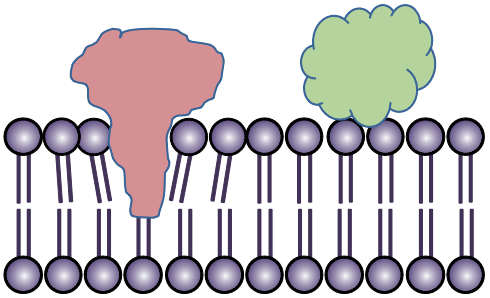

FIGURE 1.5: Scheme of intrinsic and extrinsic association of proteins to a lipid bilayer membrane. Dimensional proportions might not be exact.

Amongst the many types of enzymes exist *membrane-bound* and *cytosolic* enzymes. The first type undergoes electrostatic interaction with the lipid headgroups and hydrophobic interaction with the apolar moieties of the bilayer lipid membrane (Chen et al., 2000). The latter type of enzymes appears in the cell cytosol and is not bound to the cell membrane. It may, however, associate to it by transient electrostatic interactions (Krajewska, 2009). Cholesterol oxidase and urease are model enzymes of these two types and are used in this Dissertation for immobilization on clay supported lipid interfaces.

1.4.2 Virus and Antigen Immobilization

The structure of viruses is explained at the example of the Influenza virus which has been used in this Thesis. A virus consists of three structural components: the core, a viral envelope and matrix proteins forming the bridge between the first two components (Figure 1.6) (Nayak et al., 2004). The viral core contains the genetic information of the virus (helical ribonucleocapsids) and is surrounded by the viral envelope. It consists of a lipid bilayer membrane and contains the embedded proteins hemagglutinin (HA) and neuraminidase (NA) which are characterized by transmembrane spikes as anchor moiety (El Karadaghi et al., 1984). The combination of hemagglutinin and neuraminidase with different antigenic characteristics defines the various subtypes of the Influenza virus. The nomenclature of these subtypes is based on these combinations, e.g. H1N1, H5N9, or H1N2 etc. The main *antigen* of the Influenza virus is hemagglutinin. It triggers by a *key-lock* recognition reaction the *antibody* production of an infected organism.

Immobilization of virus particles or specific viral antigens on solid supports such as aluminum hydroxide, which are acting as adjuvants, is often necessary in the preparation and administration of vaccines (Coffman et al., 2010). Adsorption mechanism may involve ionic interaction between the charged virus surface and the adsorption site. This has been considered as basic mechanism in the immobilization of Influenza A virons on xanthan modified sepiolite fibers (Ruiz-Hitzky et al., 2009). The Influenza A virus is positively charged due to ionization of functional groups in the amino acid chains of the membrane proteins. On the other side, the carboxylic groups of the polysaccharide xanthan are deprotonated under the used physiological conditions. Functional groups of the virus proteins or the membrane itself may give rise to hydrogen bonding, ion-dipole interactions or disulfide bonds. Appropriate immobilization mechanism are of great importance since they may induce distortion of the protein structure of supported antigens (Clapp et al., 2010). A consequence would be diminished antibody production and hence, insufficient immunization of the organism. Therefore, biomimetic immobilization of these sensitive species is of great concern.

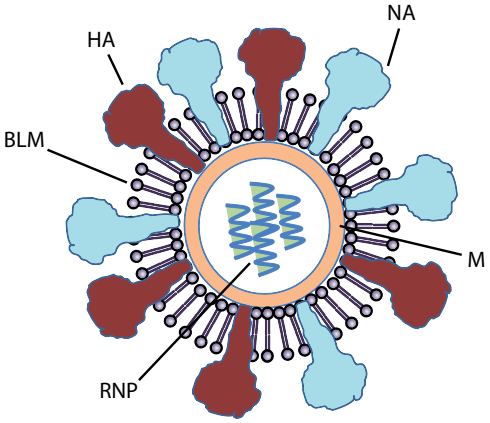

FIGURE 1.6: Scheme of an Influenza virus showing the bilayer lipid membrane (BLM) together with the transmembrane proteins hemagglutinin (HA) and neuraminidase (NA) as well as the core (RNP) and the matrix protein layer (M). For the sake of visualization, the proportions of the components are not exact.

1.5 Objectives of the Dissertation

The chief objective of this Dissertation is the study of self-assembly processes of different biosurfactants at the solid/liquid interface of clay minerals and electrode surfaces, respectively. The resultant materials display biomimetic interfaces which allow for the association of various types of biological species to originate a diversity of agricultural and clinical applications.

Four main objectives can thus be formulated:
In the first Section, the self-assembly processes of biosurfactants to different solids is subject of investigation as well as the properties of the resultant biomimetic surfaces. The self-assembly of phospholipid molecules to the clay minerals sepiolite and montmorillonite will be studied in organic and aqueous media. The choice of the solvent is considered as a crucial issue in the preparation of these clay-lipid materials. Furthermore, lipid molecules are adsorbed on nanometric platelets of layered double hydroxides by a novel co-precipitation route. Another type of studied biomembranes are mixed layers constituted of lipids and sugar-based surfactants that may provide additional functionalities owing to the incorporation of sugar moieties. Special attendance is given to the physico-chemical characterization of the various interfaces.

The second scope of the presented Dissertation comprises the study of possible technological applications based on enzymes associated to biomimetic lipid interfaces on sepiolite. These interfaces are considered favorable for the maintenance of enzymatic activity. Two model enzymes, obeying different membrane association modes, are studied in this context; urease and cholesterol oxidase. The enzyme-loaded biohybrids will henceforth be subjected to the exploration as active phase of a voltammetric biosensor for urea and as cholesterol oxidase bioreactor. A further example where clay-lipid biohybrids may find usage is the sequestration of mycotoxins. These fungi expressed, pathogenic compounds are frequently found in animal food stocks and represent a severe hazard for the health of animals and humans. The retention capacity of the clay-lipid biomaterials for the mycotoxins aflatoxin B1 and deoxynivalenol will be examined and compared to quaternary

alkylammonium based organoclays, showing the potential interest of this new type of bio-organoclays.

The third aim is in response to a constant request for suited vaccine carriers. These adjuvants are required to procure improved properties with respect to conformational and thermal stability of the associated antigenic species. In accordance with this demand, an Influenza vaccination adjuvant based on the biomimetic lipid interfaces on sepiolite and layered double hydroxides, respectively, will be investigated. Biomimetic immobilization and its study is of great importance since antibody recognition, the basis of immune reaction and accompanied immunization, relies on the native protein conformation of the immobilized antigens. Additionally, with regard to enhance the efficacy of vaccine doses, two strategies will be employed in the immobilization of the Influenza antigens: i) The association of the entire, inactivated virus particle and ii) the immobilization of the membrane protein hemagglutinin which is one of the main antigens of the Influenza virus. The efficacy of the latter approach is assessed in immunization tests in mice.

The final goal is founded in the development of a rapid, sensitive and user-friendly impedimetric biosensor for the selective detection of the H1N1 and H5N9 subtypes of the Influenza virus. The designed biosensor obtains these qualities from the association of specific sialic acid groups to a mixed self-assembled bilayer presenting external galactoside residues. This set-up would make cumbersome sample preparation, as in case of many other virus sensors or standard clinical methods, superfluous. A detailed investigation of the layer formation processes will constitute a mayor part of this forth Section.

Chapter 2

Materials and Methods

2.1 Starting Materials

2.1.1 Supports for Lipid-based Biohybrids

The biohybrid materials within this Thesis were prepared by surface modification of various layered and fibrous inorganic materials acting as solid supports for the biomimetic layers. In this context, clay minerals such as montmorillonite, belonging to the smectite group, and the microfibrous silicate sepiolite were used. Other supports were muscovite mica and the Al/Mg type layered double hydroxide.

2.1.1.1 Montmorillonite

Montmorillonite (MMT) of the type SWy1 with the composition $(Si_{7.98}Al_{0.02})^{IV}(Al_{3.01}Fe_{0.41}Mn_{0.01}Mg_{0.54}Ti_{0.02})^{VI}O_{20}(OH)_4{\cdot}(Ca_{0.12}Na_{0.32}K_{0.05})$ from Crook County, Wyoming (USA), with a cationic exchange capacity of 76 meq/100 g (according to the specifications of its supplier) was obtained from Source Clay Minerals Repository of the Clay Minerals Society, Columbia, Missouri (USA). For the preparation of MMT-biohybrids only the particle diameter fraction of $< 2\,\mu$m was used. Therefore, this fraction was extracted by applying the Stokes law to the settling of a crude MMT suspension (12.5 g/l)

in a graduated 2 l cylinder allowing for the removal of a certain upper part of the suspension after 24 h sedimentation time (Gómez Avilés, 2010). In a next step, homoionic Na^+-montmorillonite was prepared by complete ion exchange by treatment with 1.0 N NaCl solution. The sample was washed and dialyzed with bidistilled water until complete removal of chloride ions, proved with the AgCl test.

2.1.1.2 Sepiolite

Sepiolite (SEP) from Vallecas, Madrid (Spain) of $> 95\,\%$ purity and commercialized as Pangel S9 with a CEC value close to 15 meq/100 g was furnished by Tolsa S.A. (Spain) and used as supplied. The total specific surface area of this sepiolite was determined by BET measurements and found to be $310\,m^2/g$, whereof the external specific surface area are $165\,m^2/g$.

2.1.1.3 Mica

Mica is a non-swelling layered clay of the aluminum phyllosilicate family whose empirical formula is $KAl_3Si_3O_{10}(OH)_{1.8}F_{0.2}$ (Brigatti et al., 2006). Exfoliation of the clay lamellae renders atomically flat mineral sheets which served as planar support for biomimetic thin films in this work (Section 3.4.1). Muscovite mica sheets were purchased from Ted Pella Inc., California (USA).

2.1.2 Biomolecules: Phosphatidylcholine, Enzymes, Proteins, Influenza Viruses, and Mycotoxins

- Three batches of phospholipids (PL) with different L-α-phosphatidylcholine (PC) content were used in this work for the synthesis of the various lipid-hybrid materials. Phospholipids from egg yolk of 60 % and 99 % PC content (determined by thin layer chromatography (TLC)) were supplied by Aldrich. Among the residual 40 % of the

first batch are lipids belonging to the ethanolamine and lyso class as well as cholesterol. The fatty acid composition of this egg yolk PC lot consisted of approximately 27 % 16:0, 13 % 18:0, 31 % 18:1, 17 % 18:2 and 5 % 20:4 (other fatty acids being minor contributors). This nomenclature describes the number of carbon atoms and the saturation of the individual fatty acid chains. Accordingly, the 60 % PC product has an average molecular weight of approximately 770 g/mol and the average number of acyl chain carbon atoms was n=17.5. Adsorption isotherms on sepiolite and montmorillonite from organic solvent were sampled with this PC batch. Clay-lipid materials for mycotoxin adsorption were also prepared from this lot.

The highly pure 99 % PC batch was used for preparation of biohybrids applied in immunization tests for Influenza vaccination. It was also employed in model studies based on PC layer deposition on mica as well as for confirmation of preferential PC adsorption from the 60 % batch by thermal analysis. The use of this 99 % PC batch was limited due to its elevated cost as compared to other PC products used in this work.

Phospholipids from soy bean which contained 92 % PC were mostly used for liposome preparation and biohybrids which were utilized in enzyme, protein, and virus immobilization. This phospholipid product is commercialized as Emulmetik^{TM} 930 which was kindly provided as a gift from Lucas Meyer Cosmetics, Germany. Among the residual 8 % are lipids belonging to the lyso class as well as phosphorous compounds and moisture.

- Two different types of enzymes were selected for the immobilization on clay-lipid materials: The cytosolic enzyme urease and the membrane-bound enzyme cholesterol oxidase.

  Urease (URE) is present in many plants, bacteria, fungi, and algae (Hirayama et al., 2000). Extracellular urease is often found in soil and humic mater forming organo-mineral complexes and shows a great affinity for silicates (Marzadori et al., 1998). Urease was the first enzyme isolated as crystalline protein in 1926 by Sumner (Sumner, 1926). This enzyme adopts a hexametric structure composed of six subunits with

a molecular mass of 460 kDa (Figure 2.1A). The active catalytic site is known to comprise two nickel ions per each subunit (Dixon et al., 1980). Urease from *Canavalia ensiformis* (Jack Bean) Type XI E.C. 232.656.0 with 50590 u/g solid was obtained from Sigma and employed as received in the preparation of an electrochemical urea biosensor.

Cholesterol oxidase (COx), on the other side, is a membrane-bound, monomeric flavoenzyme of 65 kDa molecular mass that catalyzes the oxidation and isomerization of cholesterol to cholest-5-en-3-one (Kreit and Sampson, 2009). The reactive center of this enzyme is the flavin adenine dinucleotide (FAD) cofactor (Figure 2.1B). A remarkable feature of this enzyme is its water-solubility while its substrate is highly hydrophobic and practically insoluble in water. The hydrophobic active center of COx is deeply buried in a cavity inside the protein and the accessing tunnel is shielded from aqueous solvent by amphiphathic protein loops to ensure water-solubility of the enzyme (Chen et al., 2000). Binding with cholesterol will lead to an alteration of the loop conformation and eventually allow the entrance of the substrate to the catalysis center. COx from *Brevibacterium sp.* E.C 1.1.3.6 with 33 u/mg solid was supplied by Sigma and was used as received in the preparation of a cholesterol bioreactor.

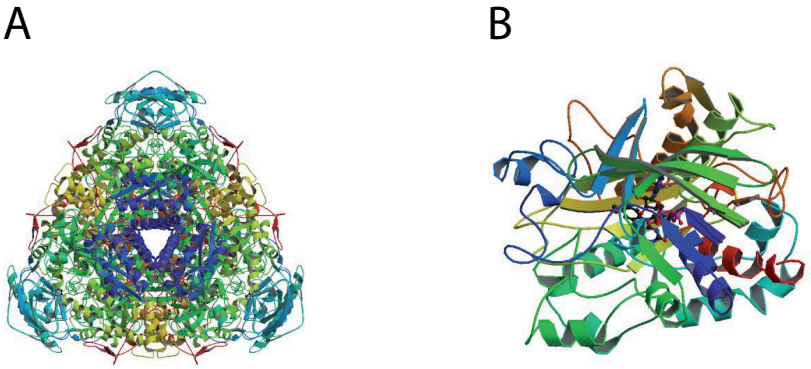

FIGURE 2.1: Representation of the molecular protein structure of urease (A) and cholesterol oxidase (B).

- Influenza viruses used in this Thesis were of the human PR8/34 (H1N1) subtype (Figure 2.2A) and the porcine A/swine/Spain/40564/2002 (H1N2) subtype. They were produced in fertilized chicken eggs of infected hens and purified (850 μg/ml

and 436 μg/ml, respectively) according to protocols from the World Heath Organization (Cox, 2002). Other used viruses were present in egg serum at different concentrations; A/turkey/Wisconsin (H5N9) at ca. 800 μg/ml which is a low pathogenic avian Influenza virus kindly donated by Dr. Adolfo García-Sastre from Mount Sinai School of Medicine of New York; A/swine/Spain/50047/2003 (H1N1) from swine (ca. 500 μg/ml); and PRRS (porcine reproductive and respiratory syndrome virus). Viruses were inactivated by exposure to UV light for 5 min prior to use. However, in some cases, active viruses were used in biosensor tests. All viruses were obtained from Dr. Gustavo del Real (INIA, Spain).

- The membrane protein hemagglutinin (HA) (Figure 2.2B) originating from the PR8 Influenza virus strain was synthetically produced in insect cells (*Baculovirus* system) and provided by Dr. J. Rodríguez Aguirre (Centro Nacional de Biotecnología (CNB-CSIC), Spain).

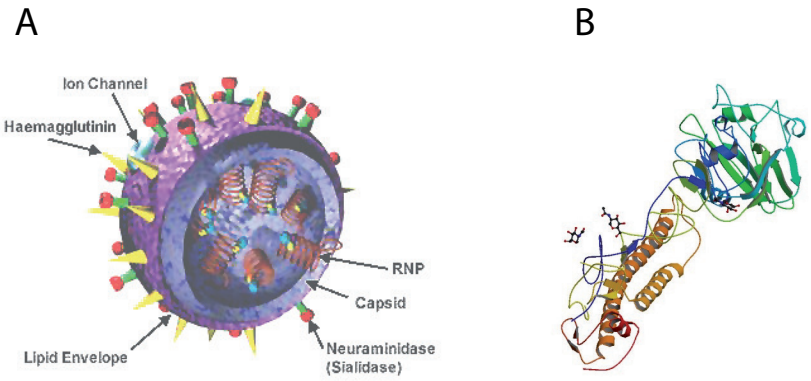

FIGURE 2.2: Representation of the Influenza virus (A) and the protein structure of hemagglutinin (B).

- Sialylation of galactoside moieties on biomimetic thin films was performed by two types of sialyltransferase enzymes (SAT); the α-2,6-SAT from *Photobacterium damsela* (EC 2.4.99.1) with $\geq$5 units per mg protein specific activity and α-2,3-SAT from *Pasteurella multocida* (EC 2.4.99.4) with $\geq$2 units per mg protein specific activity. Both enzymes are recombinant expressed in *Escherichia coli* and were purchased from Sigma. The substrate for the sialylation process was cytidine-5'-monophospho-N-acetylneuraminic acid sodium salt (CMP-sialic acid), that was also obtained from Sigma.

- Mycotoxins used in the sequestration study were aflatoxin B1 (AfB1) from *Aspergillus flavus* (Figure 2.3A), a toxin which is considered to be amongst the most carcinogenic substances known (Betina, 1989; Heathcote and Hibbert, 1978). The second tested mycotoxin was deoxynivalenol (DON), also known as vomitoxin, produced by *Fusarium moulds genera* (Figure 2.3B). Both mycotoxins were supplied by Sigma.

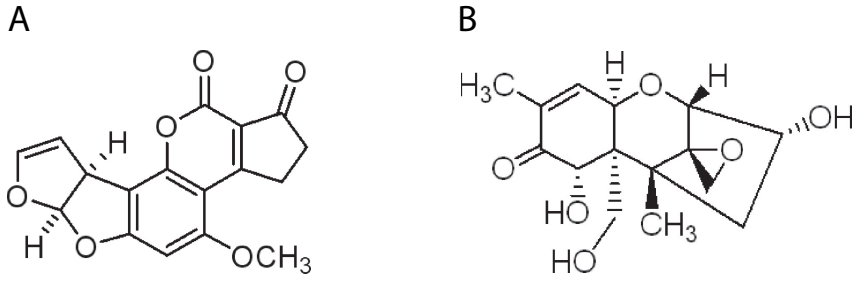

FIGURE 2.3: Representation of the molecular structure of aflatoxin B1 (A) and deoxynivalenol (B).

2.1.3 Other Chemicals and Materials

- Solvents: Iso-propanol, hexane, methanol and ethanol. All were of synthesis grade (Sigma-Aldrich). Deionized water (resistivity $> 18.2\,\mathrm{M}\Omega$ cm) was used throughout this work and obtained from a Maxima Ultrapure Water system from Elga. In experiments with viral species and in related activity assays, a commercial phosphate buffer saline (PBS) at physiological pH 7.3 and 6.7 mM PO_4 was used (Lonza). Sterile PBS was used in animal tests. In experiments with enzymes phosphate buffer (PB) solutions at pH 7.0 - 7.5 of varying concentrations were prepared from monopotassium phosphate (KH_2PO_4).

- Acids: Sulfuric acid (96 %) and phosphoric acid (85 %) were reagent grade, (Sigma-Aldrich). Ascorbic acid (AA) and 5,5'-Dithiobis(2-nitrobenzoic acid) (DTNB) were received from Fluka.

- Bases: Sodium hydroxide (NaOH), $\geq$98 %, pellets (anhydrous) and potassium hydroxide (KOH), 90 %, flakes. Both were of reagent grade (Sigma-Aldrich).

- Salts: Monopotassium phosphate (KH_2PO_4), potassium nitrate (KNO_3), potassium ferrocyanide ($K_4Fe(CN)_6 \cdot 3H_2O$), and potassium ferricyanide ($K_3Fe(CN)_6$) were from Sigma. Aluminium chloride ($AlCl_3 \cdot H_2O$) was purchased from Fluka and magnesium chloride ($MgCl_2 \cdot H_2O$) from Carlo Erba. All salts were of reagent grade.

- Reagents used in the enzyme activity study were albumin from bovine serum (BSA), urea ($\geq 98\,\%$), cholesterol ($\geq 98\,\%$), 2,2'-azino-bis(3-ethylbenzothiazoline-6-sulphonic acid (ABTS), horseradish peroxidase (HRP), TrizmaBase, and Triton X-100. All reagents were purchased from Sigma.

- Sugar-based surfactants: Octyl-β-D-glucoside (OGlu) was delivered by Sigma-Aldrich and octyl-β-D-galactoside was obtained from Carbosynth.

Other used chemicals were polyvinyl alcohol (PVA) with $> 99\,\%$ hydrolysis grade and MW of 89 000-98 000, Coomassie Brilliant Blue G, octanethiol (all from Aldrich), aluminum hydroxide gel (Alhydrogel®) from Sigma, 30 % hydrogen peroxide solution, and phenol (both from Sigma-Aldrich).

- Gold supports: Biosensors were prepared on home-made polycrystalline gold disc electrodes as well as on interdigitated polycrystalline gold electrodes which were obtained from Dr. C. Fernández-Sánchez (Centro Nacional de Microelectrónica - Instituto de Microelectrónica de Barcelona CNM-IMB (CSIC), Spain). Gold chips were used in model studies as electrode substitute and subjected to various characterization methods. The employed gold chips were also received from Dr. C. Fernández-Sánchez and consisted of Si as base material with subsequent layers of SiO_2 (1 μm), Cr (20 nm) and a 100 nm finish of polycrystalline gold.

- Reference organophilic clays: Cetyl trimethylammonium (CTA) modified sepiolite was prepared by Dr. S. Letaief (Aranda et al., 2008) and kindly provided as gift. The commercial organoclay Cloisite® 30B was received from Southern Clay Products (TX, USA). In brief, Cloisite® 30B is a natural montmorillonite modified with the quaternary ammonium salt tallow bis-(2-hydroxyethyl) methyl ammonium chloride.

2.2 Materials Syntheses

2.2.1 Synthesis of Lipid-based Biohybrids

(a) **Clay-Lipid Biohybrids**

For adsorption isotherms, phospholipid solutions of 10 ml methanol and ethanol, respectively, with a lipid concentration ranging from 0.1 to 12.5 mM, were prepared under consideration of the phospholipid purity (typically 60 %). In each phospholipid solution, 20 mg of Na-montmorillonite or sepiolite were suspended. Accordingly, the initial clay to lipid ratio was between 27:1 and 0.2:1. The suspensions were stirred for 24 h at ambient temperature (approx. 25 °C). The resultant biohybrids were collected by centrifugation (8000 rpm, 15 min), vacuum-dried at room temperature and ground to powder for further analysis. The lipid content of the biohybrids is denoted as mmol PC per 100 g clay if not stated otherwise.

For the synthesis from aqueous solution, liposomes were prepared by the extrusion method (Hope et al., 1985; Mayer et al., 1986). PC (from the 92 % batch) was dissolved in chloroform which was subsequently evaporated under a stream of nitrogen. To ensure complete chloroform removal, the sample was kept under reduced pressure for at least 2 hours. Then, the dried lipid cake was hydrated under vigorous agitation in aqueous solvent to yield the desired concentration (typically between 5 and 15 mM). The solution was consecutively extruded at least 11 times through Nuclepore® track-etched polycarbonate membranes from Whatman with regular pore sizes of 400, 200 and 100 nm. After passing each membrane, the liposome diameter decreased and eventually reached ca. 130 nm as confirmed by dynamic light scattering measurements (Malvern Instruments Zetasizer Nano ZS). Liposomes were prepared in bidistilled water as well as in 50 mM PB solution, depending on the final purpose. For adsorption on powdery supports, an aliquot of liposome solution was contacted with the adsorbents and stirred overnight (16 hours). Recovery of the resultant hybrids proceeded as described above.

(b) **Layered Double Hydroxide-Lipid Biohybrids**

Biohybrids based on 2:1 Mg/Al LDH were obtained by a co-precipitation method. In the synthesis, 4.69 mmol $AlCl_3 \cdot H_2O$ and 9.387 mmol $MgCl_2 \cdot 6H_2O$ were dissolved in 500 ml bidistilled water. The salt solution was added slowly (2 ml/min) under constant stirring to 100 ml of a 0.5 mM PC liposome solution. Both solutions are constantly purged thoroughly with N_2 and the pH was controlled using a Metrohm 765 Dosimat to keep the pH constantly at 9.0. The suspension was stirred for 24 h at room temperature and the solid fraction was separated by centrifugation. The Mg/Al LDH-PC biohybrids were washed three times with water and kept as gel (5.4 wt.% solid content) until further usage except for some characterization methods (infrared spectroscopy, chemical microanalysis, and powder X-ray diffraction) where the gel was dried at 40 °C.

(c) **Preparation of Lipid-based Thin Films on Mica**

Mixed PC/OGal layers were prepared by the formation of a bottom PC monolayer on a freshly cleaved mica support and subsequent deposition of a OGal layer. The PC monolayer on mica was obtained by spin-coating according to a protocol described elsewhere (Simonsen and Bagatolli, 2004). From a 5 mg/ml PC stock solution composed of hexane and methanol (95/5 vol%), 50 μl were spread on 1 cm^2 of mica. Samples were spun at 3000 rpm for 40 s in air atmosphere to evaporate the solvent. To ensure complete solvent removal, samples were placed under reduced pressure overnight. The PC layer was then hydrated in distilled water for 2 h, rinsed thoroughly, and blown dry under N_2. This step removes excess of lipid and leaves a PC monolayer behind. The OGal layer was then deposited from a 5 mM solution by sample immersion for 2 h at ambient temparature. The surface was rinsed with copious water and blown dry for further analysis.

2.3 Characterization Methods and Instrumentation

The characterization of the resultant materials was conducted with the purpose to obtain information about structure, composition, stability and bioactivity. Structural information was provided by X-ray diffraction, ^{29}Si and ^{31}P nuclear magnetic resonance spectroscopy, Fourier transform infrared spectroscopy, specific surface area, and contact angle measurements. Composition and thermal stability were assessed by chemical microanalysis and thermal analysis, respectively. The biological activity was evaluated by means of electrochemical instrumentation comprising potentiostats and a frequency analyzer. The morphology of the samples was observed by field-emission scanning electron microscopy, transmission electron microscopy, and atomic force microscopy, while particle size was assessed through dynamic light scattering. Surface potentials were also determined by dynamic light scattering. A full description of these methods is beyond the scope of this Section, instead, the basics are provided as far as it concerns the interpretation of the experimental results and reproduction of the analysis.

2.3.1 Elemental Analysis

The lipid quantity of biohybrid materials was calculated from data obtained by chemical microanalysis (PerkinElmer 2400 Series II CHNS/O Elemental Analyzer) of the organic content of the solids. This technique permits the quantification of the amount of hydrogen, nitrogen, carbon, and sulfur of solid samples by combustion at 950 °C. Samples were generally analyzed as duplicates.

2.3.2 Thermal Analysis

Thermogravimetry (TG) is an analytical technique used to determine the materials thermal stability by recording the weight changes during heating. Weight changes are related to thermally induced transitions involving, for instance, dehydration or decomposition processes. Evaporation of volatile components or formation of reaction products may

also give rise to weight changes (Willard et al., 1988). These processes can also be monitored by changes in the materials heat flux with the surrounding, denoted as differential thermal analysis (DTA). Thermal stability of the biohybrids was investigated by TG and DTA on a SSC/5200 Seiko analyzer. TG and DTA measurements were simultaneously performed under dynamic conditions of 20 ml/min air flux with aluminum as reference.

2.3.3 Fourier Transform Infrared Spectroscopy

Fourier transform infrared spectroscopy (FT-IR) is a broadly used technique for chemical analysis, molecular and materials structure determination and information of electronic properties (Willard et al., 1988). FT-IR absorption spectra were recorded on a NICOLET 20SXC and on a Bruker IFS 66v/S Spectrometer with 2 cm^{-1} resolution. Sepiolite based samples were prepared as self-standing films for higher sensitivity with respect to the Si-OH stretching vibration. Films were obtained by casting of an aqueous 2 wt.% slurry on Mylar foil from where the dried film can be peeled off. Other materials were suspended in a KBr matrix (∼1 wt.%) and pressed with 4 t/cm^2 to IR transparent pellets.

In some cases, samples were analyzed on an attenuated total reflectance infrared spectrometer (ATR-IR) and the obtained spectra were converted by an algorithm implemented in the equipment software OMNIC 8.1 (Thermo Fisher Scientific Inc.) into FT-IR absorbance spectra. In this method, a small amount of specimen (ca. half a spatula tip) was placed on a ruby and measured without suspension in a matrix. Therefore, this technique permits recording with high resolution and the detection of weak bands such as the one of the P=O function from the phosphatidylcholine headgroup. The used equipment was a Nicolet Avatar 320 FTIR, using a MIRacle ATR device with a diamond crystal plate (Pike Technologies, Madison, WI). These measurements were conducted at the laboratory of Prof. G. Rytwo (Migal Technological Center, Israel).

2.3.4 UV-visible Spectroscopy

Ultraviolet-visible spectroscopy (UV-Vis) is another analytical technique to prove the formation of complexes. In the present Thesis, however, UV-Vis spectroscopy was used to determine the concentration of mycotoxins, proteins, and sugar-based surfactants in aqueous solutions as well as enzymatic activity. These measurements are based on the application of the Lambert-Beer law, relating the measured optical density to the concentration of the UV-Vis active solute (Willard et al., 1988). Transmission UV-Vis spectra were recorded on an Shimadzu UV-2401 PC UV-Vis spectrometer at high scan rate in the 800-200 nm range and with a grid slide of 1 nm.

2.3.5 Powder X-ray Diffraction

Structural information was provided from powder X-ray diffraction (XRD) which was run on a Bruker D8-ADVANCE with Cu anode and Ni filter. The diffractometer was equipped with a goniometer of 0-20 ° and a SOLX detector. The radiation generator was operated at 40 kV and 30 mA. The powdery samples were cast from aqueous 1 wt.% slurries on glass sample holders and dried to films. Diffraction patterns were recorded at a scan speed of 3 ° / min in the range of 1-70 ° (2Θ). Special attention was given to the reflections of the (00l) planes from montmorillonite and Mg/Al LDH based biohybrids, respectively, to ascertain possible intercalation detected by the increase of basal distances.

2.3.6 Nuclear Magnetic Resonance

Sepiolite-lipid interaction was investigated by ^{29}Si CP MAS NMR and proton non-coupled ^{31}P MAS NMR which were recorded on a Bruker Avance 400 spectrometer, using a standard cross-polarization pulse sequence. In the case of the montmorillonite based bio-hybrids, the paramagnetism of Fe, which is always present in the MMT structure, impeded the recording of useful NMR spectra. Powder samples were spun at 10 kHz whereas PL was measured in ethanol solution. Spectrometer frequencies were set to

79.49 and 161.97 MHz for ^{29}Si and ^{31}P, respectively. A contact time of 2 ms and a period between successive accumulations of 5-10 s were used. The number of scans was 400-800. Chemical shift values were referenced to tetramethylsilane (TMS) and 85 % phosphoric acid (H_3PO_4) for Si and P nucleii, respectively.

2.3.7 Specific Surface Area

Determination of specific surface area presents an important piece of information concerning structure and morphology of hybrid materials. Especially porous and lamellar materials such as clays and related materials are frequently subject of specific surface area determination. Brunauer-Emmett-Teller (BET) analysis of the nitrogen adsorption isotherm provides information on internal (micro- and mesoporosity) and external specific surface areas. Samples were degassed at 120 °C overnight prior to analysis. BET specific surface areas were determined from N_2 adsorption analysis at 77 K on a Micromeritics ASAP 2010 analyzer. One-point analysis of N_2 adsorption to determine the BET specific surface area was performed with a Micromeritics Flowsorb II 2300 instrument.

2.3.8 Electron Microscopy

- Field Emission Scanning Electron Microscopy

  Scanning electron microscopy is a widely used technique to study materials morphology and texture on a submicron scale. Therefore, backscattered and secondary electrons generated by a scanning electron beam are detected and imaged. The used microscope in this work was a field emission scanning electron microscope (FE-SEM) from FEI company (NOVA NANOSEM 230) that operates at high and low vacuum. The microscope is equipped with various detectors (vCD and STEM amongst others) and adjustable electron landing voltage which allows sample analysis without prior conductive sputtering. The powdery samples were finely dispersed on a conductive carbon patch to avoid electrostatic charging. The aluminum and magnesium content of Mg/Al LDH and the sodium content of Na^+-MMT biohybrids were semi-quantitatively determined

by energy-dispersive X-ray spectroscopy (EDX) with an EDAX detector TypeSDD Apollo 10 mounted on the FE-SEM. In case of sodium analysis, the data acquiring conditions were kept constant at working distance 6.3 mm, spot size 2.5, landing energy 6.0 keV, and accumulation time 100 s. The sodium content is expressed as ratio of the sodium and silicon signal. Al and Mg was detected with 6.0 keV landing energy at 800 x magnication and 77 s accumulation time.

- Transmission Electron Microscopy

  Transmission electron microscopy (TEM) instruments use a beam of highly energetic electrons to examine objects on a very fine scale with nanometer resolution. This examination can yield information about topography, morphology, composition and crystallography. Half a spatula tip of powdery sample was dispersed in a test tube of bidistilled water, vortexed vigorously and subjected to ultrasonic agitation for 5 min. A drop the suspension was placed on a carbon coated copper TEM grid (200 mess) from Fedelco® and Aname, respectively, and allowed to dry. In some cases, specimens were negative stained with 1 % uranyl acetate solution for 40 s. Observations were made on a LEO-910 STEM microscope, operating at an accelerating voltage of 80 kV.

2.3.9 Atomic Force Microscopy

Atomic force microscopy (AFM) allows with vertical subnanometer resolution imaging of surfaces. AFM can be operated in two different modes, denoted as static and dynamic mode. In the first mode, the AFM tip scans over a sample at constant height, producing topographical images as result of the deflection of the tip due to interactions with the sample surface. As consequence of the contact with the sample, the tip can be contaminated when imaging soft matter samples and hence, loose resolution. Therefore, the non-contact, dynamic mode is applied for these kind of materials. The AFM tip oscillates above the sample surface at a certain frequency close to the cantilever resonance frequency. Electrostatic interactions between the sample and the tip alter the frequency and a feedback mechanism of the instrument adjusts the tip height to maintain constant

frequency. This operation provides topographical images of the surface. Frequency alterations can also be used to plot phase shift images of a sample surface, offering information on the chemical composition of the surface. Images in this Thesis were acquired in dynamic mode on a Nanotec AFM instrument equipped with a Si cantilever. The force constant of the cantilever was 2.8 N/m and the resonance frequency 75 kHz.

2.3.10 X-ray Photoelectron Spectroscopy

X-ray photoelectron spectroscopy (XPS) is a highly sensitive analytical technique that allows for detection of chemical elements of surfaces at (sub)nanometer lateral resolution. Samples are irradiated under ultra-high vacuum (UHV) with X-rays which provokes the emission of electrons from the upper electron shell of surface atoms. These emitted electrons are termed *photoelectrons* and contain a specific energy (binding energy) according to the atom number and electron shell from which they originated. This is the basis for the use of XPS in elemental chemical analysis. A CCD chip captures the photoelectrons and binding energy spectra can be plotted. Evaluation of the peak position and half-width provide information on i) the chemical element, ii) the oxidation state, and iii) coordination of the atoms at the surface.

In this Thesis, two different XPS equipments came to use. The thin films prepared on gold chips (Section 3.4.2.2) were analyzed on a VG Escalab 200 R using monochromatic Al Kα radiation at 1486.7 eV (200 W, 12 kV) in the non-focusing mode under UHV of 10^{-10} - 10^{-9} mbar. The instrument was equipped with an electron source (FG-500) for charge compensation. The photoelectron energy was analyzed with a PHOIBOS 150 9MCD and a multi-channeltron detector. Mica supported thin films (Section 3.4.1) were studied using monochromatic Mg Kα radiation at 1253.6 eV (200 W, 12 kV) under UHV. The photoelectron energy was analyzed with a PHOIBOS HSA3500 150 R6-HiRes MCD-9 detector. The binding energies for each spectrum were calibrated with respect to the C1s band at 284.6 eV.

2.3.11 Electrochemical Instrumentation

Cyclic voltammetry (CV) and electrochemical impedance spectroscopy (EIS) are means to study redox behavior at interfaces as well as electrical properties and morphologies of interfacial and bulk materials. CV of enzyme associated biohybrids was carried out on a minipotentiostat μSTAT 100 from DropSens® in a typical three electrode set-up, comprised of a working electrode, a platinum auxiliary electrode and an Ag/AgCl reference electrode. A Solartron 1480 MultiStat potentiostat was used for CV during the preparation of biomimetic thin films supported on gold electrodes. Cycling potentials and scan rates were in each case adjusted according to the application and system under investigation. The experimental conditions are indicated in the text. EIS was performed on a Frequency Response Analyzer SI 1255 HF from Schlumberger connected to the Solartron 1480 MultiStat potentiostat. A typical frequency range was set to 100 kHz - 1 Hz at the redox potential of -8 mV using a modulation amplitude of 10 mV with 10 data points per decade. The Nyquist representations of the EIS spectra were fitted to a Randles equivalent circuit model (Figure 2.4) (Mendes et al., 2004).

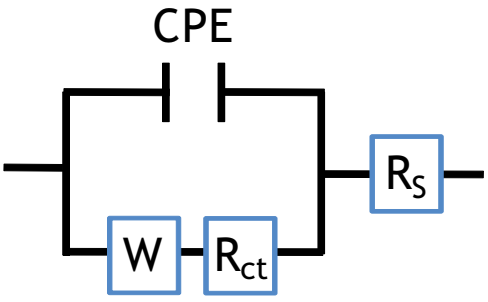

FIGURE 2.4: Representation of a Randles equivalent circuit model.

2.3.12 Dynamic Light Scattering

Dynamic light scattering (DLS), also often referred to as photo correlation spectroscopy, makes particle size accessible by determination of particle velocity caused by Brownian motion. The average mean displacement of the Brownian motion is related to the translational diffusion coefficient, rendering the hydrodynamic particle diameter according to

the Stokes-Einstein equation. The DLS technique applies Rayleigh and Mie scattering theory to determine the diffusivity.

A convenient way to evaluate colloidal stability is to measure the zeta potential of particles. This method utilizes the fact that many dispersed particles exhibit a surface potential caused by either ionisation of surface groups, differential loss of ions from the crystal lattice or adsorption of charged species like ions and ionic surfactants. The zeta potential can be measured due to the fact that charged particles interact with applied electric fields. Charged particles will travel to the opposite charged electrode and the optically measured electrophoretic mobility is linearly related to the zeta potential by the Henry equation (Pugh and Bergström, 1994).

In the present Thesis, particle size and zeta potential were determined on a Malvern Instruments Zetasizer Nano ZS. Sepiolite-lipid suspensions of 0.05 wt.% were prepared in 50 mM PB solution (pH 7.0) for zeta potential measurements while liposomes were analyzed in 10 mM NaCl. Particle size information was obtained from suspensions sufficiently diluted until data quality requirements were fulfilled.

2.3.13 Water Sorption

Water sorption is a method to study the wettability and texture of a materials surface. The analysis and fitting of the experimental data to appropriate models permits to characterize the surface. Water adsorption isotherms were sampled at 25 °C with a Gravimetric Water Sorption Analyzer (Aquadyne DVS) from Quantachrome Instruments (Florida, USA). Prior to measurements, the samples were purged at 80 °C until the sample weight remained constant. In a stepwise fashion, the relative humidity in the sample compartment is increased from 0 and 95 %. At each interval, the mass gain relative to the initial sample weight is recorded when the system has reached equilibrium and the weight remained constant. The mass change data is used to construct the sorption isotherm.

2.3.14 Contact Angle Measurement

Water contact angle measurements on surfaces render valuable information of interfacial properties such as hydrophobicity or surface tension as well as their alteration due to surface modification. Dynamic and static water contact angle measurements were performed on a Krüss drop shape analysis system. Powdery sepiolite-lipid samples were cast from aqueous 1 wt.% slurries on glass sample holders and dried to films. Measurements were performed in static mode with an average drop volume of 0.12 μl. For angles below 30 ° the drop shape was circle fitted and for angles above 30 ° the contact angle was measured according to the Laplace-Young method. Measurements of organically modified surfaces of gold chips and mica platelets were conducted in dynamic mode with 10 μl/min drop velocity.

2.4 Protocols and Applications

2.4.1 Immobilization Protocols for Biological Species

(a) **Enzyme immobilization**

Enzyme immobilization (urease and cholesterol oxidase) on sepiolite-lipid biohybrids took place in 50 mM phosphate buffer solution (PB) at pH 7.0 with 0.3 wt.% adsorbent material dispersed. Enzyme stock solutions were prepared in 50 mM PB at pH 7.0 with urease concentration of 1 mg solid/ml and 2 mg solid/ml for cholesterol oxidase. The enzyme concentration in the adsorption suspension was fixed to 1 mg solid/ml for urease and 0.267 mg solid/ml for cholesterol oxidase. The incubation time was 2 h at ambient temperature (21 °C) under gentle agitation on a magnetic stirrer. Adsorbents were separated by centrifugation at 4000 rpm for 15 min.

(b) **Immobilization of viral particles and proteins**

The supports for the viral particles and proteins were prepared as suspensions of 1 mg/ml in PBS. Between 1 and 21.5 μg of purified PR8 virus from a stock solution

(850 μg/ml) were added to aliquots of 50 μg solid to give final PR8 concentrations of 6-122 μg/ml. In case of hemagglutinin immobilization, 125 μg solid were contacted with 5-50 μg HA (from a 313 μg/ml stock solution) to render a final protein concentration of 16.7-166.7 μg/ml. Incubations in both cases were performed at 4 °C for 2 h. The solids were recovered by centrifugation (13000 rpm, 30 min, 4 °C) and resuspended in PBS for subsequent analysis.

2.4.2 Quantification and Activity Protocols for Biological Species

(a) **Quantification of lipid content in PC-based biohybrids**

The amount of adsorbed lipid on clay and Mg/Al LDH was determined by chemical microanalysis as described in Section 2.3.1. The molar quantity of PC per 100 g solid can be calculated from the measured carbon content (in wt.%) under consideration of the average molecular mass of the used PC (770 g/mol) and the molar fraction of carbon per lipid (500 g/mol) according to the average acyl chain length of 17.5 carbon atoms.

(b) **Total protein assay**

Protein adsorption quantities were determined colorimetrically following the Bradford total protein assay (Bradford, 1976) using bovine serum albumin (BSA) as reference protein for calibration (Figure 2.5). The Bradford reagent was prepared by dissolving 25 mg Coomassie Brilliant Blue G in 12.5 ml ethanol and subsequently adding 25 ml phosphoric acid (85 %). The mixture was under stirring added up to 250 ml volume with water and stirred overnight. Prior to use, the solution was filtered two times with Whatman No 1 cellulose filters. In order to improve sensitivity, a micro-Bradford assay was followed (Kruger, 2002) where 5-100 μl aliquots of a 100 μg/ml BSA standard (in 50 mM PB , pH 7.4) are brought up to 100 μl with water and 1 ml Coomassie solution is added. Samples were analyzed in duplicates and the mixtures were gently stirred and allowed to rest for 5 min prior to analysis with a Shimadzu UV-2401 PC UV-Vis spectrometer. The absorbance value at

595 nm is read and evaluated for the determination of the protein concentration under consideration of the Lambert-Beer law. The concentration of Influenza viruses can also be determined with this method since the viral membrane contains a high quantity of proteins.

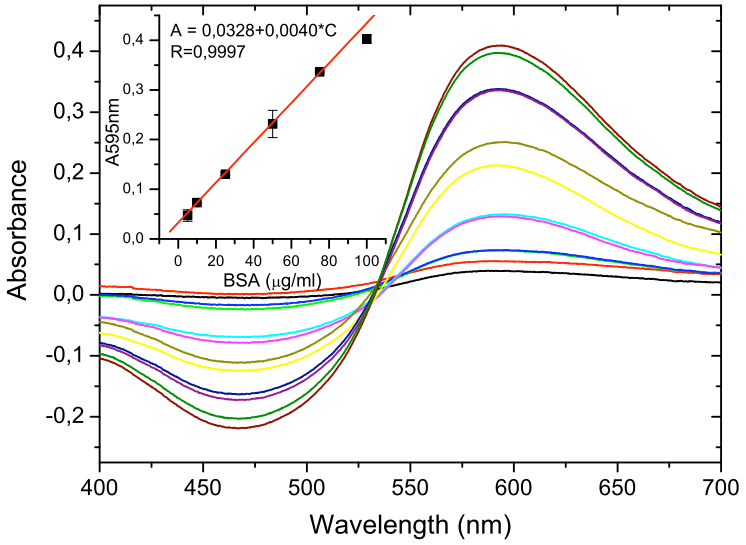

FIGURE 2.5: UV-Vis spectra and calibration curve of BSA (5-100 μg/ml) as obtained by the micro-Bradford method.

(c) **Sugar quantification**

The quantification of adsorbed sugar derivatives was performed according to the phenol-sulfuric acid method (Dubois et al., 1956). Sugars and related substances undergo a hydrolysis caused by H_2SO_4 and subsequently react with phenol to produce a color evolution detectable by means of a UV-Vis spectrometer. A 150 μl aliquot of a 5 % phenol solution was added to 196 μl of the solution containing the sugar derivative. Addition of 1.5 ml sulfuric acid (96 %) was followed. The mixture was heated up to 90 °C in a silicon bath for 5 min. Subsequently, the solution was cooled down in an ice bath and subjected to UV-Vis analysis where the absorbance at 483 nm was measured and the concentration was calculated applying the Lambert-Beer law. The baseline was recorded with a solution containing the same quantities of phenol and sulfuric acid and with water in stead of the sugar solution.

The calibration curve is shown in Figure 2.6. In the cases where sugar-based surfactants (SBS) were adsorbed on powdery samples, the supernatant was analyzed and the amount of adsorbed SBS was estimated by subtraction from the initial concentration. In cases where SBS were adsorbed on gold surfaces, the chips were immersed in the phenol/sulfuric acid solution and proceeded as described above. The adsorbed SBS were stripped off by the highly concentrated H_2SO_4 solution and available for reaction with phenol to provoke a color revelation.

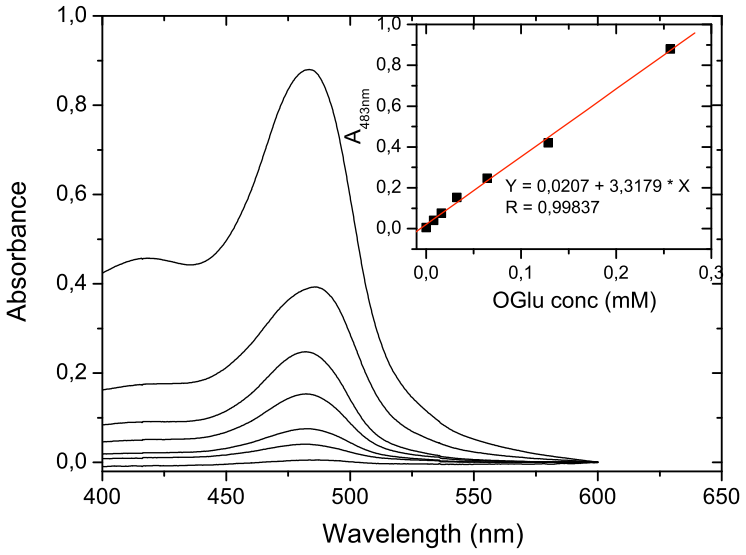

FIGURE 2.6: UV-Vis spectra and calibration curve of octyl-glucoside (0-0.26 mM) as obtained by the phenol-sulfuric acid method.

(d) **Hemagglutination test**

The hemagglutination test quantifies the capacity of HA or HA containing species to prevent red blood cells from sedimentation by forming a coagulated net of agglutinated erythrocytes. These results can be used for quantification of HA containing species or to evaluate the bioactivity of these compounds (Cox, 2002). In the hemagglutination test, red blood cells, extracted from chicken, were washed and diluted to a 0.5 % solution in PBS. The analyzed sample is dispensed as 50 μl aliquot in a 96-well microtiter plate and diluted stepwise from 1/2 to 1/4096 under the maintainance of the 50 μl volume. An aliquot of 50 μl red blood cell solution is added to

each well and allowed to rest on ice for 1 h. Thereafter, the plate is examined for sedimented red blood cells and the reciprocal of the dilution corresponding to this well (HA titer) provides a measure for the hemagglutination capacity of the sample, e.g. the higher the HA titer of the sample, the larger is the hemagglutination activity.

(e) **Viral neuraminidase activity assay**

The neuraminidase activity assay can be used to investigate the biological integrity and denaturation of viral particles containing neuraminidase (NA) in their membrane. In short, this assay is a colorimetric method where the NA activity is expressed as optical density (OD) at a wavelength of 549 nm. An aliquot of virus sample is mixed with fetuin and incubated at 37 °C overnight. Subsequently, periodate, arsenite, and thiobarbituric acid reagents are added and the mixture is placed in boiling water during 15 min allowing for the color development. In a next step, an aliquot of *Warrenoff* reagent is added and the mixture is centrifuged at 200 rpm for 10 min. The supernatant is analyzed with a photospectrometer at 549 nm. A detailed description of the procedure can be found in the protocols on animal Influenza diagnosis of the World Health Organization (Cox, 2002). This assay was carried out at the laboratory of Dr. G. del Real (INIA, Spain) and the used reagents were provided there.

(f) **Quantification of mycotoxins**

The adsorbed amount of toxin was estimated from the difference of the initial toxin concentration and the concentration in the supernatant. Toxin concentrations were determined under consideration of the Lambert-Beer law by means of a UV-Vis spectrometer using the absorbance values of AfB1 at 362 nm ($\epsilon = 18395$) and of DON at 217 nm ($\epsilon = 5052$). These values were derived from calibrations curves.

2.4.3 Enzyme Activity Assays and Preparation of an Urea Biosensor

(a) **Conditioning of electrodes**

Activity assays of immobilized urease and the preparation of an urea biosensor were accomplished with home-made polycrystalline gold disc electrodes. In both tasks, the electrode conditioning protocol was the same. Gold disc electrodes were polished with 1.0 μm diamond suspension (Bühler), rinsed with water and sonicated for 10 min in an ultrasound bath. The electrodes were subjected to electrochemical cleaning in 0.1 M NaOH solution with the potential held at -1.5 V for 1 min. Afterwards, the electrodes were activated in 0.1M H_2SO_4 with the potential kept at +2.0 V for 5 s and then at -0.35 V for 10 s, followed by 2 min of potential cycling between -0.2 and +1.5 V with a scan rate of 4.5 V/s. The electrodes were rinsed with water and immediately dipped into a 10 mM solution of 5,5'-dithiobis(2-nitrobenzoic acid) (DTNB) in ethanol. A DTNB monolayer was allowed to form on the gold surface within 3 h at room temperature. The DTNB modified electrodes were subjected to cyclic voltammetry (CV) in 50 mM PB (pH 7.0) at 0.05 V/s over the potential range of +0.1 to -0.8 to confirm the formation of a DTNB layer by the appearance of two cathodic peaks at -0.53 and -0.75 V (Casero et al., 1999). Holding the potential at -0.53 V for 3 s triggers the generation of a reversible, surface-confined redox couple with a formal potential of 0.035 V. This redox couple is pH dependent, resulting in a corresponding peak shift and thus, the DTNB modified gold electrode can be used as potentiometric sensor. The electrochemical redox reaction can be described as

$$(S - AR - NHOH)_2 - 4e^- - 4H^+ \rightleftharpoons (S - AR - NO)_2 \tag{2.1}$$

with AR as aromatic ring system. From this reaction equation the pH dependence of the redox couple becomes evident. Cyclic voltammetry of the DTNB modified gold electrode was performed at varying pH to estimate the pH sensitivity of the

electrode. The redox potential shifted linearly with pH at a rate of -0.059V/pH (Figure 2.7). This is exactly the Nernstian value as expected for electrochemical reactions where equal numbers of electrons and protons are involved (Eq. 2.1).

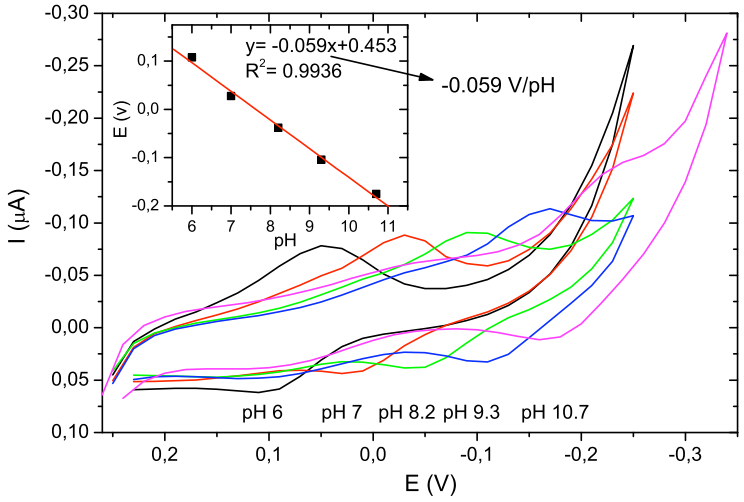

FIGURE 2.7: Cyclic voltammetry of DTNB modified Au electrode in pH range of 6 to 10.7 to confirm the pH sensitivity. The shift of the peak potential per unit pH coincides with the Nernstian value of 59 mV.

(b) **Enzyme activity assays using cyclic voltammetry**

Cyclic voltammetry is an electrochemical method used to study redox processes. Reverse linear potential sweeps at controlled scan rate are performed around the formal redox potential of a redox couple. This will oxidize and reduce the redox species and result in a measurable current which is manifested as anodic and cathodic peaks in the cyclic voltammogram.

In this work, DTNB was used as redox couple, being sensitive to pH changes caused by the catalytic activity of urease according to Eq. 2.2:

$$(NH_2)_2CO + H_2O \rightarrow 2NH_4^+ + HCO_3^- + OH^- \tag{2.2}$$

For measurement of urease activity, URE-biohybrids were deposited as film on a DTNB modified gold electrode surface. A 10 μl aliquot from a PVA suspension (0.5 wt.%) containing 1 wt.% URE-biohybrid was placed on the electrode surface

and allowed to dry at ambient temperature. Cyclic voltammetry was carried out with a minipotentiostat μSTAT 100 from DropSens® in 10 mM PB (pH 7.4) with a typical three electrode setup consisting of the surface modified gold electrode as working electrode, a platinum auxiliary electrode and a Ag/AgCl reference electrode (Figure 2.8A). The potential range was set to +0.2 and -0.3V with a scan rate of 50 mV/s. Prior to use, the electrodes were conditioned in PB solution for 30 min to ensure sufficiently well hydrated films. Urea aliquots were added from a 0.1 M standard stock solution that was prepared weekly and stored at 4 °C.

Activity of immobilized cholesterol oxidase (COx) was deduced from measuring hydrogen peroxide (H_2O_2) oxidation currents by cyclic voltammetry. The H_2O_2 occurrence is result of the enzymatic oxidation of added cholesterol aliquots according to Eq. 2.3:

$$cholesterol + O_2 \overset{COx}{\rightarrow} cholest - 4 - en - 3 - one + H_2O_2 \tag{2.3}$$

COx-biohybrids were directly suspended in a supporting electrolyte (50 mM PB at pH 7.5) at a concentration of 0.5 wt.%. The electrode setup comprised a Pt wire as working electrode, a Pt auxiliary electrode and a Ag/AgCl reference electrode (Figure 2.8B). Cholesterol stock solutions of 0.1 M in iso-propanol were prepared weekly and stored at -18 °C. Cholesterol working solutions of 0.25 mM were prepared prior to use by adding an aliquot of the cholesterol stock solution to PB (50 mM, pH 7.5) containing 1 wt.% Triton X-100 as cholesterol solubilizer. The addition happened under vigorous stirring and then slowly warmed up to 60 °C until the solution became clear. Aliquots of cholesterol working solution were added to the measurement suspension giving a final cholesterol concentration of 0-19 μM. CV measurements were conducted between 0 and +0.65 V with 50 mV/s and H_2O_2 was detected at +0.6 V.

(c) **Urea biosensor**

The preparation of an urea biosensor was based on the electrode protocols described

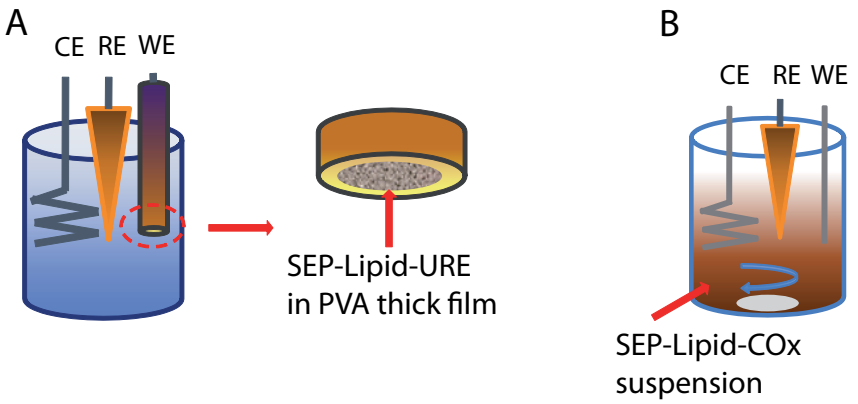

FIGURE 2.8: Schematics of the three electrode setups used in enzyme activity assays. In case of urease activity experiments the working electrode (WE) was modified with DTNB and the active phase was deposited on top of it (A). For the COx activity measurements, a platinum wire was used as working electrode in COx-biohybrid suspensions (B). In both setups, the counter electrode (CE) was a platinum wire and the reference electrode (RE) was Ag/AgCl.

in Sections 2.4.3(a) and (b). The biosensor characteristics were assessed with regard to response time, sensitivity, shelf-life time, and interferences with ascorbic acid.

2.4.4 Preparation and Measurements of Influenza Virus Biosensor

(a) **Preparation of biosensors for Influenza virus detection**

Virus biosensors were prepared on interdigitated polycrystalline gold electrodes with gold as counter and pseudo-reference electrodes (Figure 2.9). At the same time, gold chips were surface modified with the same procedure as for the electrodes. The chips served as 'easy to handle' model for the Au-electrodes and were subjected to different characterization methods such as measurement of dynamic contact angle, AFM, XPS, or colorimetric sugar quantification.

Gold electrodes and chips were subsequently rinsed with acetone, iso-propanol and ethanol to remove resin residues and greasy stains. A treatment with freshly prepared *piranha* solution (7:3 concentrated sulfuric acid to 35 % hydrogen peroxide solution) at 70 °C for 20 minutes followed to oxidize away any organic matter. The cleaned gold surfaces were immersed overnight (ca. 16 h) in 1 mM 1-octanethiol

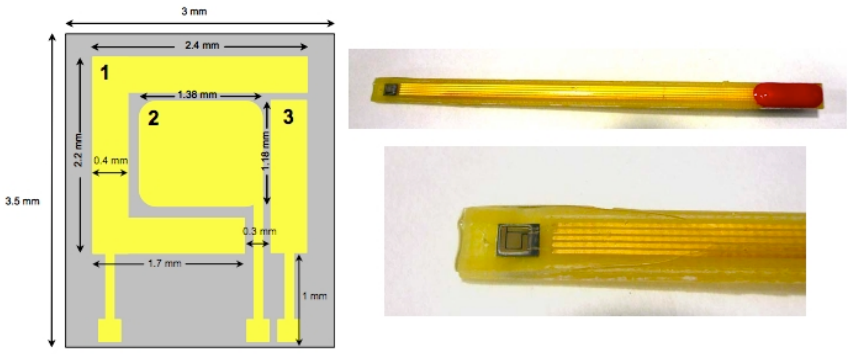

FIGURE 2.9: Interdigitated gold electrode used for virus sensing with 1) being the counter electrode, 2) being the working electrode, and 3) the pseudo-reference electrode. The electrodes and wires are imbedded in ebecryl resin. The images are courtesy of Dr. C. Fernández-Sánchez (CNM-IMB (CSIC), Spain).

solution in ethanol. The surfaces were rinsed with copious ethanol and contacted with aqueous octyl-glucoside (OGlu) solution at different concentration and varying incubation times. These optimization experiments were carried out with OGlu instead of octyl-galactoside (OGal) since it is much cheaper and available in larger quantities. However, under the optimized conditions, OGal was used to proceed with the incorporation of sialic acid which binds only to galactose residues. The adsorption was carried out by means of an α-2,6-sialyltransferase enzyme (SAT). 18 μl of α-2,6-SAT stock solution (160 μg/ml) were mixed with 180 μl of the substrate cytidine-5'-monophospho-N-acetylneuraminic acid sodium salt (CMP-sialic acid) (at 5 mg/ml) and 1080 μl PBS. The as-modified gold surfaces were kept in this solution for 4 h at 37 °C, subsequently rinsed with PBS and placed overnight in 2 % BSA solution to block any unspecific adsorption sites. Until usage, the sialylated electrodes were stored in PBS at 4 °C. The gold chips were employed for comparative Influenza virus detection using Western Blot assays (Kurien and Scofield, 2009).

(b) **Influenza virus detection using electrochemical impedance spectroscopy**

Virus detection was carried out by electrochemical impedance spectroscopy (EIS) with modified gold electrodes as described above (Section 2.4.4(a)). EIS spectra were recorded on a frequency response analyzer and the measurement electrolyte was composed of PBS (6.7 mM, pH 7.3) containing 0.5 M KNO_3 and 2 mM

$Fe(CN)_6^{3-}/Fe(CN)_6^{4-}$ as redox pair. The frequency range was set to 100 kHz - 1 Hz at the redox potential of -8 mV using a modulation amplitude of 10 mV. The as-prepared bioelectrodes were subjected to an EIS measurement in order to collect the blank values. Subsequently, the electrodes were incubated with virus containing aliquots obtained from a purified PR8/34 (H1N1) stock solution at 800 μg/ml. This H1N1 stock had been inactivated by exposure to UV light prior to the biosensing assays. Working solutions of different H1N1 concentrations were prepared on a daily basis and always kept at 4 °C. Drops of 50 μl were placed on the electrode and kept under humid atmosphere to prevent solvent evaporation. After 15 min the electrode was rinsed with PBS and submersed in the measurement electrolyte for EIS. Control measurements were conducted with the PRRS virus and the H5N9 Influenza virus which were kept in serum/BSA/PBS.

2.4.5 Cholesterol Bioreactor

The setup of the cholesterol bioreactor was according to a stirred batch reactor where the particulate biocatalyst is suspended in a buffer solution. The biocatalysts were composed of sepiolite-lipid hybrids supporting cholesterol oxidase (COx). The COx enzyme was immobilized from a 2000 μg/ml stock solution by contacting 3 mg support with 160 μg COx. After 2 h incubation at ambient temperature the solid was separated and washed with copious amounts of PB solution.

The enzymatic activity of COx-biocatalysts was determined from spectrophotometric experiments. Cholesterol working solutions of 0.5 mM in PB were prepared as described above. The biocatalyst (3 mg) was suspended in 2 ml PB and an aliquot of cholesterol working solution was added. The mixture was thermostated for 7 min at 25 °C in a water bath shaker. The solid was then separated by centrifugation and the supernatant was analyzed for the amount of enzymatically produced H_2O_2 using a Shimadzu UV-2401 PC UV-Vis spectrophotometer. Therefore, 1 ml of supernatant was mixed with 10 μl of 10 mM ABTS and 50 μl of 23 μM HRP and brought up to 2 ml with PB. After 2 min a UV-Vis spectrum was collected and the absorbance at 728 nm was measured. The

recyclability of biocatalysts was also evaluated. After each addition of 31 μM cholesterol, the activity assay was conducted as described above. The biocatalyst was separated and washed thoroughly in PB before starting a new catalysis cycle.

2.4.6 Mycotoxin Adsorption Study

Methanolic stock solutions of 500 μg AfB1/ml and 1200 μg DON/ml were prepared and aliquots diluted in bidistilled water. Adsorption isotherms of AfB1 on pristine and modified clays were obtained from 5 ml of 1 mg/ml sorbent dispersions and the addition of 4 - 100 μl of AfB1 stock solution aliquots. Deoxynivalenol adsorption was evaluated by a rapid screening method conducted as a single concentration sorption study. Dispersions of 0.375 mg/ml sorbent containing 5 μg/ml DON were prepared. Employed sorbent materials were MMT-24 wt.% PC and SEP modified with 11 and 23 wt.% PC and as reference materials Cloisite® 30B and SEP-12 wt.% CTA. All mixtures were agitated on a magnetic stirrer for 20 hours at ambient temperature and then centrifuged for 10 min at 8000 rpm. (Caution!: *Mycotoxins are extremely toxic compounds*)
For retention experiments of AfB1, one milligram of sample, previously loaded with AfB1, was suspended in 3 ml of an extraction solution of 60 methanol / 40 water (v/v) and in water. The mixtures were stirred for 3 hours at room temperature, centrifuged and the mycotoxin concentration of the supernatant was determined.

Chapter 3

Results and Discussion

3.1 Synthesis and Characterization of Lipid - Nanohybrids

Clay-lipid biohybrids are prepared by adsorption of phosphatidylcholine (PC) on the lamellar clay montmorillonite (MMT) and the microfibrous mineral sepiolite (SEP). The deposition of the lipid membranes is carried out from both organic and aqueous phase. The adsorption processes in these two media are based on different mechanism; in most organic media phospholipids are present as individually dissolved molecules while in aqueous phase lipids form micellar structures such as liposomes. Hence, the involved adsorption mechanism on the clay support in terms of solvent influence or adsorption efficiency are expected to be different. The investigation of the underlying mechanism, both from an experimental and a mechanistic perspective are the prime subject of this Chapter.

A further point under investigation are the interfacial properties of different sepiolite supported lipid membranes. Therefore, membranes of diverse structure and composition have been prepared, e.g. lipid mono- and bilayers and mixed lipid/sugar-based surfactant layers. These interfaces find further application as biomimetic supports for the immobilization of enzymes (Section 3.2) or viral compounds (Section 3.3).

Biohybrids based on layered double hydroxides (LDHs) represent another versatile and promising approach toward biocompatible materials (Darder et al., 2005a). In this Section, Mg/Al type LDHs were prepared with lipid interfaces by a novel co-precipitation route. These materials are employed in the stabilization and vectorial administration of Influenza viruses as well as its membrane protein hemagglutinin with the aim to develop new, improved vaccine adjuvants (Section 3.3). The choice of the Mg/Al type of LDHs to prepare PC based biohybrids is accounted for comparative purposes to the SEP-PC system and because of their structural similarity to commercial aluminum hydroxides that are widely used as vaccine adjuvants.

3.1.1 Clay-Lipid Interactions

Lipid adsorption processes are investigated by sampling adsorption isotherms from methanol, ethanol and aqueous media. Further investigation comprises the study of the surface potential of the hybrids in the course of lipid adsorption, performing thermal analysis (TA) for the confirmation of preferential phosphatidylcholine (PC) adsorption, and recording X-ray diffraction (XRD) pattern in case of montmorillonite to ascertain PC intercalation. Spectroscopic methods are applied to investigate clay-lipid interactions.

3.1.1.1 Sepiolite-Lipid Adsorption Mechanism

- Lipid Adsorption from Organic Phase

Sepiolite-lipid biohybrids are prepared by PC adsorption from ethanol using the 60 % (TLC) batch. Preliminary experiments using methanol as solvent yielded lower adsorption quantities and indicated incomplete lipid bilayer formation. The corresponding adsorption isotherm and a brief discussion of these findings are provided in Appendix A. Thermal analysis (Figure A.2 in Appendix A) of the resultant sepiolite-lipid hybrids from ethanol confirmed the preferential adsorption of L-α-phosphatidylcholine over the other present species in this lipid batch, e.g. cholesterol, proteins, and other phospholipid classes. The obtained materials are henceforth denominated as SEP-PC.

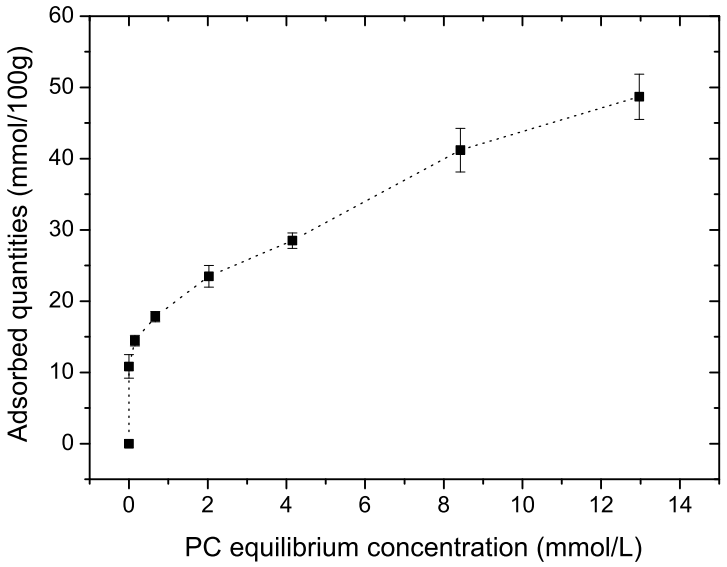

FIGURE 3.1: PC adsorption isotherm from ethanol on sepiolite. Adsorption took place at 25 °C for 24 hours. The dotted line serves to guide the viewer's eye.

A PC adsorption isotherm from ethanol was sampled at 25 °C (Figure 3.1). Adsorption is expected to take place only at the external surface of sepiolite since the diameter of a PC molecule is about 0.9 nm whereas the smallest dimension of a sepiolite tunnel is 0.4 nm (Ruiz-Hitzky, 2001). Therefore, the possibility of lipid penetration into the tunnel system can be ruled out. The isotherm reveals a first plateau at about 25 mmol/100g and a second at 50 mmol/100g. Inflection points in isotherms are known to correspond to the formation of a saturated adsorption layer (Giles et al., 1960). Therefore, the observed plateaus can be attributed to the formation of a monolayer and a bilayer of PC molecules. Moreover, the determined PC quantity at the upper plateau is exactly the double of the first plateau. This emphasizes that the molecular packing density in both layers is equal. The packing density can be calculated from the molecular lipid cross-section area (0.72 nm^2 (Small, 1967)) and the specific external surface area of sepiolite (165 m^2/g). The resulting value is estimated to 0.92 lipid molecules per nm^2. This packing density is however somewhat lower than in PC liposomes or in supported bilayer lipid membranes (sBLM) on planar and smooth surfaces, being 1.39 lipids per nm^2 (Zimmermann et al., 2009). The reduced packing density might be ascribed to the micro-roughness of the sepiolite fibers owing

the channels and crystalline steps (Figure 1.2), which impede the same layer regularity as on smooth surfaces. Alternatively, an effect of the regular disposition of silanol groups as possible preferential center for interaction could be involved.

In fact, the adsorption curve could not be fitted to any of the common isotherm models such as Langmuir, Freundlich, or Dubinin. The reason for that might lie in the characteristics of the sepiolite fiber. Sepiolite contains various possible adsorption sites like microcavities, coordinated water molecules, silanol groups, and exchangeable cations (Ruiz-Hitzky, 2001). Additionally, a cooperative adsorption mechanism is expected for lipid molecules which interact strongly *via* van der Waals attraction between fatty acid chains of adjacent molecules. A lot of these characteristics are essentially neglected in many isotherms models such as for instance the Langmuir model.

For the use in subsequent studies, the sepiolite biohybrids with 25 and 50 mmol/100g PC are taken as model systems for the supported lipid monolayer and lipid bilayer. The corresponding materials are henceforth denominated as SEP-ML-PC and SEP-BL-PC.

- Lipid Adsorption from Aqueous Phase

Lipids are practically insoluble in water. However, lipids show colloidal stability in aqueous media when prepared as liposomes and can thus easily be solubilized. Prior to adsorption on sepiolite vesicle size and ζ-potential of PC liposomes (from the 92 % batch) had been characterized by dynamic light scattering which provides information about particle size and surface potential. In many adsorption processes on clays participate electrostatic and ionic interactions (Ruiz-Hitzky and Van Meerbeeck, 2006). Therefore, it is of great importance to know the surface charge of an adsorbate at a given solution pH. The surface charge of extruded liposomes is approximated as ζ-potential which is the electric potential measured at the shear plan of a diffusing particle (Pugh and Bergström, 1994). The ζ-potential value as function of the solution pH is shown in Figure 3.2. As expected for zwitterionic compounds, the ζ-potential was found to be close to zero. Only at the borders of the studied pH range, the ζ-potential slightly deviated from zero. This can be explained with the acid-base behavior of the two ionic groups of the PC head

group. The pK values of choline (-$N^+(CH_3)_3$) and phosphatidyl (-OPO_3^-) groups are ≈9 and ≈3, respectively (Abramson et al., 1964). Hence, the phosphatidylcholine headgroup is neutral over the pH range from 3 to 9. However, toward theses boundary limits, H^+ or OH^- adsorption is gradually increasing with the effect of turning PC slightly positive or negative.

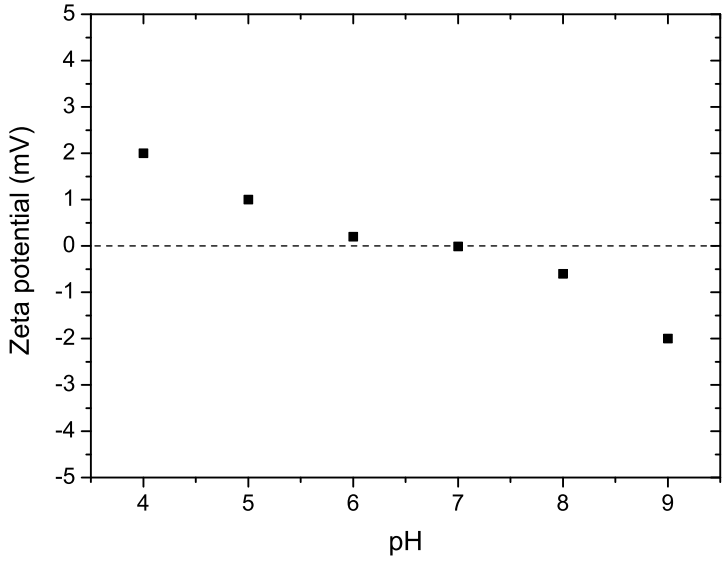

FIGURE 3.2: The ζ-potential value of a 0.5 mM liposome solution as function of the pH. The ionic strength of each measurement solution was kept constant at 10 mM NaCl and the pH was adjusted with HCl and NaOH.

The liposomes prepared by extrusion through 100 nm polycarbonate membranes showed a narrow size distribution (polydispersity index of 0.083) centered around 128±2 nm as the hydrodynamic diameter (Figure A.3 in Appendix A). This value corresponds to the typical diameter of large unilamellar vesicles (LUV) (Hope et al., 1985; Mayer et al., 1986).

The incubation time for LUV adsorption on sepiolite was fixed to 16 h which has been shown to be sufficient for the establishment of an adsorption equilibrium on silica (Rapuano and Carmona-Ribeiro, 1997). Liposome adsorption was carried out at the natural pH (8.0) of the sepiolite suspension in the presence of 5 mM NaCl in order to keep the ionic strength constant at the different liposome concentrations.

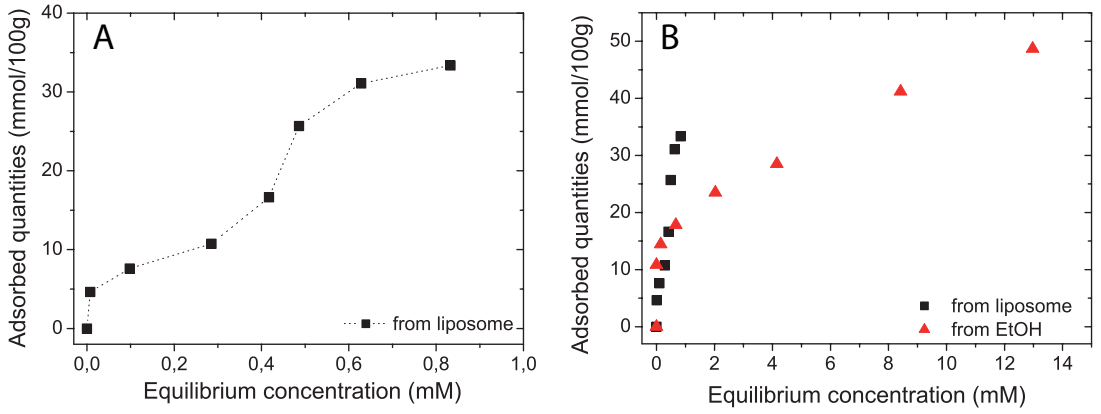

FIGURE 3.3: PC adsorption isotherms on sepiolite prepared from aqueous liposome solution (A) and compared with the adsorption isotherm obtained from ethanol solution (B).

Solutions of extruded liposomes at varying PC concentration were contacted with sepiolite and the corresponding adsorption isotherm is presented in Figure 3.3A. Two adsorption plateaus at 15 and 35 mmol/100g can be observed which are attributed to a mono- and bilayer formation of the PC molecules. Comparing the adsorption quantities, it is obvious that more PC is adsorbed from ethanol solution. There are several possible explanations. It has been shown that ethanol molecules can enter into the tunnel system of sepiolite (Serna and Vanscoyoc, 1978). Such small organic molecules can easily remain entrapped due to blocking of the entrances by subsequently adsorbed larger molecules (Ruiz-Hitzky, 2001; Kuang et al., 2003). The entrapped ethanol (by adsorbing PC molecules in this case) would contribute then to the total carbon content as determined by elemental analysis and hence, result in an overestimated PC content. It is difficult to proof this possibility experimentally since ethanol would not be distinguished from PC for instance by infrared spectroscopy. However, rough estimations based on TA results suggest that ethanol penetration would not sum up to the observed difference of 15 mmol/100g. Therefore, another explanation might be considered which is based on different adsorption mechanism due to different electrostatic interactions. In aqueous media, the ion-exchange capacity of sepiolite is likely to dominate stronger during the first stage of PC adsorption as compared to adsorption from ethanol solution, where ion-exchange processes are less likely expected to occur. The cation exchange capacity (CEC) of sepiolite is 15 mequiv/100g which exactly matches the measured 15 mmol of adsorbed PC per 100 g sepiolite at the first isotherm

plateau. This can be an indication that the initial stage of liposome adsorption is governed by a cation exchange mechanism.

Further comparison of the two adsorption isotherms makes evident that bilayer formation by liposome adsorption requires significantly lower equilibrium concentrations (Figure 3.3B). The principle difference is that in aqueous media PC adsorbs as aggregates while in ethanol single PC molecules associate to the sepiolite surface (Figure 3.4). Liposome adsorption on solid interfaces can be described as multistage process including i) first contact ii) liposome deformation iii) liposome rupture and iv) lateral lipid molecule diffusion for complete surface coverage (Richter et al., 2006; Anderson et al., 2009). This mechanism is believed to make bilayer deposition more efficient than molecular self-assembly.

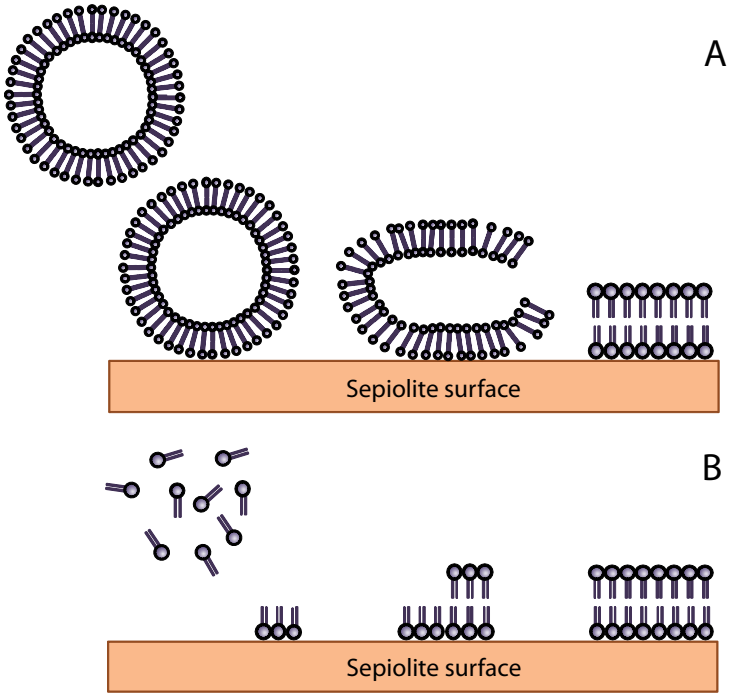

FIGURE 3.4: Scheme of PC adsorption on sepiolite from aqueous by liposome deposition (A) and from ethanol phase by molecular self-assembly (B).

Rapuno and Carmona-Ribeiro have assumed that the surface density of Si-OH groups is crucial for successful liposome rupture and lipid bilayer formation on silica particles (Rapuano and Carmona-Ribeiro, 1997). Tris(hydroxymethyl)aminomethane (Tris) adsorption on silica has been found to increase the -OH density sufficiently to afford bilayer stabilization. In contrast to these results, PC bilayers could be stabilized on the sepiolite

surface without additives. The reason is assumed to be related to the high surface density of silanol groups on sepiolite (0.35 nm nearest distance between adjacent Si-OH (Ruiz-Hitzky, 1974)) as well as the multiple other possible adsorption sites such as coordinated water molecules, cation exchange sites, or microcavities (Ruiz-Hitzky, 2001).

Another dissimilarity in organic and aqueous media are the electrostatic interactions applying to the adsorption process. These interactions are generally diminished by the lower dielectric constant of organic solvents and could therefore influence the affinity between an adsorbate and a substrate. In the present case of ethanol, this reduction is however not expected to be dramatic since ethanol has a moderate dielectric constant of $\epsilon = 25.3$ for an organic solvent. This should allow electrostatic interaction between the ionic lipid headgroups and the different adsorption sites on the sepiolite surface. However, more importantly, surface confined water molecules are always present on sepiolite even though adsorption takes place in organic solvent. These physisorbed water molecules have been found crucial in adsorption of lipid molecules on silica/silicate surfaces for the formation of stable bilayer lipid membranes (Radler et al., 1995; Cremer and Boxer, 1999).

An important issue in the preparation of sBLM on particulate materials in contrast to planar surfaces is the size and curvature of the substrate (Bayerl, 2004; Bayerl and Bloom, 1990; Naumann et al., 1992). In the present case, the diameter of the sepiolite microfibers is in the range of 100 nm. It has been shown that high curvatures of nanometric silica beads inflict certain restrictions on bilayer spreading from liposomes related to reduced contact area and distorted lipid molecule packing (Cremer and Boxer, 1999; Ahmed and Wunder, 2009). However, this effect has been only marginal when approaching particle sizes of > 100 nm (Ahmed and Wunder, 2009). Thus, it can be assumed that curvature induced impediments should not arise in the present case of sepiolite.

- Molecular Interactions of Sepiolite-Lipid Biohybrids

The molecular interaction between PC and the sepiolite surface was further investigated by NMR and FT-IR spectroscopy. A special focus was laid on the functional silanol

groups, which represent one of the principal adsorption sites on sepiolite (Kuang et al., 2003). Figure 3.5A shows the ^{29}Si CP/MAS NMR spectra of the starting sepiolite. The three characteristic Q^3 signals at -92.3, -94.7 and -98.3 ppm are assigned to the near-edge, center and edge crystallographic positions of Si atoms in sepiolite. The low intensity signal at -85.2 ppm has been attributed to the Q^2(Si-OH) group, situated at the edges and ends of the sepiolite channels (Barron and Frost, 1985; Sanz, 1990). Upon PC adsorption, this signal diminishes in intensity and being almost hidden on the background (Figure 3.5A). This is indicative for interaction of the silanol group with polar species (Kuang et al., 2003).

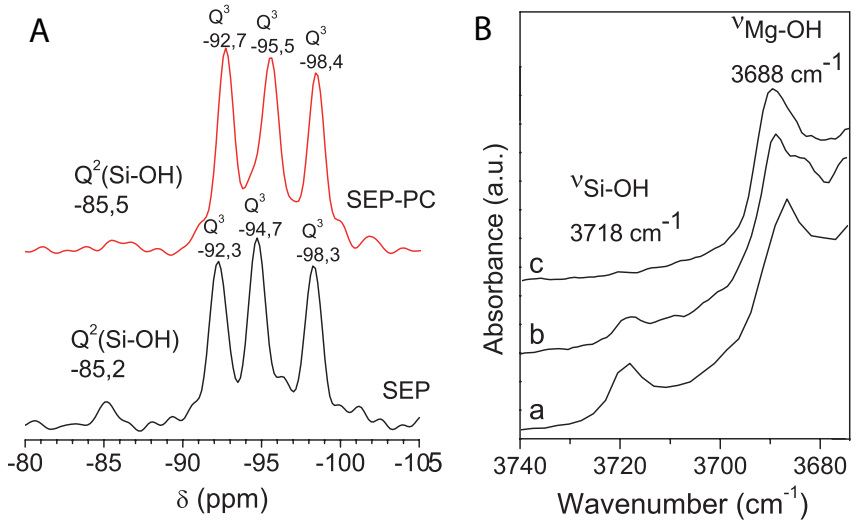

FIGURE 3.5: ^{29}Si CP/MAS NMR (A) and FT-IR (B) of neat sepiolite (SEP) and sepiolite-lipid hybrids (SEP-PC). The wavenumber range of the OH stretching vibrations of Si-OH and Mg-OH is depict in (B) with (a): neat sepiolite; (b): 7 mmol /100 g; (c) 16 mmol /100 g lipid content in the biohybrid. All samples were prepared by PC adsorption from ethanol. The FT-IR spectra were recorded from self-standing films.

These findings are also supported by IR spectroscopy. Stretching vibrations of structural hydroxyl groups are depicted in Figure 3.5B which were obtained from pure sample for avoidance of interaction with KBr. The band at 3718 cm^{-1} is assigned to the OH stretching vibration υ_{Si-OH} of the silanol group in natural sepiolite (Nagata et al., 1974; Ahlrichs et al., 1975). This band is shifted toward lower frequencies with increasing PC content and eventually disappears due to overlapping of adjacent bands. This observation is ascribed to the strong interaction of the freely accessible silanol groups with the polar headgroup of adsorbing phospholipids. Similar electrostatic interactions of the Si-OH

groups have also been observed in other systems (Ruiz-Hitzky, 2001; Aranda et al., 2008). The band at 3688 cm^{-1} corresponds to the stretching vibration of magnesium hydroxyl groups (Ruiz-Hitzky, 2001). It remains unaltered in the course of PC adsorption since Mg-OH groups are located inside the sepiolite structure and hence, inaccessible for the lipid molecules.

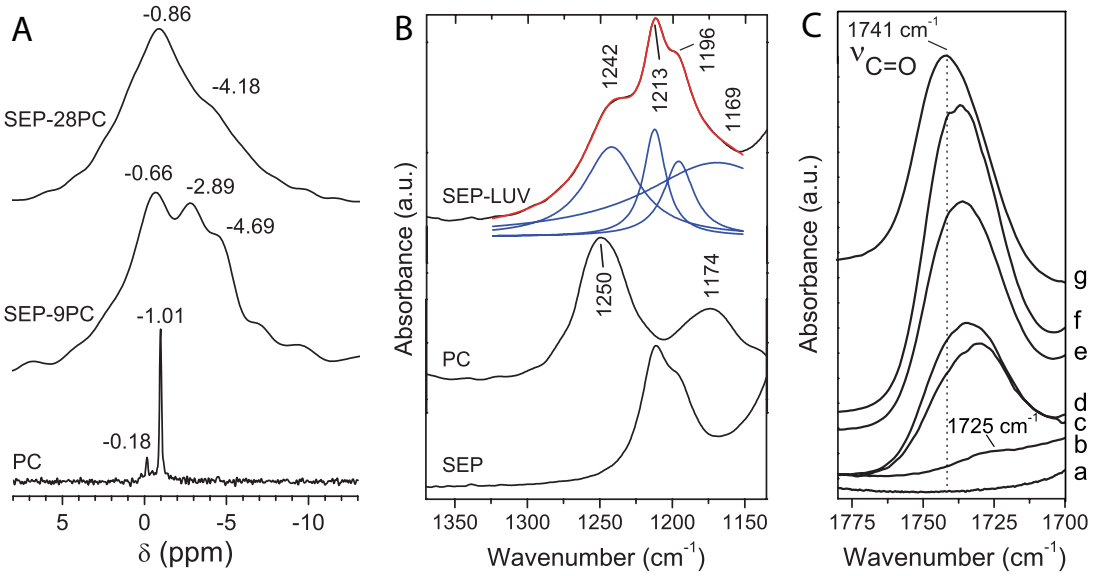

FIGURE 3.6: Proton non-decoupled ^{31}P MAS NMR (A) of phospholipid (60 % TLC) and sepiolite-lipid biohybrids containing 9 and 28 mmol PC per 100 g sepiolite, respectively. The reference of phospholipid was obtained from a 10 mM ethanol solution and the peak at -0,18 ppm is associated with impurities. The FT-IR spectra (B) show the phosphatidyl (P=O) and ester (C-O-C) region of a SEP-LUV hybrid (33 mmol PC per 100 g sepiolite). Neat sepiolite and PC (92 % batch) are included for comparison. The peak fitting was performed with Lorentz distribution. The FT-IR spectra (C) shows the C=O band of PC in (a): neat sepiolite; (b): 7; (c) 17; (d): 25; (e): 34; (f): 40 mmol/100 g lipid content and (g): PC of 60 %TLC purity. The samples were prepared from EtOH solution and the spectra were recorded of cast, self-standing SEP-PC films.

Spectroscopic changes of specific PC headgroup moieties in the course of adsorption are also investigated. The proton non-decoupled ^{31}P MAS NMR spectrum of SEP-9PC (Figure 3.6A) shows a signal at -2.89 ppm that could be related to phospholipid molecules which are in electrostatic interaction with a siliceous surface (Snyder and Madura, 2008; Murray et al., 2005). Based on ^{1}H and ^{2}D NMR data, Chunbo and co-workers reported hydrogen bonding between the phosphate headgroup moiety and silanol groups as interaction mechanism for adsorption of dipalmitylphosphatidylcholine on silica (Chunbo et al.,

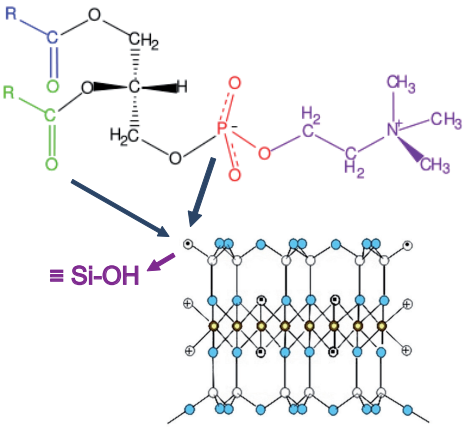

FIGURE 3.7: Scheme of proposed interaction mechanism between the headgroup of PC molecules and the Si-OH group of sepiolite.

1995). Additional evidence for the involvement of the phosphatidyl group in H-bonding is also concluded from IR spectroscopy using the matrix-free methodology of the ATR setup (Figure 3.6B) which allows for the detection of the relatively weak asymmetric phosphate stretching vibration $\upsilon_{P=O}$. The position of $\upsilon_{P=O}$ is shifted from 1250 cm^{-1} in neat PC to 1242 cm^{-1} for the sepiolite-lipid hybrid, being also a sign for H-bonding (Tsai et al., 1987).

Furthermore, there is indication that the glycerol ester group also participates in hydrogen bonding with the sepiolite surface. Figures 3.6B and C show the stretching vibrations of the carbonyl $\upsilon_{C=O}$ and ester group υ_{C-O-C}. The positions of $\upsilon_{C=O}$ and υ_{C-O-C} are shifted from 1741 cm^{-1} and 1174 cm^{-1} in neat PC to 1725 cm^{-1} and 1169 cm^{-1}, respectively, for the sepiolite-lipid biohybrid. A red shift of the carbonyl band is generally attributed to hydrogen bonding (Korn and Killmann, 1980). Hence, the spectroscopic examinations strongly suggest hydrogen bonding both of the ester and the phosphatidyl group with the silanol groups of the sepiolite fibers.

Examination of the structural formula of phosphatidylcholine reveals that C=O are part of the ester groups which connect the hydrocarbon chains to the glycerol backbone (Figure 3.7). Hence, the C=O groups would be rather far away from the mineral surface. However, it is well-known that the axis of the PC head group is oriented in a perpendicular fashion to the principal axis of the lipid molecule (Seelig, 1978). Consequently, the carbonyl

groups are situated near the kink which brings the C=O groups in closer vicinity to the sepiolite surface. The scheme in Figure 3.7 illustrates the interaction of the different involved groups.

- Lipid Assembly in Sepiolite-Biohybrids

Molecular assembly and structure of the phospholipid layers on the sepiolite surface was investigated by water contact angle measurements, ^{31}P MAS NMR, and IR spectroscopy. Contact angle measurements were conducted to follow the change of surface hydrophilicity upon PC adsorption from EtOH (Figure 3.8). Until the first plateau of the adsorption isotherm, the contact angle increases slightly, whereas during the subsequent slope the contact angle decreases. The rise of the water contact angle can be related to increased hydrophobicity of the sepiolite fibers. This is the case for a lipid monolayer coverage with the hydrocarbon chains oriented bottom-up. With beginning bilayer formation gradually more polar headgroups are exposed at the air interface of the upper membrane leaflet and hence, the hydrophilicity increases.

Additional evidence for controlled lipid mono- and bilayer formation on sepiolite is provided by solid state ^{31}P MAS NMR. This technique became a powerful and well-established

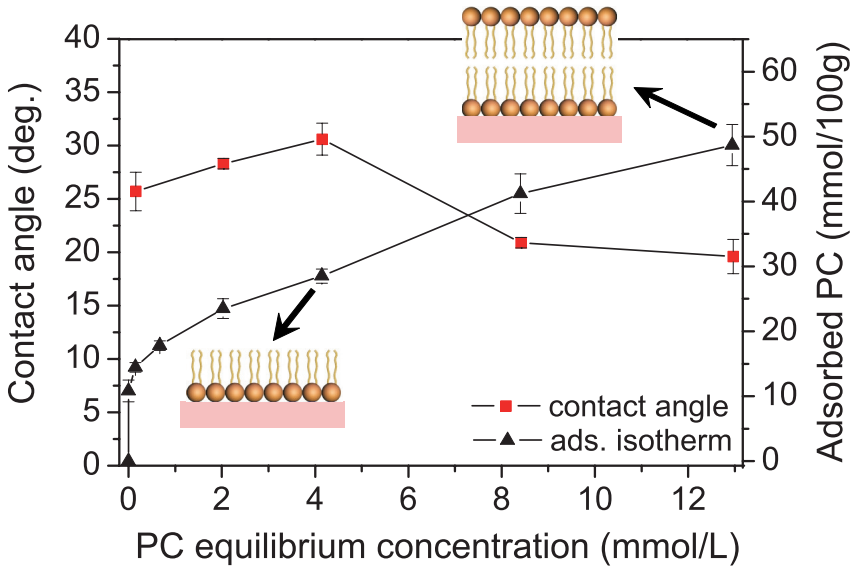

FIGURE 3.8: Water contact angles on cast SEP-PC films are plotted together with the corresponding adsorption isotherm of PC on sepiolite obtained in ethanol.

tool to study lipid-lipid and lipid-substrate interaction and furthermore, the line shape is characteristic for different lipid assemblies (Seelig, 1978; Auger, 1997). The two samples under investigation are SEP-9PC, corresponding to a PC submonolayer and SEP-28PC, at the beginning of PC bilayer formation according to the adsorption isotherm (Figure 3.1). Proton non-decoupled ^{31}P MAS NMR spectra of these two samples and the reference spectra of phospholipid dissolved in ethanol have already been displayed in Figure 3.6A and is now subjected to a closer inspection. A sharp, isotropic signal at -1.01 ppm is obtained from dissolved phospholipid. This signal is shifted and broadened in the SEP-9PC sample, attributed to i) proton-phosphorous dipolar interaction and ii) chemical shift anisotropy of the phosphorous nuclei (Seelig, 1978). These contributions are averaged out by diffusion of the lipid molecules in the case of dissolved PC and thus, yielding the observed isotropic peak (Seelig, 1978). The spectrum of SEP-28PC displays a maximum at -0.86 ppm and a shoulder at -4.18 ppm. The shape of this spectrum is indicative for lamellar lipid phases (Seelig, 1978) and hence, it is in accordance with the conclusions retrieved from the adsorption isotherm (Figure 3.1).

Further information on the lipid layer formation can be retrieved from the evolution of the carbonyl IR band in Figure 3.6C. At low PC content, $\upsilon_{C=O}$ experienced a maximum red shift of 16 cm^{-1} (spectrum b). In subsequent spectra of samples with increased PC content, this band is shifted back toward the vibration frequency of neat PC (1741 cm^{-1}). A possible interpretation could be as follows: At low PC content all lipid molecules are in close contact with the sepiolite surface. Interaction with the adsorption sites causes a significant shift of the $\upsilon_{C=O}$ band. As the adsorbed lipid amount is increased, the additionally assembled molecules are not anymore in direct interaction with the adsorption centers since they are already occupied. The molecules of the upper membrane leaflet are then adsorb *via* intermolecular interactions, namely van der Waals forces. Consequently, these carbonyl groups are less perturbed and the recorded carbonyl band of these hybrids is the overall spectrum of all present carbonyl groups.

3.1.1.2 Montmorillonite-Lipid Intercalation Mechanism

- Lipid Adsorption from Organic Solvent

Methanol (MeOH) was used as organic solvent for the adsorption of phospholipid (60 % TLC) on Na^+-montmorillonite. Ethanol (EtOH) was also tested, but resulted in incomplete lipid bilayer formation. A brief discussion on this observation can be found in (Appendix A). Like in case of sepiolite, thermal analysis confirmed preferential adsorption of L-α-phosphatidylcholine (Figure A.5 in Appendix A) and the obtained materials are henceforth denominated as MMT-PC. An adsorption isotherm of PC from MeOH was sampled at 25 °C and is presented in Figure 3.9. It was found that the isotherm could be

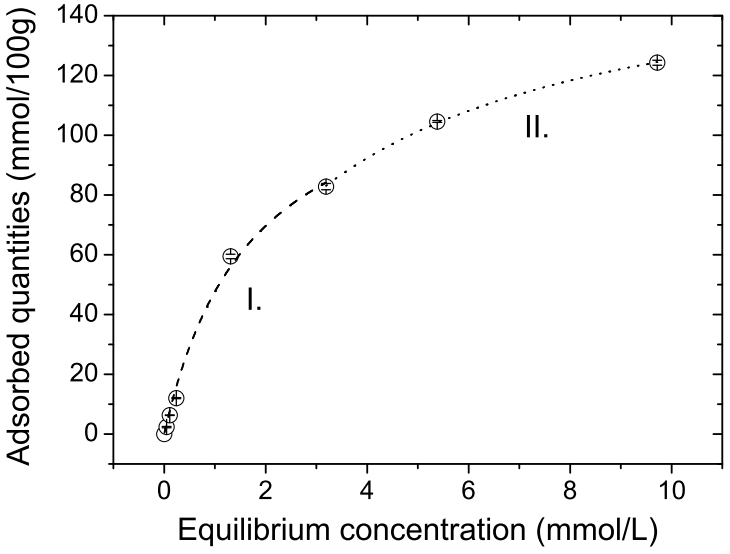

FIGURE 3.9: Adsorption isotherm from methanol of phospholipid on Na^+-montmorillonite. The dashed and dotted lines represent the Langmuir fitting curves. Adsorption took place at 25 °C for 24 hours under agitation of a magnetic stirrer.

fitted more adequately in two separate regions than with one overall fit. The best fitting was obtained for the L type (Langmuir) of adsorption isotherms (Giles et al., 1960),

$$\Gamma = \frac{bx_m C_s}{1 + bC_s} \tag{3.1}$$

region	x_m (mmol $100g^{-1}$)	b (L $mmol^{-1}$)	ΔG_{ads} (kJ mol^{-1})	R^2
I.	130	0.58	-52.0	0.9938
II.	164	0.32	-49.0	0.9995

TABLE 3.1: Langmuir fitting parameters of the PC adsorption isotherm on Na^+-MMT and Gibbs free energy of adsorption.

where Γ is the adsorbed amount of lipid, b the affinity constant between lipid and clay interaction sites, x_m the maximum adsorbed amount, and C_s the equilibrium lipid concentration. For ionic species the affinity constant can be related to the Gibbs free adsorption energy ΔG_{ads} through the relation $K=(b\rho/4)^2$ where ρ is the ratio of the solvent density to its molecular weight, $\rho \approx 247\,\text{mol L}^{-1}$ (Miller et al., 2002)

$$\Delta G_{ads} = -RTlnK \tag{3.2}$$

where R is the gas constant and T is the adsorption temperature. The calculated data are presented in Table 3.1.

The Gibbs free energy of adsorption could be calculated to -52.0 kJ mol^{-1} from fitting of region I. This value is comparable to results obtained by microcalometry for the intercalation of crown-ether macrocyclic compounds in homoionic montmorillonite which are known to form very stable coordination compounds with the intracrystalline alkaline cations (Aranda et al., 1994). Hence, the calculated value in the present work is indicative for strong adsorption and high affinity of phosphatidylcholine toward the mineral surface, although the mechanism of interaction must be different in the MMT-PC system as pointed out further below. Fitting of region II renders a maximum adsorption capacity x_m of 164 mmol/100 g. This value agrees with the adsorption plateau of didodecyldimethylammonium vesicles on Na^+-montmorillonite as reported by Undabeytia and co-workers (Undabeytia et al., 2003). The adsorption quantity of 164 mmol/100 g corresponds to a molecular cross-section area of 0.71 nm^2 for the adsorbed PC molecules (specific surface area of Na^+-MMT: 700 m^2/g) that is in excellent agreement with reported values of PC in supported bilayers (0.72 nm^2) (Small, 1967; Zimmermann et al., 2009). In contrast, the packing density of the PC layer on sepiolite is about a half as compared MMT. A reason could be that the MMT platelets afford a rather large (several

hundred nm^2) and atomically smooth surface while the sepiolite fibers display microroughness and crystalline steps. In a consequence, lipid self-assembly and layer growth proceed on MMT with little disorganization, and is hence similar to supported lipid bilayer membranes prepared on the surface of macroscopic substrates such as mica or glass sheets (Jurak and Chibowski, 2007). In fact, the surface of a montmorillonite platelet shows a similar crystallographic structure as the mica surface composed of hexagonally aligned SiO_4 tetrahedra (Brigatti et al., 2006).

The fact that the isotherm is best fitted in two different regions might suggest two distinct adsorption mechanism. The transition between region I and II is observed at about 80 mmol/100 g while the CEC of Wyoming montmorillonite is 76 meq/100 g (furnisher specifications). This accordance might point toward a sodium cation exchange as principal adsorption mechanism in region I. This assumption is supported by semi-quantitative EDX analysis of the sodium content of MMT-PC from region I (Figure 3.10). The sodium to silicon ratio (in at.%) indicates a depleation of sodium ions in the intracrystalline space while at the same time the PC content increases.

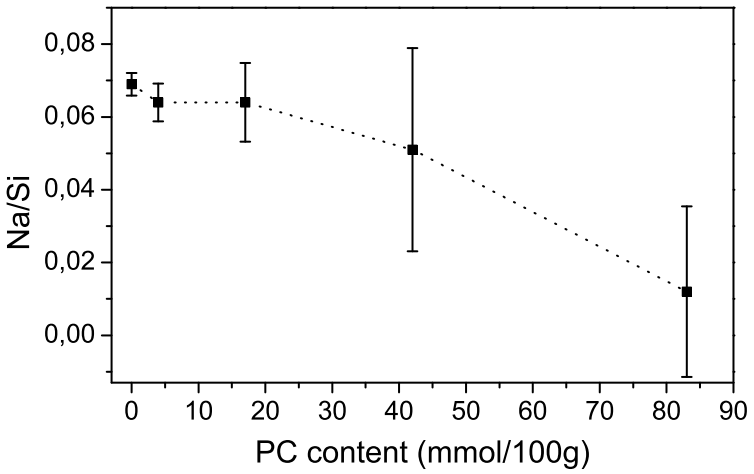

FIGURE 3.10: Sodium to silicon ratios in at.% as function of PC content in mmol/100 g of the biohybrid material. These data were obtained from EDX/FE-SEM measurements where the conditions were held constant in order to compare the results within a series of samples (working distance: 6.3 mm, spot size: 2.5, landing energy: 6.0 keV, accumulation time: 100 s). The dotted line is to guide the viewer's eye.

In region II are additional adsorption mechanism expected as Na^+ is already greatly depleted. At the end of region I the surface of montmorillonite is assumed to be relative hydrophobic owing to the presence of PC hydrocarbon chains. This will lead to enhanced hydrophobic interaction between the lipid tails and consequently, give rise to a cooperative adsorption mechanism. This mechanism is also typical for adsorption of conventional alkylammonium cations on smectite clays (Ruiz-Hitzky et al., 2004).

There remains the question how zwitterionic lipid molecules can participate in an exchange process with sodium cations. It is known that highly polarized water molecules are present in the intracrystalline space of montmorillonite (Fripiat et al., 1971). A mechanism could then be based on the uptake of protons originating from these polarized, acidic water molecules by the anionic phosphate group rendering PC molecules cationic. In this respect, it has been discussed by Petelska and co-workers that the cationic form of PC dominates when hydrogen ions are in excess (Petelska and Figaszewski, 2000). Hence, it seems reasonable to propose that cationic PC molecules in the specific environment of Na^+-MMT may well participate in a cation exchange mechanism. Similar zwitterion sorption mechanism with accompanied proton uptake have been reported for the intercalation of organic species such as antibiotics (Figueroa et al., 2004).

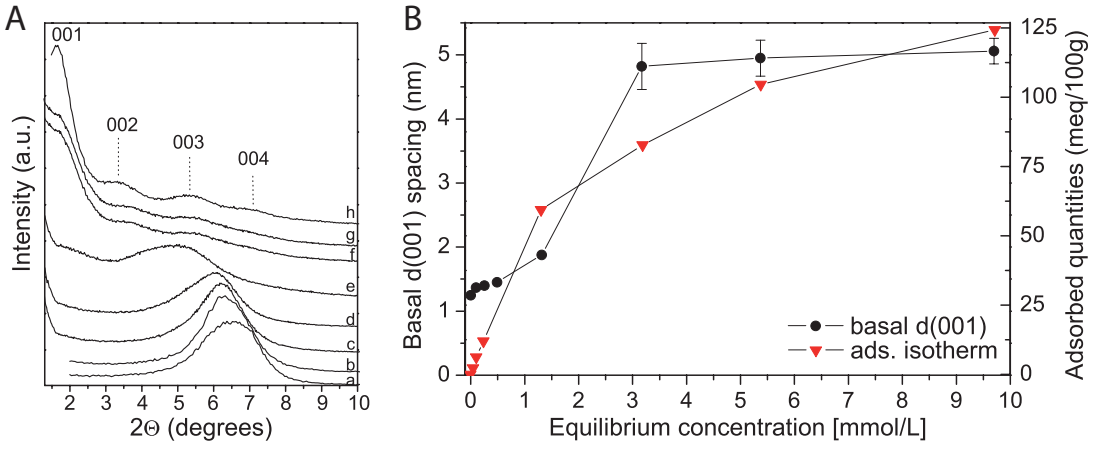

FIGURE 3.11: (A) XRD patterns of MMT-PC biohybrids obtained from methanol with increasing amounts of adsorbed phospholipid, given in mmol/100g, with (a): 2; (b): 6; (c): 12; (d): 18; (e): 59; (f): 84; (g): 105; (h): 125. (B) The basal d_{001} spacing is plotted with the corresponding adsorption isotherm from methanol. The d_{001} values of the last three samples were calculated from the average over the higher reflections.

The intercalation of PC into montmorillonite is investigated by powder X-ray diffraction (XRD). Figure 3.11A shows the XRD pattern of MMT-PC. Pattern h in this Figure, corresponding to the MMT-125PC sample, shows four reflections at 1.65, 3.47, 5.32, and 7.06 °. Taking into account the silicate layer thickness of 0.96 nm (Aranda et al., 1994), an interlayer distance of 4.2 ± 0.2 nm is estimated over an average of these four reflections. This is a common method in order to decrease measurement errors often associated with low angle reflections of intercalated molecules (Brown and Brindley, 1980). The obtained value is slightly lower than the 4.6 nm thickness of a lipid bilayer calculated with $1.64 + 0.17\,n$ (Karlovska et al., 2006), where n is the average number of carbon atoms in the acyl chains of the used 60 % TLC egg yolk PC (n=17.5). An explanation for this difference might be rendered from a comparsion to organoclays prepared with long chain alkylammonium cations. It has been observed that these molecules tend to arrange into bimolecular films typically displaying certain inclination angles depending amongst others on the intercalation quantity (Lagaly, 1986). Based on this findings a tilt angle of about 66 ° with respect to the interlayer surface can be calculated from the layer expansion provoked by the intercalated PC molecules. This lower interlayer distance could also be explained with the higher flexibility of the lipid molecule chains as compared to a rather stiff alkylammonium. The PC molecule is constituted of two acyl chains and one containing an unsaturated C=C bond. This originates in lower degree of molecule alignment and packing density, and can therefore allow a higher compression of the lipid membrane which would result in the observed lower basal swelling.

Figure 3.11B shows the interlayer expansion of MMT-PC together with the corresponding adsorption isotherm. At low PC adsorption a first slope until 1.45 nm layer expansion is observed, which can be attributed to a monolayer arrangement of lying lipid molecules (Lagaly, 1986). Subsequent PC adsorption at the beginning of region II results in a drastic layer expansion until 4.2 nm which thereafter remains constant. This is interpreted as follows: The cooperative adsorption mechanism in region II leads to strong incorporation of lipid molecules into the intracrystalline space. As a consequence of increasing molecular packing density, a small number of lipid bilayer zones is formed. This is manifested by the rather broad (001) reflection (pattern f in Figure 3.11A) and a layer expansion value

compatible with the calculated hight of a PC bilayer. With increasing PC adsorption these domains are gradually spreading out along the clay platelets and hence, decreasing the width of the (001) reflection but leaving the expansion constant. Therefore, PC adsorption in region II is considered as a consolidation stage for the compactness and layer arrangement of the intercalated lipid bilayer.

- Lipid Adsorption from Aqueous Phase

The liposome adsorption isotherm on Na^+-montmorillonite was sampled at room temperature at the natural pH (7.8) of the clay suspension and at an ionic strength of 5 mM NaCl (Figure 3.12A). The resultant materials are denominated as MMT-LUV, emphasizing the preparation method based on deposition of large unilamellar vesicles (LUV). The adsorption isotherm has the shape of a *high affinity* curve (H type) according to the Giles classification (Giles et al., 1960). Comparison to the isotherm derived from methanol phase makes evident the high affinity of PC liposomes for montmorillonite and the efficiency of this preparation method Figure 3.12B).

Spectroscopy characterization of the materials suggests that the adsorption mechanism is again based on the exchange of sodium cations. FT-IR spectroscopy shows the diminished intensity of the δ_{HOH} band of crystalline water while the carbonyl band increases due to PC adsorption (Figure 3.13A). The intensity of the δ_{HOH} band is normalized for the

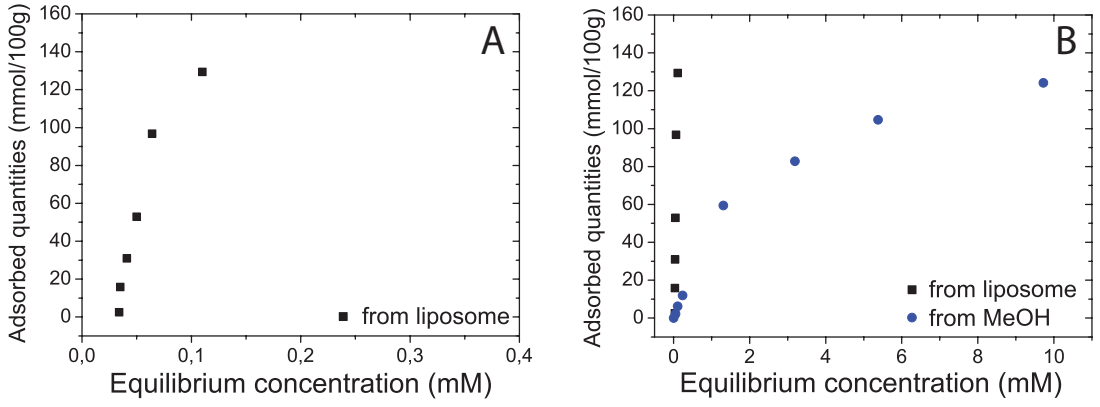

FIGURE 3.12: PC adsorption isotherms on Na^+-montmorillonite prepared from aqueous liposome solution (A) and compared with the adsorption isotherm obtained from methanol solution (B).

structural vibration υ_{Si-O} at 1045 cm^{-1} (Tyagi et al., 2006) and plotted as function of the PC concentration (Figure 3.13B). The results clearly show a decrease in δ_{HOH} intensity compared to the structural MMT vibrations. This could be interpreted as removal of water molecules from the intracrystalline space as consequence of the release (exchange) of Na^+ ions. This is possible since water molecules are strongly associated with sodium ions (Fripiat et al., 1971) and would be simply carried away with them.

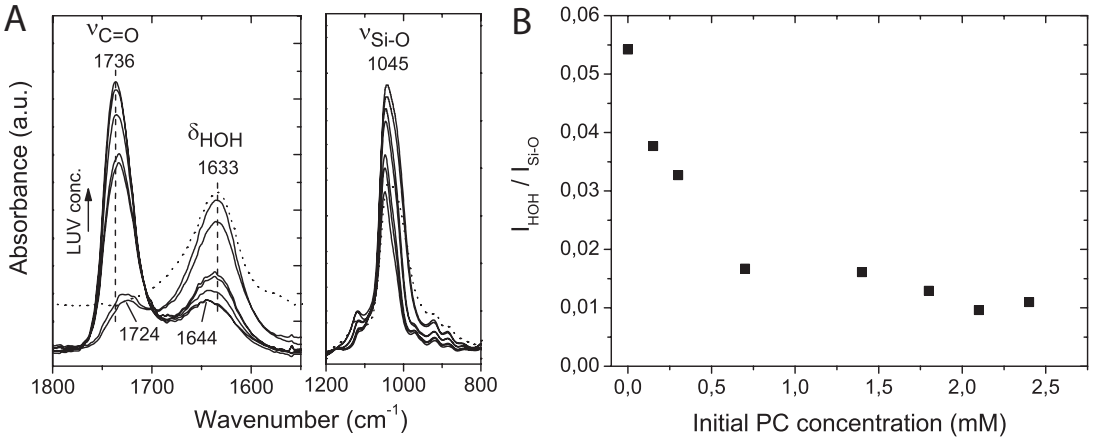

FIGURE 3.13: FT-IR spectra of MMT-LUV biohybrids (A) and the normalized intensity of δ_{HOH} as function of the PC concentration (B). The dotted spectra are pristine Na^+-montmorillonite

XRD pattern of MMT-LUV biohybrids are presented in Figure 3.14. The (001) reflection of the basal plane of pristine Na^+-MMT appears at 7.15 ° (Aranda et al., 1994). A second reflection at 3.82 ° appears which can be related to an increased basal distance d(001) of 2.31 nm. At higher liposome concentrations this low angle reflection increases in intensity while the full width at half maximum (FWHM) of the peak is reduced. At the same time, the peak of the basal spacing of pristine Na^+-MMT gradually vanishes. This process shows the progressive increment of intercalation with increasing lipid adsorption. At low LUV concentrations, small lipid domains are formed within the intracrystalline space. At elevated concentrations, these zones grow and eventually form an intercalated PC bilayer membrane as evidenced from the reflection at 1.67 °, equivalent to an interlayer expansion of 4.33 nm. The appearance of various reflections which are not (00l) indicate that the lipid bilayer is still not homogeneously distributed in all galleries and hence, cause reflections according to the different layer distances. These findings are essentially

similar to the intercalation process from methanol despite of the different aggregation form of the intercalating lipid molecules in both solvents. A reason could be the mobility of the lipid molecules in the liposome (Sackmann, 1996) which permits their release from the vesicle and diffusion into the clay galleries.

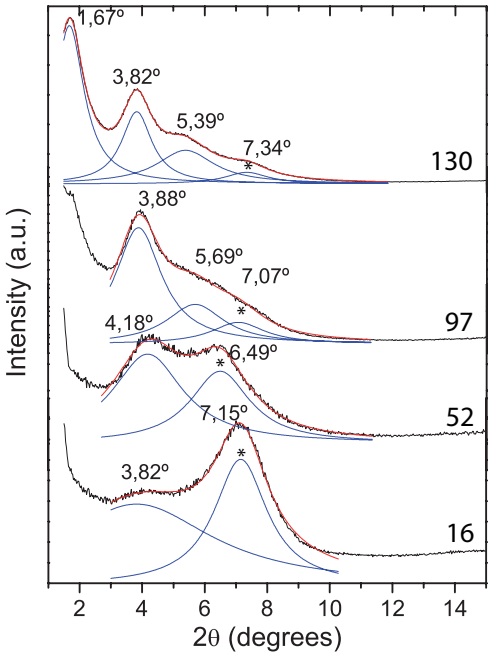

FIGURE 3.14: XRD pattern of MMT-LUV biohybrids with increasing PC content (in mmol/100g) obtained from liposome adsorption. The asterix indicates the position of the reflection ascribed to the basal spacing of pristine Na^+-MMT.

- Molecular Interactions of between PC and Na^+-MMT

Interaction between montmorillonite and phosphatidylcholine is investigated using IR spectroscopy. A red shift of the $\upsilon_{P=O}$ band is revealed (Figure 3.15). This indicates again the involvement of the phosphatidyl group in hydrogen bonding with the clay surface. A finding which is comparable to the sepiolite-lipid biohybrids. Figure 3.13A displays the bands of the carbonyl group $\upsilon_{C=O}$ and intracrystalline water δ_{HOH}. As in the case of the sepiolite-PC hybrids, a shift of $17\,cm^{-1}$ of the $\upsilon_{C=O}$ band compared to neat PC can be observed. This shift is likely to be attributed to electrostatic interaction with hydroxyl groups from water molecules in the interlayer region which are known to be important adsorption sites on montmorillonite (Ruiz-Hitzky et al., 2004). The latter mechanism is confirmed by the strong perturbation of the δ_{HOH} position. The HOH

bending vibration is known to shift to higher frequencies and their half-widths increase upon hydrogen bonding (Pimentel and McClellan, 1960; Paul and Ford, 1986). These perturbations are even an indication for the strength of the H-bond (Xu et al., 2000). In the present case, it can be concluded, that water molecules which are not removed from the intracrystalline space are subjected to increasing hydrogen bonding with the growing amount of intercalated lipid molecules. This is in agreement with the high affinity of the lipid headgroup for water molecules (Tsai et al., 1987).

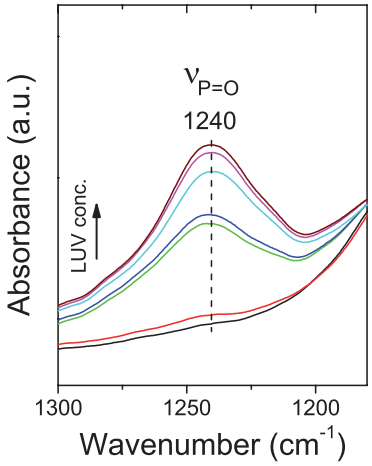

FIGURE 3.15: FT-IR spectra of MMT-LUV biohybrids showing the $\upsilon_{P=O}$ band.

The influence of intracrystalline water on the adsorption behavior of PC from MeOH was also investigated. Prior to adsorption Na^+-MMT powder samples were exposed for ten days to different relative humidity of 0, 33, 55 and 98 %. The results suggest a trend in which adsorbed PC quantities increase with increasing relative humidity (Figure 3.16). This finding indicates an important influence of intracrystalline water on the adsorption mechanism. It is known that water molecules on mineral surfaces can act as water bridges for phospholipid molecules forming an interlayer between the lipid layer and the silicate surface (Rapuano and Carmona-Ribeiro, 2000; Bayerl, 2004; Wiegart et al., 2005). These water molecules themselves are bridging to residual sodium ions in the interlayer space of montmorillonite. In this way, water molecules enhance the electrostatic interaction of the headgroup moieties with the mineral surface. Consequently, the affinity of the phospholipids toward Na^+-montmorillonite is increased.

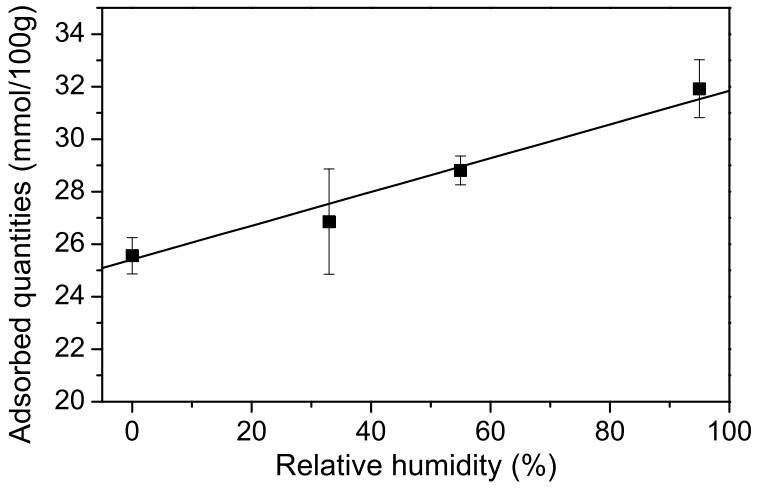

FIGURE 3.16: PC adsorption quantities on Na^+-montmorillonite, that had been exposed to different relative humidities prior to PC adsorption from methanol.

Further evidence for this lipid-water association might be obtained from thermal gravimetry (TG). The TG curve of the sample MMT-22PC (equivalent to 15 wt.% PC as estimated from chemical analysis) shows three weight losses with the maxima centered at 63, 305, and 629 °C (Figure 3.17). These weight losses are attributable to removal of water, combustion of PC, and dehydroxylation of the montmorillonite structure. A detailed discussion of the latter two observations is provided in Appendix A while here only the water removal will be discussed. The first weight loss from room temperature until 100 °C (endothermic effect) is hence assigned to the removal of residual interlayer water molecules. This process occurs at slightly higher temperatures than in neat montmorillonite. Strong association of intracrystalline water molecules to the lipid head group might be responsible for this (Tsai et al., 1987). However, the elevated water elimination temperature might equally well be explained in terms of hindered escape of the intracrystalline water molecules due to the presence of intercalated lipid molecules.

In summary, it has been shown that both clays, the fibrous one and the layered one, preferentially adsorb phosphatidylcholine and form mono- and bilayers on the external surface of sepiolite and additionally in the interlayer space of montmorillonite. The packing density of the lipid layers on sepiolite is lower than on montmorillonite due

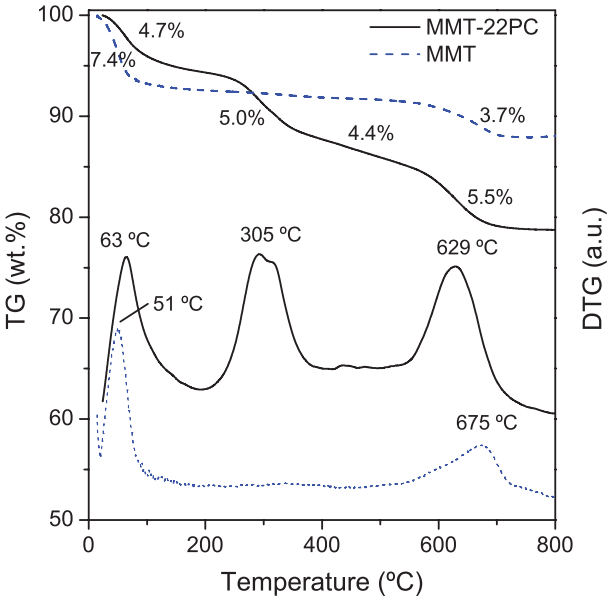

FIGURE 3.17: Thermal gravimetry and differential thermal gravimetry curves of neat montmorillonite (dashed curve) and a MMT-PC biohybrid (22 mmol/100 g PC adsorbed from methanol). The gravimetric curves were recorded under air flow conditions with a heating rate of 10 °C/min.

to the microcrystalline roughness and crystalline steps of this clay fiber. On both clays, the layer deposition is more efficient from a liposome solution than by molecular assembly from solution in an organic solvent. The underlying clay-lipid interaction mechanism are however similar in both systems. In case of sepiolite, the main interaction mechanism is based on hydrogen bonding of the lipid headgroup moieties C=O, C-O-C, and PO_4 with Si-OH surface groups. In case of Na^+-montmorillonite, the interaction mode is more complicated. The acidic environment of the intracrystalline space induces a positive charge on the PC headgroup which permits a cation exchange mechanism. Moreover, association with interlayer water molecules proofed to be of great importance by acting as water bridges between the clay surface and the lipid membrane. Like with sepiolite, the involved lipid groups are the carbonyl, ester, and phosphate moieties. The intercalation of PC molecules is evidenced from powder X-ray diffraction.

3.1.2 Mixed Lipid/Octyl-Galactoside Layers on Sepiolite and Characteristics of Supported Interfaces

Self-assembly allows for the preparation of mixed lipid membranes that can be considered as a further development of the artificial bilayer lipid membrane (Hubbard et al., 1998a; Plant, 1999). These hybrid layers are constituted of individual membrane leaflets, each consisting of different compounds. This strategy gives rise to a great variety of lipid-based membranes with diverse functionalities that can be important in different technological applications (Plant, 1999). Nonionic sugar-based surfactants (SBSs), for instance, are a type of biosurfactants which are worth to be investigated for incorporation into these hybrid layers. The reason that makes them an interesting compound for interfaces is the fact that SBSs are regarded as a class of mild detergents (Baron and Thompson, 1975) which generally do not affect enzyme activity (Stubbs et al., 1976). Therefore, a hybrid PC-OGal interface supported on sepiolite is presumed to be a good scaffold for non-degenerative enzyme immobilization which is studied further below (Section 3.2). This hybrid interface is composed of an inner phosphatidylcholine monolayer (ML-PC) and an outer leaflet of n-octyl-β-D-galactoside (OGal).

Additionally, layers of different interfacial properties supported on sepiolite are compared in terms of surface potential, layer packing density, and hydrophilicity. Sepiolite with e.g. a hydrophobic surface is obtained from PC and cetyltrimethylammonium monolayer formation, respectively. Hydrophilic surface layers are afforded by PC bilayers (BL-PC) and mixed PC/OGal layers, respectively. The characterization comprises measurements of ζ-potential by dynamic light scattering (DLS) and surface hydrophilicity by sampling of water adsorption isotherms.

- Preparation of Mixed Lipid/Octyl-Galactoside Layers on Sepiolite

Layer formation of OGal is investigated by sampling the adsorption isotherm of this biosurfactant on SEP-ML-PC (containing 25 mmol/100g PC). Figure 3.18 reveals that the isotherm follows a sigmoidal shape. This type of adsorption isotherm is typical for

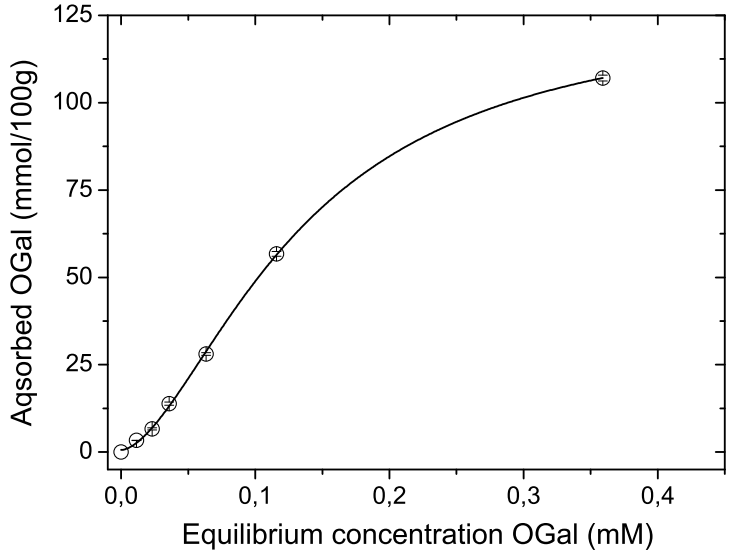

FIGURE 3.18: Adsorption isotherm of OGal on SEP-ML-PC from water at 21 °C. The solid line represents the fitting curve of a logistic growth model (R^2=0.9997).

adsorbates that show intermolecular cooperativity based on van der Waals interaction between hydrophobic moieties (Giles et al., 1974). In particular, nonionic surfactants have been observed to adsorb at hydrophobic solid/water interfaces in this manner (Kumar et al., 2004). The saturation level is calculated as 127 mmol/100g which corresponds to a molecular packing density of 4.7 OGal molecules per nm^2. This is about 2 times the monolayer packing density of n-octyl-β-D-glucoside at the air/water interface (Shinoda et al., 1961). It is assumed that the PC monolayer serves as anchor and nucleation site for the growth of the OGal outer membrane leaflet by hydrophobic interaction between the hydrocarbon chains (Zhou and Somasundaran, 2009). This assumption is also supported by Persson and co-workers who investigated adsorption of n-dodecyl-β-D-maltoside on hydrophobized surfaces based on silane and concluded insertion of alkyl chains of the sugar-based surfactant into the hydrophobic silane layer as anchoring mechanism (Persson et al., 2002).

The excess of OGal might be explained in terms of hydrophobic aggregation or hemimicelle formation (Gu and Rupprecht, 1990; Darder et al., 2000) which can occur even at surfactant concentrations considerably below the critical micelle concentration (Dick

et al., 1971). This is a phenomenon observed for both ionic and nonionic surfactants on a variety of hydrophobic surfaces such as carbon nanotubes (Richard et al., 2003), graphite (Kawasaki et al., 2004), or hydrophobized solids (Brumaru and Geng, 2010) and should therefore also be noted on SEP-ML-PC due to the hydrophobic character of its surface (Section 3.1.1.1). As additional feature, on hydrophobic layers the hydrocarbon tail of the surfactant can penetrate into the hydrophobic surface layer. This case has been observed for sodium dodecyl sulfate adsorption on C18-derivatized mesoporous silica particles (Brumaru and Geng, 2010). In consequence, this can lead to increased molecule packing density and might explain in the present case the elevated packing density of OGal on SEP-ML-PC (Figure 3.19B). On the other side, this value could equally well be achieved by assuming the formation of an OGal bilayer with the octyl chains of the outer OGal layer facing the liquid phase (Figure 3.19C). However, hydration repulsion between the sugar head groups of SBSs is known to occur (Waltermo et al., 1996) and hence, would impede the assembly of an OGal bilayer in this fashion. Figure 3.19 shows schematically the assumed PC-OGal layer arrangement in form of hemimicelles (B) and the two unlikely assemblies of an OGal monolayer and bilayer (A and C).

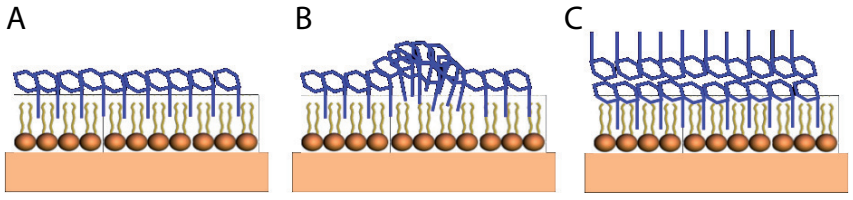

FIGURE 3.19: Schematic of possible OGal layer assemblies on SEP-ML-PC. OGal monolayer (A), OGal hemimicelle (B), and OGal bilayer (C).

- Surface Characteristics of Sepiolite and Sepiolite Hybrids

The neat sepiolite used in this thesis was reported to have an isoelectric point (iep) of 2.2-3.2 (Pajares, 1984; Knapp et al., 1997). Consequently, the observed ζ-potential at pH 7 in 50 mM PBS was -27.8 $\pm$ 0.3 mV. The negative surface charge is accounted to isomorphous substitutions of Mg^{2+} by Al^{3+} in the octahedral layers giving rise to cation exchange ability, typically in the 15-20 mEq / 100 g range (Ruiz-Hitzky, 2001). Another

suggested origin of the negative surface charge was attributed to the presence of Si-O^- groups, resulting from deprotonization of surface hydroxyl groups and adsorption of OH^- ions (Alkan et al., 2005).

As studied in Section 3.1.1.1, a PC monolayer with 25 mmol/100g was formed on sepiolite (SEP-ML-PC), yielding a packing density of 0.92 lipid molecules per nm^2. The ζ-potential of SEP-ML-PC decreased to -18.5 $\pm$ 0.7 mV. Similar observations were made by other authors in the silica-liposome system (Savarala et al., 2010; Chibowski et al., 2011). This phenomena has been attributed to a shielding effect imposed on surface charges by adsorbed PC molecules. As a result, PC shifts the electrokinetic slip plane of the particle outwards and thus, decreases the absolute value of the ζ-potential.

The sepiolite supported lipid bilayer (SEP-BL-PC) contained 50 mmol/100g and revealed a molecular density of 0.92 lipids per nm^2 in each membrane leaflet of the bilayer. This indicates that both membrane leaflets are exact complements. However, since the packing density is lower as compared to PC liposomes or supported bilayer lipid membranes on even surfaces (1.39 lipids per nm^2), a less compact but more mobile bilayer membrane is expected. This may well be ascribed to irregularities of the fiber surface giving rise to microroughness and crystalline steps which can be a reason for the reduced layer packing density. ζ-Potential measurements of SEP-BL-PC revealed a value of -18.1 $\pm$ 0.7 mV.

The ζ-potential of SEP-PC-OGal (109 mmol OGal/100g) was measured to -21.6 $\pm$ 1.3 mV which remained close to the value of SEP-ML-PC. As expected for the adsorption of a nonionic compound, OGal adsorption imposed only little alteration on the ζ-potential (Zhou and Somasundaran, 2009). Even though the hybrid as such is apparently ionic, its surface is composed of assembled nonionic galactoside residues. Furthermore, the alteration of surface hydrophilicity upon OGal adsorption was studied by sampling water adsorption isotherms on the prepared SEP-PC-OGal biohybrids. Figure 3.20 shows the water isotherms on pristine sepiolite, SEP-ML-PC and SEP-PC-OGal with increasing OGal content. The isotherms were analyzed according to Park's model (Park, 1986), rendering the Langmuir capacity constant A_L (water monolayer coverage) from the initial slope of the curves. This value can be interpreted as measure for hydrophilicity of the

exposed interface. The Park equation can be expressed as

$$c = \frac{A_L b_L a}{1 + b_L a} + K_c a^n + k_H a \tag{3.3}$$

where c is the amount of adsorbed water per gram substrate, a the activity of water, K_c the equilibrium constant for the clustering reaction, k_H the Henry's type solubility constant, n the mean number of water molecules per cluster, A_L the Langmuir capacity constant and bL the Langmuir affinity constant. From Table 3.2 it becomes evident that pristine sepiolite fibers are very hydrophilic while the PC monolayer turns the surface more hydrophobic. The successive increment of OGal quantities at the ML-PC surface caused gradually increasing A_L values. Another effect owing to the hydrophobicity of a non-swelling interface is clustering of water molecules (Gouanve et al., 2006). The corresponding parameter n describes the average number of clustered water molecules and can be derived from the Park model. On the sepiolite surface water clustering is low (n=14) related to spreading of water molecules along the hydrophilic surface. On

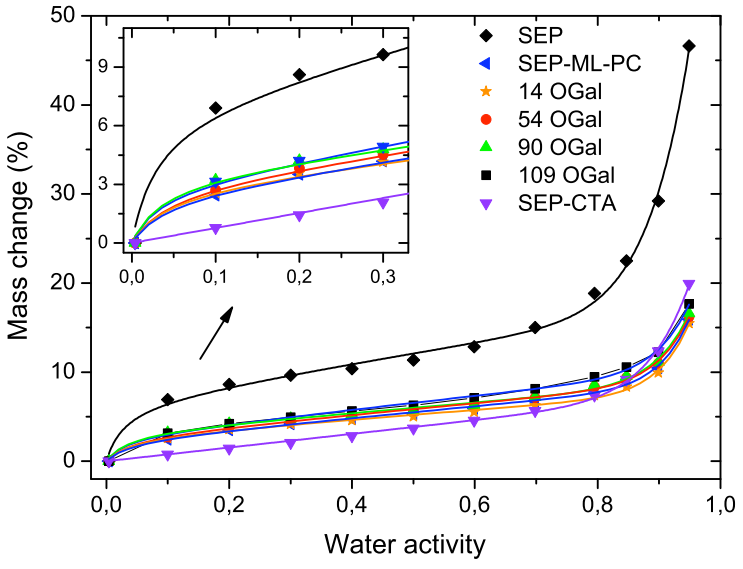

FIGURE 3.20: Water adsorption isotherms at 25 °C on the surface of bare sepiolite (SEP), SEP-CTA, SEP-ML-PC and SEP-PC-OGal with increasing OGal quantities (14, 54, 90, and 109 mmol/100g). The solid lines are calculated from Parks equation. The inset shows the regime of Langmuir adsorption.

the other side, the ML-PC interface shows a value of n=19. This value is gradually decreasing on the SEP-PC-OGal hybrids with increasing OGal content, indicating the change in hydrophobicity. Finally, it should also be mentioned that the hybrid containing 109 mmol/100 g OGal does not follow the general trends of A_L or n even though the water adsorption at the region of elevated humidity is the highest of all OGal hybrids (Figure 3.20). The formation of hydrophobic aggregations of OGal molecules, as suggested above, may offer an explanation. At low water activity, they might act as nucleation sites for the water adsorption, perturbing the formation of a water monolayer. At higher water activity however, the elevated number of OGal molecules provides more interaction sites and is thus responsible for the enhanced overall water adsorption. Together, the results suggest hydrophilization of the ML-PC surface due to assembly of OGal molecules, which present the galactoside headgroup at the solid/liquid interface.

	SEP	ML-PC	CTA	14 OGal	54 OGal	90 OGal	109 OGal
A_L (g/100 g)	6.92	2.51	1.73	2.86	2.97	3.44	2.97
n	14	19	14.2	18.3	17.7	16.5	17.6
R^2	0.9973	0.9976	0.9536	0.9972	0.9978	0.9960	0.9974

TABLE 3.2: Water adsorption data of sepiolite and sepiolite based hybrid materials. The data is obtained from fitting of the adsorption isotherms to the Park model.

The surface properties of a sepiolite hybrid presenting an interface composed of the alkylammonium surfactant cetyltrimethylammonium (CTA) are characterized. The intention is to provide a comparison between the monolayers of the biosurfactant PC and the organo-surfactant CTA. This can be of importance for subsequent studies related to the association of biological species on these materials (Section 3.2).

The examined SEP-CTA material was prepared by Aranda and co-workers and kindly provided (Aranda et al., 2008). This material is prepared by adsorption of cationic CTA^+ molecules which changes the ζ-potential of sepiolite to a value close to zero. This charge compensation is result of Coulomb interactions between CTA^+ and the negative charge sites on sepiolite. But also cation exchange is well known to govern part of this adsorption process (Aranda et al., 2008). The obtained SEP-CTA material contains 34 mmol CTA / 100g sepiolite which corresponds to a packing density of 1.25 molecules

	SEP	ML-PC	CTA	BL-PC	PC-OGal
Ads. quantities (mmol/100g)	-	25	34	50	25 + 127
Molecule density (nm^{-2})	-	0.92	1.25	0.92	4.70
Z-potential (mV)	-27.8 $\pm$0.3	-18.5 $\pm$ 0.7	-3.7 $\pm$ 0.3	-18.1 $\pm$ 0.7	-21.6 $\pm$ 1,3

TABLE 3.3: Surface characteristics of sepiolite based hybrid materials. ζ-Potential was measured in 50 mM PB (pH 7.0) of 0.1 wt. % suspensions.

per nm^2 (or 0.8 nm^2 per molecule) of the resulting CTA layer. This value is higher than the cross-section area of 0.5 nm^2 of a CTA molecule in a monolayer on silicon dioxide (Birch et al., 1994). The microscopic roughness of sepiolite may reduce the ideal packing density of the CTA monolayer. However, according to the water adsorption isotherm, the CTA monolayer is significantly more hydrophobic than the PC monolayer (Figure 3.20) with an A_L value of 1.73 g/100 g. Together, these findings suggests a denser molecule packing of the CTA monolayer than in case of the lipid monolayer, where the double bond in the acyl chain may impede the same high degree of ordering. Consequently, it can be assumed that the ML-PC structure is looser and allows for partial penetration of water molecules into the layer giving rise to higher A_L and n values.

The above discussed surface properties are listed in Table 3.3.

3.1.3 Mg/Al Layered Double Hydroxide-Lipid Biohybrids

Another clay-PC system are layered double hydroxide (LDH) lipid biohybrids. These materials can be used as alternative to SEP-PC in various explored applications (Section 3.3). Inspired by the work of Begú and co-workers (Begú et al., 2009), a new intercalation route was followed for the preparation of Mg/Al LDH-PC biohybrids based on co-precipitation in presence of a liposome solution.

This strategy was developed since in preliminary experiments, the method of ion-exchange with the zwitterionic PC to intercalate into Mg/Al LDH was found to be very little effective. Inspection of XRD pattern, for instance, suggested only partial intercalation at the most. The results from this attempt can be found in Appendix A. Owing to the anion exchange mechanism of LDHs and their elevated anion exchange capacity, the intercalation approach for neutral molecules is often not feasible (Forano and Prevot, 2008). Therefore, it was decided to prepare Mg/Al LDH-lipid biohybrids by co-precipitation with liposomes.

The as-precipitated Mg/Al LDH-PC was not subjected to thermal treatment or any further drying but was kept as gel instead. The reasons are the avoidance of possible loss of colloidal behavior inflicted by particle growth due to ripening processes. Also re-dispersion issues for later immobilization of viral compounds and the formulation of vaccine adjuvant systems (Section 3.3) were considered in this context.

- Characterization of Mg/Al LDH Biohybrids from Co-Precipitation

According to the synthesis described in Section 2.2.1(b) Mg/Al LDH-PC co-precipitated at low supersaturation of Mg^{2+} and Al^{3+} at 2:1 molar ratio in the presence of a 0.5 mM liposome solution (prepared from the 92 % batch). The XRD pattern can be seen in Figure 3.21 together with the diffractogram of pristine Mg/Al LDH. Both patterns are poorly defined, even though the one of Mg/Al LDH-PC is a bit less noisy. It is quiet common for many LDHs and their organic hybrids to show badly defined diffraction pattern (Evans and Slade, 2005). This is related to poor crystallinity especially when the

structure has not been consolidated by a thermal treatment. However, a closer inspection of the pattern reveals that both diffractograms show all the typical reflections assigned to a Mg/Al LDH structure and thus, confirm the formation of the desired material. This observation is also supported by EDX analysis revealing Mg and Al at an molar ratio of 1.8 (Figure A.7). A deviation from the theoretic molar ratio is a common phenomenon in co-precipitation of hybrid LDHs.

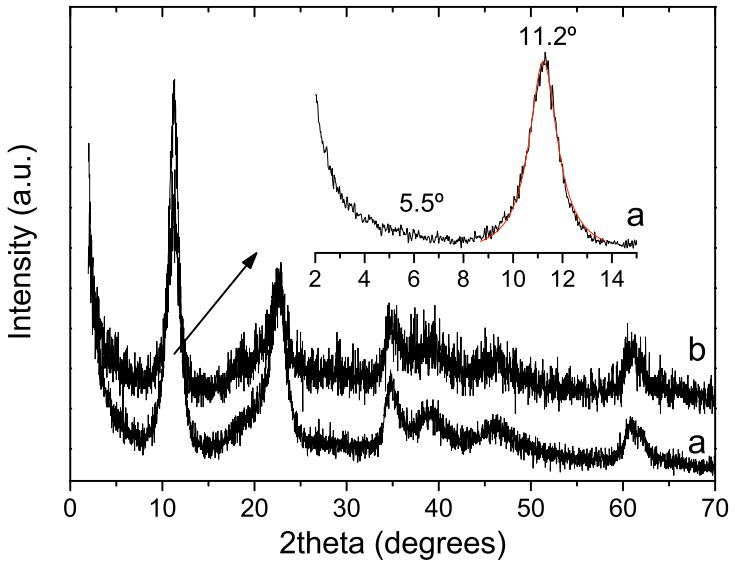

FIGURE 3.21: XRD pattern of co-precipitated Mg/Al LDH-PC (a) and pristine Mg/Al LDH (b). The inset shows the low angle region of Mg/Al LDH-PC with a Lorentz peak fit of the (003) reflection.

Typical (00l) reflections of the Mg/Al LDH exchanged with Cl^- ions appear at 11.2 °, 23 °, and 35 ° 2θ. The (01l) reflections are present at 38 ° and 47 ° 2θ while the in-plane (110) and (113) reflections are found above 60 ° 2θ (Evans and Slade, 2005). The insert in Figure 3.21 shows a very weak and broad peak at around $2\theta = 5.5$ ° that may be ascribed to the first (00l) reflection peak of an intercalated phase. The interlayer spacing calculated from this reflection gives a value of 1.13 nm. This value together with the low intensity of the reflection indicate that only insignificant intercalation took place. However, elemental analysis of this biohybrid revealed a PC content of 28 mmol/100g. Therefore, is can be

assumed that the assembled lipid molecules are situated at the external surface of the particles instead.

A basal spacing of 0.777 ± 0.011 nm for both Mg/Al LDH-PC and pristine Mg/Al LDH was calculated as average value from the three (00l) reflections (003), (006), and (009). With the subtraction of 0.48 nm brucite layer thickness (Meyn et al., 1990) follows an interlayer spacing of 0.30 nm. This value is in agreement with the presence of interlayer Cl^- anions (Evans and Slade, 2005; Begú et al., 2009) which are also detected by EDX analysis (Figure A.7) and confirm therewith the absence of an anion exchange process.

The Scherrer equation is applied to the (00l) and (110) reflections which will render the domain size along the c and a axis, respectively. The Scherrer equation is presented as

$$t = \frac{K\lambda}{\beta cos\theta} \tag{3.4}$$

where t is the Scherrer crystal size, K is the shape factor (typically 0.9), λ is the wavelength of the Kα X-ray radiation, β the line broadening at full width half maximum (FWHM) of the reflection intensity and θ is the Bragg angle (Scherrer, 1918). Table 3.4 reports the Scherrer sizes of the crystalline domains in a and c direction of pristine Mg/Al LDH and Mg/Al LDH-PC. The stacking size in c direction is for both materials in the nanometer regime (14.0 and 11.5 nm, respectively). The number of lamellae in c direction can be calculated from the division of the domain size by the basal spacing. This estimation renders stacks of 14 to 20 lamellae. The crystalline domain size in a direction is of similar nanometric dimensions as in a direction ($\approx$16 nm).

The small Scherrer domains are in agreement with the relatively poor defined XRD pattern. Diffraction intensities decrease and FWHM increases with decreased crystal size (Jenkins and Snyder, 1996). Also the low intensity of the in-plane (110) and (113) reflections suggest short-range intralamellar organization.

Table 3.4 also reports particle sizes measured with dynamic light scattering (DLS). Mg/Al LDH-PC shows a trimodal size distribution (by scatter intensity) of 80 ± 10, 243 ± 10, and 1450 ± 158 nm while the size distribution by number revealed a monomodal population of

	Mg/Al LDH	Mg/Al LDH - lipid
Domain size in *c* direction (nm)	14.0	11.5
Number of lamellae	20	14
Domain size in *a* direction (nm)	16.3	15.6
Particle size (nm)	32 ± 6	75 ± 10

TABLE 3.4: Scherrer size of crystal domains in *a* and *c* directions of pristine and PC modified Mg/Al LDH. The values are calculated from the (110) and (00l) XRD refections, respectively, and the number of lamellae is estimated from the stacking size in *c* direction. The (110) peak was deconvoluted and fitted according to the Gauss distribution. The particle size was determined by DLS measurements and the size distribution is presented by number.

nanometric colloids around 75±10 nm. Pristine LDH has a multimodal size distribution ranging from colloidal 28 nm up to aggregates around 950 nm. DLS distribution graphs are presented in Figure A.8 in Appendix A. The difference between the distributions is that scatter intensity emphasizes aggregates since large particles scatter more than small particles. Number-based distributions, on the other hand, pronounce more the small particles and provide an estimate of the ratio between differently sized populations (Malvern, 2011). Bearing this in mind, the DLS results indicate nano-scaled colloids as principal population. The particle size is about the double of the crystalline domain size, suggesting finely dispersed crystals in the suspension.

Particle morphology was further studied by TEM microscopy (Figure 3.22). The co-precipitated biohybrid displays transparent, platelet-like particles of 40-50 nm lateral size and even some apparently exfoliated LDH sheets (Figure 3.22B). The particle size is in the same order of magnitude as the DLS derived particle size. Many platelets also showed dark rims (black arrows in Figure 3.22A), supposedly originating from bending of thin LDH sheets. Pristine Mg/Al LDH was observed to show some extend of aggregation (Figure 3.22C). Electron microscopy therewith confirms the prevailing colloidal morphology of the prepared LDH materials and is in accordance with the XRD and DLS results. Similar nanosized Mg/Al LDH materials were also reported elsewhere (Xu et al., 2006). However, in these cases the sheet-like morphology was obtained from hydrothermal aging processes. Another frequently made observation is aggregation of the primary LDH crystallites to micrometric agglomerates. This process is effectively avoided in the present case of Mg/Al LDH-PC.

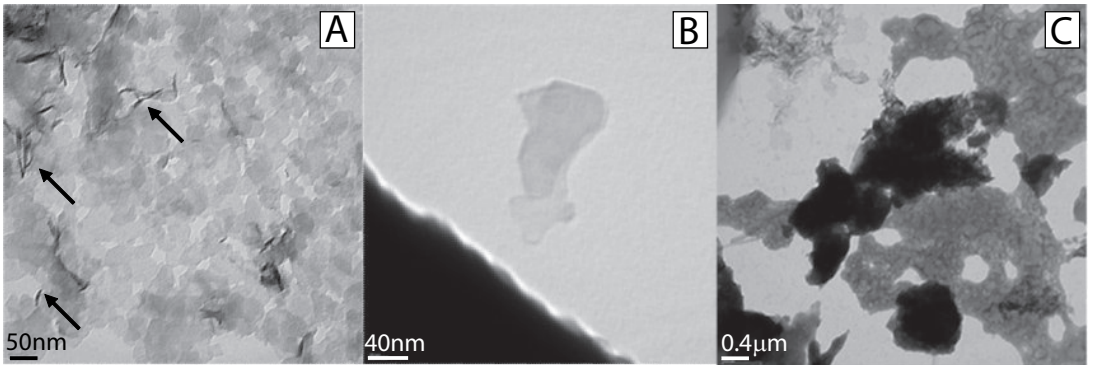

FIGURE 3.22: TEM images of co-precipitated Mg/Al LDH-PC (A, B) and pristine Mg/Al LDH (C).

- Mg/Al LDH-PC Biohybrid Formation Mechanism

Interaction of PC with Mg/Al LDH was investigated by IR spectroscopy. Figure 3.23 shows the spectrum of Mg/Al LDH-PC with the stretching vibrations ν_{O-H} of hydroxyl groups centered at around 3460 cm^{-1} and lattice vibrations (Mg-O, Al-O) below 800 cm^{-1} (Hernandez-Moreno et al., 1985). Particular attention should be payed to the band at 447 cm^{-1} which is evidence for a Mg_2Al-LDH (Hernandez-Moreno et al., 1985; Labajos et al., 1992). The band at 1370 cm^{-1} is likely to be attributed to the ν_3 vibrational mode of carbonate anions, which are common contaminants in the LDH synthesis and originate from atmospheric CO_2 (Camacho et al., 2009). PC specific bands are observed at 2925 and 2855 cm^{-1} (ν_{CH_2}), at 1736 cm^{-1} ($\nu_{C=O}$), at 1457 cm^{-1} (δ_{C-H}), and at 1230 cm^{-1} ($\nu_{P=O}$). The perturbed IR bands of C=O and P=O indicate H-bonding of the lipid molecules with the Mg/Al LDH framework similar to case of the clay-PC materials. Support for this assumption is provided by Wang and co-workers who observed a red shift for the S=O band of sulfonate surfactant molecules that adsorbed on layered double hydroxides (Wang et al., 2005). This finding has been interpreted as hydrogen bonding between S=O and surface hydroxyl groups (HO-M, M = Al or Mg). The chemical similarity between the S=O group and the P=O function present in the PC molecule may allow to conclude that similar interactions are arising in the Mg/Al LDH-PC material. In this sense, the perturbed ν_{O-H} band of the surface hydroxyl groups (HO-M, M = Al or Mg) on Mg/Al LDH-PC (3469 cm^{-1} *versus* 3460 cm^{-1} of pristine Mg/Al LDH) may be interpreted as a result of these interactions.

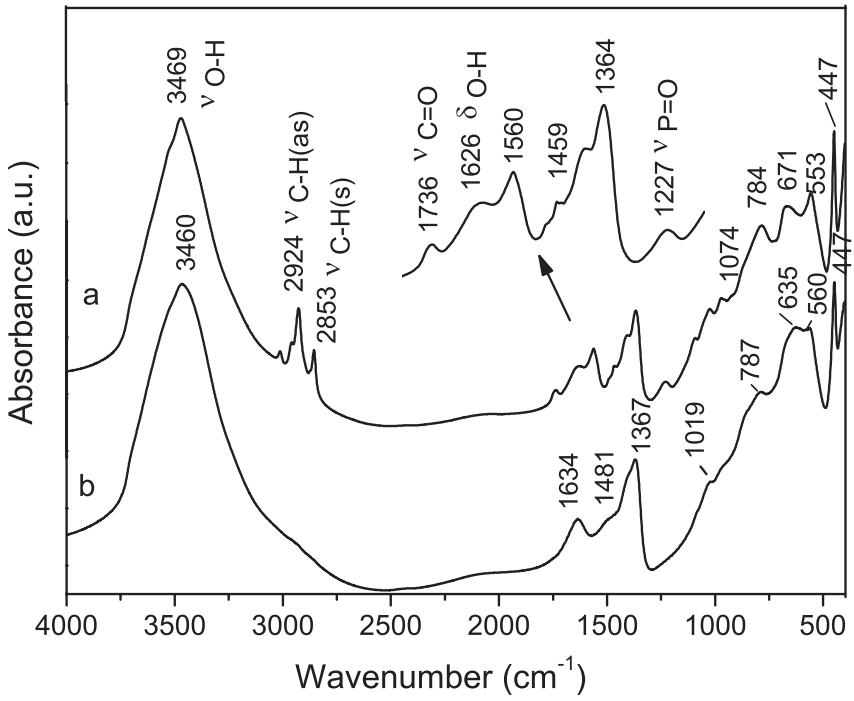

FIGURE 3.23: FT-IR spectra of co-precipitated Mg/Al LDH-PC (a) and pristine Mg/Al LDH (b). The spectra were recorded in KBr pellets.

Unfortunately however, a more detailed, mechanistic mechanism for the formation of Mg/Al LDH-PC is difficult to postulate. A major problem lies in the simultaneous crystallite nucleation and growth during co-precipitation since salt solution is continuously added to the reaction (Crepaldi et al., 2000). This implies the coincidental presence of clusters, crystallites and aggregates during all stages of the synthesis and makes a detailed study of the influence of liposomes on the LDH formation cumbersome. It would require a relatively sophisticated synthesis apparatus to effectively separate these processes (Zhao et al., 2002), which however was not available during this work. Therefore, it can only be hypothesized, that the external surface of the liposomes may serve as nucleation site for Mg/Al LDH crystallites (Figure 3.24). The pH value during co-precipitation was adjusted to 9, at which point the phosphatidylcholine liposomes develop a small negative surface charge, as concluded from ζ-potential measurements (Figure 3.2). This charge could induce the precipitation of positively charged brucite layers. Additionally, H-bonding presumingly favors the association of the metal hydroxides to the polar PC headgroups at the liposome surface. The brucite lamellae might grow on the liposomes

and eventually rupture the vesicles to convert them into a surface membrane. The nano-sized, sheet-like morphology of this material could also be a result of the precipitation at isolated nucleation sites, e.g. on individual liposomes. A templating effect of the intercalation compound on the resultant LDH morphology in co-precipitation was also noticed by Darder and co-workers (Darder et al., 2005b). Smaller stacking sizes have been obtained for branched polysaccharides while larger crystals were formed in presence of lineal biopolymers (e.g. alginate).

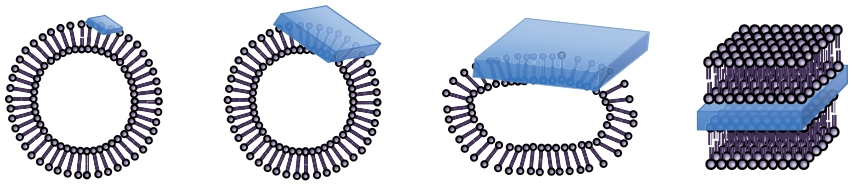

FIGURE 3.24: Scheme of the proposed Mg/Al LHD-PC formation mechanism including the nucleation step, crystallite growth, liposome deformation, and eventually the rupture and layer formation.

3.1.4 Concluding Remarks

The clay-lipid biohybrids obtained from adsorption of phosphatidylcholine display precisely controlled lipid layers. Furthermore, the adsorption mechanism in organic solvent and the resultant lipophilic interlayer space of montmorillonite can be compared to adsorption of alkylammonium species in the preparation of conventional organo-clays. Therefore, this material can be regarded as true bio-organoclay due to the biological origin of the employed surfactant. This new type of lipophilic clay has the additional advantage of being composed of biocompatible components and should find suitable applications in e.g. agriculture or other sensitive sectors.

The concept of supported hybrid layers could also successfully be transfered to the surface of sepiolite fibers. The controlled adsorption of the sugar-based surfactant octyl-galactoside on a lipid monolayer rendered biohybrid materials with more divers interfaces. The degree of OGal immobilization could be systematically analyzed by interface sensitive techniques such as sampling of water adsorption isotherms. Combined with supported

mono- and bilayer lipid membranes, a variety of different biointerfaces was prepared with interfacial properties as divers as ionic and nonionic, hydrophilic and hydrophobic, low and high molecular packing density. These properties are examined in the succeeding Section 3.2 for biomimetic immobilization of model enzymes.

The novel co-precipitation method with PC liposomes rendered a Mg/Al LDH-PC biohybrid material, that provides the desired nanometric, colloidal morphology and lipid interface. In contrast to other methods, this approach permits the preparation of nano-LDHs with readily incorporated biological species as it is performed under avoidance of biodegrading conditions such as hydrothermal aging. These characteristics are generally considered to be advantageous for use of LDHs as drug vectors (Choy et al., 1999; Choy et al., 2000; Xu et al., 2007b). The additional lipid interface is expected to provide appropriate immobilization conditions for influenza virus antigens in terms of adsorption quantity, stabilization of biological activity, and vector properties for antigen administration to animals.

3.2 Applications of Clay-Lipid Biohybrids for the Immobilization of Enzymes and Mycotoxins

In the present Section, bioinspired interfaces are studied as possible immobilization hosts for bioactive species. In this way, the association of the enzymes urease (URE) and cholesterol oxidase (COx) to sepiolite supported lipidic interfaces is evaluated. Also the sequestration of mycotoxins on clay-lipid biohybrids is subject of investigation.

As discussed in the previous Section 3.1.2, a variety of sepiolite supported layers have been prepared; a mixed lipid/sugar-based surfactant layer constituted of an inner phosphatidylcholine (PC) monolayer and an outer leaflet of n-octyl-β-D-galactoside (OGal), a bilayer lipid membrane (BL-PC), and monolayers of phosphatidylcholine (ML-PC) and of the long-chain alkylammonium surfactant cetyltrimethylammonium (CTA). For comparison, the bare sepiolite surface is also tested as immobilization site for bioactive species. The principal surface characteristics of these materials are summarized in Table 3.5.

	pristine SEP	ML-PC	BL-PC	CTA	PC-OGal
ionic	+	+/-	+	-	+/-
hydrophilicity	+	+/-	+	-	+

Table 3.5: Summary of physico-chemical properties of sepiolite supported interfaces and surface groups.

Two different types of enzymes were studied. Urease, which is a cytosolic enzyme that is present in many plants, bacteria, fungi, and algae (Krajewska, 2009). Cholesterol oxidase on the other side is a membrane-bound flavoenzyme that catalyzes the oxidation and isomerization of cholesterol to cholest-5-en-3-one (Kreit and Sampson, 2009) and is related to coronary heart diseases, arteriosclerosis, cerebral thrombosis and miscellaneous other dysfunctions (Nauck et al., 2000). The choice of these enzymes reflects two general schemes of enzyme association to membranes: extrinsic and intrinsic association. The first one is often adopted by cytosolic enzymes while the latter one is frequently found for membrane-bound enzymes presenting a hydrophobic side chain for insertion into the lipid membrane. Enzyme immobilization was characterized by the total protein assay while enzymatic activity was assessed by cyclic voltammetry. This electro-chemical method is

very convenient to study biocatalytic activity of enzymes (Griffiths and Hall, 1993). The reason is the precise and feasible detection of changes in a physico-chemical property (e.g. pH, solution conductivity, impedance, etc.) in the vicinity of or on an electrode surface provoked by an enzymatic reaction. The magnitude and velocity of these changes can be related to enzyme sensitivity toward corresponding substrates and to reaction kinetics, whose analysis renders parameters to characterize possible denaturation of immobilized enzymes.

Urease immobilized on SEP-BL-PC is further tested as active phase of a voltammetric urea biosensor. The principle of an electro-chemical biosensor is the employment of a biological specie that allows highly selective recognition of a analyte. Specific interactions between recognition moiety and substrate provoke a change in a chemical or physical property, which is transduced through a metal electrode as a readable, electrical signal (Turner et al., 1987; Sethi, 1994). In another application of technological interest, COx/SEP-lipid biohybrids are exploited as biocatalyst in a stirred batch reactor.

A different kind of application with agricultural background is evaluated by assessing phospholipid modified sepiolite and montmorillonite as sequestration agents for mycotoxins. These are highly toxic compounds produced as secondary metabolites by many species of fungi after infesting grain and other food crops and thus, are potentially inflicting economic and sanitary harm (Niyo, 1989).

3.2.1 Urease and Cholesterol Oxidase Immobilization on Sepiolite Supported Biointerfaces

3.2.1.1 Adsorption Processes on Different Biointerfaces

- Total Protein Assay

Urease was adsorbed from phosphate buffer (PB) solution at pH 7.0 on neat sepiolite and the different sepiolite based hybrid materials. Figure 3.25 shows the uptake of urease from where can be seen that any kind of surface modification enhanced urease retention with

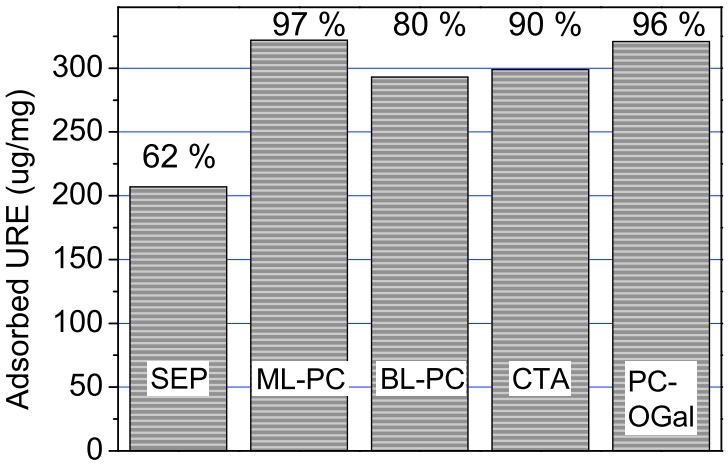

FIGURE 3.25: Urease adsorption on bare sepiolite and sepiolite hybrid materials with ML-PC, BL-PC, CTA, and PC-OGal interfaces. The urease uptake is given in percentage of available enzyme quantity.

respect to pristine sepiolite. Interestingly however, the lowest adsorption was observed on ionic surfaces.

Pristine sepiolite and BL-PC modified sepiolite display ionic interaction sites as negatively charged centers on the clay surface and trimethyl ammonium and phosphatidyl groups of the lipid molecules. Moreover, the ζ-potential of both materials is negative (sepiolite: -27 mV; SEP-BL-PC: -18 mV). On the other side, under the conditions of immobilization (pH 7.0), the surface of URE is negatively charged (isoelectric point (iep) of urease is 5.0-5.2 (Cesareo and Langton, 1992)) and ionic repulsion is likely to counteract attractive forces and consequently, reduces adsorption quantities. On the other side, in case of SEP-BL-PC might arise attractive forces such as H-bonding between the lipid headgroup and cysteine, tyrosine, or histidine side chains of URE. Additionally, glutamate, being present in URE (Vial et al., 2008), is known to strongly interact electrostatically with the phosphatidylcholine headgroup (Wang et al., 2011).

On sepiolite are several more adsorption sites present such as silanol groups, coordinated water molecules, and cation exchange sites that give rise to H-bonding and electrostatic attraction with urease. Surprisingly however, FT-IR and ^{29}Si NMR (Figure 3.26 A and B)

revealed an unperturbed silanol band upon urease adsorption, which is contrary to many electrostatic protein adsorption mechanism on sepiolite. Garcia-Segura and co-workers suggested hydrophobic interactions for sepiolite supported urease (Garcia-Segura et al., 1987) which might offer an explanation for the observed spectra and retention data.

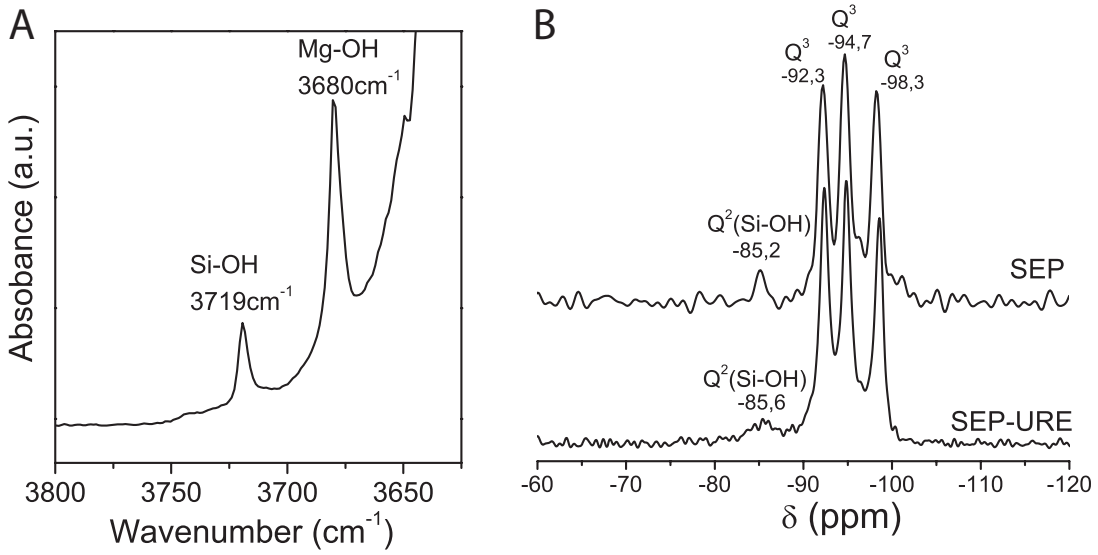

FIGURE 3.26: FT-IR spectrum of SEP-URE showing the silanol band around 3719 cm^{-1} and the Mg-OH band centered at 3680cm cm^{-1} (A). ^{29}Si MAS NMR spectra of pristine sepiolite and SEP-URE (B).

Urease adsorption on SEP-PC-OGal (109 mmol/100g OGal) yielded very high retention. This can be attributed to the polar head group of OGal, comprising four slightly acidic hydroxyl groups (pKa 12.35) (Andrews, 1986) and two etheric oxygen atoms. These are prone to form dipole-dipole and even dipole-ion interactions with the polar and ionic regions of the urease surface. Also H-bonding with urease side chains cysteine, tyrosine, or histidine is likely to occur. Together, these interactions are supposedly strong enough to compensate for the ionic repulsion between the anionic URE and SEP-PC-OGal.

High adsorption quantities were also determined on the hydrophobic PC and CTA monolayers. On urease, a large hydrophobic patch is surrounding the binuclear nickel catalyst center (Remaut et al., 2001) that may well interact and adsorb on hydrophobic surfaces (Hou et al., 2002). This might explain the observed high retention.

Cholesterol oxidase adsorption on the different interfaces was also assessed, and it was found to be equally high for all tested materials. Enzyme concentration in the supernatant

was below detection limit of the used total protein assay and gave an adsorption of ca. 45 μg/mg, corresponding to a 100 % uptake of all available enzyme.

The iep of COx is around 4.7 (Supplier data) which renders the COx surface negative at the pH value used in the immobilization step. However, attractive interactions are apparently stronger. Sampson and co-workers observed COx binding constants to vary only little with membrane surface charge, ionic strength, or pH which suggests that surface binding to membranes is mainly driven by hydrophobic interaction (Chen et al., 2000). This may explain the equally high retention on different interfaces such as lipid layers, CTA membrane, or pristine sepiolite. The high retention of COx on pristine sepiolite in contrast to the lower adsorption of URE might be attributed to entrapment in microcavities of the clay fibers. The COx protein has a significantly smaller molecular mass (64 kDa), corresponding to a molecular cross-section of 15 nm^2 (Ferraz et al., 2011), than URE (460 kDa) and might therefore easily enter the microcavities.

- Stabilization of Enzyme Biohybrids

The amide I and II infrared bands of the amino acid chains provide indications for protein structure deformation caused by strong support - enzyme interaction or by other denaturation processes. Protein degradation can in many cases easily be investigated by IR spectroscopy. The assignment of urease IR absorption bands designated to amide groups are: Amide I attributed to C=O stretching mode at 1650 cm^{-1}; amide II assigned to stretching vibration of NH at 1545 cm^{-1} (Ogura et al., 1999).

FT-IR spectra of free and immobilized urease were recorded (Figure B.1 in Appendix B). However, the amide I band in all cases is largely superimposed by the HOH vibrations at 1660-1626 cm^{-1} of structural and zeolitic water molecules that are present in the pores of sepiolite (Figure B.1). Hence, only the weaker amide II band could be used to assess possible protein structure distortion. But in most cases, this band was too weak to be examined. The IR study of immobilized COx has also been found to provide very limited insight. The adsorbed protein quantities are at the order of 4 wt. % which results in very weak signals.

Therefore, electrochemical enzyme activity measurements were carried out to provide information on possible protein degradation.

3.2.1.2 Immobilization Model Based on Bioactivity and Enzyme Orientation

- Immobilized Urease

Kinetics of immobilized urease were assessed electrochemically by means of a reagentless voltammetric pH probe (Wildgoose et al., 2003; Streeter et al., 2004) based on the redox compound DTNB assembled to the gold electrode surface. As detailed in the Experimental Section 2.4.3, the redox signal due to the couple NHOH/NO derived from DTNB is shifted toward more negative potential values as pH increases. Thus, this potential shift is useful to detect the increase of pH as result of the catalyzed oxidation of urea:

$$(NH_2)_2CO + H_2O \rightarrow 2NH_4^+ + HCO_3^- + OH^- \tag{3.5}$$

The produced peak shift is plotted as function of urea concentration in the supporting electrolyte (Figure 3.27). The linear slope of the curves provides a measure for the preserved enzymatic activity on the different interfaces (Table 3.6). Owing to the sigmoidal curve shape, the data is fitted to the Hill model (Kurganov et al., 2001) for kinetic evaluation of the immobilized enzyme:

$$I = \frac{([C]/[C_{0.5}])^h}{1 + ([C]/[C0.5])^h} I_{max} \tag{3.6}$$

where I_{max} is the maximum rate of the enzymatic reaction, $[C_{0.5}]$ is the concentration at half saturation, and h is the Hill coefficient.

Lipid containing interfaces provide high urease activity with the lipid bilayer affording the highest of all studied interfaces. The good maintenance of bioactivity on this material may be ascribed to the close resemblance of the supported lipid bilayer to biological lipid structures and thus, providing optimal immobilization conditions. This is also reflected

by the high catalytic efficiency $I_{max}/[C_{0.5}]$ (Table 3.6). Pristine sepiolite on the other side, did not conserve enzymatic activity at all. This could be attributed to the fact, that catalytic activity may be compromised due to interaction with the support.

At the CTA interface, a high amount of urease is adsorbed but the sample demonstrates low activity and catalytic efficiency. This may be explained in terms of protein orientation and hydrophobic interactions. As explained earlier, urease possesses a large hydrophobic patch surrounding the Ni catalyst center. Hydrophobic interaction with the CTA interface is likely to orientate the enzyme with its catalyst center toward the support surface and hence, hampering the access of urea to the catalyst site.

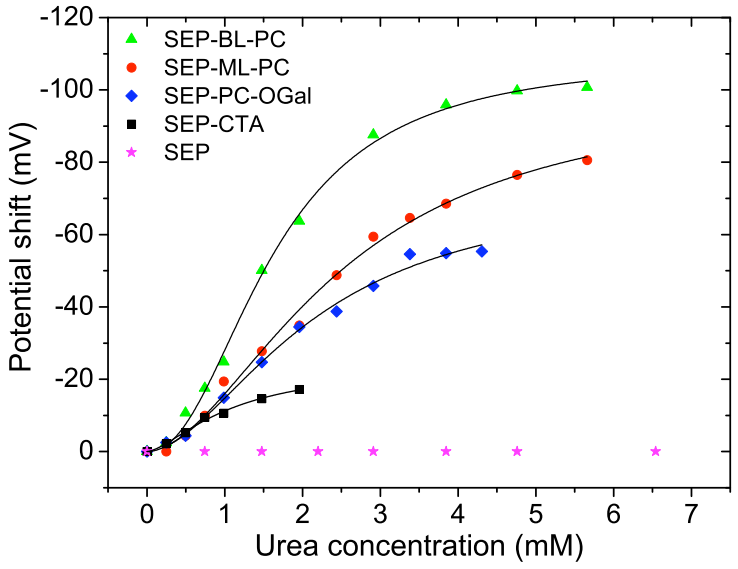

FIGURE 3.27: Potential shift of DTNB as result of pH increase produced by urea oxidation and plotted as function of urea concentration. The solid lines represent the fitting curves to the Hill model. Urease was immobilized on the pristine sepiolite and sepiolite displaying interfaces such as BL-PC, ML-PC, PC-OGal, and CTA.

Similar reasons may apply in case of SEP-ML-PC, however to a smaller extend. Here again, the activity is lower than for SEP-BL-PC. But the lower packing density as compared to the CTA monolayer, and therewith accompanied higher membrane fluidity may allow the enzyme to re-orientate and thus, recover some of its activity. This assumption is also supported by the significant long-term conservation of enzymatic activity on SEP-ML-PC over a period of several weeks (data not shown). It indicates that the reduced

Interface	pristine SEP	PC monolayer	PC bilayer	CTA	PC-OGal
Slope (mV/mM)	0	-21.3	-33.3	-10.2	-16.8
I_{max} (mV)	-	-99.8	-109.0	-23.9	-73.3
$[C_{0.5}]$ (mM)	-	2.5	1.62	1.1	2.1
$I_{max}/[C_{0.5}]$ (VM^{-1})	-	39.9	67.3	21.7	34.9

TABLE 3.6: Activity of immobilized urease as indicated by the slope of the potential shift as function of substrate concentration. The kinetic parameters I_{max} and $[C_{0.5}]$ as well as the catalytic efficiency $I_{max}/[C_{0.5}]$ are derived from fitting to the Hill model.

activity is less related to hydrophobic induced degradation processes which eventually will decline the activity to zero, but rather to conformational obstructions. This long-term activity, for instance, is not observed for SEP-CTA.

Urease activity at the mixed PC-OGal interface is inferior to the genuine lipid bilayer. Galactoside residues on the outer surface seem not to stabilize urease sufficiently. Nonionic sugar-based surfactants such as alkyl glucosides are known as versatile protein solubilizers under the avoidance of typical denaturation effects caused by many ionic detergents (Baron and Thompson, 1975). Consequently, it might be reasonable to consider the different type of electrostatic interaction between OGal and URE, as compared to PC, as possible cause for the decayed activity. This result indicates the necessity of a fully developed lipid bilayer that mimics cellular membranes for optimal enzyme immobilization and activity.

For all cases, the Hill coefficient h was between 1.5 and 2, indicating a slight deviation from classical Michaelis-Menten kinetics (Kurganov et al., 2001) as result of allosteric effects (Magana-Plaza et al., 1971).

- Immobilized Cholesterol Oxidase

Activity of immobilized COx is assessed by plotting calibration curves (Figure 3.28A) from the oxidation current response that originates from the H_2O_2 produced in the COx catalyzed reaction:

$$cholesterol + O_2 \overset{COx}{\rightarrow} cholest - 4 - en - 3 - one + H_2O_2 \tag{3.7}$$

Interface	SEP	ML-PC	BL-PC	CTA	PC-OGal	free COx
Sensitivity (mA M^{-1})	62	154	138	0	24	47
Linear range (μM)	up to 4.9	up to 4.9	up to 3.7	-	2.5-4.9	up to 4.9
K_M^{app}	2.1	5.0	4.4	-	8.7	
I_{max}	0.43	1.31	1.10	-	0.26	0.65

TABLE 3.7: Analytic and kinetic parameters for COx immobilized on different surfaces.

The deduced analytical parameters are reported in Table 3.7. Apparent kinetics of immobilized enzymes are determined amongst others by two factors: (1) enzyme structure degradation due to support - enzyme interactions and, (2) mass transport limitations both in the external bulk solution and the supporting matix (Bunting and Laidler, 1972). Fitting the obtained substrate conversion data to appropriate models may reveal these processes. Lineweaver-Burk plots (Figure 3.28B) were constructed from the reaction data to determine the values of the apparent Michaelis-Menten constant K_M^{app} and the maximum current I_{max}.

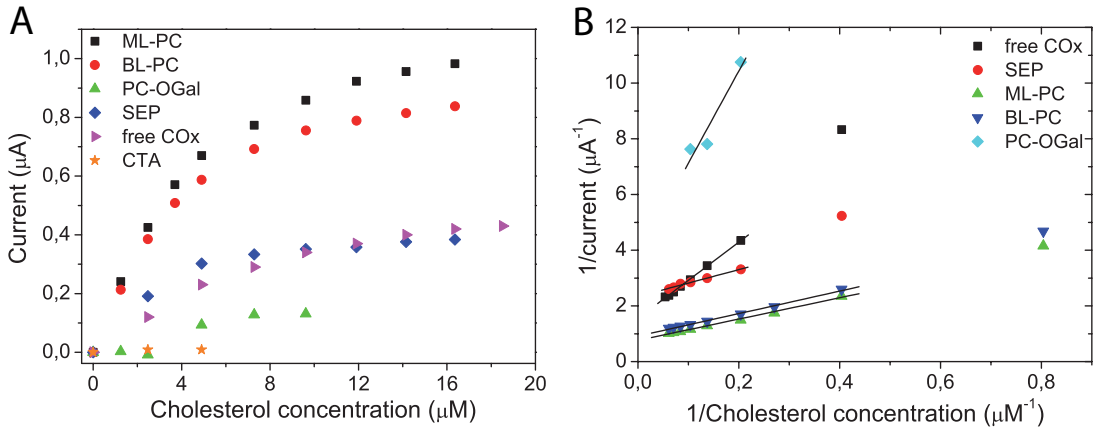

FIGURE 3.28: Calibration plots of COx immobilized on sepiolite displaying biointerfaces such as BL-PC, ML-PC, mixed PC-OGal, CTA, and pristine surface (A). Lineweaver-Burk plots were derived from the conversion data (B)

The brought linearity of the Lineweaver-Burk plots indicates the absence of mass transport restrictions (Bunting and Laidler, 1972; Hamilton et al., 1973) owing to free substrate access to COx which is adsorbed on the surface of the suspended hybrid materials. Furthermore, since all studied materials contained similar enzyme quantities according to

the total protein assay, all observed kinetic variations should be solemnly associated to variations in enzyme activity.

In this way, COx immobilized on SEP-ML-PC produced the largest response. The linear range and sensitivity are found to be 0-4.9 μM and 154 mA M^{-1}, respectively. Slightly inferior sensitivity is detected on SEP-BL-PC. The results demonstrate good immobilization at the lipid interface with even enhanced sensitivity in comparison to free COx. Reduced activity is detected on the mixed PC-OGal interface and on pristine sepiolite while no enzymatic activity is registered at the CTA interface. These findings are supported by the kinetic parameters obtained from Lineweaver-Burk plots. COx, immobilized on both PC mono- and bilayer, shows a decreased K_M^{app} of about 5.0 and 4.4 μM, respectively, when compared to free COx (8.8 μM). Immobilization at the PC-OGal interface renders an apparent Michealis-Menten parameter in the range of free COx while pristine sepiolite provides the lowest K_M^{app} with 2.1 μM but also a low I_{max} value (0.43 μA). Low K_M^{app} values are indicative for fast kinetics and high substrate affinity. It is a frequently made observation that enzymes immobilized on adequate supports may show faster kinetics than the soluble, free enzyme (Kato et al., 2003; Kouassi et al., 2005). Hence, it is obvious that BL-PC offered the best environment of all tested interfaces for COx immobilization. Also when comparing the long-term stability after four weeks, the K_M^{app} value from SEP-BL-PC is lower than from SEP-ML-PC (15 μM and 104 μM, respectively) (Figure B.2 in Appendix B). Both K_M^{app} increased (2.3-fold for SEP-BL-PC and 22.6-fold for SEP-ML-PC) due by slow protein degradation, but the PC bilayer limited this fate to a lower extent.

Sampson and co-workers showed that the amphiphathic active-site loop (residues 78-87) interacts with the lipid headgroup moiety choline while amino acid chains of this loop insert ca. 0.8 nm into the cellular lipid bilayer for spatial orientation of the active center (Chen et al., 2000). It is presumed that this twofold specific interaction with the PC bilayer supported in the present case on sepiolite enables the high and long-lasting activity of COx.

Contrarily, COx did not preserve any activity on the monolayer composed of CTA. Strong hydrophobic interaction between CTA alkyl chains and the hydrophobic region of COx are possibly accounted for this observation. Additionally, COx amino acid chains are possibly hindered to penetrate into the membrane since the CTA monolayer is more densely packed. The mixed interface of PC and OGal rendered diminished activity despite of its close structural resemblance to the PC bilayer. Here, the amino acid chains are likely to insert with more ease due to the lower packing degree of the outer membrane leaflet. But on the other side, electrostatic stabilization as with the choline moiety on a lipid bilayer is not possible.

3.2.2 Application of Supported Enzymes as Urea Biosensor and Cholesterol Bioreactor

The good immobilization properties of SEP-BL-PC are exploited as active phase of an biosensor for urea detection and as biocatalyst in a cholesterol bioreactor.

3.2.2.1 Sensing Characteristics of Urea Biosensor

- Response Time, Sensitivity, and Shelf-Life Time

An important biosensor characteristic is the time until the biological recognition moiety produces a signal strong enough to be measured by the electrode system. Mass transportation of substrate and product to the catalytic centers, and restraints originating from the immobilization process are generally the determining factors for response time. In order to develop a compact biosensing device, the enzyme-containing solid was dispersed in polyvinyl alcohol (PVA) and spread on the surface of a DTNB modified gold electrode, leading to the formation of a film by solvent casting. PVA is a biocompatible polymer and used extensively as hydrogel and enzyme support (Ichijo et al., 1990). Films are known as permeable for electrolytes and many biomolecules, allowing sufficient diffusivity of substrates and products (Hoffman, 2002).

The enzyme-modified sensor was immersed in 10 mM PB at pH 7.4 and the solution was magnetically stirred for 30 s upon urea addition to ensure homogeneous substrate concentration. A peak shift was produced almost instantaneously reaching a constant value after 60-70 s (Figure 3.29A). The quick response time is ascribed to fast enzyme kinetics enabled by good immobilization at the SEP-BL-PC interface. It also indicates significant diffusivity of both the substrate and the products of the urea conversion through the PVA film. The pH change produced within the confined space is in close proximity to the DTNB-modified electrode surface. Therefore, urea is quickly detectable and allows for high sensitivity. The sensitivity of the biosensor was 30.8±0,7 V M^{-1} with a linear range of 0.19-3.39 mM (Figure 3.29B).

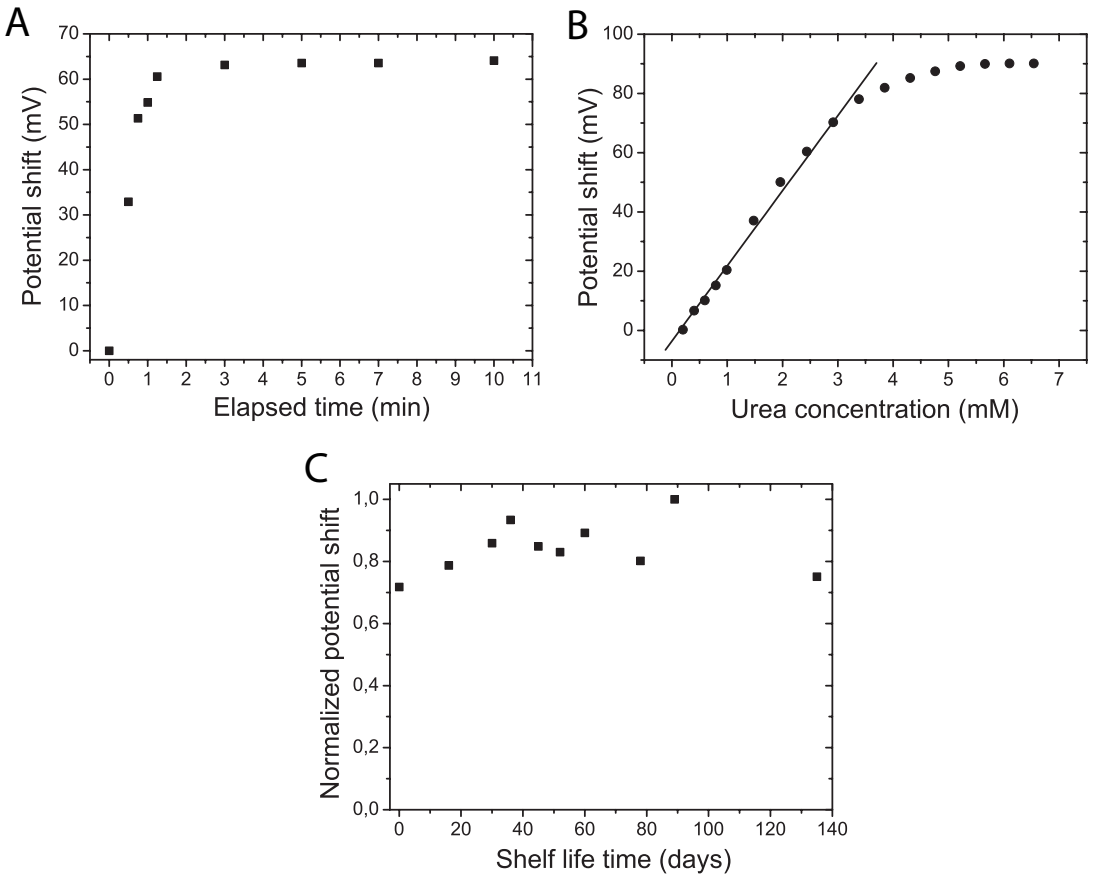

FIGURE 3.29: Response time (A), calibration curve (B), and shelf-life time (C) of urease-biosensor based urease immobilization on a lipid bilayer. The response time was measured in 10 mM PBS (pH 7.4) with 4.8 mM urea. After urea addition, the solution was 30 s magnetically stirred and the time henceforth referred to as elapsed time. The produced peak shift was determined by CV (+0,2 to -0,25 V, 50 mV/s). The calibration curve was recorded in 10 mM PBS (pH 7.4). The shelf-life time is referred to supported urease on SEP-BL-PC which has been stored as dry powder at 4 °C before usage.

For shelf-life time investigation, the urease-biohybrid was kept as dry powder at 4 °C before usage. Enzymatic activity could be maintained up to six months without significant decay of sensitivity indicating a very good storage performance (Figure 3.29C).

- Interferences

In blood serum or urine, many electrochemically active substances may interfere with the recognition moiety and alter the biosensor sensitivity (Mizutani et al., 1997). One of the most important interferences originates from ascorbic acid (AA).

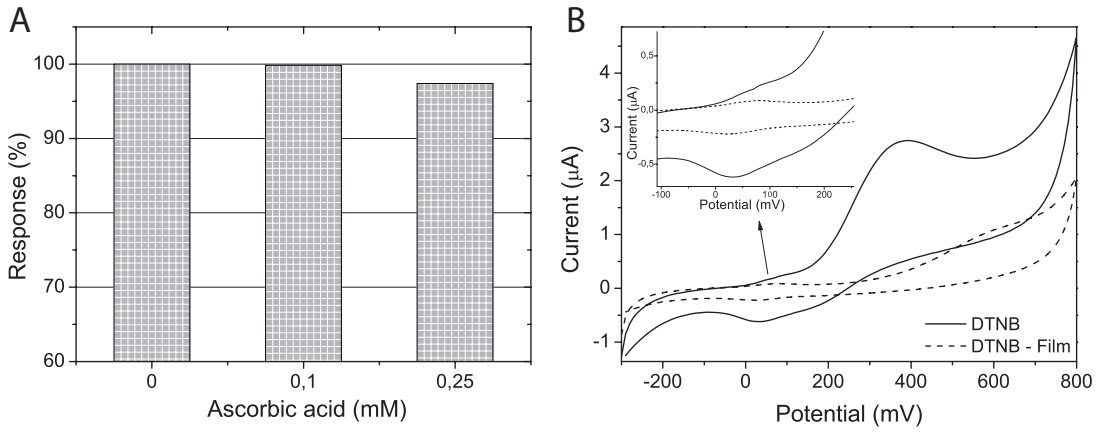

FIGURE 3.30: Interference of urease-biosensor with ascorbic acid. Urease was immobilized on SEP-BL-PC and deposited as PVA based film on DTNB modified Au electrode. Urea concentration was initially 2 mM in 10 mM PB at pH 7.4 (A). CV of 0.25 mM AA in 10 mM PB at pH 7.4 with a DTNB modified Au electrode and a PVA-biohybrid coated electrode (B).

Ascorbic acid may affect the signal of the urease-based sensor by two different ways. Firstly, the oxidation peak of AA appears at a positive potential around 350 mV at pH 7.4, which does partially overlap with the redox couple of DTNB (inset in Figure 3.30B). Secondly, oxidation products of AA are dehydro-L-ascorbic acid and hydronium ions which will locally decrease the pH. This will lead to a shift of the pH sensitive DTNB redox couple towards positive potentials and thus, counteracting the negative potential shift caused by urea conversion. The initial potential produced by addition of 2 mM urea (referred to as 100 % response) is practically unaffected in 0.1 mM AA, and reduced by only 2.6 % in the presence of 0.25 mM AA (Figure 3.30A). The physiological level of AA in serum, however, is only 0.05 mM (Mizutani et al., 1998). This demonstrates that the observed interferences are rather low. The reason is that the PVA layer acts as permselective barrier. This follows a widely used strategy to avoid interferences by limiting the access of electrochemically active substances to the electrode surface (Vaidya and Wilkins, 1994; Madaras and Buck, 1996).

3.2.2.2 Cholesterol Bioreactor

The results of the COx activity assays promoted the application of sepiolite-lipid biohybrids (mono- and bilayer) as possible candidates for COx based bioreactors. The hybrids

contained 53 μg/mg COx, corresponding to 100 % uptake, and the biocatalysts were dispersed in PB solution following a stirred batch reactor set-up (as detailed in Experimental Section 2.4.5). Figure 3.31 shows the catalytic activity as a function of the number of catalytic cycles. It can be noted that the activity of COx after 10 cycles is still very high: 100 % on the lipid monolayer and around 60 % on the bilayer.

Another important characteristic is resistance against mechanical stress. Therefore, after cycle # 4, both bioreactor suspensions were vigorously vortexed. As it can be observed from the activity of the subsequent cycle, COx immobilized on SEP-ML-PC did not show any sign of denaturation, while in case of SEP-BL-PC, the activity decayed by 35 %. Furthermore, a recovery effect of the enzyme activity can be noticed after storage of both materials for one night in PB solution at 4 °C. This behavior can be explained by reorganization and conformational changes of the enzyme if immobilized on a support that provides sufficient mobility. Therefore, this observation can be interpreted as indication of the good biocompatible nature of the sepiolite-supported lipid layers.

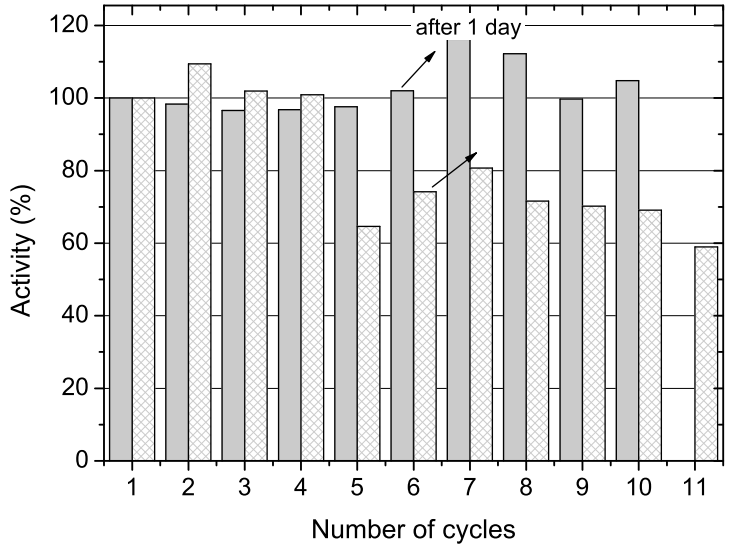

FIGURE 3.31: Catalytic activity of COx bioreactors as function of number of catalytic cycles. SEP-ML-PC (filled columns) and SEP-BL-PC (checked columns) were loaded with 53 μg COx per mg support. After each catalytic cycle, the biocatalyst was separated and the supernatant was subjected to analysis. Before starting a subsequent cycle, the biocatalysts were washed in PB.

3.2.3 Clay-Lipid Biohybrids as Adsorbents for Mycotoxins

Mycotoxins have probably been with humans since the beginning of time, and several historically reported plagues and diseases could be afterwards connected to the infestation of foodstuffs with mycotoxins. But not until relatively recently, a greater awareness and interest in them arose (Goldblatt, 1977). As a consequence of the universal occurrence of mycotoxins and difficult avoidance of molds on stored crops and the subsequent mycotoxin production, several methods of detoxification have been developed. These approaches include kernel separation, heat treatments, or ozonation (Lemke, 2000). However, most mycotoxins are exceptionally resistant to many of these methods and thus, dietary approaches have come into focus. Mycotoxins are known to be strongly retained by soil materials (Jaynes et al., 2007; Desheng et al., 2005). Consequently, soil minerals such as hydrated sodium calcium aluminosilicate (HSCAS) clay and smectites were added to animal diets and demonstrated to act effectively as enternosorbents. In the gastrointestinal tract aflatoxins bind strongly to these materials, and are hence inactivated (Phillips, 1999). The mycotoxins used in the present study are aflatoxin B1 (AfB1) (Figure 2.3A), a toxin which is considered to be amongst the most carcinogenic substances known (Betina, 1989; Heathcote and Hibbert, 1978). Aflatoxin is a very potent poison and represents a true threat to the health of animals and humans as well as a severe economic impact. The second used mycotoxin was deoxynivalenol (DON), also known as vomitoxin, produced by *Fusarium moulds genera* (Figure 2.3B). AfB1 and DON adsorption on bio-organoclays was compared to the commercial alkylammonium organoclay Cloisite® 30B and to cetyltrimethylammonium (CTA)-exchanged sepiolite (SEP-12 wt.%CTA) (the synthesis procedure can be found elsewhere (Aranda et al., 2008)).

3.2.3.1 Aflatoxin B1 Adsorption and Release Study

In this study, montmorillonite and sepiolite based bio-organoclays of different PC content were used. The PC content is given in wt.% and indicated in the sample denotation. AfB1 adsorption isotherms of the organo- and bio-organoclays as well as of the corresponding pristine clays are shown in Figures 3.32A and 3.32B, respectively.

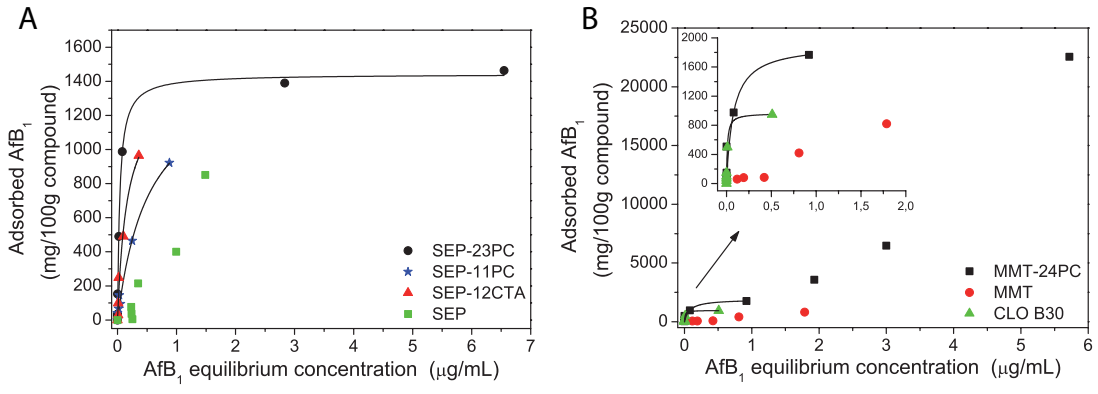

FIGURE 3.32: Aflatoxin B1 adsorption isotherms and corresponding Langmuir fits if procurable of sepiolite (A) and montmorillonite (B) based materials. The isotherms were obtained at ambient temperature after 20 h magnetic stirring. The modified clays were MMT-24PC, SEP-23PC, SEP-11PC, SEP-12CTA and CLO 30B (modifier content in wt.%). In (B) the entire isotherm of MMT-24PC is presented with the inset showing the low concentration tail.

All the modified clays exceeded the adsorption capacity of their pristine correspondents. This finding may indicate an enhanced compatibilization with the hydrophobic mycotoxin due to the organic and bio-organic surface modification. The adsorption curves were subjected to isotherm fitting to obtain information about the maximum adsorption capacity x_m and the Gibbs adsorption energy ΔG_{ads}. Most curves could be fitted to the Langmuir type isotherm. The two sepiolite biohybrids SEP-11PC and SEP-23PC adsorb AfB1 to a similar extent (about 1440 mg/100 g) indicating a toxin saturation level. By contrast, the reference material SEP-CTA was found to possess a smaller retention capacity. The montmorillonite based materials MMT-24PC and CLO 30B also adsorbed AfB1 following the L3 type of the Giles classification (Giles et al., 1960) but to different degrees. While CLO 30B shows an adsorption capacity of 966 mg/100 g, MMT-24PC revealed a first threshold of 1915 mg/100 g and a subsequent strong adsorption (Figure 3.32B). This difference can be explained by the small specific surface area of CLO 30B (12 m^2/g). The question if AfB1 penetrates into the intracrystalline space of Na^+-MMT is a controversially discussed topic in literature (Phillips et al., 2002; Desheng et al., 2005; Kannewischer et al., 2006). Interestingly however, lipid modified montmorillonites increase the retention of AfB1. This greater AfB1 adsorption is assumed to be related

Clay hybrids	x_m [mg/100 g]	ΔG_{ads} [kJ/mol]	R^2
MMT-24PC	1915	-38.0	0.881
SEP-23PC	1442	-39.7	0.997
SEP-11PC	1473	-33.2	0.988
SEP-12CTA	1376	-36.1	0.976
CLO 30B	966	-43.2	0.939

TABLE 3.8: Results of Langmuir isotherm fitting of AfB1 adsorption on modified clays. For calculation of Gibbs adsorption energy an approach for toxic dyes was used. PC content is referred to wt.%.

to AfB1 penetration into the hydrophobic region of the lipid layer (hydrophobic interactions) rather than hydrogen bonding, van der Waals and other interactions as can be postulated for pristine smectite.

When comparing AfB1 adsorption on MMT and SEP biohybrids, one should bear in mind the different specific surface areas of these two minerals. The specific intracrystalline surface area (BET) of Wyoming montmorillonite was determined to about 700 m^2/g (van Olphen, 1977). This value exceeds the external surface area (BET) of sepiolite (165 m^2/g), which is the only adsorption site for AfB1 due to impeded penetration into the sepiolite tunnels according to molecular size considerations. This difference in available adsorption area may well explain the deviation in adsorption capacity of the two clay biohybrids.

The calculation of the Gibbs adsorption energy (Table 3.8) from the adsorption isotherms was based on an approach for toxic dyes (Mittal, 2006). Lower ΔG_{ads} were estimated for increased lipid content in the PC composites and hence, suggesting an enhanced toxin affinity of the clay hybrids with increased lipid content. According to the calculated x_m values, the toxin adsorption of the montmorillonite-PC hybrid was up to 100 % higher compared to the alkylammonium organoclays CLO 30B and SEP-12CTA.

3.2.3.2 Deoxynivalenol Adsorption Study

Adsorption of DON was performed by a single concentration study (Figure 3.33). This is a commonly applied method to conduct rapid screenings of potential sorbents. The tested clays MMT-24PC, SEP-23PC, SEP, and MMT (modifier content in wt.%) were agitated

for 20 h at ambient temperature at a deoxynivalenol concentration of 5 μg/ml. It has been revealed that both SEP-23PC and MMT-24PC adsorbed about 80 % of the available deoxynivalenol in solution. In both cases, the adsorption capacity exceeded the ones of the pristine clays which is indicative for increased affinity due to the presence of the lipid layer. Unlike to AfB1, in the DON system was no higher adsorption observed by the lipid modified MMT adsorbent as compared to its sepiolite equivalent. A possible explanation may be related to the molecular structure of DON (Figure 2.3B). Deoxynivalenol is more hydrophilic than aflatoxin B1 due to its three hydroxyl groups and the smaller aromatic ring system. Thus, penetration into the hydrophobic lipid interlayer space of montmorillonite is less favoured and the beneficial intracrystalline lipid modification for AfB1 adsorption is of minor importance in the case of DON. There might also be steric considerations as the AfB1 molecule is more rigid and planar than the somewhat bulky DON molecule. It is assumed that planar molecules intercalate with greater ease into the organically modified intracrystalline space of smectites. Supporting observations have been made for the adsorption of different herbicides on organically modified bentonites (Nir et al., 2000). Based on these assumptions, the external surfaces are considered as the principal adsorption sites for DON.

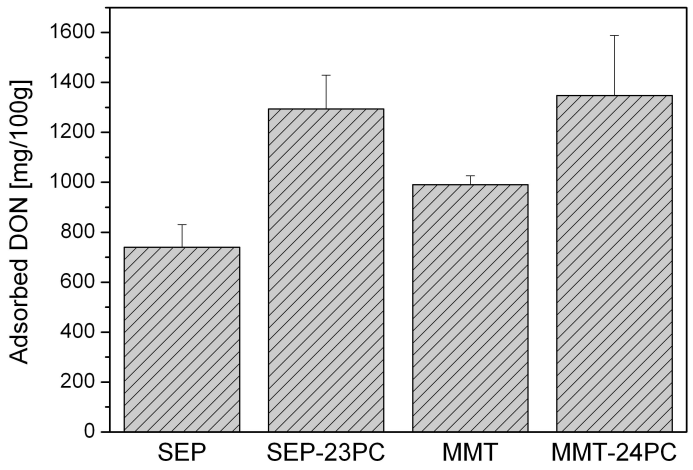

FIGURE 3.33: Deoxynivalenol adsorption from a 5 μg/mL aqueous solution.

3.2.4 Concluding Remarks

Immobilization of biological species was used to probe the biomimetic properties of the diverse biointerfaces on sepiolite as well as to examine possibilities for technological applications. Protein quantification and bioactivity assays helped to elucidate the different adsorption modes of the two model enzymes urease and cholestrol oxidase.

Both enzymes showed highest activity on SEP-BL-PC as could be expected for these enzymes. This interface resembles the native immobilization environment of URE and COx, which is the bilayer lipid membrane (BLM). Urease associates peripherically on a BLM while COx binds cooperatively with the aid of an inserted side loop. This association mode is on the other prepared interfaces less possible which is eventually reflected in the lower enzymatic activity. Urease, for instance, is less active on the hydrophobic ML-PC and CTA interfaces. On the former material, this is likely to be attributed to the orientation of the hydrophobic active side toward the lipid monolayer, and therewith limited substrate assess, while on the latter material additional severe protein degradation can be expected, related to the high hydrophobicity of the CTA membrane.

The immobilized enzymes were tested in an urea biosensor and a cholesterol bioreactor. In case of the biosensor, rapid analyte detection could be achieved owing to the compact active phase confined in a PVA film. Moreover, this film effectively impeded interferences with typical physiological substances such as ascorbic acid. The immobilized urease retained its activity over several months which can be economically significant. Similarly, the COx-biocatalysts are recyclable under conservation of elevated enzymatic activity. The good dispersion properties of the sepiolite fibers additionally contribute to a homogeneously mixed reaction media offering a large accessible surface area that affords high exploitation of the enzymatic activity and thus, high conversion rates.

The application of clay-lipid biohybrids as sequestration agent for mycotoxins is conducted with the intention to evaluate a possible substitution of conventional alkylammonium organoclays by lipid based bio-organoclays as prepared in this Thesis. The uptake data suggests increased affinity of the mycotoxin aflatoxin B for the clay-lipid biohybrids. This

is in part due to penetration of aflatoxin into the hydrophobic space of the lipid membrane. This intercalation is also considered as responsible for the low release in water (data not shown) permitting a safe removal of the sequestered mycotoxin.

3.3 Lipid Bio-Nanohybrids as Influenza Vaccine Adjuvants

The principle of vaccination is the stimulation of a specific immune response of the body against an infectious agent in such a way that the organism is immunized against future infections (Boog, 2009; Pulendran and Ahmed, 2011). Vaccines act in a similar way as natural infectious material but do not subject the recipient to the disease. Vaccines are composed of antigens which are recognized by the immune system as being foreign. The organism reacts with the induction of humoral and/or cellular immune responses which are specific to antigens. These immune responses are ready to protect against future infections (Amorij et al., 2010).

Some vaccines consists in the administration of inactivated viruses that are not able to multiply in an organism but maintained their antigenic properties. The advantage is that they are safer than *live vaccines*, but they are less immunogenic, and require therefore carriers and adjuvants (Coffman et al., 2010; Heegaard et al., 2010). Often, a second administration (*booster*) is needed to ensure sufficient immunogenicity. Adjuvants (from the Latin *adjuvare*, to help) are substances that enhance the antigenic immune response (Coffman et al., 2010). They may also carry the antigen and ensure its slow release. Aluminum hydroxide gel ($Al(OH)_3$) is one of the most frequently applied inorganic adjuvant and antigen carrier, and which is also often used as control in adjuvant development (Gupta, 1998). Besides, some adjuvants can elicit a local inflammatory reaction, typically in the mucosa, that helps to trigger the immunization (Heegaard et al., 2010; Amorij et al., 2010). In the present work, sepiolite is used as carrier due to its high antigen retention capacity and co-adjuvant properties. Sepiolite fibers may provoke irritation of mucous tissue and thus, enhance the immune response (Ruiz-Hitzky et al., 2009). Apart, the protein flagellin (Fla) from *Salmonella typhi* was applied as co-adjuvant to further enhance immunogenicity (Huleatt et al., 2007).

As pointed out above, inactivated antigentic agents usually require an adjuvant in the

administration of the vaccine. However, solid adjuvants as carriers may inflict conformational alterations on the antigen by strong interactions and thus, diminish its immunogenic potential (Clapp et al., 2010). Hence, the preservation of native conformation of antigens is important to ensure successful production of conformational antibodies critical for protection. Therefore, lipid-based interfaces supported on sepiolite fibers and Mg/Al layered double hydroxide (LDH) platelets are explored here and expected to accommodate the antigenic species in a non-degenerative fashion. This approach can be regarded as development of existing antigen carrier systems based on freely suspended liposomes (Heegaard et al., 2010).

The reason for using a Mg/Al LDH-lipid hybrid as support are its multiple similarities to the commercial $Al(OH)_3$ gel. Both materials present aluminum hydroxide groups at their surface, disposable for electrostatic interaction with biological adsorbates. Moreover, both compounds show morphological resemblance with respect to colloidal behavior and ability to form gels. Mg/Al LDH, like $Al(OH)_3$, is biocompatible and approved by U.S. Food and Drug Administration for pharmaceutical formulations (Costantino et al., 2008). In addition, interfacial lipid modification of Mg/Al LDH is believed to ensure minimum denaturation of immobilized viral species.

In a first approach, inactivated H1N1 influenza A virus particles of the PR8 subtype were adsorbed on solid supported lipid interfaces using ($Al(OH)_3$) gel as control.

In a second approach, a partial reconstruction of the viral surface was intended by incorporating the virus membrane protein hemagglutinin (HA) on supported lipid membranes as model of a *sub-unit vaccine*. HA is the main protective Influenza antigen and antibodies that are directed to it are able to neutralize virus infections (Johansson and Brett, 2007). Another important point is, that at present, virus particles are produced in embryonated eggs which can be scarce in case of a global pandemic (Johansson and Brett, 2007). On the other side, recombinant DNA methods are available for large-scale production of HA and thus, a higher number of vaccine doses can be produced (Brett and Johansson, 2005; Johansson and Brett, 2007). Another advantage arises from a materials point of view. The assembly of proteins can be easier controlled, avoiding possible

aggregation and thus, the amount of immobilized antigen can be increased, which in turn will reduce the quantity of required dose rate.

The investigation of thermal stability of immobilized H1N1 virus and HA with respect of the applied support is a further objective of this work. The thermal resistance of immunoactive species is an important issue in the preparation and especially in the distribution of vaccines (Clapp et al., 2010). Shipment to Third World countries with limited refrigeration possibilities may put in danger the efficacy of vaccines and therefore, threaten the health of many. Adequate carriers for the antigens may hold the keys to improved thermal stability. But also lyophilization of the vaccine formulation is often an issue, especially in case of aluminum containing adjuvants which tend to agglomerate during this process and therewith loose their colloidal properties (Clapp et al., 2010). In this respect, sepiolite based adjuvants are envisaged as specially advantageous owing to the good freeze-drying properties of this clay mineral (Darder et al., 2011).

Ultimately, the biohybrid materials were assessed in immunization tests with mice. The serum was analyzed to check specific immunoglobulin G (IgG) levels which are used to assess the immunogenicity (*seropositivity*) of the applied vaccines. The presence of serum antibodies against viral HA is a correlate of protective immune response (Hobson et al., 1973). These *in vivo* tests were carried out in close collaboration with the group of Dr. Gustavo del Real (INIA, Spain).

3.3.1 Influenza Virus Immobilization on Sepiolite- and Mg/Al LDH-Lipid Hybrids

- Exploratory Adsorption Study

In a preliminary adsorption test, PR8/34(H1N1) virus was immobilized on sepiolite, presenting a lipid mono- and bilayer (SEP-ML-PC and SEP-BL-PC), and compared to $Al(OH)_3$ gel. The virus to solid ratio was fixed at $10\,\mu g/100\,\mu g$ and the incubation time was set to 30 min. From Figure 3.34 can be learned that 69 % of the available virus,

equivalent to 6.9 μg per 100 μg support, was retained by the PC bilayer sample and only 38 % by SEP-ML-PC. However, both were inferior as compared to the $Al(OH)_3$ gel with over 90 % retention.

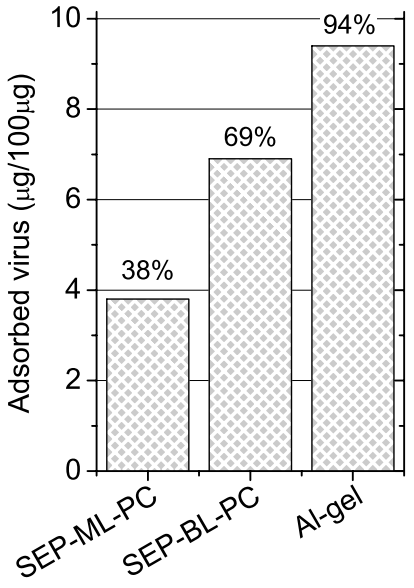

FIGURE 3.34: PR8/34(H1N1) virus retention on SEP-ML-PC, SEP-BL-PC, and $Al(OH)_3$ gel. This particular adsorption experiment has been carried out by Dr. M. Yuste Parra from the INIA, Madrid.

In accordance with the retention data, TEM micrographs show more immobilized virus on SEP-BL-PC than on SEP-ML-PC (Figure 3.35). Furthermore, it appears that the virus particles tend to aggregate on the PC monolayer while the bilayered interface allows for a higher degree of particle dispersion along the sepiolite fibers (arrows in Figure 3.35).

As for a possible adsorption mechanism, one should recall the negative ζ-potential of SEP-BL-PC (Section 3.1.2). The virus surface, on the other side, is positively charged. This is attributed to hemagglutinin that has an isoelectric point of $\approx$8.4 and hence, is protonated under the physiological conditions used in this experiment (Huang et al., 2002; Gasparini et al., 2004). Thus, Coulombic attraction between these two surfaces would be expected. However, SEP-ML-PC also has a negative ζ-potential of similar magnitude (-18.5 mV). Therefore, Coubombic attraction seems not to be the only driving force for the virus adsorption and would not explain the observed difference in retention on these two lipid interfaces.

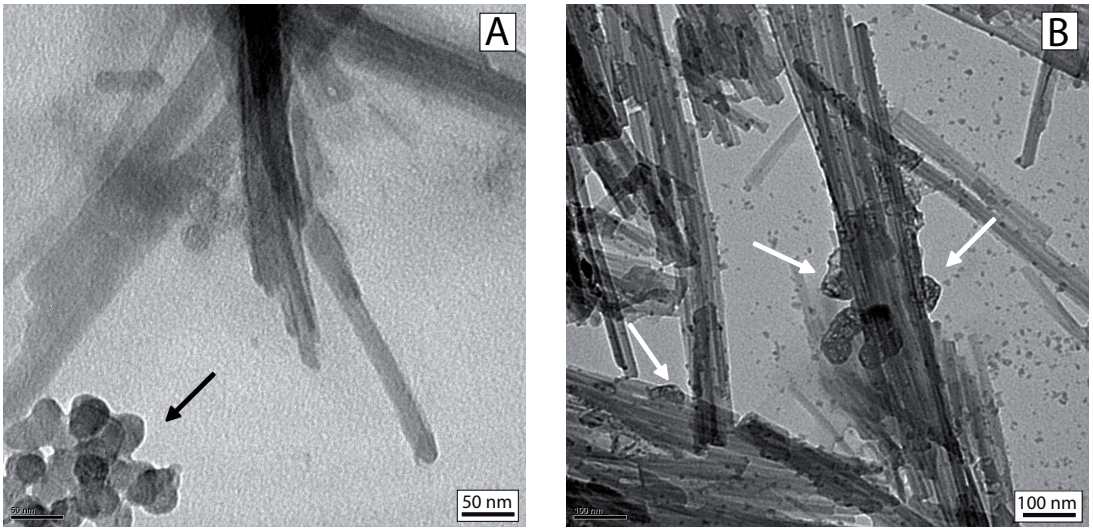

FIGURE 3.35: TEM micrographs of virus particles immobilized on sepiolite supported PC (A) mono- and (B) bilayer. The black arrow in A indicates viral particle aggregation and the white arrows in B point to individually adsorbed virus particles.

An additional attractive interaction in case of SEP-BL-PC might arise from H-bonding between the virus particle surface and lipid headgroups at the external interface of the bilayered hybrid. Amino acid side chains of the virus membrane proteins could induce hydrogen bonding and ion-dipole interactions with lipid headgroups (El Karadaghi et al., 1984). This possibility is essentially disabled on the PC monolayer configuration, presenting apolar hydrocarbon chains at the external interface. Hence, a lower virus retention quantity would be expected as observed in Figure 3.34.

On the other side, the commercial $Al(OH)_3$ adjuvant retained the highest amount of virus particles. This type of adjuvant is known to adsorb large quantities of antigens by ionic interaction (Gupta, 1998). But also H-bonding, hydrophobic, and van der Waals interactions as well as dipolar interactions with exposed Al atoms, Al-O bonds, and hydroxide groups are important in the retention process (Gupta, 1998). XRD analysis of this $Al(OH)_3$ gel confirmed a mixed composition of γ-Al_2O_3 and Boehmite α-AlO(OH) (Figure C.1A in Appendix C). The commercial $Al(OH)_3$ adjuvant has a positive surface potential at neutral pH (Gupta, 1998), implying electrostatic repulsion with the cationic Influenza virus particles. The fact that $Al(OH)_3$ still adsorbed large amounts of PR8 virus might point toward another quality of this adjuvant: The colloidal, gel-forming morphology. As confirmed by DLS (data not shown) and TEM (Figure C.1B in Appendix

	PR8 (μg/ml)	OD
SEP-BL-PC	20	0.148 ± 0.062
Mg/Al LDH-PC	20	0.107 ± 0.008
free PR8	21	0.094 ± 0.030

TABLE 3.9: NA activity assay rendering optical density (OD) values for free and supported PR8/34(H1N1) virus on SEP-BL-PC and Mg/Al LDH-PC. The amount of supported virus was 2 μg/100μg solid in 100 μl being equivalent to a concentration of 20 μg/ml. Samples were analyzed in duplicates.

C), $Al(OH)_3$ gel contains micron-sized particles around 3 μm which seems to be an optimal size for antigen uptake (Gupta, 1998; Clapp et al., 2010). Colloidal and/or gel systems can retain large quantities of adsorbates attributed to their increased specific surface area and entrapment of adsorbates within the gel network (Willaert and Baron, 1996). The applied $Al(OH)_3$ gel has therewith an important advantage over the two sepiolite based materials.

Based on these observations, a lipid modified layered double hydroxide (Mg/Al LDH-PC) was synthesized to combine the qualities of a gel and the biocompatible interface of a lipid membrane. This biohybrid was subjected to an extended virus immobilization study together with SEP-BL-PC and $Al(OH)_3$ gel.

- Extended Adsorption Study

The concentration of PR8/34(H1N1) virus was increased to 2-43 μg/100 μg or equivalent to 6-122 μg/ml and contacted at prolonged incubation time of 2 h. The objective herein was to enhance the retained virus quantity for the formulation of higher immunogenic vaccine doses. The total protein assay revealed virus concentrations below the detection limit (0.5 μg/ml) in all supernatants and therefore, retention is considered as close to 100 %.

Transmission electron micrographs of PR8 virus supported on SEP-BL-PC and Mg/Al LDH-PC are presented in Figure 3.36 and demonstrate clearly the increased amount of immobilized virus particles. Especially on the sepiolite based material, the association of the individual virus particles becomes evident.

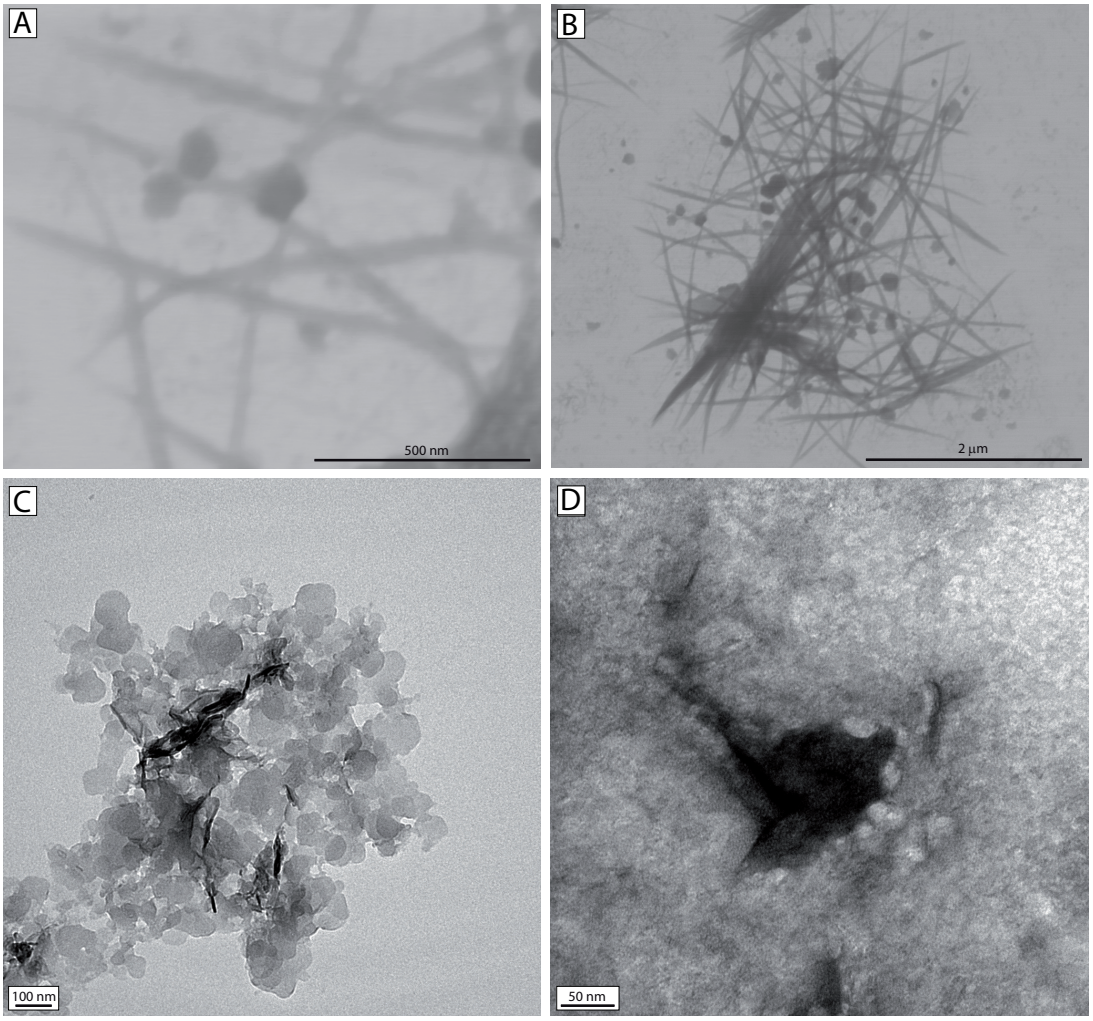

FIGURE 3.36: Micrographs of PR8/34(H1N1) virus supported on SEP-BL-PC (A,B) and Mg/Al LDH-PC (C,D). Images A and B were obtained on a FE-SEM in STEM mode while image C shows Mg/Al LDH-PC before negative staining with uranyl acetate and image D after negative staining. Both last micrographs were recorded on a TEM at 80 kV. The virus concentration on both materials was 43 μg/100 μg.

The retained bioactivity of the immobilized PR8/34(H1N1) virus (2 μg/100μg solid) was investigated by the NA activity assay. Table 3.9 shows the optical density (OD) values for SEP-BL-PC, Mg/Al LDH-PC, and free virus at 20 μg/ml. It can be noted that immobilized PR8/34(H1N1) virus does not loose NA activity which can be interpreted as sign for non-degenerative immobilization on the two lipid nanohybrids.

The quantity of immobilized PR8 was further increasing to study possible effects of aggregation on viral activity. Figure 3.37 reveals an increment of NA activity with rising PR8 content. These findings suggest an absence of aggregation induced denaturation.

This reasoning is also supported by STEM micrographs of dispersed viral particles on SEP-BL-PC fibers (Figure 3.36A and B). These results become crucial in the light of increment of immunogenicity per dose under the avoidance of antigen denaturation. A further important result of this study is the significantly lower NA activity on $Al(OH)_3$ gel (Figure 3.37). This could be interpreted as benevolent contribution of the biocompatible surface afforded by the lipid membrane toward non-degenerative PR8 virus stabilization.

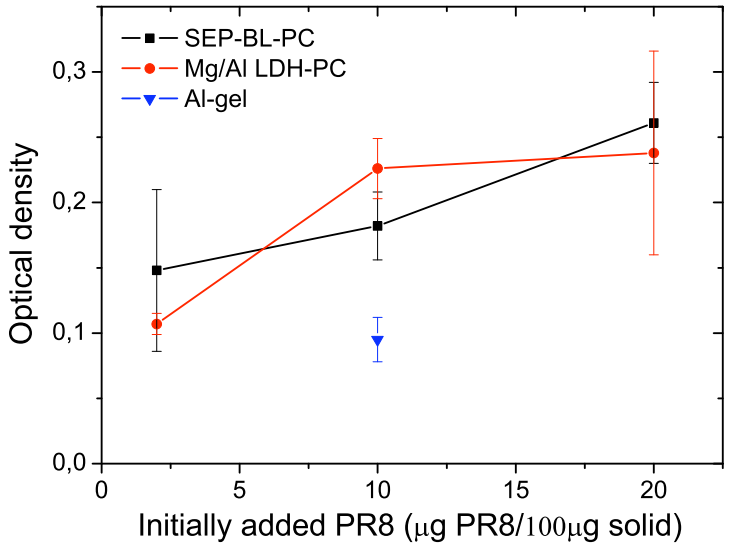

FIGURE 3.37: NA activity assay for PR8/34(H1N1) virus immobilized on SEP-BL-PC and Mg/Al LDH-PC as well as control on $Al(OH)_3$ gel. The virus concentration was 2-20 μg/100 μg solid or equivalent to 6-56 μg/ml. Samples were analyzed in duplicates.

According to these promising results from PR8/34(H1N1) virus immobilization, hemagglutinin as the crucial antigen in influenza immunization was directly immobilized on the lipid nanohybrids in the challenge to reconstruct a solid-supported viral membrane.

3.3.2 Hemagglutinin Immobilization on Sepiolite- and Mg/Al LDH-Lipid Hybrids

Recombinant hemagglutinin (HA) from 43.3 and 166.7 μg/ml solution was immobilized on SEP-BL-PC and Mg/Al LDH-PC and as control on $Al(OH)_3$ gel. As can be observed from Figure 3.38, the retained quantity of HA was over 80 % for all the tested materials. Similar as before, the gel-like materials Mg/Al LDH-PC and $Al(OH)_3$ achieved the highest retention values close to 100 % of all available protein. The recombinant HA

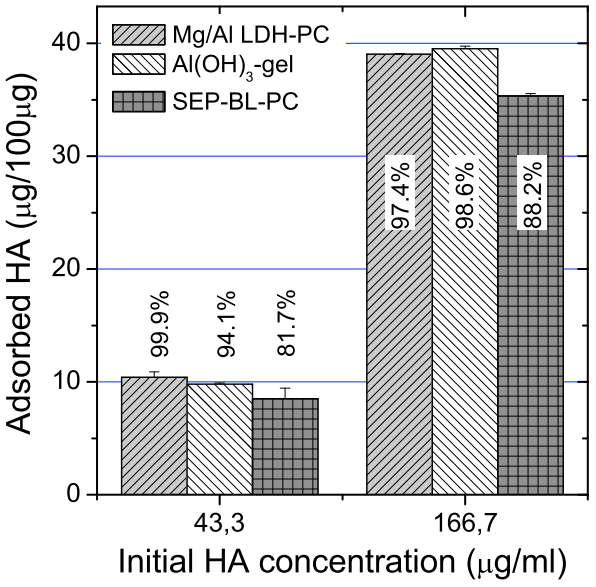

FIGURE 3.38: Quantity of immobilized HA on SEP-BL-PC, Mg/Al LDH-PC, and $Al(OH)_3$ gel. The initial HA concentration was 43.3 and 166.7 μg/ml or equivalent to 10.4 and 40.0 μg/100 μg solid.

lacks of the transmembrane domain (Rodríguez, 2011). This will essentially disable transmembrane anchoring as found on the membrane in native Influenza viruses. Instead, the immobilization mechanism on the artificial lipid membrane is suggested to be governed by electrostatic interactions comparable to those proposed for the entire PR8 virus (Section 3.3.1).

In case of Mg/Al LDH-PC an additional feature can be taken into account. As observed in Section 3.1.3, Mg/Al LDH-PC displays a high degree of exfoliation and accompanied

large specific surface area. This is regarded as favorable for enhanced protein retention (Forano and Prevot, 2008).

Biological activity of supported HA is investigated by means of hemagglutination tests. This assay evaluates the capacity of HA to agglutinate red blood cells and is hence an indicator for the biological intactness of this protein (expressed as HA titer). However, also the used solids alone can induce agglutination and has therefore to be taken as background value. The HA titer of supported hemagglutinin alone might not be as insightful, but the comparison to the HA titer of immobilized PR8 virus could provide valuable information about the efficacy of this approach. Therefore, the mass ratio of HA embedded on PR8 has to be considered. As a rough estimate, 1 g of PR8 virus contains 1/3 g of HA (del Real, 2011). Figure 3.39 depicts the HA titer ratio of immobilized PR8 to HA. Values below 1 mean higher agglutination capacity of HA as compared to the complete PR8 virus. As can be noticed, supported HA on lipid interfaces shows similar agglutination activity as the whole virus particle and in the case of SEP-BL-PC it is even slightly enhanced. This strongly suggests that supported HA has not lost its bioactivity compared to PR8 and furthermore implies that Influenza vaccination doses formulated on basis of hemagglutinin alone could be equally immunogenic. This hypothesis is investigated in Section 3.3.4 by means of an immunization test in mice.

3.3.3 Thermal Stability of Immobilized Viral Species

Even though aluminum based compounds present one of the most abundant adjuvants, they face serious limitations in terms of thermal stability of the associated vaccine at elevated temperatures and at sub-zero conditions related to particle agglomeration (Gupta, 1998; Clapp et al., 2010). Therefore, this stability study aims to evaluate the thermal performance of the lipid-nanohybrids as antigen support.

Aliquots of immobilized and freely suspended A/swine/Spain/50047/2003 (H1N1) virus and recombinant HA were thermostated in a water bath at 21, 28, 37, 48, and 60 °C for

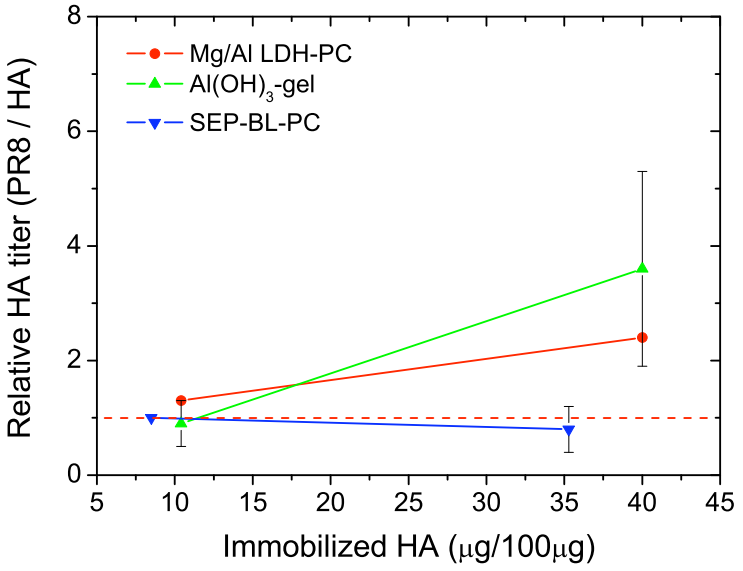

FIGURE 3.39: HA titer of immobilized PR8 virus relative to the HA titer of immobilized HA. For comparison, the HA titer had to be normalized to the amount of immobilized species per gram support. Furthermore, the weight ratio of 1 PR8 virus particle to 1/3 HA had to be considered. The supports are SEP-BL-PC, Mg/Al LDH-PC, and $Al(OH)_3$ gel and all samples were analyzed in duplicates.

20 min at low temperatures and for 10 min at 60 °C. After the thermal treatment, the samples were cooled down in ice and subjected to bioactivity assays.

In case of H1N1 thermal stability was assessed by residual NA activity (Figure 3.40A). It was found that immobilization on SEP-BL-PC provided the highest thermal stability. NA activity of free H1N1 decayed rapidly, suggesting beginning denaturation of the enzyme and accompanying thermal degradation of the viral particle. However, neither $Al(OH)_3$ nor Mg/Al LDH-PC could effectively prevent this fate. A possible explanation for the good thermal stabilization on the sepiolite bio-nanohybrid is assumed to be related with the good thermal insulation properties of these mineral fibers (Chen et al., 2011). This property is supposedly attributed to the microporous texture of the internal sepiolite tunnels, diminishing the thermal conductivity of the crystals to ca. 0.04 W/m·k (Shijiazhuang, 2011). Sepiolite fibers tends to form agglomerates in aqueous suspension and hence, provide some kind of protective scaffold for the immobilized species. $Al(OH)_3$

and Mg/Al LDH-PC, on the other side, form gels of finely dispersed colloids. In this case, the immobilized species are less occluded and more exposed to the environment.

Thermal stability of immobilized HA was studied by hemagglutination assay. The results reveal comparable high stability until 48 °C on all carriers and even for the free protein (Figure 3.40B). The surprisingly high thermal resistance of HA as compared to the virus particles can prove advantageous in the design of stable vaccine formulations and be regarded as another argument for the preparation of vaccines from HA alone.

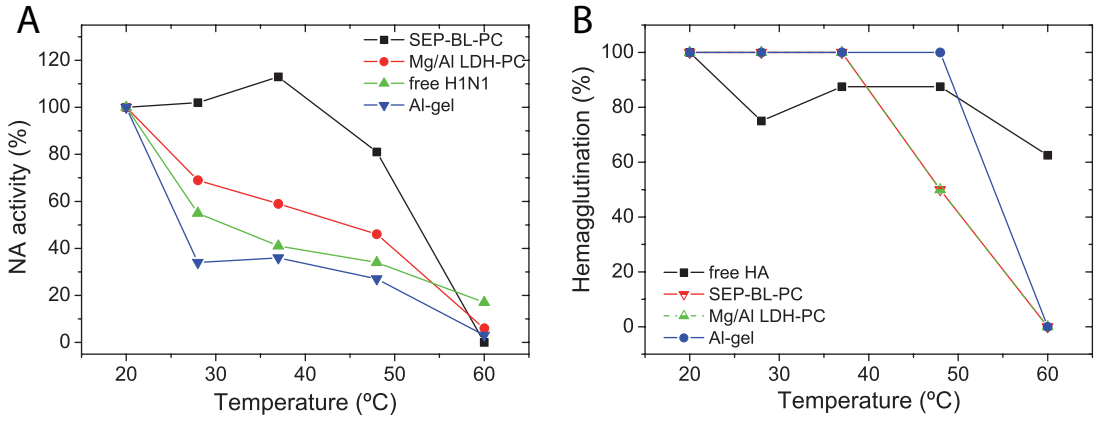

FIGURE 3.40: Thermal stability of immobilized H1N1 virus (A) and HA (B) assessed by NA activity and hemagglutination, respectively. The viral species were immobilized on SEP-BL-PC, Mg/Al LDH-PC, and $Al(OH)_3$ gel and compared to the thermal stability of the freely suspended species. The amount of immobilized H1N1 was 15 μg/100 μg solid or equivalent to 150 μg/ml free virus while 12 μg/100 μg HA were adsorbed corresponding to 120 μg/ml free HA.

The approach presented here to ensure thermal stability of the antigenic agent is a physical one and thus, deviates from other common methods, being based on adjustment of solution pH or surface ionization of the adjuvant / antigen pair by a mixture of adequate buffers. However, for many of these methods the applying mechanism is still not fully understood (Clapp et al., 2010).

Another property of great concern to vaccine manufacturers and physicians is the lyophilization behavior of the adjuvant / antigen system. It has been reported that aluminum based adjuvants can cause diminishment in antigenic activity related to aggregation of the solid and accompanied distortion of the antigen protein structure (Warren et al., 1986; Gupta, 1998). Therefore, the freeze-drying behavior of the two biohybrid adjuvants and $Al(OH)_3$

gel as control (all samples without virus) was investigated by FE-SEM microscopy (Figure 3.41) and by NA activity of samples with immobilized H1N2 virus after thawing and re-suspension (Figure 3.42).

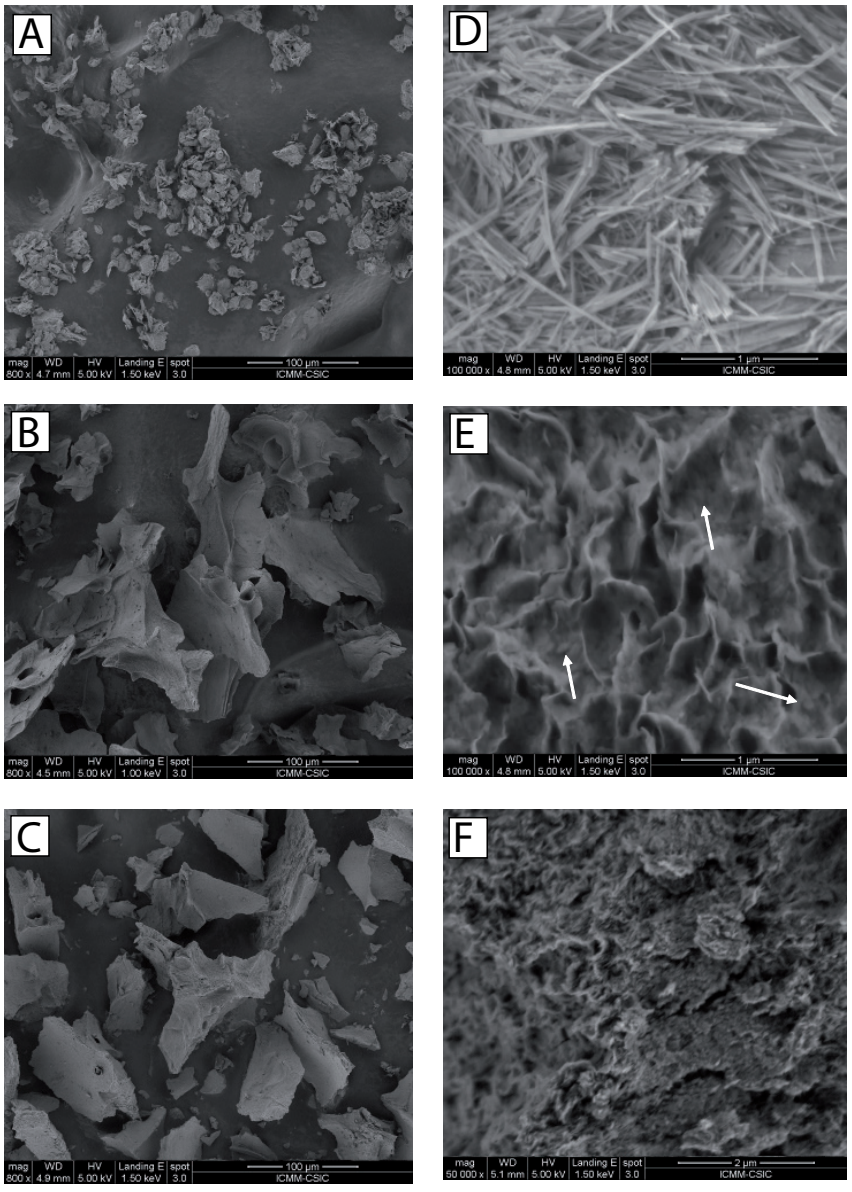

FIGURE 3.41: FE-SEM images of lyophilized SEP-BL-PC (A,D), Mg/Al LDH-PC (B,E), and $Al(OH)_3$ gel (C,F). The samples were prepared from 1 mg/ml suspensions in PBS.

The morphological characterization revealed agglomerates of SEP-BL-PC in the 10-25 μm range (Figure 3.41A and D). At higher magnification it becomes obvious that the sepiolite fibers are disperse and present as individuals. On the other side, both Mg/Al LDH-PC and $Al(OH)_3$ undergo severe aggregation with particle sizes up to 200 μm (Figure 3.41B

and C). The surface of $Al(OH)_3$ particles appears compact while the Mg/Al LDH-PC particles show a structured, cellular surface. At many points the presence of nanosized LDH platelets of about 50 nm can be observed (indicated by white arrows in Figure 3.41E). This could be important for the stabilized antigens.

The effect of lyophilization and subsequent thawing on the biological activity of Influenza virus is assessed by NA activity measurements of immobilized virus and compared to free virus in physiological solution. The NA activity is determined before and after the freeze-drying process, and therefore expressed as retained activity. As can be noticed from Figure 3.42, virus stabilized on SEP-BL-PC conserved ca. 80 % of its NA activity whereas the activity decayed to ≈45 % on both Mg/Al LDH-PC and $Al(OH)_3$. This result strongly suggests an influence of the aggregation behavior of the support on the immobilized antigenic compound. In this way, SEP-BL-PC, which agglomerates in relatively small units (Figure 3.41A), compromises little the biological activity of the virus. However, in

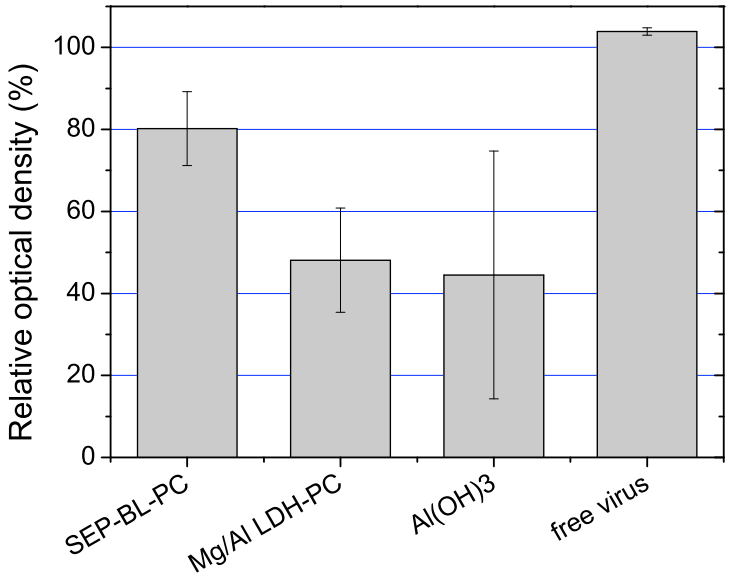

FIGURE 3.42: NA activity of immobilized H1N2 virus particles on thawed adjuvants after lyophilization. The activity is given in percentage of retained activity related to the initial activity before lyophilization. The virions were immobilized on SEP-BL-PC, Mg/Al LDH-PC, and $Al(OH)_3$ gel and compared to the NA activity of freely suspended virus that underwent the same thermal treatment. The amount of immobilized H1N2 virus was 20 μg/100 μg solid or equivalent to 133 μg/ml free virus.

accordance with the FE-SEM observations, the tendency to aggregate of Mg/Al LDH-PC and $Al(OH)_3$ might have distorted the protein structure of NA. Likewise, the conformation of HA may have been affected which could severely reduce its antigenic properties and therewith, diminish the immunogenic efficacy.

3.3.4 Immunization Test with Supported Viral Species

The efficacy of the sub-unit vaccines composed of HA is tested in an immunization test in mice. The antigen HA alone and together with flagellin (Fla) were immobilized on the sepiolite bio-nanohybrid SEP-BL-PC for this purpose. As negative control, BSA was adsorbed on the biohybrid in stead of HA. After two subcutaneous injections, mice were bled and virus-specific antibodies in the sera were measured by hemagglutination inhibition and ELISA. A more detailed description of the immunization and analysis procedures is provided in Appendix C. As anticipated, the negative control with BSA did not provoke the production of specific antibodies, whereas the HA sub-unite vaccine elicits high titers of the virus-specific antibody IgG1 which are indicative of protection efficacy (Hobson et al., 1973). This strongly suggests that the native conformation of the antigen is preserved which is important to ensure successful production of conformational antibodies (epitopos). Moreover, in the presence of the adjuvant Fla, the IgG1 titer was enhanced by a 100 %. These findings are also supported by results of the hemagglutination inhibition test that revealed a similar enhancement in serum titers (1/320 *versus* 1/160). Altogether, these observations demonstrate that the antigenic carrier SEP-BL-PC can accommodate other active immunostimulating molecules accompanying the antigens.

These promising results are currently promoting further investigation and *in vivo* assays, extending the range of carriers and immunogenic molecules.

3.3.5 Concluding Remarks

One of the mayor objectives of the work presented in this Section is the development of an adjuvant which could overcome certain limitations inflicted by particulate antigen carriers

such as aluminum containing systems. These are namely protein structure deformation induced by strong interaction of the antigen with the support and insufficient thermal stabilization.

Therefore, two clay-based biohybrids presenting a biomimetic lipid interface were prepared and explored in *in vitro* bioactivity assays and in immunization tests. The bioactivity examination showed no loss in NA activity of Influenza virus immobilized on these materials. Moreover, the NA activity was even superior to the one of $Al(OH)_3$ supported virus. This result is believed to be associated with the lipid membrane that afforded sufficient biocompatibility and modulated support / antigen interactions. A further manifestation of the good host properties of the tested materials is provided by a thermal stability study which revealed enhanced stability of immobilized virus on SEP-BL-PC. This observation is tentatively attributed to a physical mechanism that involves thermal insulation afforded by the clay fibers. Moreover, SEP-BL-PC demonstrated good lyophilization properties in comparison to the other two solids which is revealed by a lower degree of agglomeration. Based on the findings from NA activity measurements, this quality is thought to be advantageous for the preservation of antigenic activity of immobilized vaccines. Additionally, the good dispersion behavior of sepiolite fibers may also contribute to more homogeneous mixtures obligatory for aliquatation of vaccine formulations.

An advantage of the tested Mg/Al LDH-PC biohybrid is that this material class is safe, non-toxic, biocompatible and can be dissolved by the organism, making it biodegradable. This property is highly valued in adjuvant science making the vaccination more compliant for the recipient.

The HA based sub-unit vaccine prepared on the sepiolite-biohybrid has been tested in an immunization assay in mice and revealed a strong induction of Influenza virus specific sera antibodies. The co-adsorption of the adjuvant Fla enhanced the immunization by a factor two. These results emphasize the suitability of the sepiolite-biohybrid as potential adjuvant in Influenza vaccination.

3.4 Biomimetic Lipid-Based Thin Films

Biomimetic thin films such as supported hybrid bilayers are an interesting development of the bilayer lipid membrane (Plant, 1999; Richter et al., 2006; Mechler et al., 2009). The two halves of the membrane may consist of different (bio)-surfactants and held together by hydrophobic interaction of the hydrocarbon chains facing each other. This concept can provide enhanced versatility in the design of functional interfaces and mimetism of biological surfaces. Illustrative examples are genetic biochips (Xu et al., 2003) or hybrid red blood cell membranes (Hubbard et al., 1998b). Typically, the anchoring bottom leaflet consists of alkane thiols or silanes, which provide strong covalent adsorption on metal or silica/silicate surfaces, respectively. The resultant configuration is designated as self-assembled monolayer (SAM) which presents a hydrophobic surface. The upper leaflet can be constituted of biosurfactants to introduce specific functionalities to the surface. Especially those of natural origin such as lipids (Menger et al., 2005), glycolipids, lipopolysaccharides (Gharaei-Fathabad, 2011), or lipopeptides (surfactin) (Deleu et al., 1999) are frequently used. Other biocompatible surfactants are sugar-based surfactants (SBS), DNA-surfactants, or full peptide surfactants (Molina-Bolivar and Carnero Ruiz, 2009; Lu et al., 2007).

Based on promising results from mixed phosphatidylcholine/octyl-galactoside (PC-OGal) biointerfaces on sepiolite, this concept was extended to the planar surface of muscovite mica. This is due to a twofold reason: Firstly, the flat surface of mica provides the possibility for the application of surface sensitive techniques such as atomic force microscopy (AFM), X-ray photoelectron spectroscopy (XPS), or dynamic contact angle measurements for a detailed study of the layer formation process which are in case of the sepiolite particles less applicable. Secondly, the external surface of the crystalline structure of mica sheets is identical with the hexagonal SiO_4 sheets of the external ribbons of sepiolite (and other phyllosilicates). The major difference, however, is the minor content in silanol groups in case of the mica surface. This circumstance offers the possibility to study whether these particular surface groups influence or not lipid adsorption on silicate clays.

Octyl-galactoside containing hybrid biofilms are also prepared on a gold surface using 1-octanethiol (Othiol) as substitute for phosphatidylcholine as surface anchoring entity. The resultant Othiol-OGal biofilm is applied in an impedimetric biosensor specific to subtypes of the Influenza virus. The specificity of the conceived sensor lies in the affinity of sialic acid groups for specific virus membrane proteins (hemagglutinin). The incorporation of these sialic acid molecules occurs *via* sialylation of galactoside residues with the corresponding transferase enzymes. This process makes clear the reason for the employment of this particular biosurfactant in the hybrid membrane.

The employed virus sensing technique is electrochemical impedance spectroscopy (EIS) (Guan et al., 2004), which can detect slightest changes in impedance of an electrode surface caused by virus adsorption.

3.4.1 Lipid-based Films on Mica

In the preparation of the mixed PC-OGal bilayer on mica, the bottom PC monolayer was formed according to a protocol reported by Simonsen and Bagatolli (Simonsen and Bagatolli, 2004) and described in Section 2.2.1c. The PC leaflet was obtained by the deposition of a PC multilayer from a hexan/methanol solution and subsequent hydration and removal of the upper layers leaves a monolayer behind. Figure 3.43 depicts topographical AFM images of the multi- and monolayer structures. The line scan of the multilayer sample shows typical steps with heights as multiplies of ≈2 nm, being comparable to the monolayer thickness of PC (Oberts and Blanchard, 2009). The root mean square (RMS) of the roughness is 2.8 nm. After the hydration step, the RMS value drops to 0.6 nm, emphasizing that the surface has become smooth on a large scale. For comparison, the bare mica surface shows a RMS value of 0.5 nm.

The next step comprises the adsorption of OGal molecules that constitute the outer leaflet. Water contact angle measurements are performed to follow the change in surface hydrophilicity. Table 3.10 reports the contact angle values. The data clearly shows the changes in surface hydrophilicity along with the interfacial modifications. Bare mica has

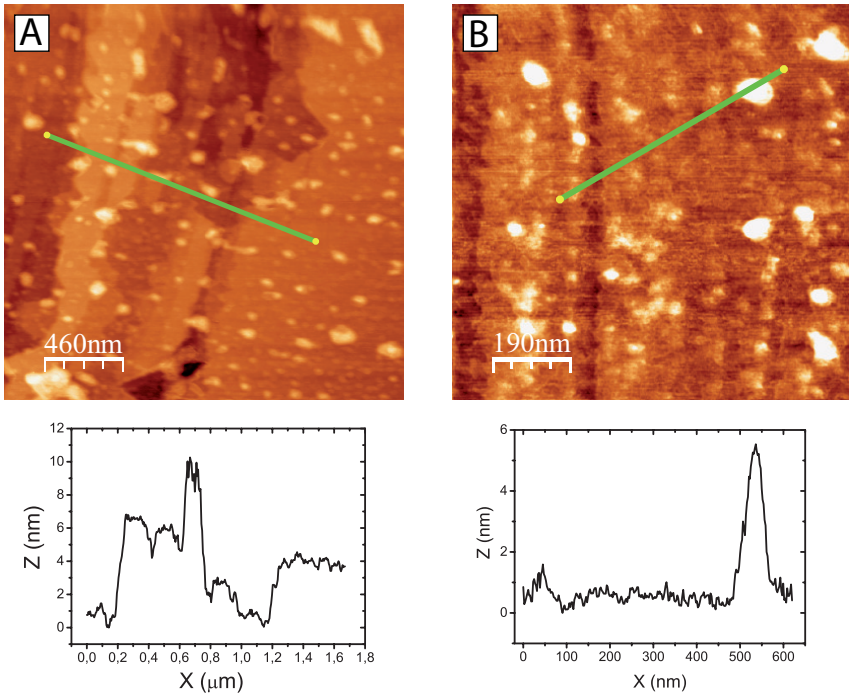

FIGURE 3.43: Topographical AFM images of PC multilayer (A) and monolayer (B) supported on mica. Line scans and the corresponding profiles are also presented.

the lowest contact angle, attributed to its high hydrophilicity and wetting properties related to the abundant presence of surface hydroxyl groups (Maslova et al., 2004). The PC multilayer reveals a contact angle value typical for lipid layer configurations where headgroups are present at the solid/liquid interface (Oberts and Blanchard, 2009). The subsequent hydration step results in a considerable increase in hydrophobicity (69°), suggesting the presence of hydrocarbon chains at the solid/liquid interface. The measured value is comparable to other contact angle data obtained for PC monolayers on silicate surfaces (Phang and Franses, 2006). By contrast, thiol or silane SAMs present water contact angle values above 110° (Bain et al., 1989), indicating a higher degree of hydrophobicity than in case of lipid monolayers. Phang and Franses provided a possible explanation based on penetration of water molecules into the lipid monolayer and hydrating the polar headgroup (Phang and Franses, 2006). Additionally, single-chained,

	bare mica	PC multilayer	PC monolayer	PC-OGal
Contact angle [°]	13 ± 3	34 ± 3	69 ± 3	45 ± 1

TABLE 3.10: Dynamic water contact angle values of the bare mica surface and supported PC and PC-OGal films.

chemisorbed SAMs such as alkane thiols are usually more densely packed which impedes water penetration (Bain et al., 1989). Finally, the incubation in OGal solution increased again the surface wettability, evidenced by a reduced contact angle of 45°. Interfacially arranged galactoside residues are considered to be responsible for this alteration as they are polar and hydrophilic groups (Molina-Bolivar and Carnero Ruiz, 2009).

Further support for the presumed interfacial modifications was provided from X-ray photoelectron spectroscopy (XPS). Figure 3.44 shows survey scans and high resolution spectra of the PC multilayer, the PC monolayer and the mixed PC-OGal bilayer samples.

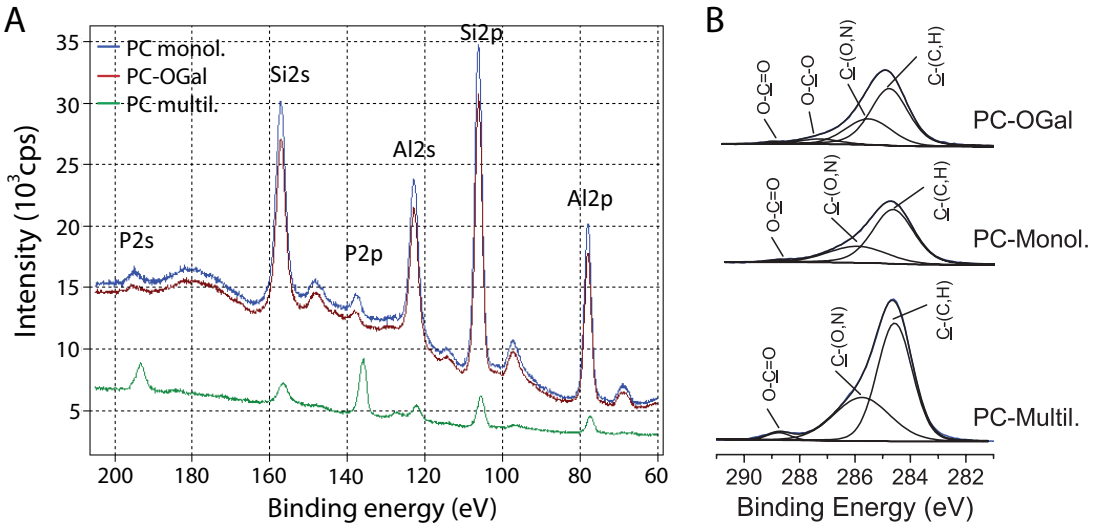

FIGURE 3.44: XPS survey scans (A) and C1s (B) core level bands from PC multilayer, hydrated PC layer and mixed PC-OGal layers supported on mica.

From the survey scan of the PC multilayer sample it can be noticed that the Al2s, Al2p, Si2s, and Si2p bands are significantly attenuated as compared to the other two samples. These bands are assigned to Al-O and Si-O bonds of the crystal structure of the mica support (Liu and Brown, 1998). The attenuation is presumably associated to the presence of a relatively thick lipid layer, hampering the escape of photoelectrons from the underlying Al and Si atoms. On the other side, bands designated to the presence of phospholipids, N1s, P2s and P2p, are more intense for the multilayer sample.

After the hydration step, the P2s and N1s band intensities diminish while the structural mica bands increase in intensity. This leads to the assumption that a significantly thinner

lipid layer has been formed. Incubation with OGal attenuated again the Al and Si bands as well as the P2s and N1s bands. This behavior can be rationalized by the addition of an OGal layer, attenuating the bands of both PC and mica.

Further evidence is gained from carbon C1s core level spectra (Figure 3.44B). The multilayer configuration yields the most intense band whereas the hydrated layer has the weakest peak. Incubation with OGal increases again the C1s intensity, indicating the addition of OGal. The presence of OGal molecules is also verified by deconvolution of the C1s band of the PC-OGal sample. This analysis reveals at 287.6 eV the hemiacetal group O-C-O of the galactose ring (Gerin et al., 1995). Other observed components are the O-C=O function (289.0 eV) of the esterified glycerol backbone of the PC molecule, C-(O,N) (285.5 eV) which attributable to the choline moiety of the PC headgroup, and C-(C,H) (284.6 eV) (Benavente et al., 2011).

Together, the surface analysis data confirm the presence of OGal groups at the surface of the mixed layers. Figure 3.45 illustrates the assumed interfacial layer configurations along the preparation of the mixed PC-OGal layer on mica. These results from the mica based system helped to characterize this layer configuration more precisely than it would have been possible from the particulate sepiolite system.

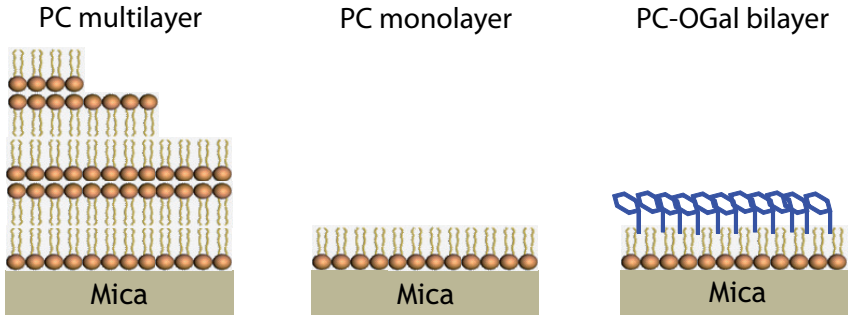

FIGURE 3.45: Illustration of PC multilayer, PC monolayer, and mixed PC-OGal layer supported on mica.

Moreover, the obtained analytical data confirm stable adsorption of PC molecules on the mica surface in spite of the lower quantity of silanol groups as compared to the sepiolite surface. The mica surface consists of an hexagonal arrangement of SiO_4 tetrahedrons

with apical oxygen atoms at the surface. These atoms are polarized and may induce ion-dipole interactions with the cationic $N^+(CH_3)_3$ group of the lipid headgroup.

3.4.2 Biomimetic Thin Films Applied in Influenza Virus Biosensors

The approach of mixed lipid/octyl-galactoside bilayers was employed in the preparation of an impedimetric *affinity biosensor* for the selective detection of different subtypes of the Influenza virus. The incorporation of the Influenza virus *receptor* sialic acid gives rise to specific *ligand-receptor* affinity adsorption of the distinct subtypes (Wiley and Skehel, 1987; Stephenson et al., 2003). Influenza virus subtypes are amongst others classified by the antigenic characteristics of specific hemagglutinin proteins at their membrane surface, acting as *ligands* for sialic acid. The resultant electrode surface resembles therewith the surface of erythrocytes or cell membranes of the upper respiratory tract, presenting sialic acid moieties that are linked to galactose terminals of glycoproteins (Figure 3.46) (Traving and Schauer, 1998; Schauer, 2000). These sialic acid groups are responsible for the high specificity of these cells toward different hemagglutinin subtypes based on ligand-receptor reactions (Stephenson et al., 2003).

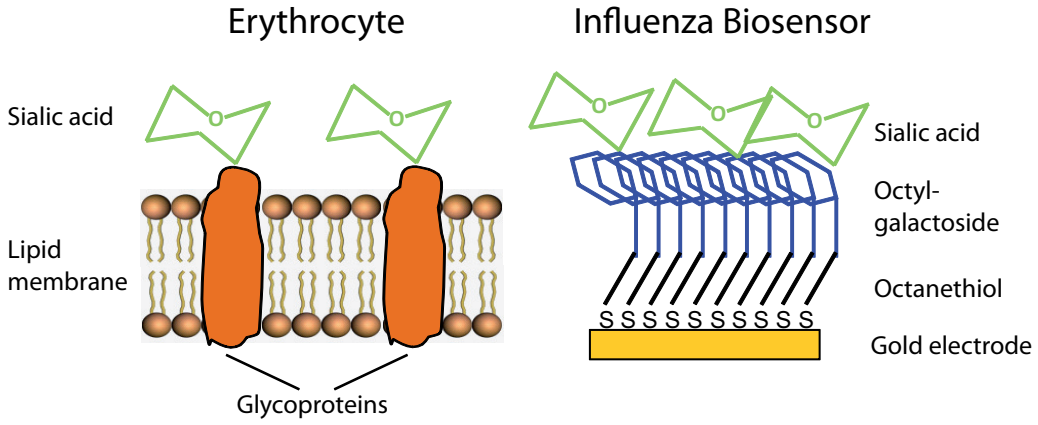

FIGURE 3.46: Schematic of an erythrocyte membrane and a mixed Othiol-OGal film supported on a gold electrode surface presenting sialic acid groups.

The employed sensing method is based on electrochemical impedance spectroscopy. Therefore, the concept of mixed bilayers had to be transfered onto a gold electrode surface to provide electrical conductivity. 1-Octanethiol (Othiol) was used as substitute for the phosphatidylcholine bottom leaflet as this compound is known to form close-packed self-assembled monolayers (SAM) on gold (Bain et al., 1989). The assembly of the upper

leaflet (octyl-galactoside), giving eventually rise to a hybrid Othiol-OGal bilayer, can be accomplished by two distinct approaches: i) By adsorption onto a previously formed Othiol SAM, denoted as *sequential* formation process, or ii) by *simultaneous* self-assembly from a solution containing the two compounds (Figure 3.47).

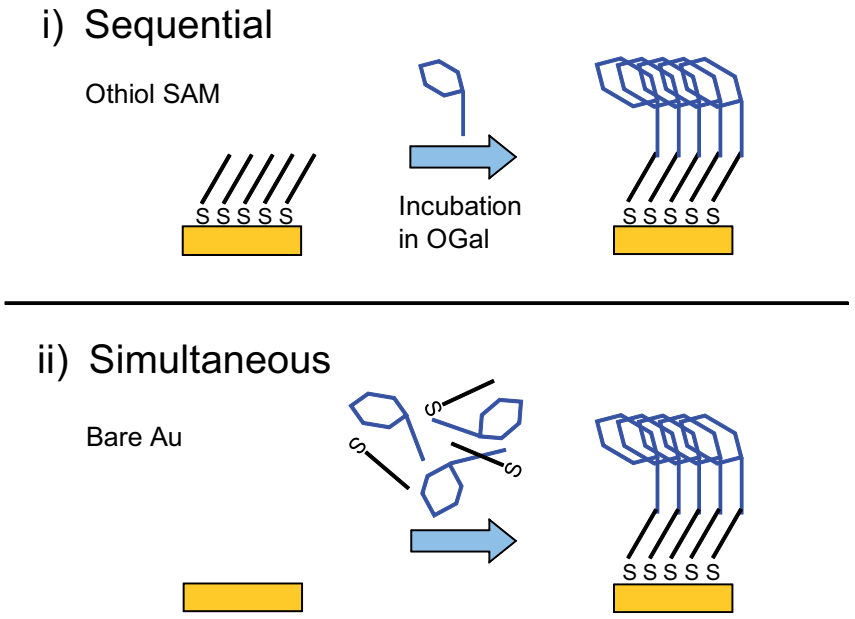

FIGURE 3.47: Scheme of self-assembly approaches for the preparation of mixed Othiol-OGal films. (i) Depicts a sequential formation process and (ii) shows the simultaneous self-assembly from a 1-octanethiol/octyl-galactoside solution. The resultant bilayer arrangement is drawn in idealized fashion.

In the latter case, the bottom Othiol monolayer is anticipated to be formed preferentially due to the strong specific interaction between the sulfur atoms and the gold surface (Nuzzo et al., 1987). This might overrate possible OGal deposition since it is known that glucose, for instance, shows only weak adsorption on gold (Wu et al., 2006). The layer formation processes were investigated by electrochemical impedance spectroscopy (EIS), cyclic voltammetry (CV), water contact angle measurements, atomic force microscopy (AFM), and X-ray photoelectron spectroscopy (XPS). An estimate of the quantity of adsorbed sugar-based surfactant was assessed with the phenol-sulfuric acid method.

3.4.2.1 Characterization of the Self-Assembly Process of 1-Octanethiol / Octyl-Glucoside Hybrid Bilayers on the Gold Surface

Optimization and characterization experiments were for economic reasons carried out with octyl-glucoside (OGlu) instead of octyl-galactoside (OGal). This is under the assumption that OGal and OGlu show the same adsorption behavior owing to the fact that both surfactants have similar solubility and critical micelle concentration (CMC) values (16 and 20 mM, respectively (Matsumura et al., 1990)). The characterization study was conducted in close cooperation with the group of Dr. C. Fernández-Sánchez from the CNM-IMB (CSIC) in Barcelona (Spain) and experiments were performed in complementary manner. In this way, the 1-octanethiol desorption experiments and the EIS recordings of OGlu adsorption as function of incubation time and concentration were performed by Dr. C. Fernández-Sánchez and conceded with courtesy.

i) Sequential *versus* Simultaneous Layer Formation

The evaluation of the layer formation methods was conducted in a rather preliminary study utilizing home-made gold disc electrodes encapsulated in glass. The formation of the mixed bilayer was studied by EIS and CV using the $Fe(CN)_6^{4-/3-}$ redox couple as electrochemical probe. In the simultaneous method, the molar Othiol/OGlu ratio was 1/4 while the layers in the sequential approach were prepared from immersion in 1 mM Othiol for one day and subsequent incubation in 5 mM OGlu for three days. The incubation time was one day for the simultaneous approach.

The Nyquist plots (Figure 3.48) were fitted to a simple Randles equivalent circuit model which helps to interpret the obtained spectra. In this model, the capacitance is introduced as constant phase element (CPE) which accounts for non-ideal capacitive behavior arising from surface roughness and layer imperfections (Mendes et al., 2004). The CPE contains contributions both from the capacitance of the formed organic layer and the electric double layer. The fitting also renders values for the charge transfer resistance R_{ct} which is related to the diameter of the semi-circle of the spectrum. This value reflects the barrier properties of surface layers which may hamper the transfer of charges from the

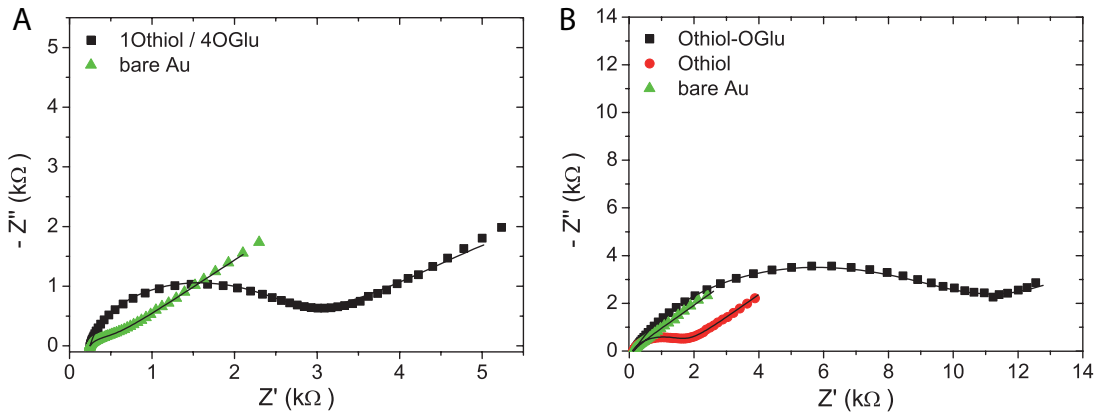

FIGURE 3.48: Nyquist diagrams (Z' vs. Z") from the impedance measurements of hybrid Othiol/OGal bilayers prepared by simultaneous (A) and sequential (B) self-assembly. Impedance measurements were performed in 2 mM $Fe(CN)_6^{4-/3-}$ solutions prepared in 0.1 M KNO_3. The solid lines represent the fittings to the Randles equivalent circuit.

bulk solution to the electrode surface and can easily be probed with a redox pair such as $Fe(CN)_6^{4-/3-}$.

The bare Au surfaces yield almost straight capacitive lines, typical for metal conductors. The simultaneous surface modification with Othiol and OGlu gives rise to increased charge transfer resistance, manifested in the semi-circular shape of the Nyquist plot (Figure 3.48A). At the same time, CPE is decreasing (Table 3.11) which indicates the capacitive character of the formed organic layers. In the sequential approach the relative charge transfer resistance $R_{ct}(layer)/R_{ct}(blank)$ increased with each deposited layer. Compared to the simultaneous formation process, the relative R_{ct} value of the Othiol-OGlu bilayer

Surface	R_{ct} [Ω]	rel. R_{ct} [-]	surface coverage [%]	CPE [μF]
sequential:				
bare	140	-	-	1.3
Othiol	1358	9.7	89.7	0.23
Othiol-OGlu	9536	68.1	98.5	0.28
simultaneous:				
bare	274	-	-	1.75
Othiol-OGlu	2210	8.1	87.6	0.08

TABLE 3.11: R_{ct} and CPE data obtained from fitting of EIS spectra to a Randles equivalent circuit model. The goodness factor chi-square of the fitting was in all cases below 0.04. The spectra were recorded of sequentially and simultaneously prepared mixed 1-octanethiol/octyl-glucoside bilayers on a gold electrode surface.

was found to be higher in the sequential layer formation approach. High R_{ct} values are generally indicative of densely packed surface layers hampering the transfer of charges (Ding et al., 2005). Decreasing CPE on the other side can be related to increasing thickness of the deposited layers according to $C = \epsilon\epsilon_o A/d$, where C is the capacitance, ϵ is the dielectric constant of the surface layer, ϵ_o is the permittivity of the free space, A is the electrode area, and d is the layer thickness (Wang, 2000). Altogether, the results led to the assumption that the sequential approach yielded a more close-packed layer. In the simultaneous method, the presence of OGlu at the electrode interface might disturb the Au-S bond formation during Othiol adsorption. As a consequence, layers of lower degree of order and alignment might be formed. This hypothesis might also be reflected in the surface layer coverage θ of the various layers which can be estimated as $\theta = 1 - R_{ct}(bare)/R_{ct}(layer)$ (Shervedani et al., 2006) (Table 3.11). The simultaneous method only rendered a coverage of 87,6 % while the sequential approach yielded a densely packed bilayer of 98,5 %. Therefore, the sequential method was chosen for further investigation using smooth, white-room prepared polycrystalline gold electrodes.

With such an electrode, voltammetric measurements of sequentially prepared Othiol-OGlu bilayers were performed. Figure 3.49 shows the cyclic voltammograms of the corresponding interfaces. On bare Au, a well-defined, characteristic wave of the $Fe(CN)_6^{4-/3-}$ redox couple is recorded. The layer formation changes the wave to the characteristic capacitive shape of an electric double layer. The reason is that the organic layers are sufficiently dense to act as electron barriers. This is reflected in voltammograms by decreasing peak currents (Ding et al., 2005). In accordance to that, it can be observed that the double layer current decreases stepwise during the sequential bilayer formation which is in agreement with the above obtained EIS data.

ii) Variation of Incubation Time

Another important parameter in self-assembly processes is the incubation time. Therefore, octanethiolated gold chips were immersed in 5 mM OGlu for 2, 6, 16, 24, and 72 hours. The amount of adsorbed OGlu was estimated with the phenol-sulfuric acid method. In this protocol, concentrated H_2SO_4 dissolves the organic layers and hydrolyzes

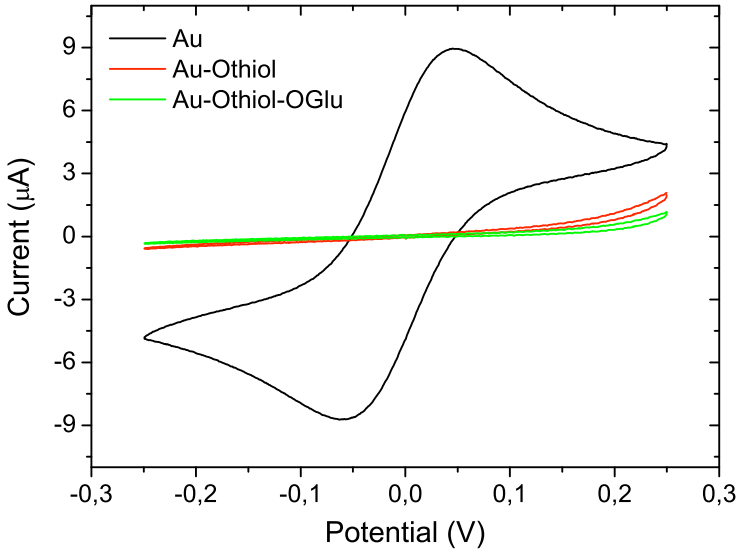

FIGURE 3.49: Cyclic voltammograms of a bare Au surface, a Othiol SAM and a mixed Otiol-OGlu bilayer. The layers were prepared from 1 mM Othiol solution and subsequent immersion in 5 mM OGlu solution. Voltammetric measurements were performed in 2 mM $Fe(CN)_6^{4-/3-}$ against Ag/AgCl.

the glucose moiety of the OGlu molecules. The reaction with phenol results in a color evolution which can be detected photospectroscopically at 477 nm wavelength. Comparison with a calibration curve yields the amount of dissolved OGlu which correlates to the quantity of previously adsorbed OGlu. However beforehand, the phenol-sulfuric acid method was applied to Othiol-OGlu modified electrodes and EIS measurements with these electrodes showed that sulfuric acid could strip off all surface layers and hence, ensuring that all absorbed OGlu molecules were available for the reaction with phenol (Figure D.1 in Appendix D). Eventually, the amount of dissolved OGlu from the gold chips as function of incubation time is shown in Figure 3.50A. It can be observed that during the first 24 hours the adsorbed OGlu quantity remained constant while after 72 hours the OGlu content increased significantly. This is a rather uncharacteristic behavior, as self-assembly of sugar-based surfactants on hydrophobic surfaces is generally a fast process due to large hydrophobic interaction (Waltermo et al., 1996).

Advancing water contact angle measurements were performed to investigate the change of surface hydrophobicity during the subsequent layer depositions (Figure 3.50B). The

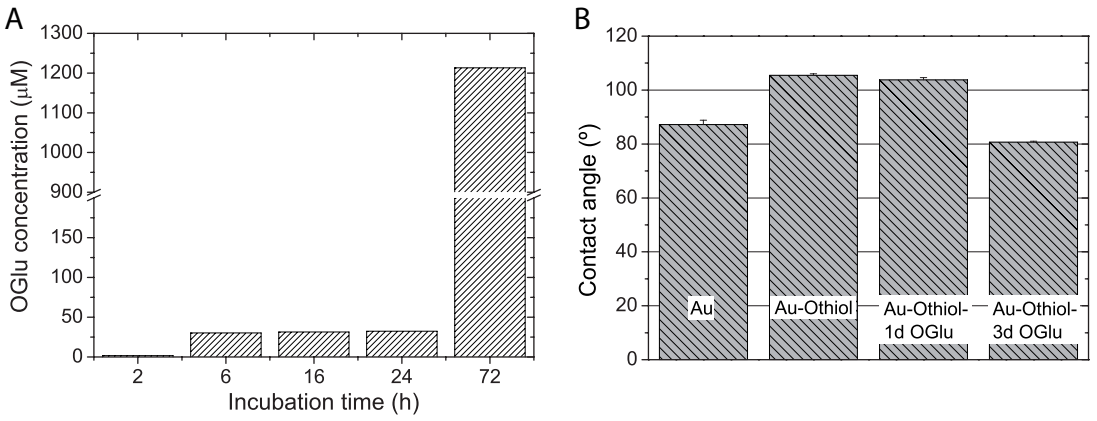

FIGURE 3.50: Concentration of dissolved OGlu according to the phenol-sulfuric acid method (A). The liberated OGlu had been previously adsorbed on octanethiolated gold chips after incubation in 5 mM OGlu for 2, 6, 16, 24, and 72 hours. Advancing water contact angle measurements (B) on a bare Au surface and octanethiolated gold chips incubated in 5 mM OGlu for 1 and 3 days.

contact angle on Au increased from 85 to 106 ° after the Othiol SAM formation. This value is comparable to reported data of 1-octanethiol SAMs (Bain et al., 1989). After one day incubation in 5 mM OGlu solution the contact angle decreased only marginally but three days incubation resulted in a substantial decay to 81 °. Waltermo and co-workers measured a water contact angle of 85 ° after OGlu adsorption (from 5 mM) on hydrophobized mica (Waltermo et al., 1996) which is a value in good agreement with the data obtained in the present work. The drop in surface hydrophobicity is assumed to be related to an increased amount of glucose headgroups at the solid/liquid interface which renders the surface more hydrophilic. This reasoning seems to be supported by the OGlu concentration data, also indicating an elevated OGlu content after three days of incubation.

OGlu adsorption as function of the incubation time was also investigated by impedance measurements. Octanethiolated gold electrodes were immersed in 5 mM OGlu solution for 1, 2 and 5 days. The Nyquist plots are presented in Figure 3.51 and fitting to the Randles equivalent circuit model provided the corresponding R_{ct} and CPE values which are reported in Table 3.12.

It is apparent that the relative R_{ct} decreased with extended OGlu incubation even though the absolute $R_{ct}(OGlu)$ was always above $R_{ct}(Othiol)$. At the same time, the CPE value

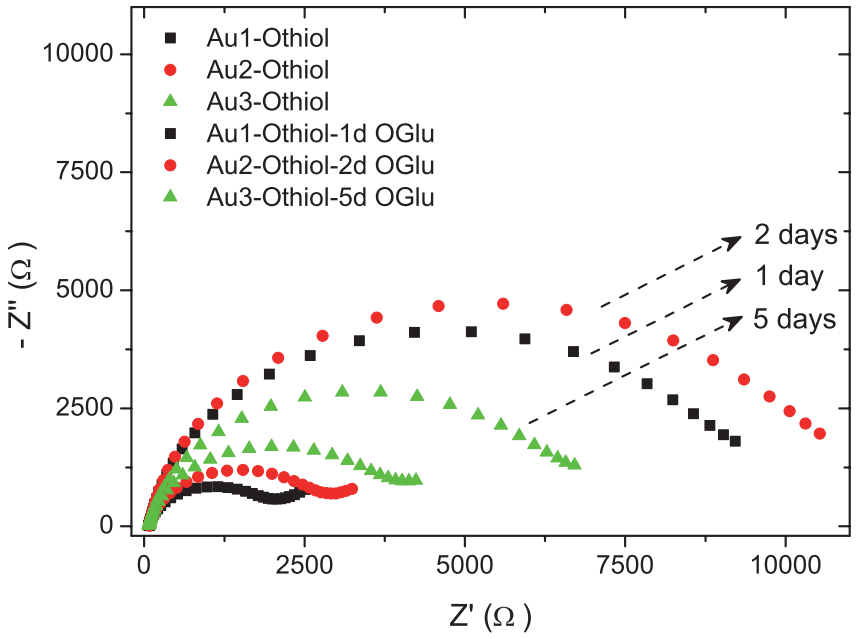

FIGURE 3.51: Nyquist diagrams (Z' vs. Z") of thiolated gold electrodes that were incubated in 5 mM OGlu for 1, 2, and 5 days. The impedance measurements were performed in 2 mM $Fe(CN)_6^{4-/3-}$.

increases. This is indicative for reduced compactness of the formed Othiol-OGlu bilayer upon prolonged incubation.

In order to clarify whether Othiol molecules were replaced by OGlu or simply removed without substitution, voltammetric thiol desorption experiments were performed. Representative voltammograms are displayed in Figure 3.52A showing two characteristic cathodic peaks at -0.54 and -0.86 V which are attributed to the reduction of adsorbed Othiol molecules (Widrig et al., 1991). The corresponding electrode reaction can be expressed as

$$CH_3(CH_2)_7SAu + 1e^- \rightarrow Au(0) + CH_3(CH_2)_7S^- \tag{3.8}$$

Electrode / incubation time	R_{ct} [Ω]			CPE_{dl} [μF]	
	Othiol	OGlu	OGlu/Othiol	Othiol	OGlu
1 / 1 day	2026	9508	4.69	4.8	3.3
2 / 2 days	2855	10907	3.82	4.4	3.0
3 / 5 days	3999	6561	1.64	5.0	4.2

TABLE 3.12: R_{ct} and CPE data obtained from fitting of Nyquist plots to the Randles equivalent circuit model. The spectra were recorded of thiolated gold electrodes that were incubated in 5 mM OGlu for 1, 2, or 5 days.

Integration over the cathodic peaks yields the charge Q_{red} associated to the Othiol reduction. Knowledge of Q_{red} allows for the calculation of the surface coverage Γ with $\Gamma = Q_{red}/nFA$. Comparison to the theoretical surface coverage of long-chain n-alkanethiols ($7.6 \cdot 10^{-10}$ mol cm^{-2}) renders a percentaged surface coverage (Widrig et al., 1991). The results in Figure 3.52B demonstrate a decrease in Othiol surface coverage with increased immersion time. This observation suggests a damage of the initially formed 1-octanethiol SAM upon prolonged incubation. The fact that the absolute $R_{ct}(OGlu)$ value is still higher than $R_{ct}(Othiol)$ and CPE(OGlu) lower than CPE(Othiol) could indicate that the removed Othiol molecules were partially replaced by OGlu and thus, passivated the bared Au surface sites to some extent. This assumption is also consistent with the results from OGlu quantification and the water contact angle measurements which suggest elevated OGlu presence at the surface despite of the obvious Othiol SAM damage.

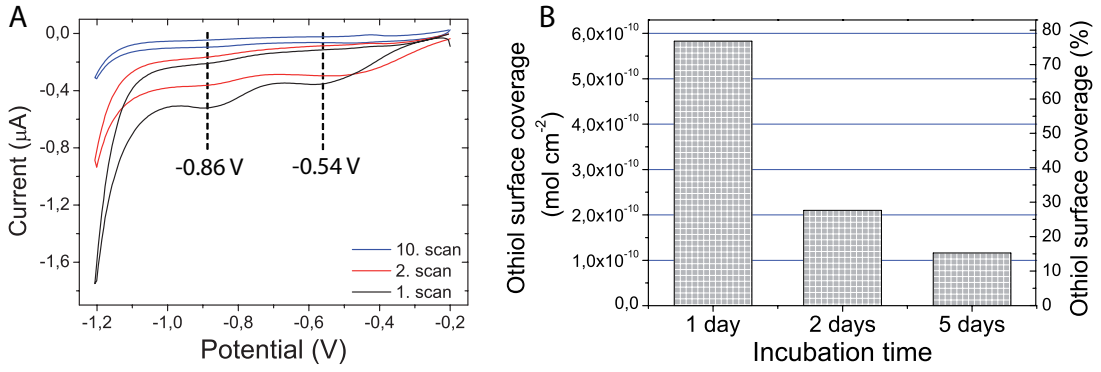

FIGURE 3.52: Cyclic voltammograms from Othiol desorption of hybrid Othiol-OGlu layers on gold electrodes (A). The CV measurements were performed in 2 mM $Fe(CN)_6^{4-/3-}$ against Ag/AgCl. The surface coverage of Othiol on Au electrodes as function of OGlu incubation time is shown in (B). These values were derived from integration of Othiol desorption peaks in cyclic voltammagrams of the first two scans. The layers were prepared by incubation in 5 mM OGlu for 1, 2, and 5 days.

iii) Optimization of Octyl-Glucoside Concentration

The next parameter under investigation is the OGlu concentration of the incubation solution. The concentration was varied between 0.5 and 5 mM. Octanethiolated Au electrodes were immersed in the various OGlu solutions for one day and EIS spectra were recorded to deduce the relative R_{ct} values (Figure 3.53A). The results show a slight rise in the relative R_{ct} for increased OGlu concentration even though the dispersion of the data is

quit high. 1-Octanethiol desorption experiments, however, revealed a decreased Othiol surface coverage at high OGlu concentrations (Figure 3.53B). This suggests that OGlu might replace Othiol molecules of the preformed SAM similar to previous observations regarding the incubation time. Contrary however is, that the relative R_{ct} values did not decrease upon Othiol substitution. This finding points to an enhanced passivation process possibly related to a high amount of adsorbed OGlu at elevated OGlu concentrations even though the underlying SAM is partially distorted. It should be adverted that the Othiol surface coverage is lowest for the 0.5 mM OGlu concentration. This stands somewhat contrary to the general observed trend. However, this series of experiments was carried out with a single electrode for each concentration and can therefore be an artifact of a defective electrode.

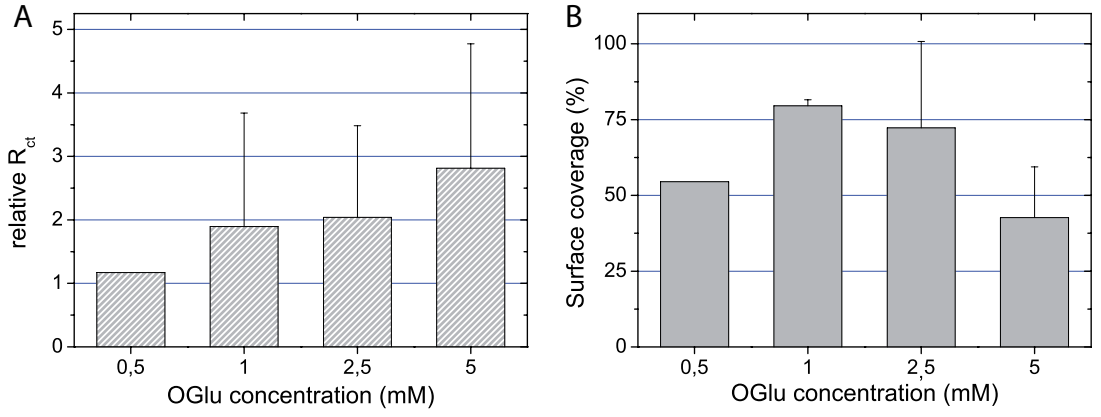

FIGURE 3.53: Relative R_{ct} (A) and Othiol surface coverage (B) of Othiol-OGlu modified gold electrodes as function of the OGlu concentration during incubation.

The final OGal concentration for the sialylation experiments was chosen as 5 mM. Additional support for this choice was provided from preliminary Influenza virus sensing tests. A higher signal was obtained for layers prepared from 5 mM OGal as compared to layers from lower OGal concentrations. It is assumed that the higher amount of immobilized OGal, at the expense of a partially disordered Otiol layer, allows for enhanced sialic acid adsorption which in turn is determinant for sensitive Influenza virus detection.

iv) Bilayer Characterization by Atomic Force Microscopy

Atomic force microscopy (AFM) was employed to examine the compositional homogeneity of the Othiol-OGal bilayer. For this purpose, topographic images with the corresponding surface roughness values (RMS) were collected together with a frequency shift image which can reveal variations in the chemical composition of the studied surface (Figure 3.54). The bare gold surface is reasonably smooth for being poly-crystalline and the RMS value is 2.6 nm. Upon formation of the Othiol SAM, however, the surface roughness increases to RMS = 3.0 nm. The next surface modification step is the deposition of the outer OGal leaflet. The topographic examination (Figure 3.54C) shows the disappearance of the crystalline grain structure and reveals a further rise in surface roughness (RMS = 3.5 nm). This tendency clearly confirms the successive deposition of the organic layers. On the other side, the domains of different contrast in the frequency image in Figure 3.54D indicate certain compositional heterogeneity of the bilayer even though the strongest contrasts are suspected to originate from imaging artifacts. The observed heterogeneity in AFM confirms therewith the already assumed defects upon bilayer formation as reasoned from the electrochemical characterization.

v) Proposed Bilayer Formation Model

A tentative model of the sequential Othiol-OGlu bilayer formation is proposed. In this model, both incubation time and OGlu concentration are the major determinants for the compactness and alignment of the bilayer. The highest amount of adsorbed OGlu is archived at prolonged incubation time and elevated OGlu concentration. Contrary to other reported works, the time to reach the equilibration amount of adsorbed OGlu takes very long (several days). This duration is shortened by increased OGlu concentration. It can be hypothesized that at low concentration or at short incubation times the OGlu molecules are adsorbed laying flat on the SAM aiming to maximize the hydrophobic interactions. The increment in concentration or time leads to a higher amount of OGlu molecules at the interface which gives rise to gradual uprise of the molecules in order to reach a higher degree of packing density (Zhang et al., 1997). However, the preformed

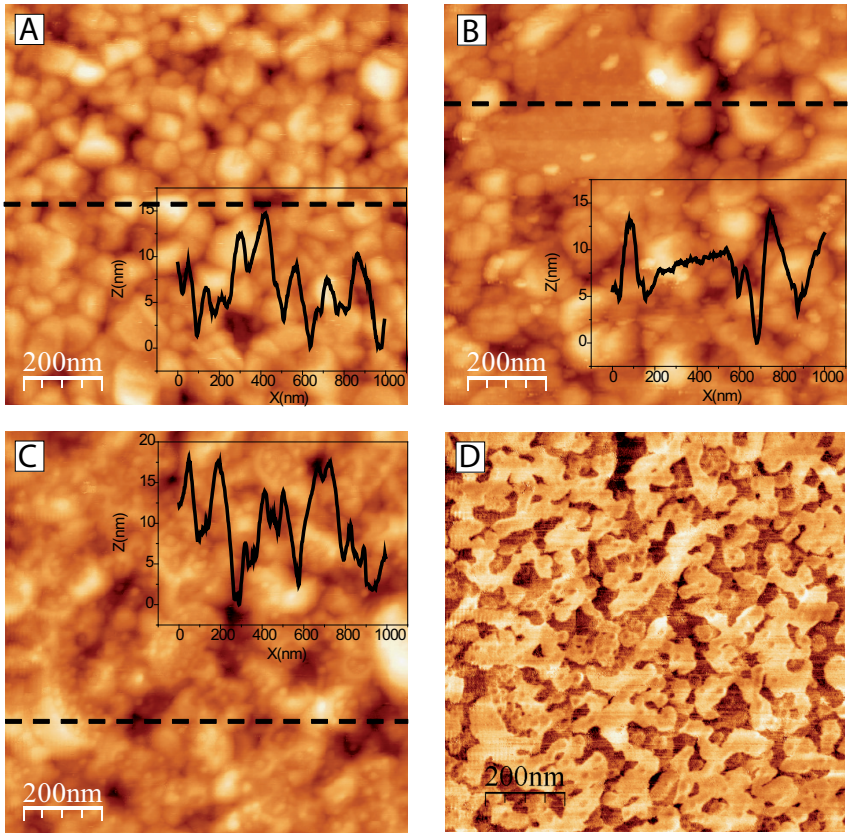

FIGURE 3.54: Topographic AFM images of the bare gold surface (A), the Othiol SAM (B), and the Othiol-OGal bilayer (C) as well as a frequency shift image of the bilayer (D). The topographic profiles of the various cross-sections are provided. The AFM imaging was conducted in dynamic, non-contact mode.

Othiol SAM is found to be most distorted exactly under these conditions. The incorporated OGlu molecules are capable to displace and at least partially passivate the electrode surface.

As for a hypothesis, it is known that OGlu is a good solubilization agent for proteins and other delicate biological molecules (Stubbs et al., 1976). However, it remains surprising that OGlu is strong enough to distort a covalently bound alkanethiol SAM. Nevertheless, it is also known that short chain alkanethiols ($n < 10$) form more defective and less compact SAMs which consequently are even prone to desorption (Bain et al., 1989). This may allow the intercalation of OGlu molecules into the Othiol SAM and even permit access to the gold surface where they eventually may replace Othiol molecules. This assumption is also supported by experiments where the SAM was formed with 1-dodecylthiol that gives rise to more compact layers. It has been noticed that the amount of adsorbed

OGal molecules was significantly below the quantity that adsorbed on a 1-octanethiol SAM (data not shown). Therefore, these findings can be interpreted that OGal interpenetration was impeded on the 1-dodecylthiol SAM while the higher OGal content on the 1-octanethiol SAM should be due then to intercalation. This might also explain to some degree the passivation of the Au surface by the OGlu molecules. A refined representation of the Othiol-OGlu bilayer formation process is depicted in Figure 3.55.

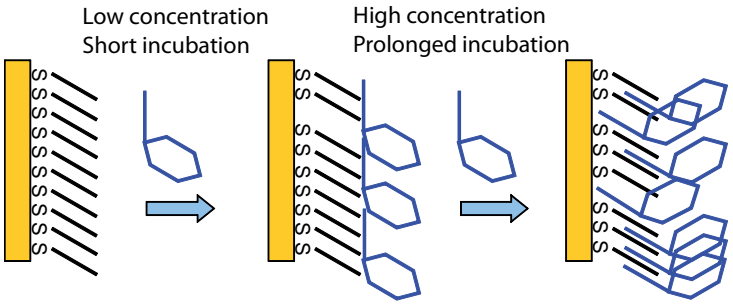

FIGURE 3.55: Scheme of the formation process of a mixed Othiol-OGlu bilayer based on the proposed model as conclusion of the experimental findings.

3.4.2.2 Sialic Acid Functionalization of the Othiol-OGal Interface

Mixed Othiol-OGal bilayers on gold chips (one day incubation in 5 mM OGal) were sialylated using a sialyltransferase (SAT) enzyme which bonds sialic acid (SA) molecules to the galactose groups. The sialylation in this study was according to a standard protocol comprising incubation at 37 °C for 4 h in 160 μg/ml α-2,6 SAT and 703 μg/ml CMP that is the SA containing substrate. X-ray photoelectron spectroscopy (XPS) was employed to verify the presence of α-2,6 linked sialic acid molecules by examining the photoelectron bands of C1s, O1s and N1s. The sialylation with α-2,3 SAT was studied by carrying out a Western Blot (WB) assay.

Figure 3.56 shows the survey scans of the α-2,6 SA terminal surface together with the underlying Othiol and OGal layers for comparison. The survey confirms that all expected elements are present. Deconvolution of the C1s band revealed components at 288.9 eV, 287.2 eV, and 285.7 eV which can be attributed to $\underline{C}OO^-$, $\underline{C}$=O, and $\underline{C}$-N functions (Gerin et al., 1995), respectively, which are only present in the sialic acid molecule. The

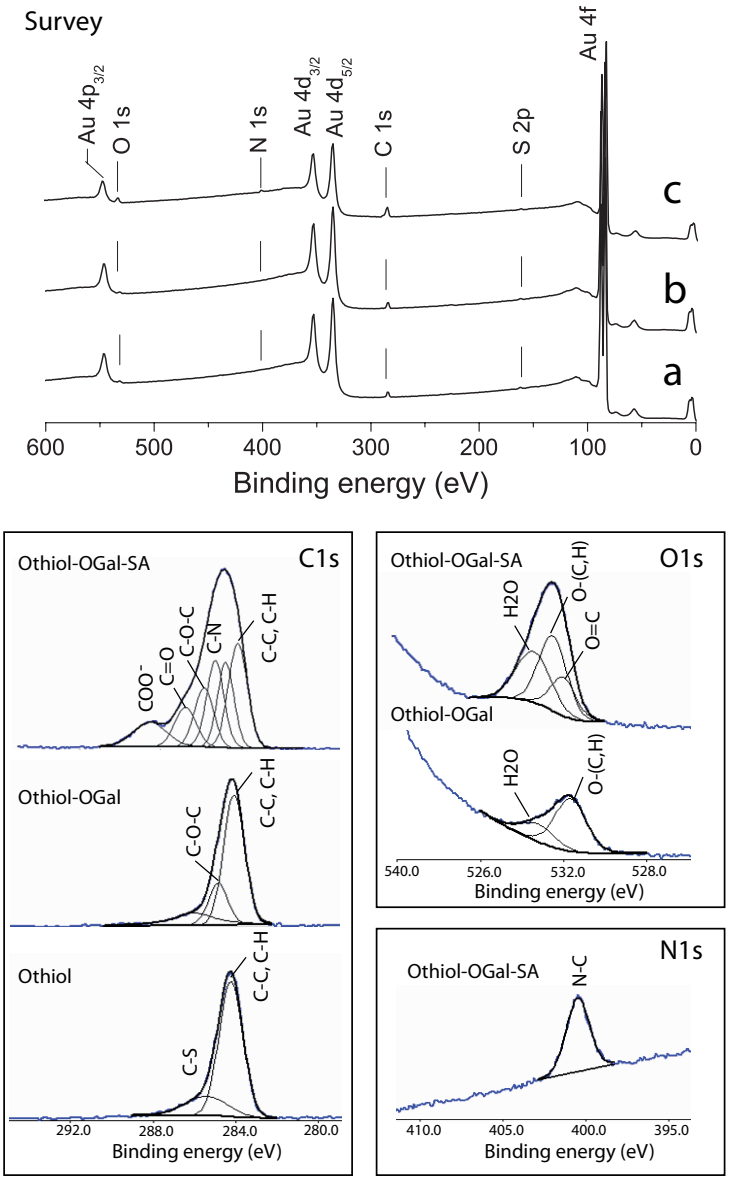

FIGURE 3.56: XPS survey scans and deconvoluted core level bands of C1s, O1s, and N1s photoelectrons emitted from self-assembled Othiol (a), Othiol-OGal (b), and Othiol-OGal-SA (c) layers which were prepared on Au chips. Peak deconvolution was performed with 90 % Gaussian / 10 % Lorentzian peak shapes and the baseline was adjusted with the Tougaard model. The chi-square value was always below 0.1 for all deconvolutions.

underlying OGal and Othiol molecules contribute with bands at 286.5 eV (acetal group), at 284.6 eV (C-(C,H)), and at 285.8 eV attributed to the thiol group C-S of Othiol. The N1s band at 400.5 eV revealed the presence of unprotonated amine groups (Gerin et al., 1995), attributable to the neuraminic acid moiety of the sialic acid molecule. Nitrogen has not been detected in the underlying Othiol-OGal bilayer, confirming SA as only source

of the observed N1s band. The deconvolution of the O1s peak reveals a band at 531.2 eV which is attributed to carboxylic acid functions (O=C) (Gerin et al., 1995) and is therefore associated to the presence of the sialic acid moieties. Furthermore, the O1s peak from the OGal terminated surface is decomposed into a band at 533.4 eV (H_2O molecules) and at 531.8 eV that can be associated to hydroxyl (C-OH) and acetal (C-O-C) functions of the galactose ring (Gerin et al., 1995). Altogether, the results confirm the presence of the expected molecules and that the OGal layer has been successfully sialylated with the α-2,6 SAT enzyme.

The sialylation using an α-2,3 SAT was probed by incubation with H5N9 Influenza virus particles. The hemagglutinin protein of this Influenza subtype binds specifically to α-2,3 linked sialic acid groups. The adsorbed viral particles can then be revealed by a WB assay. Figure 3.57 shows typical stains on a sialylated surface which confirms the presence of adsorbed H5N9 viruses and therewith, the specific functionalization with α-2,3 bonded SA groups. No staining is observed for the control with the BSA protein, excluding unspecific protein adsorption.

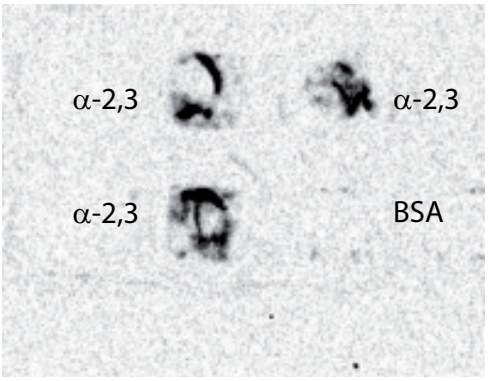

FIGURE 3.57: Western Blot image of α-2,3 sialylated gold chips after incubation with a H5N9 Influenza virus solution (1 μg/ml, 1 h, in triplicate). The control chip was incubated with 1 %BSA.

3.4.3 Influenza Virus Sensing

The development and controlled formation of the multilayer structure terminating in Influenza virus specific sialic acid moieties provided the basis for a reagentless, label-free *affinity* biosensor. The Influenza virus detection was performed by electrochemical impedance spectroscopy (EIS). The study consisted in the detection of purified PR8 virus (human subtype H1N1), especially at low concentrations, and investigating the detection kinetics. A series of controls with an avian subtype Influenza virus (A/turkey/Wisconsin H5N9) as well as with the PRRS virus (porcine reproductive and respiratory syndrome virus) (Rossow, 1998) is carried out to establish the selectivity of the envisaged electrode layer setup displaying α-2,3 and α-2,6 linked sialic acid moieties, respectively. All used viruses were inactivated by exposure to UV irradiation if not stated otherwise.

3.4.3.1 Detection Tests for PR8 Influenza Virus

Unspecific adsorption of PR8 virus was tested on electrodes that presented a Othiol/OGal interface and compared to sialylated electrodes. From Figure 3.58A it becomes obvious that functionalization with α-2,6 sialic acid (α-2,6 SA) significantly increases the R/R_{blank}, while on the other side, only a slight increment in R/R_{blank} is observed for the non-sialylated electrode. These findings suggest enhanced specific PR8 adsorption due to α-2,6 sialylation whereas in the other case only weak unspecific PR8 adsorption occurred. Additional support is also provided from WB assays using sialylated gold chips. The inset WB images in Figure 3.58A clearly confirm the specific adsorption of PR8 virus particles on the α-2,6 SA surface by the appearance of dark stains whereas in the absence of sialic acid no adsorption was observed.

The α-2,6 sialylated biosensor was tested for sensitivity of PR8 virus at low concentrations which is one of the two most important characteristics of a sensor. The other characteristic is selectivity, which is assessed further below (Section 3.4.3.2). For the sensitivity test, three concentrations of 0.05, 0.075, and 0.1 μg/ml where chosen. Figure 3.58B shows the increased R/R_{blank} over the total incubation time. For a fixed incubation time the signal

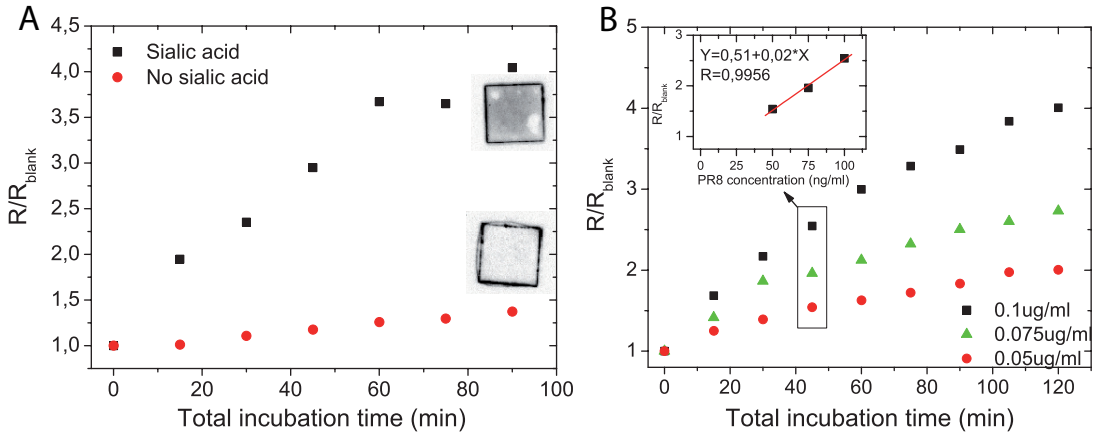

FIGURE 3.58: PR8 virus adsorption from 0.1 μg/ml on sialylated and non-sialylated electrodes (A) and PR8 detection at various concentrations (B). The incubation time refers to the total time in which the electrode surface was successively incubated in virus solution. The charge-transfer resistance values were derived from circle-fits of impedance spectra and corresponding R/R_{blank} values are calculated from individual blank measurements in PBS. The inset micrographs in Figure A show Western Blot images of sialylated and non-sialylated gold chips after incubation in PR8 solution. These assays were carried out by Ms. Martin del Burgo at the INIA (Spain).

follows a linear relationship with the added PR8 concentration and gives a sensitivity value of 20.1 $(\mu g/ml)^{-1}$ at 45 min total incubation time (inset in Figure 3.58B). Furthermore, it can be noticed that the R/R_{blank} curves flatten at levels according to the measured PR8 concentration. This saturation limit should be related to the amount of affinity sites for the PR8 virus present on the electrode surface, or in other words, being related to the concentration of immobilized α-2,6 SA. A variation in immobilized sialic acid quantity might be possible but should be ruled out due to reproducibility tests with individually prepared electrodes showing similar PR8 detection curves (Figure 3.60A). Adsorption of agglomerated virus particles could be another explanation. However, atomic force microscopy (AFM) imaging of electrode surfaces after virus detection reveals individually adsorbed viral particles (Figure 3.59) and may therefore discard this explanation. On the other side, it is commonly observed for immunosensors that the amount of adsorbed antigen rather depends on the equilibrium concentration in the analyte solution than on the quantity of affinity sites on the sensor surface (Eddowes, 1987). Thus, given that the maximum concentration of added PR8 (0.1 μg/ml) is below the true saturation limit of the present sialic acid sites, the observed plateaus could be explained in these terms.

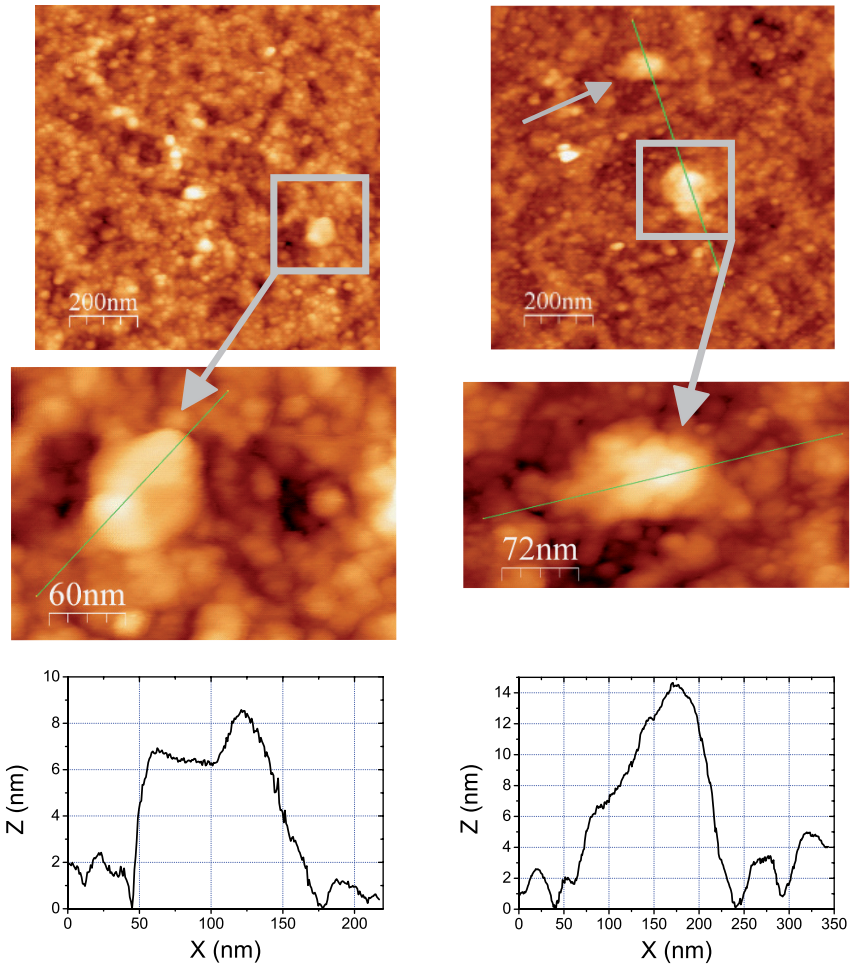

FIGURE 3.59: Topographic AFM images (dynamic mode) of biosensor surfaces after detection of 0.1 μg/ml PR8 solutions. The measured hight is lower than a typical influenza virus diameter (70-120 nm). This is possibly due to a collapse of the viral particle as consequence of the dehydration in the course of the sample preparation (i.e. ambient AFM measurements).

A further characteristic of this biosensor is the low detection limit (inset in Figure 3.58B). The theoretical detection limit is determined at 0.024 μg/ml (interception point of *calibration curve* with $y = 1$). This is by two orders of magnitude lower than other reported impedimetric Influenza biosensors (Diouani et al., 2008; Wang et al., 2009) based on whole virion detection without special sample pre-treatment. In other biosensors, the genetic material of viruses is used for detection which implies extraction of DNA or RNA, and in some cases even their amplification by the polymerase chain reaction (PCR) method (Bonanni et al., 2010). This, however, makes the whole process tedious and not user-friendly.

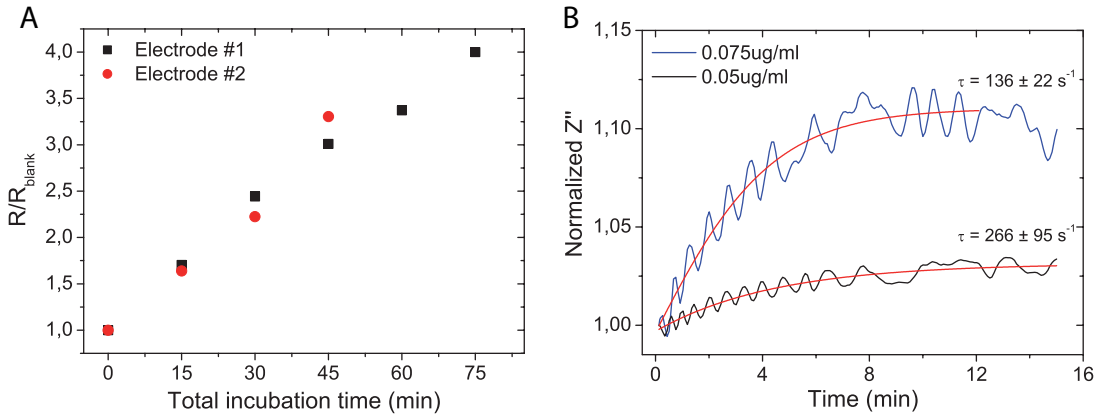

FIGURE 3.60: Reproducibility of PR8 virus detection from a 0.5 μg/ml solution (A) and PR8 adsorption kinetics on a virgin α-2,6 sialylated electrode surface (B). These measurements were performed at constant frequency (ν=50 Hz) at 0 mV *versus* open circuit potential. The resultant $Z''(t)$-curves were nonlinearly fitted with the Boltzmann function to derived the time constant τ of the adsorption process. The frequency value is picked from the linear range in a Bode plot ($\log|Z|$ *vs.* $\log\nu$) that is indicative for capacitive behavior of the system.

As already observed in Figure 3.58B, the detection time of this biosensor is very short. After only 15 min a significant signal can be recorded. These fast detection kinetics were investigated by *in situ* recording of PR8 virus adsorption on the α-2,6 sialylated electrode surface. Figure 3.60B shows the normalized imaginary impedance (Z'') at constant frequency (50 Hz) as function of the incubation time in two different PR8 virus solutions. The value of Z'' is related to the electric double layer capacity C_{dl} of the electrode surface by $Z'' = 1/\omega C$, and its recording over time can therefore be used to determine the time constant τ, or also called apparent association rate constant k^a_{app} of the PR8 adsorption. For the determination of this constant, the curves were nonlinearly fitted to the Boltzmann function (Gill et al., 1996). The fittings reveal a smaller time constant but a higher saturation plateau Z''_{max} for the 0.075 μg/ml PR8 solution as compared to the 0.05 μg/ml solution. The kinetics of the present biosensor system can be treated similar to kinetic analysis of antibody-antigen reactions. In this context, two general limiting cases for antigen adsorption to antibody functionalized electrode surfaces can be considered: i) The *adsorption site* limited case, and ii) the *bulk solution antigen concentration* limited case (Eddowes, 1987). The latter case implies independence of the fractional response $Z''(t)/Z''_{max}$ on the antigen concentration. This case can be excluded here since

$Z''(t)/Z''_{max}$ demonstrated a clear antigen concentration dependence (Figure D.2 in Appendix D). By contrast, in the *adsorption site* limited case kinetic analysis predicts the time to reach a fractional response to be dependent on antigen concentration in such way, that antigen adsorption takes longer at decreased concentration (Eddowes, 1987). And in fact, this is being revealed by the kinetic examination of the virus adsorption as manifested by the higher τ value for the 0.05 μg/ml PR8 solution.

The curves in Figure 3.60B further show that the plateau Z''_{max} is reached after only ca. 6 min (for the 0.075 μg/ml PR8 solution) confirming reliable Influenza virus detection at very short response times. This furnishes the present biosensor with a great advantage over many standard clinical methods such as real-time RT-PCR (Poon et al., 2009), antigen tests, immunofluorescence, ELISA, or viral culture (Voller et al., 1976; anonymous, 2009) which are in some cases condemned to large revelation periods over several hours or even days.

3.4.3.2 Selectivity of Influenza Virus Subtypes

The Influenza virus appears in many different subtypes, differentiated by the combination of the membrane proteins hemagglutinin (H) and neuraminidase (N). The Influenza virus nomenclature is based on these combinations, e.g. H1N1, H5N9, or H5N1 etc. Therefore, an important requisite of a biosensor for Influenza viruses is the capacity to discriminate between the various Influenza subtypes since some are harmless but others potentially lethal. The design of the present biosensor accounts for this characteristic by sialylation with α-2,6 and α-2,3 sialyltransferase, respectively, providing the possibility for selective detection of H1 and H5 subtypes (Stephenson et al., 2003). Figure 3.61 illustrates the combinations of sialylated electrodes for the selectivity between H1N1 (PR8) and H5N9 viruses.

The selectivity of the α-2,6 sialylated biosensor is revealed in Figures 3.62A and B. The R/R_{blank} value is 2.6 in presence of H1N1 while no signal above the blank is obtained for H5N9. Also for functionalization with α-2,3 a significant selectivity toward the corresponding H5N9 virus can be observed although unspecific adsorption of H1N1 on the

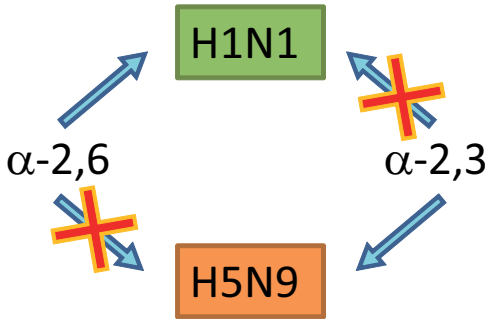

FIGURE 3.61: Scheme for selectivity of α-2,6 and α-2,3 sialylated electrodes toward H1N1 and H5N9 Influenza viruses.

α-2,3 sialylated surface occurred to some extent. These results confirm the conceived concept of selectivity afforded by the choice of the corresponding sialyltransferase.

Clinical samples may also contain other types of viruses which can show structural features similar to Influenza viruses (e.g. proteins, capsid, lipid membrane) and might therefore cause wrong diagnoses. Given this, the present biosensor is tested for selectivity toward the PRRS virus that commonly accompanies Influenza viruses from porcine. Figure 3.63 displays the detection curve for the PRRS virus together with serum. The reason is that this PRRS sample was suspended in serum which gives rise to a background signal owing to unspecific adsorption on the electrode. As can be noticed, the test with PRRS virus did not give a signal above the serum background and the biosensor can therefore be considered as unspecific for this virus. Regarding the structural features, Influenza viruses belong to a class of viruses which are surrounded by a lipid membrane (also termed *envelope*) (Nayak et al., 2004). The PRRS virus, belonging to the same class but presenting different membrane proteins (Rossow, 1998), served as control to examine the influence of the lipid envelope on the adsorption to the electrode surface. The present results imply that the adsorption mechanism is not related to the lipid envelope but only to the specific interactions between the viral hemagglutinin and the sialic acid sites.

A further control was conducted with not inactivated PR8 virus to rule out potential alterations of the virus membrane structure inflicted by the UV treatment and which

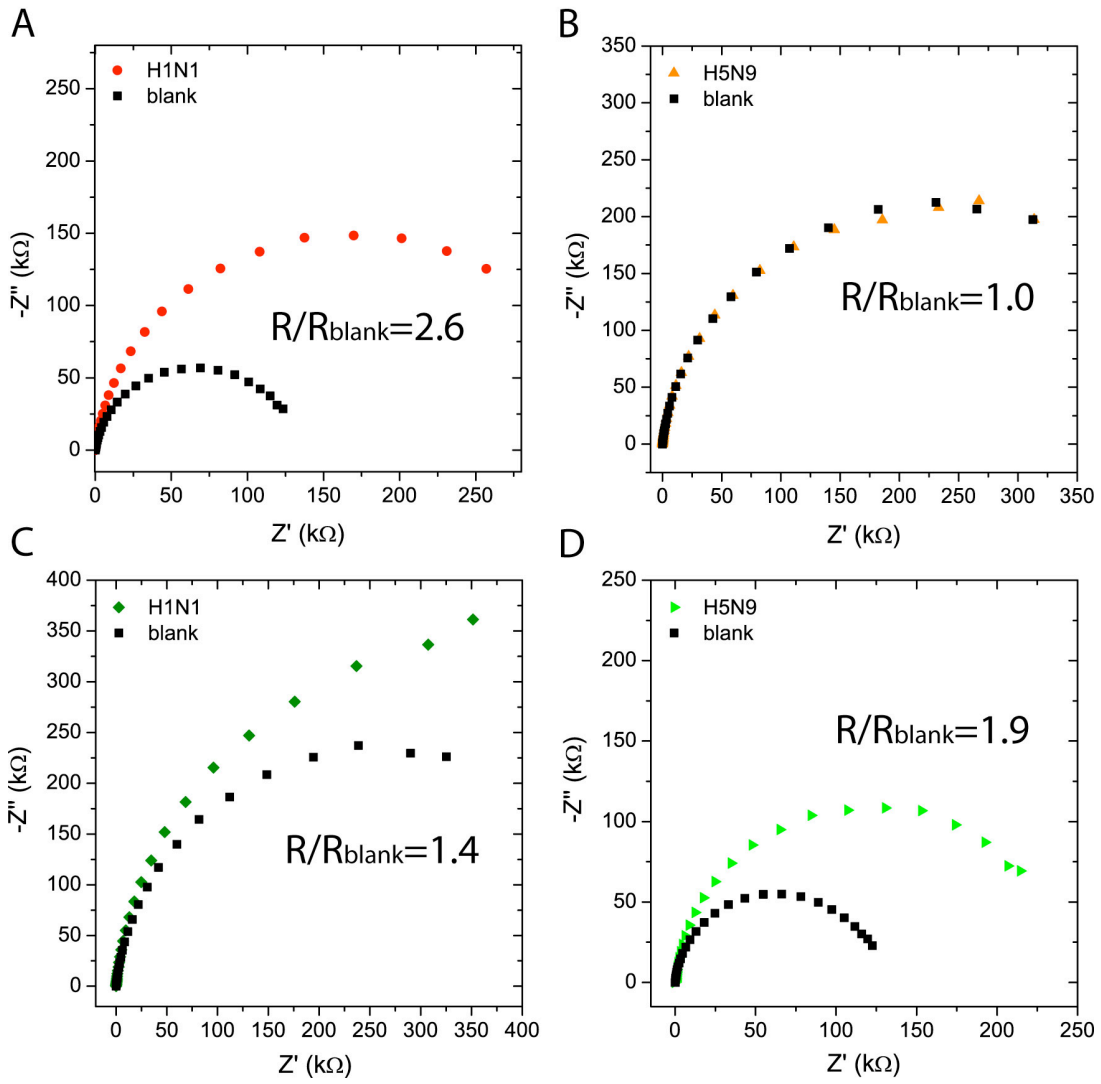

FIGURE 3.62: Nyquist plots of α-2,6 and α-2,3 sialylated electrodes after 45 min incubation in solutions of H1N1 (PR8) and H5N9 virus. Figure A and B refer to α-2,6 sialylated electrodes and Figures C and D refer to α-2,3 sialylated electrodes. The H1N1 virus sample was purified and for the EIS measurements suspended in 0.5 % BSA/PBS solution at a virus concentration of 0.1 μg/ml. The corresponding blank recordings were performed with 0.5 % BSA/PBS solution. The H5N9 virus was present in serum at a stock concentration of 800 μg/ml and diluted with 0.5 % BSA/PBS to 0.75 μg/ml.

could consequently affect the correct detection. The R/R_{blank} curve of active PR8 in Figure 3.63 shows a steady increase with incubation time. The R/R_{blank} value at 45 min is 1.9 which is comparable to the one from the 0.075 μg/ml concentration of inactive PR8 virus. Given the low concentration of 0.01 μg/ml of the active virus, this signal substantiates a very high sensitivity of the sensor for active PR8 viruses. Considering these observations, it can be suggested that the inactivated PR8 virus might have suffered from protein damage which reduced its detectability by the present biosensor setup based

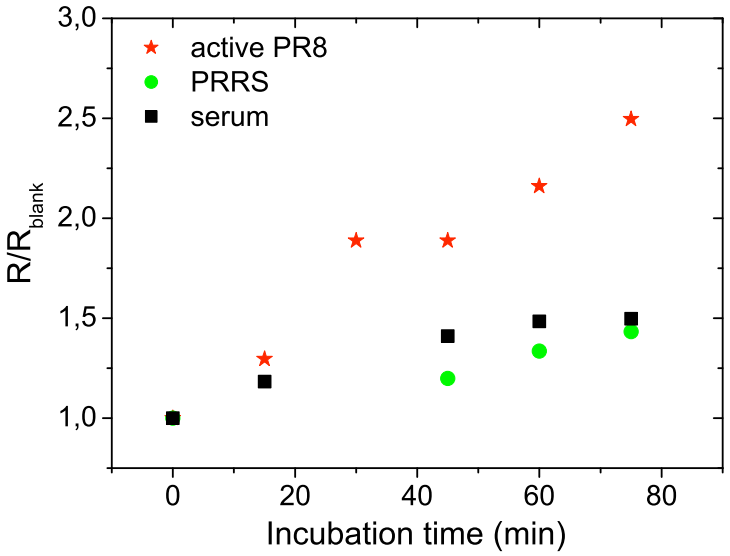

FIGURE 3.63: Unspecific PRRS virus adsorption from 0.07 μg/ml together with the signal from the serum background and detection of active PR8 virus from a 0.01 μg/ml solution.

on ligand-receptor affinity. On the other side, these results also demonstrate the high sensitivity of the sialylated electrode for very low Influenza virus concentrations.

3.4.4 Concluding Remarks

It has been shown that the sequential Othiol-OGlu adsorption yields a more compact, and therewith better ordered bilayer than the simultaneous approach. Furthermore, the preformed Othiol SAM was found to be distorted by adsorbing OGlu molecules. This event is most pronounced at high OGlu concentrations and extended incubation. On the other side, impedance measurements indicate an elevated amount of adsorbed OGlu from 5 mM solutions. Since the objective is to prepare well-ordered bilayers with high loadings of galactoside groups, the optimized conditions were found to be incubation for one day at an OGal concentration of 5 mM.

The sialylation of these bilayers with the specific sialyltransferase enzymes could provide α-2,3 and α-2,6 linked sialic acid groups, respectively. Their presence was confirmed

both by XPS and WB assays. This allowed for the preparation of Influenza virus selective biosensors based on the affinity between the specific sialic acid groups and the hemagglutinin protein of the Influenza subtypes.

The resultant affinity biosensor could successfully detect and distinguish between the H1N1 and H5N9 subtypes as well as the PRRS virus. The impedimetric sensing method proofed to allow for short response times and high sensitivity. A further advantage of the present biosensor is the unnecessity of sample preparation as in case of impedimetric genosenosors. This type of Influenza biosensors shows very high sensitivity and low detection limits, but requires elaborate sample preparation and biotechnological training of the technician to perform extraction the viral RNA or DNA for hybridization and so forth. Contrarily, Influenza biosensor conceived and prepared in this work is "easy to handle", fast, cheap, and could be very convenient in field-operation acting as sort of Influenza alarm device.

Chapter 4

Conclusions

In this Dissertation, a new class of biohybrid materials based on the self-assembly of biosurfactants on the surface of clay minerals and gold electrodes is studied. The resulting materials expose biomimetic interfaces which ensure biocompatible immobilization of different types of biological species. In detail, the conclusions are:

- The self-assembly process of phospholipid molecules on the clay minerals sepiolite and montmorillonite was studied in water as well as in organic solvent. It was found that lipid bilayer formation from liposome adsorption is more effective than molecular self-assembly from solution in organic media. However, physico-chemical characterization revealed that the fundamental interaction mechanism are in both cases similar: ion-exchange and hydrogen bonding.

  Furthermore, it could be demonstrated that established self-assembly concepts could be successfully transfered. This holds both for the preparation of organophilic clays with phospholipids substituting quaternary alkylammonium surfactants and for the controlled formation of mixed lipid membranes on the surface of sepiolite.

  A novel method for the preparation of lipid membranes on Mg/Al LDH was introduced which additionally gave rise to nano-scaled LDH sheets. This specific texture is considered as mandatory for successful employment in biological vector applications.

- The biomimetic quality of the surface of sepiolite biohybrids was demonstrated by immobilization of the two model enzymes urease and cholesterol oxidase. Bioactivity assays showed that enzymatic activity of the enzymes depend on the provided interface structure. The membrane-associated cholesterol oxidase and the cytoplasmic enzyme urease showed both highest activity on their native supporting environment, the lipid bilayer membrane. These results emphasized the controlled formation of biomimetic interfaces supported on sepiolite. Furthermore, the enzyme-loaded biohybrids were tested for the exploration as active phase of an interference-free electrochemical urea biosensor and as cholesterol bioreactor with considerable recyclability.

  Clay-lipid biohybrids were also evaluated as sequestration agent for the mycotoxins aflatoxin B1 and deoxynivalenol. The adsorption study revealed increased toxin uptake compared to the commercial organoclay Cloisite® 30B and cetyltrimethylammonium exchanged sepiolite. These promising results could lead to a potential usage of these bio-organoclays as biocompatible feed additives for *in vivo* toxin adsorption in animals.

- Lipid biohybrids based on sepiolite and Mg/Al LDH were evaluated as biomimetic supports for antigenic material in vaccines against the Influenza A virus. By providing a lipid membrane, the support-antigen interactions could be controlled to preserve the native conformation of the antigen. Two strategies were successfully carried out for comparison of whole virion and hemagglutinin stabilization. This last strategy is especially important for the development of large-scale vaccines. Bioactivity assays demonstrated for both routes that the sepiolite-lipid biohybrid offers better immobilization conditions than a standard aluminum hydroxide adjuvant. This was found for thermal stability at elevated temperatures as well as for lyophilization. Therefore, this biohybrid could be a promising alternative to aluminum hydroxide adjuvants as antigenic carriers.

  Hemagglutinin together with flagellin were assembled on the sepiolite supported bilayer lipid membrane and assessed as sub-unit vaccine in an immunization test in mice. A high level of virus specific antibodies was produced which is indicative for protection

efficacy against Influenza and proofs the suitability of the sepiolite-lipid biohybrid as adjuvant in vaccinations.

- The development of a rapid, sensitive, and selective biosensor for the detection of the Influenza A virus was a further objective of this Thesis. This was archived by a bioinspired approach mimicking the surface of erythrocytes. The thorough study of the self-assembly of a hybrid octanethiol/octyl-galactoside bilayer allowed a controlled formation of galactoside residues at the interface which permitted the association of specific sialic acid moieties. These are the basis for the selectivity of the detector toward different Influenza subtypes by receptor-ligand affinity reactions.

  The impedimetric affinity biosensor proofed to be sensitive with a detection limit at $0.024\,\mu$g/ml and a response time of less than 10 minutes. The design of the sensor afforded the discrimination between the subtypes H1N1 and H5N9 and furthermore, was insensitive to the non-Influenza virus PRRS. An additional advantage of this sensor setup is the user-friendliness by label-free specimen detection which makes preparative sample treatment superfluous.

Appendix A

Synthesis and Characterization of Lipid-Biohybrids

- Phosphatidylcholine Adsorption on Sepiolite from Methanol

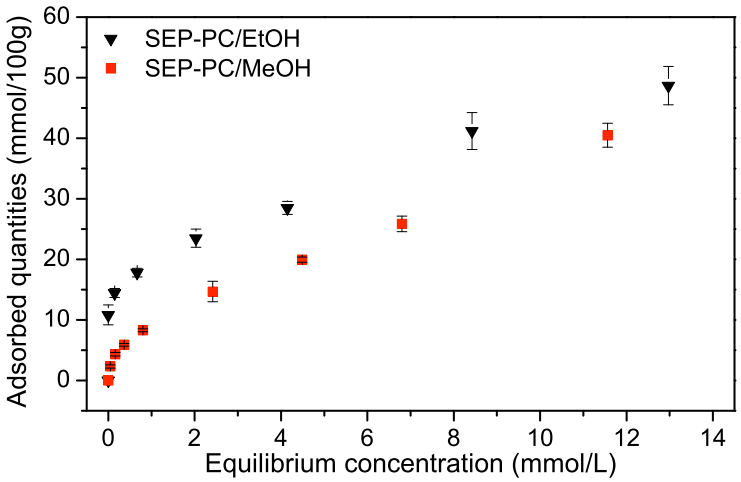

FIGURE A.1: Adsorption isotherms of PC from methanol and ethanol on sepiolite. Adsorption took place at 25 °C for 24 hours under agitation of a magnetic stirrer.

Figure A.1 shows the phosphatidylcholine (PC) adsorption isotherms from methanol and ethanol. It can be noticed that adsorption quantities from methanol are inferior compared to ethanol. A tentative hypothesis explaining the solvent influence on PC adsorption

might be based on competitive adsorption. As pointed out in Section 3.1.1.1, superficial water molecules can act as adsorption sites for PC molecules. On the other side, methanol interacts strongly with coordinated water at the external surface of sepiolite. Serna has even shown that methanol can facilely replace these water molecules (Serna, 1973). In turn, this may disadvantage the adsorption of PC in the presence of methanol. Hence, the more coordinated water molecules are substituted, the less PC would adsorb on sepiolite. This effect is less pronounced in case of ethanol as solvent since ethanol is a less polar molecule as compared to methanol.

- Investigation of Preferential PC Adsorption on Sepiolite

According to the synthesis of the sepiolite-PC materials from phospholipid solution prepared from the 60 % (TLC) PC batch, an approach to ascertain the composition of the

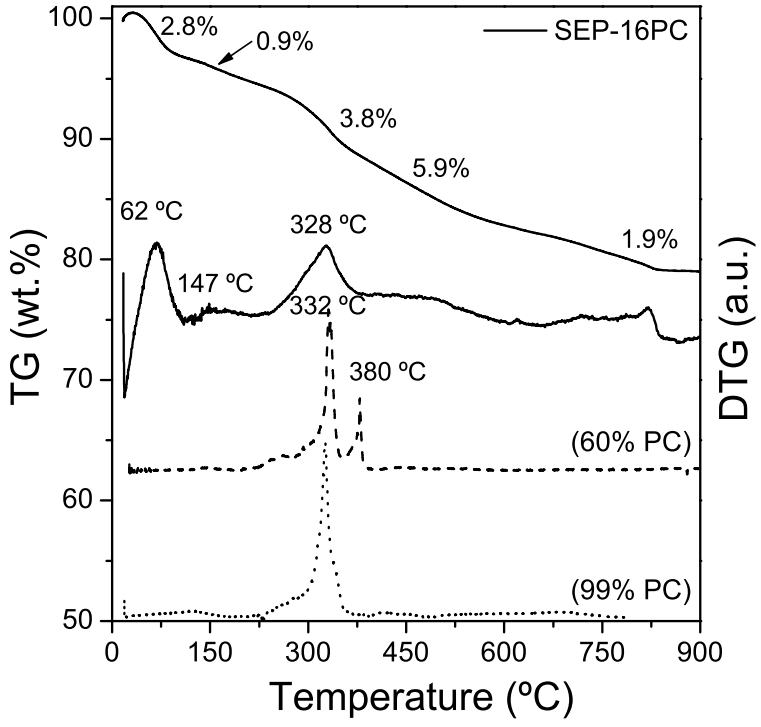

FIGURE A.2: Thermogravimetric analysis of a sepiolite-lipid biohybrid (16 mmol/100 g PC adsorbed from ethanol) and L-α-phosphatidylcholine of 60 and 99 % TLC purity in the temperature range of 20-900 °C, recorded under air flow conditions with a heating rate of 10 °C/min.

resultant biohybrids is proposed by means of thermal analysis. Figure A.2 displays the differential thermogravimetry (DTG) curves of a sepiolite-lipid biohybrid together with the 60 % PC batch and as reference the one of 99 % purity. The weight loss observed at 328 °C can be related to the combustion of L-α-phosphatidylcholine (exothermic peak in DTA curve, not shown), which is suggested from the comparison with the reference DTG curve of the 99% PC sample. The second peak at 380 °C of the 60% PC sample is likely to be attributed to the presence of other species in this phospholipid batch, such as cholesterol and proteins, as this sample is of lower purity. The absence of this peak in the DTG curve of the hybrid material strongly indicates preferential adsorption of L-α-phosphatidylcholine on sepiolite and thus, offering fairly pure sepiolite-PC composites.

The ability of sepiolite for selective PC sorption could be exploited as means for purification and enrichment of phospholipid solutions of low purity. This would be a low cost and essential *green* method since in standard procedures organic solvents are used to a large degree (Singleton et al., 1965).

- Liposome Preparation

The hydrodynamic diameter of PC liposomes prepared by the extrusion method was assessed by means of dynamic light scattering. The particle size distribution is presented in Figure A.3. The diameter is around 130 nm which is in accordance with typical values obtained from extrusion through 100 nm polycarbonate membranes (Hope et al., 1985; Mayer et al., 1986).

- PC Adsorption on Montmorillonite from Ethanol

Phospholipids from ethanol solution adsorbs with lower quantity on montmorillonite, forming a plateau at about 60 mmol/100 g (Figure A.4) which is approximately half the quantity that is adsorbed from methanol. A possible explanation for the significantly lower total adsorption quantity from ethanol might be related to the competition between the solvent and the adsorbing lipid layer. The formation of the first lipid layer is

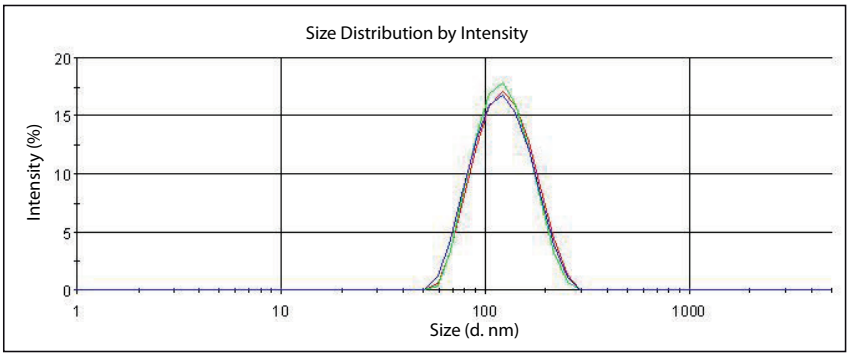

FIGURE A.3: Particle size distribution by intensity of extruded liposomes. Measurements were conducted at 0.5 mM liposome concentration and at an ionic strength of 10 mM NaCl.

mainly governed by electrostatic interaction between the silicate surface and the polar PC headgroup. Further adsorption involves intermolecular attraction between the lipid molecules, mainly van der Waals forces. Since these are generally weaker as H-bonding, polarity of the surrounding solvent gains in importance. Ethanol ($\epsilon = 25.3$) is more lipophilic than methanol ($\epsilon = 33$) (Lide, 2009) and hence, pulling the adsorption equilibrium between the PC layer and dissolved lipid molecules rather to the solvent side. On contrary, lipid-lipid attraction in slightly less lipophilic methanol seems to exceed the solvation force of methanol, resulting in a higher adsorption amount.

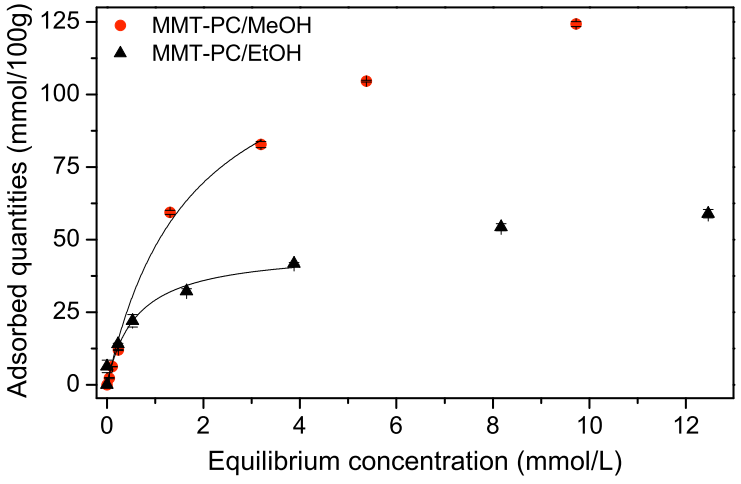

FIGURE A.4: Adsorption isotherms of PC from methanol and ethanol on Na^+-montmorillonite. Adsorption took place at 25 °C for 24 hours under agitation of a magnetic stirrer.

- Investigation of Preferential PC Adsorption on Montmorillonite

Preferential PC adsorption from a phospholipid solution prepared from the 60 % (TLC) PC batch is confirmed by thermal analysis of the sample MMT-22PC. The corresponding thermogravimetry curve in Figure A.5 shows a weight loss at 328 °C that can be related to the combustion of L-α-phosphatidylcholine (exothermic peak in DTA curve). This is suggested from the comparison with the reference DTG curve of the 99% PC sample. The second peak at 380 °C of 60 % (TLC) PC in the DTG curve is likely be associated to the presence of other species in the 60 % (TLC) PC, such as cholesterol and proteins, since this phospholipid batch is of lower purity. The absence of this peak in the DTG curve of MMT-22PC strongly indicates preferential adsorption of L-α-phosphatidylcholine on the montmorillonite and thus, offering fairly pure MMT-PC composites.

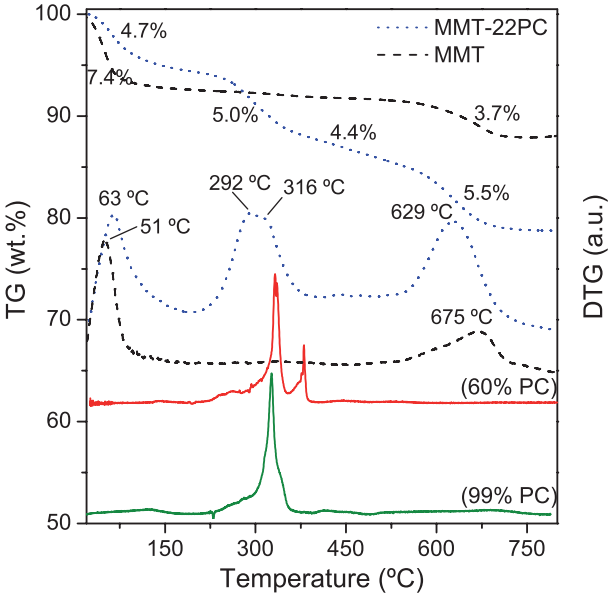

FIGURE A.5: Thermogravimetric analysis of a montmorillonite-lipid biohybrid (22 mmol/100 g PC adsorbed from methanol) and L-α-phosphatidylcholine of 60 and 99 % TLC purity in the temperature range of 20-900 °C, recorded under air flow conditions with a heating rate of 10 °C/min.

The second peak of the DTG curve which is centered around 305 °C is attributed to the combustion (exothermic peak in DTA curve, not shown) of PC and accompanied with a weight loss of 5.0 wt.%. A further weight loss of 4.4 wt.% until 580 °C is registered (TG curve in Figure A.5). This elimination step is supposedly associated with gradual removal of the combusted lipid fragments.

Another interesting finding is the dehydroxylation temperature of montmorillonite in the MMT-22PC hybrid. It appears at 629 °C which is about 40 °C lower than in pristine montmorillonite (dashed DTG curve in Figure A.5). This is a known event to occur when organic species are intercalated in smectites (Schultz, 1969) and thus, being another evidence for the intercalation of PC molecules in Na^+-montmorillonite.

- Intercalation Method for Preparation of Mg/Al LDH-PC Biohybrids

In a first attempt, LDH-lipid biohybrids were prepared by an intercalation method reported by Begú and co-workers for the anionic phospholipid 1,2-dimyristoyl-*sn*-glycero-3-phosphate (Begú et al., 2009). An adsorption isotherm of PC liposomes on Mg/Al LDH was sampled and the curve is depicted in Figure A.6.

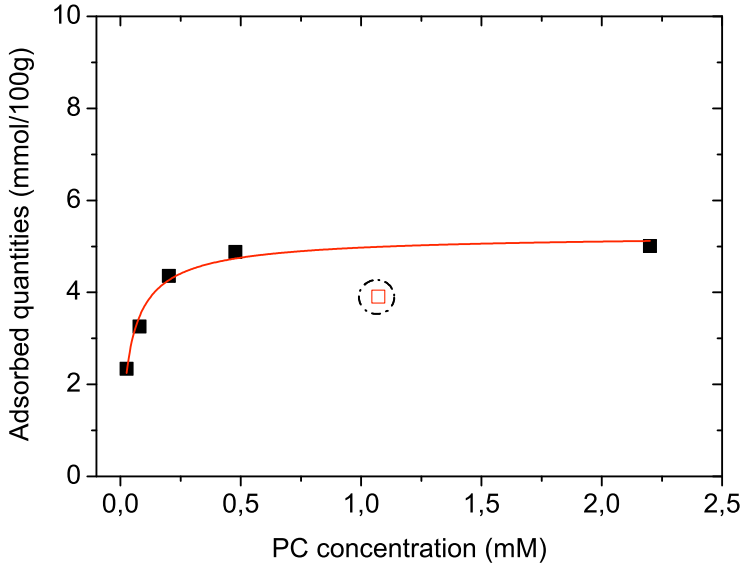

FIGURE A.6: Adsorption isotherm of PC liposomes on Mg/Al LDH from 10 mM PBS at pH 7.4. The solid line represents a fitted Langmuir adsorption isotherm for which the data point at 1.0 mM was not regarded.

The isotherm shows a steep increase in adsorption and levels off at ca. 5.3 mmol/100g. This amount is rather low when compared to the 28 mmol/100g yielded by the co-precipitation method. However, a more important issue is the high degree of agglomeration and re-dispersion difficulties of this type of LDH-PC material as evidenced from

electron microscopy. This becomes especially problematic in the application as vector for biological species which relies on the nano-sized dimensions of the carrier material. Therefore, it was decided to discard the intercalation method and follow the co-precipitation route.

- EDX Analysis of the Mg/Al LDH-PC Biohybrid

Energy-dispersive X-ray (EDX) spectroscopy was employed to determine the chemical composition of the co-precipitated Mg/Al LDH-PC biohybrid. The spectrum reveals the presence of Mg, Al, and O as basic elements and Cl and P as minor components. Integration of the peaks yields the atomic percentage of each element from which the molar ratio of Mg/Al can be calculated. The value is 1.8 which is reasonably well in range with the designed 2:1 Mg/Al type. Cl can be attributed to unexchanged interlayer anions and phosphorous originates from adsorbed lipid molecules.

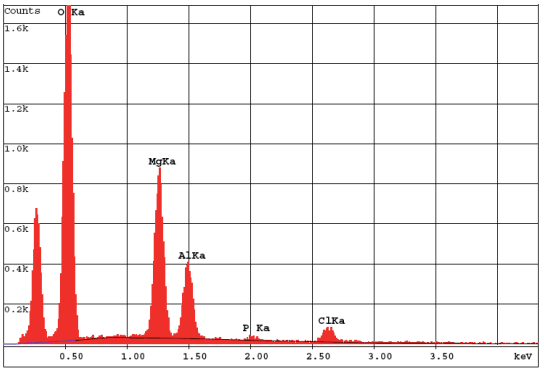

Element	Wt %	At %
O K	44.07	56.80
MgK	27.70	23.49
AlK	17.38	13.28
P K	1.35	0.90
ClK	9.50	5.53
Total	100.00	100.00

FIGURE A.7: EDX spectrum of co-precipitated Mg/Al LDH-PC and the derived atomic fraction of the present elements. The conditions were fixed to 6.0 KeV landing energy at 800 x magnification and 77 s accumulation time.

- Particle Size of the Mg/Al LDH-PC Biohybrid

The hydrodynamic diameter of pristine Mg/Al LDH and Mg/Al LDH-PC particles was assessed by dynamic light scattering. Figure A.8 shows the particle size according to the distribution by scatter intensity and number. The determined particle sizes are in reasonable agreement with data obtained from TEM observations ($\approx$ 50-80 nm).

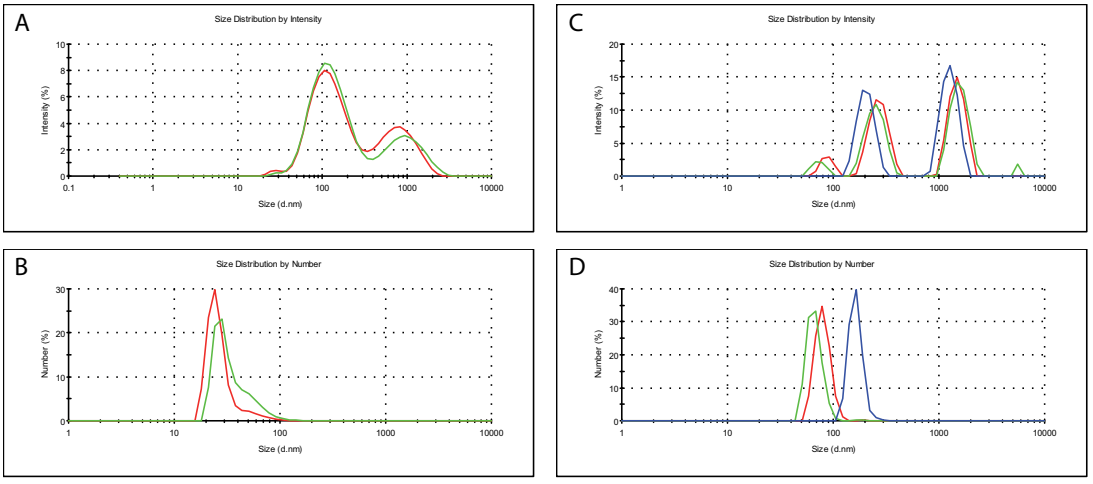

FIGURE A.8: Particle size by intensity and number distribution of pristine Mg/Al LDH (A and B) and Mg/Al LDH-lipid (C and D) obtained from dynamic light scattering.

Appendix B

Immobilization of Enzymes on Clay-Lipid Biohybrids

FT-IR spectra of immobilized urease on various sepiolite interfaces (Figure B.1).

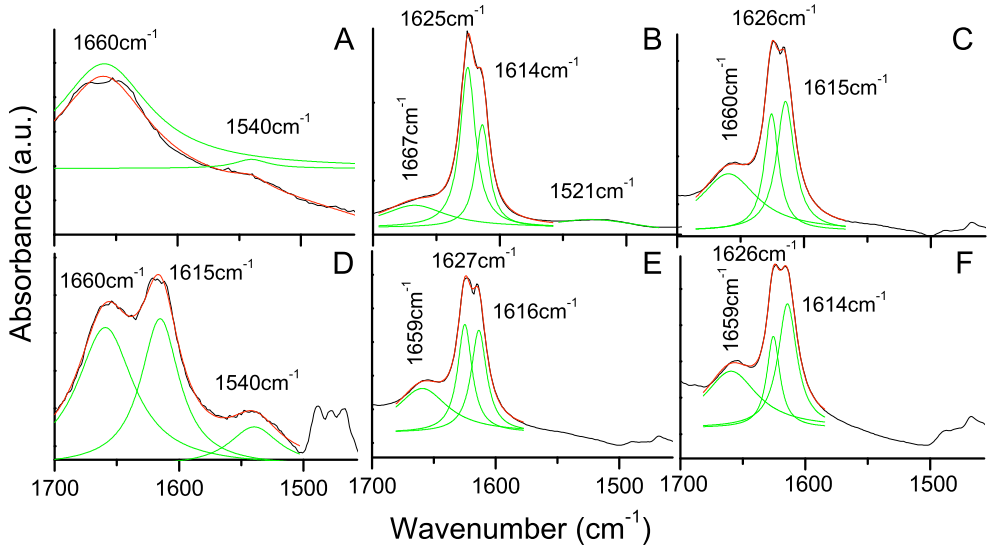

FIGURE B.1: FT-IR spectra of free urease (A) and immobilized on sepiolite displaying different interfaces such as bare surface (B), PC-OTGal (C), CTA (D), ML-PC (E), and BL-PC (F). Urease was measured in KBr while the sepiolite based samples were prepared as self-standing films.

Long-term activity of COx immobilized on SEP-BL-PC and SEP-ML-PC (Figure B.2).

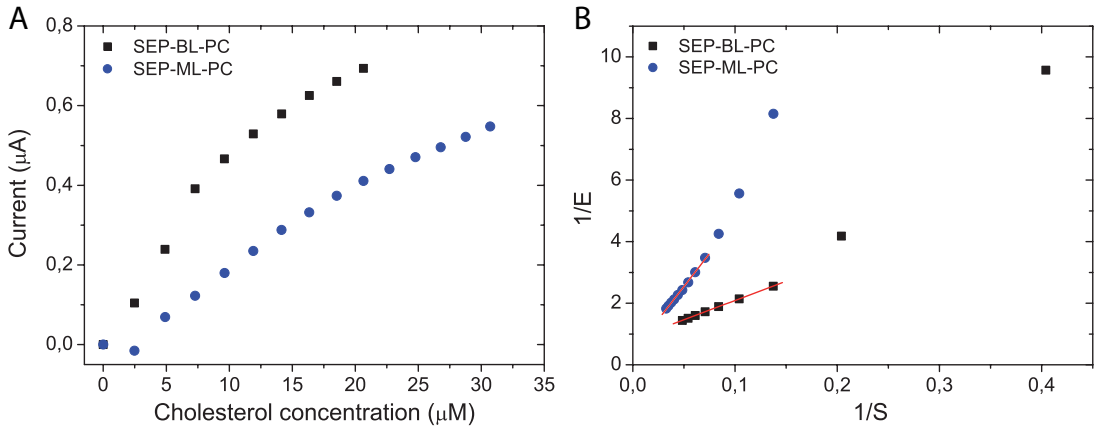

FIGURE B.2: Activity of COx four weeks after immobilization on SEP-BL-PC and SEP-ML-PC (A). Lineweaver-Burk plots derived from the conversion data (B). The hybrids were kept as dry powder at 4 °C.

Appendix C

Lipid Bio-Nanohybrids as Influenza Vaccine Adjuvant

Powder X-ray diffraction and TEM micrograph of the commercial $Al(OH)_3$ adjuvant Alhydrogel®, that has been used as standard in the development of adjuvants based on lipid bio-nanohybrids (Figure C.1).

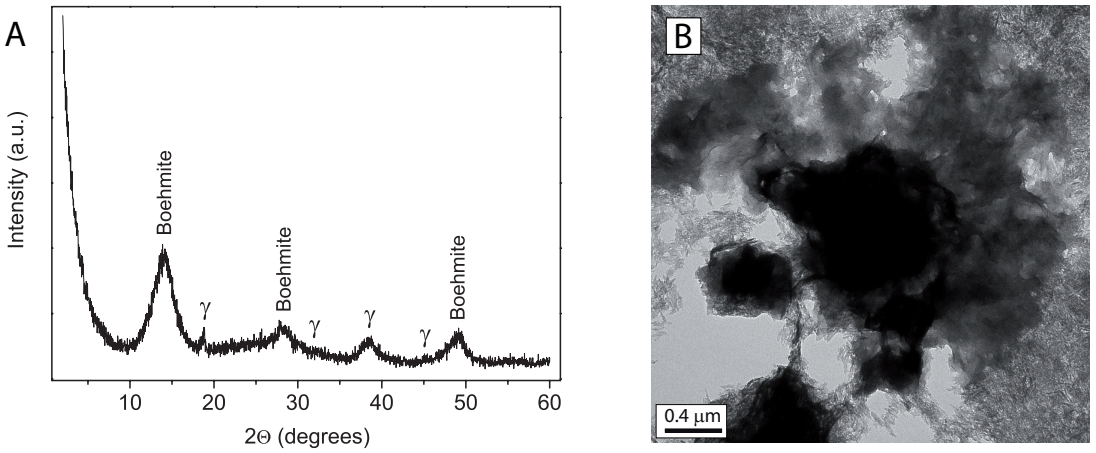

FIGURE C.1: XRD pattern (A) and TEM micrograph (B) of commercial $Al(OH)_3$ adjuvant. The mineral components γ-Al_2O_3 and Boehmite α-AlO(OH) are indicated in the diffractogram.

- Immunization Test with Hemagglutinin

The efficacy of hemagglutinin (HA) immobilized on SEP-BL-PC as model for a sub-unit vaccine was tested in an immunization test with mice. For this purpose, doses of 1 μg HA per 200 μg SEP-BL-PC were prepared. In a second group of vaccines, 6 μg Fla per dose were co-adsorbed with the antigens to show the versatility of the delivery system. A control group was composed of SEP-BL-PC and BSA only. Each vaccine was assessed with a group of 6 mice (Balb/c strain, female, 8-week-old). Animals were inoculated intraperitoneally at day 0 with a first dose and at day 18 with a second *booster* dose. Blood samples were collected 4 weeks following the second immunization and sera were analyzed for virus-specific antibodies (IgG) by a hemagglutination inhibition (HAI) test and by ELISA. In the HAI test, specific serum antibodies produced by immunized mice bind to HA from Influenza virus. This effect prevents erythrocytes to agglutinate and the titer indicates the level of total IgG present in the serum (Cox, 2002). The ELISA assay, on the other side, quantifies the presence of more specific antibodies such as IgG1. The inoculation and subsequent analyses were carried out by the group of Dr. Gustavo del Real (INIA, Spain).

Appendix D

Biomimetic Lipid-Based Thin Films

The applicability of the phenol-sulfuric acid method for the OGlu quantification from gold supported hybrid Othiol/OGlu bilayers was investigated by EIS (Figure D.1).

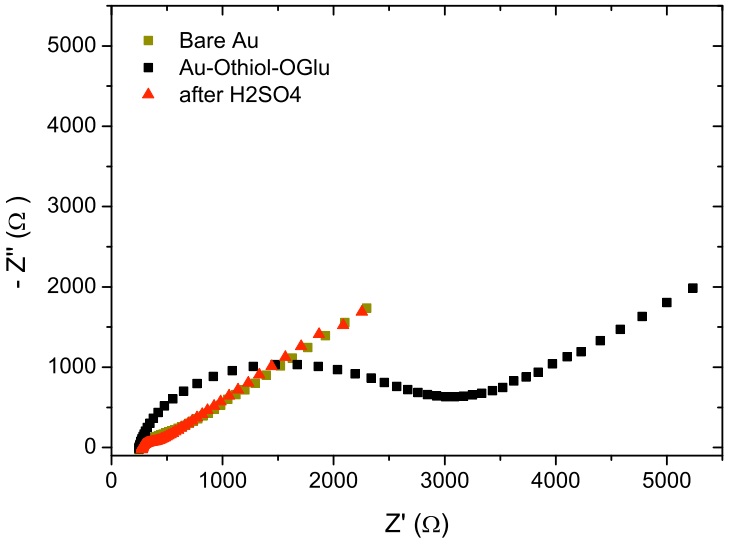

FIGURE D.1: Nyquist plots of an Othiol/OGlu modified gold electrode before and after treatment with sulfuric acid to confirm the applicability of the phenol-sulfuric acid method for the OGlu quantification from gold supported hybrid Othiol/OGlu bilayers.

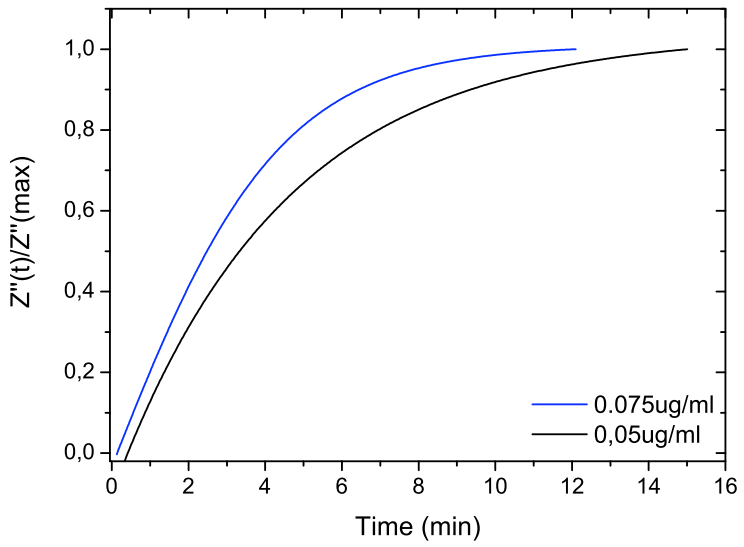

FIGURE D.2: Response profiles of α-2,6 sialylated electrodes toward PR8 Influenza viruses at 0.05 and 0.075 μg/ml concentration. The $Z''(t)/Z''_{max}$ *versus* t curves were derived from Boltzmann fits of the experimental $Z''(t)$ data.

The $Z''(t)/Z''_{max}$ *versus* t curves are plotted to examine the limiting cases for the kinetic analysis adopted from an antibody-antigen reaction. Figure D.2 demonstrates the dependence of the $Z''(t)/Z''_{max}$ *versus* t profiles on virus concentration which is a strong indication for an *adsorption site* limited case.

Bibliography

Abbate, C., Arena, M., Baglieri, A., and Gennari, M. (2009). Effects of organoclays on soil eubacterial community assessed by molecular approaches. *Journal of Hazardous Materials*, 168:466–472.

Abramson, M. B., Katzman, R., Wilson, C. E., and Gregor, H. P. (1964). Ionic properties of aqueous dispersions of phosphatidic acid. *Journal of Biological Chemistry*, 239:4066–4072.

Ahlrichs, J. L., Serna, J. C., and Serratosa, J. M. (1975). Structural hydroxyls in sepiolite. *Clays and Clay Minerals*, 23:119–124.

Ahmed, S. and Wunder, S. L. (2009). Effect of high surface curvature on the main phase transition of supported phospholipid bilayers on SiO_2 nanoparticles. *Langmuir*, 25:3682–3691.

Alcântara, A. C. S., Darder, M., Aranda, P., and Ruiz-Hitzky, E. (2011). A new type of biohybrid materials based on zein assembled to fibrous clays. submitted.

Alkan, M., Demirbas, O., and Dogan, M. (2005). Electrokinetic properties of sepiolite suspensions in different electrolyte media. *Journal of Colloid and Interface Science*, 281:240–248.

Amorij, J.-P., Hinrichs, W. L. J., Frijlink, H. W., Wilschut, J. C., and Huckriede, A. (2010). Needle-free influenza vaccination. *The Lancet Infectious Diseases*, 10:699–711.

Anastas, P. T. and Warner, J. C. (2000). *Green Chemistry: Theory and Practice*. Oxford University Press, New York.

Anderson, T. H., Min, Y. J., Weirich, K. L., Zeng, H. B., Fygenson, D., and Israelachvili, J. N. (2009). Formation of supported bilayers on silica substrates. *Langmuir*, 25:6997–7005.

Andrews, A. (1986). *Electrophoresis: Theory, Techniques and Biomedical and Clinical Applications*. Oxford Univ. Press, New York, 2 edition.

Angelatos, A. S., Katagiri, K., and Caruso, F. (2006). Bioinspired colloidal systems via layer-by-layer assembly. *Soft Matter*, 2:18–23.

anonymous (2009). Interim guidance on specimen collection, processing, and testing for patients with suspected novel influenza A (H1N1) virus infection. `http://www.cdc.gov/h1n1flu/specimencollection.htm`. Centers for Disease Control and Prevention.

Aranda, P., Casal, B., Fripiat, J. J., and Ruiz-Hitzky, E. (1994). Intercalation of macrocyclic-compounds (crown-ethers and cryptands) into 2/1 phyllosilicates - Stability and calorimetric study. *Langmuir*, 10:1207.

Aranda, P., Kun, R., Martín-Luengo, M. A., Letaief, S., Dékány, I., and Ruiz-Hitzky, E. (2008). Titania-sepiolite nanocomposites prepared by a surfactant templating colloidal route. *Chemistry of Materials*, 20:84–91.

Ariga, K., Hill, J. P., Lee, M. V., Vinu, A., Charvet, R., and Acharya, S. (2008). Challenges and breakthroughs in recent research on self-assembly. *Science and Technology of Advanced Materials*, 9.

Auger, M. (1997). Membrane structure and dynamics as viewed by solid-state NMR spectroscopy. *Biophysical Chemistry*, 68:233–241.

Avnir, D., Coradin, T., Lev, O., and Livage, J. (2006). Recent bio-applications of sol-gel materials. *Journal of Materials Chemistry*, 16:1013–1030.

Bain, C. D., Troughton, E. B., Tao, Y.-T., Evall, J., Whitesides, G. M., and Nuzzo, R. G. (1989). Formation of monolayer films by the spontaneous assembly of organic thiols from solution onto gold. *Journal of the American Chemical Society*, 111:321–335.

Bally, M., Bailey, K., Sugihara, K., Grieshaber, D., Vörös, J., and Städler, B. (2010). Liposome and lipid bilayer arrays towards biosensing applications. *Small*, 6:2481–2497.

Baron, C. and Thompson, T. E. (1975). Solubilization of bacterial-membrane proteins using alkyl glucosides and dioctanoyl phosphatidylcholine. *Biochimica et Biophysica Acta*, 382:276–285.

Barron, P. F. and Frost, R. L. (1985). Solid-state Si-29 NMR examination of the 2-1 ribbon magnesium silicates, sepiolite and palygorskite. *American Mineralogist*, 70:758–766.

Bayerl, T. M. (2004). A glass bead game. *Nature*, 427:105–106.

Bayerl, T. M. and Bloom, M. (1990). Physical-properties of single phospholipid-bilayers adsorbed to micro glass-beads - A new vesicular model system studied by ^{2}H-nuclear magnetic-resonance. *Biophysical Journal*, 58:357–362.

Beck, J. S., Vartuli, J. C., Kennedy, G. J., Kresge, C. T., Roth, W. J., and Schramm, S. E. (1994). Molecular or supramolecular templating: Defining the role of surfactant chemistry in the formation of microporous and mesoporous molecular sieves. *Chemistry of Materials*, 6:1816–1821.

Beck, J. S., Vartuli, J. C., Roth, W. J., Leonowicz, M. E., Kresge, C. T., Schmitt, K. D., Chu, C. T. W., Olson, D. H., Sheppard, E. W., McCullen, S. B., Higgins, J. B., and Schlenker, J. L. (1992). A new family of mesoporous molecular-sieves prepared with liquid-crystal templates. *Journal of the American Chemical Society*, 114:10834–10843.

Becker, A. L., Johnston, A. P. R., and Caruso, F. (2010). Peptide nucleic acid films and capsules: Assembly and enzymatic degradation. *Macromolecular Bioscience*, 10:488–495.

Begú, S., Aubert-Pouessel, A., Polexe, R., Leitmanova, E., Lerner, D. A., Devoisselle, J. M., and Tichit, D. (2009). New layered double hydroxides/phospholipid bilayer hybrid material with strong potential for sustained drug delivery system. *Chemistry of Materials*, 21:2679–2687.

Benavente, J., Vázquez, M. I., Hierrezuelo, J., and López-Romero, J. M. (2011). Physicochemical and transport parameters for a lipid coated regenerated cellulose membrane. *Vacuum*, 85:1067–1070.

Bensaude-Vincent, B., Arribart, H., Bouligand, Y., and Sanchez, C. (2002). Chemists and the school of nature. *New Journal of Chemistry*, 26:1–5.

Betina, V. (1989). *Mycotoxins. Chemical, Biological and Environmental aspects*. Elsevier Scientific: Amsterdam.

Birch, W. R., Knewtson, M. A., Garoff, S., Suter, R. M., and Satija, S. (1994). The molecular structure of autophobed monolayers and precursing films of a cationic surfactant on the silicon oxide/silicon surface. *Colloids and Surfaces A: Physicochemical and Engineering Aspects*, 89:145–155.

Bonanni, A., Pividori, M. I., and Del Valle, M. (2010). Impedimetric detection of influenza a (H1N1) DNA sequence using carbon nanotubes platform and gold nanoparticles amplification. *Analyst*, 135:1765–1772.

Boog, C. J. P. (2009). Principles of vaccination and possible development strategies for rational design. *Immunology Letters*, 122:104–107.

Bradford, M. M. (1976). Rapid and sensitive method for quantitation of microgram quantities of protein utilizing principle of protein-dye binding. *Analytical Biochemistry*, 72:248–254.

Braun, S., Rappoport, S., Zusman, R., Avnir, D., and Ottolenghi, M. (1990). Biochemically active sol-gel glasses - The trapping of enzymes. *Materials Letters*, 10:1–5.

Brauner, K. and Preisinger, A. (1956). *Mineralogische und Petrographische Mitteilungen*, 6:120.

Brett, I. C. and Johansson, B. E. (2005). Immunization against influenza a virus: Comparison of conventional inactivated, live-attenuated and recombinant baculovirus produced purified hemagglutinin and neuraminidase vaccines in a murine model system. *Virology*, 339:273–280.

Brian, A. A. and McConnell, H. M. (1984). Allogeneic stimulation of cyto-toxic t-cells by supported planar membranes. *Proceedings of the National Academy of Sciences of the United States of America-Biological Sciences*, 81:6159–6163.

Brigatti, M. F., Galan, E., and Theng, B. K. G. (2006). Structures and mineralogy of clay minerals. In Bergaya, F., Theng, B. K. G., and Lagaly, G., editors, *Handbook of Clay Science*, chapter 2. Elsevier Science Ltd.: Amsterdam.

Brown, G. and Brindley, G. W. (1980). X-ray diffraction procedures for clay mineral identification. In Brindley, G. W. and Brown, G., editors, *Crystal Structures of Clay Minerals and their X-ray Identification*, chapter 5. Mineralogical Society, London, 1 edition.

Brumaru, C. and Geng, M. L. (2010). Interaction of surfactants with hydrophobic surfaces in nanopores. *Langmuir*, 26:19091–19099.

Bunting, P. S. and Laidler, K. J. (1972). Kinetic studies on solid-supported beta-galactosidase. *Biochemistry*, 11:4477–4483.

Camacho, D. I., Morales, R., Arizaga, G. G. C., Wypych, F., and Krieger, N. (2009). Immobilization of laccase on hybrid layered double hydroxide. *Quimica Nova*, 32:1495–1499.

Casero, E., Darder, M., Takada, K., Abruna, H. D., Pariente, F., and Lorenzo, E. (1999). Electrochemically triggered reaction of a surface-confined reagent: Mechanistic and

EQCM characterization of redox-active self-assembling monolayers derived from 5,5-dithiobis(2-nitrobenzoic acid) and related materials. *Langmuir*, 15:127–134.

Cesareo, S. D. and Langton, S. R. (1992). Kinetic-properties of helicobacter-pylori urease compared with jack bean urease. *Fems Microbiology Letters*, 99:15–22.

Chemburu, S., Fenton, K., Lopez, G. P., and Zeineldin, R. (2010). Biomimetic silica microspheres in biosensing. *Molecules*, 15:1932–1957.

Chen, C., Wang, F., Liang, J., and Tang, Q. (2011). Thermal insulation coatings containing sepiolite mineral fibers and their performance. *Advanced Materials Research*, 178:318–323.

Chen, X. Y., Wolfgang, D. E., and Sampson, N. S. (2000). Use of the parallax-quench method to determine the position of the active-site loop of cholesterol oxidase in lipid bilayers. *Biochemistry*, 39:13383–13389.

Chibowski, E., Delgado, A. V., Rudzka, K., Szczes, A., and Holysz, L. (2011). Surface modification of glass plates and silica particles by phospholipid adsorption. *Journal of Colloid and Interface Science*, 353:281–289.

Choy, J. H., Kwak, S. Y., Jeong, Y. J., and Park, J. S. (2000). Inorganic layered double hydroxides as nonviral vectors. *Angewandte Chemie-International Edition*, 39:4042–4045.

Choy, J. H., Kwak, S. Y., Park, J. S., Jeong, Y. J., and Portier, J. (1999). Intercalative nanohybrids of nucleoside monophosphates and DNA in layered metal hydroxide. *Journal of the American Chemical Society*, 121:1399–1400.

Choy, J. H., Paek, S. M., Oh, J. M., and Jang, E. S. (2002). Intercalative route to heterostructured nanohybrids. *Current Applied Physics*, 2:489–495.

Chunbo, Y., Daqing, Z., Aizhuo, L., and Jiazuan, N. (1995). A NMR study of the interaction of silica with dipalmitoylphosphatidylcholine liposomes. *Journal of Colloid and Interface Science*, 172:536–538.

Clapp, T., Siebert, P., Chen, D., and Jones Braun, L. (2010). Vaccines with aluminum-containing adjuvants: Optimizing vaccine efficacy and thermal stability. *Journal of Pharmaceutical Sciences*, 100:388–401.

Coffman, R. L., Sher, A., and Seder, R. A. (2010). Vaccine adjuvants: Putting innate immunity to work. *Immunity*, 33:492–503.

Colowick, N. P., Kaplan, N. P., and Mosbach, K., editors (1998). *Immobilized enzymes and cells, Part D*, volume 137 of *Methods in Enzymology*. Academic Press, NY.

Costantino, U., Ambrogi, V., Nocchetti, M., and Perioli, L. (2008). Hydrotalcite-like compounds: Versatile layered hosts of molecular anions with biological activity. *Microporous and Mesoporous Materials*, 107:149–160.

Cox, N. (2002). WHO manual on animal influenza diagnosis and surveillance, WHO/CDS/CS/NCS/2002.5. World Health Organization.

Cracknell, J. A., Vincent, K. A., and Armstrong, F. A. (2008). Enzymes as working or inspirational electrocatalysts for fuel cells and electrolysis. *Chemical Reviews*, 108:2439–2461.

Cremer, P. S. and Boxer, S. G. (1999). Formation and spreading of lipid bilayers on planar glass supports. *Journal of Physical Chemistry B*, 103:2554–2559.

Crepaldi, E. L., Pavan, P. C., and Valim, J. B. (2000). Comparative study of the coprecipitation methods for the preparation of layered double hydroxides. *Journal of the Brazilian Chemical Society*, 11:64–70.

Darder, M., Aranda, P., Ferrer, M. L., Gutiérrez, M. C., del Monte, F., and Ruiz-Hitzky, E. (2011). Progress in bionanocomposite and bioinspired foams. *Advanced Materials*. DOI: 10.1002/adma.201101617.

Darder, M., Aranda, P., and Ruiz-Hitzky, E. (2007). Bionanocomposites: A new concept of ecological, bioinspired, and functional hybrid materials. *Advanced Materials*, 19:1309–1319.

Darder, M., Casero, E., Diaz, D. J., Abruna, H. D., Pariente, F., and Lorenzo, E. (2000). Concentration dependence of aggregate formation upon adsorption of 5-(octyldithio)-2-nitrobenzoic acid on gold electrodes. *Langmuir*, 16:9804–9811.

Darder, M., Colilla, M., and Ruiz-Hitzky, E. (2003). Biopolymer-clay nanocomposites based on chitosan intercalated in montmorillonite. *Chemistry of Materials*, 15:3774–3780.

Darder, M., López-Blanco, M., Aranda, P., Leroux, F., and Ruiz-Hitzky, E. (2005a). Bio-nanocomposites based on layered double hydroxides. *Chemistry of Materials*, 17:1969–1977.

Darder, M., Lopez-Blanco, M., Aranda, P., Leroux, F., and Ruiz-Hitzky, E. (2005b). Bio-nanocomposites based on layered double hydroxides. *Chemistry of Materials*, 17:1969–1977.

Davis, S. A., Dujardin, E., and Mann, S. (2003). Biomolecular inorganic materials chemistry. *Current Opinion in Solid State and Materials Science*, 7:273–281.

del Real, G. (2011). Personal Communication.

Deleu, M., Paquot, M., Jacques, P., Thonart, P., Adriaensen, Y., and Dufrene, Y. F. (1999). Nanometer scale organization of mixed surfactin/phosphatidylcholine monolayers. *Biophysical Journal*, 77:2304–2310.

Desheng, Q., Fan, L., Yanhu, Y., and Niya, Z. (2005). Adsorption of aflatoxin B1 on montmorillonite. *Poultry Science*, 84:959–961.

Desigaux, L., Ben Belkacem, M., Richard, P., Cellier, J., Leone, P., Cario, L., Leroux, F., Taviot-Gueho, C., and Pitard, B. (2006). Self-assembly and characterization of layered double hydroxide/DNA hybrids. *Nano Letters*, 6:199–204.

Dick, S. G., Fuerstenau, D. W., and Healy, T. W. (1971). Adsorption of alkylbenzene sulfonate (A.B.S.) surfactants at the alumina-water interface. *Journal of Colloid and Interface Science*, 37:595–602.

Dimotakis, E. D. and Pinnavaia, T. J. (1990). New route to layered double hydroxides intercalated by organic-anions - Precursors to polyoxometalate-pillared derivatives. *Inorganic Chemistry*, 29:2393–2394.

Ding, S.-J., Chang, B.-W., Wu, C.-C., Lai, M.-F., and Chang, H.-C. (2005). Impedance spectral studies of self-assembly of alkanethiols with different chain lengths using different immobilization strategies on Au electrodes. *Analytica Chimica Acta*, 554:43–51.

Diouani, M. F., Helali, S., Hafaid, I., Hassen, W. M., Snoussi, M. A., Ghram, A., Jaffrezic-Renault, N., and Abdelghani, A. (2008). Miniaturized biosensor for avian influenza virus detection. *Materials Science & Engineering C-Biomimetic and Supramolecular Systems*, 28:580–583.

Dixon, N. E., Blakeley, R. L., and Zerner, B. (1980). Jack bean urease (ec 3.5.1.5). A simple dry ashing procedure for the micro-determination of trace-metals in proteins - The nickel content of urease. *Canadian Journal of Biochemistry*, 58:469–473.

Dubois, M., Gilles, K. A., Hamilton, J. K., Rebers, P. A., and Smith, F. (1956). Colorimetric method for determination of sugars and related substances. *Analytical Chemistry*, 28:350–356.

Eddowes, M. J. (1987). Direct immunochemical sensing - Basic chemical principles and fundamental limitations. *Biosensors*, 3:1–15.

El Karadaghi, S., Zakomirdin, J. A., Shimane, C., Bucher, D. J., Tverdislov, V. A., and Kharitonenkov, I. G. (1984). Interaction of influenza virus proteins with planar bilayer lipid membranes I. Characterization of their adsorption and incorporation into lipid bilayers. *Biochimica et Biophysica Acta - Biomembranes*, 778:269–275.

Evans, D. G. and Slade, R. C. T. (2005). Structural aspects of layered double hydroxides. In Evans, D. G. and Duan, X., editors, *Layered Double Hydroxides*. Springer, Berlin Heidelberg.

Eytan, G. D. (1982). Use of liposomes for reconstitution of biological functions. *Biochimica et Biophysica Acta*, 694:185–202.

Fernandes, F. M., Manjubala, I., and Ruiz-Hitzky, E. (2011). Gelatin renaturation and the interfacial role of fillers in bionanocomposites. *Physical Chemistry Chemical Physics*, 13:4901–4910.

Ferraz, H. C., Guimaraes, J. A., Alves, T. L. M., and Constantino, C. J. L. (2011). Monomolecular films of cholesterol oxidase and S-layer proteins. *Applied Surface Science*, 257:6535–6539.

Figueroa, R. A., Leonard, A., and Mackay, A. A. (2004). Modeling tetracycline antibiotic sorption to clays. *Environmental Science & Technology*, 38:476–483.

Forano, C. and Prevot, V. (2008). Enzyme-based bioinorganic materials. In Ruiz-Hitzky, E., Ariga, K., and Lvov, Y. M., editors, *Bio-Inorganic Hybrid Nanomaterials - Strategies, Syntheses, Characterization and Application*, chapter 15, pages 443–484. Wiley-VCH,, Weinheim, 1 edition.

Fripiat, J., Chaussidon, J., and Jelli, A. (1971). *Chimie-Physique de Phenomenes de Surface*. Masson et Cie: Paris.

Garcia-Segura, J. M., Cid, C., Dellano, J. M., and Gavilanes, J. G. (1987). Sepiolite-supported urease. *British Polymer Journal*, 19:517–522.

Gasparini, R., Montomoli, E., Marinello, E., Guerranti, R., Sansone, M., Pilia, S., Sticchi, I., Icardi, G., Ansaldi, F., and Crovari, P. (2004). Purification of influenza B virus hemagglutinin by isoelectric focusing. *Journal of Preventive Medicine and Hygiene*, 45:17–20.

Gerin, P. A., Dengis, P. B., and Rouxhet, P. G. (1995). Performances of XPS analysis of model biochemical compounds. *Journal de Chimie Physique*, 92:1043–1065.

Gharaei-Fathabad, E. (2011). Biosurfactants in pharmaceutical industry: A mini-review. *American Journal of Drug Discovery and Development*, 1:58–69.

Giles, C. H., Dsilva, A. P., and Easton, I. A. (1974). General treatment and classification of solute adsorption isotherm. Part ii. Experimental interpretation. *Journal of Colloid and Interface Science*, 47:766–778.

Giles, C. H., MacEwan, T. H., Nakhwa, S. N., and Smith, D. (1960). Studies in adsorption. A system of classification of solution adsorption isotherms, and its use in diagnosis of adsorption mechanisms and in measurement of specific surface areas of solids. *Journal of the Chemical Society*, 111:3973–3993.

Gill, A., Leatherbarrow, R. J., Hoare, M., Pollard-Knight, D. V., Lowe, P. A., and Fortune, D. H. (1996). Analysis of kinetic data of antibody-antigen interaction from an optical biosensor by exponential curve fitting. *Journal of Biotechnology*, 48:117–127.

Gill, I. and Ballesteros, A. (2000a). Bioencapsulation within synthetic polymers (part 1): Sol-gel encapsulated biologicals. *Trends in Biotechnology*, 18:282–296.

Gill, I. and Ballesteros, A. (2000b). Bioencapsulation within synthetic polymers (part 2): Non-sol-gel protein-polymer biocomposites. *Trends in Biotechnology*, 18:469–479.

Girard-Egrot, A. P., Godoy, S., and Blum, L. J. (2005). Enzyme association with lipidic Langmuir-Blodgett films: Interests and applications in nanobioscience. *Advances in Colloid and Interface Science*, 116:205–225.

Goldblatt, L. A. (1977). Mycotoxins: Past, present and future. *Journal of the American Oil Chemists' Society*, 54:302–307.

Gómez Avilés, A. (2010). *Meteriales inorgnicos micro- y nano-heteroestructurados basados en sepiolita*. PhD thesis, Universidad Autónoma de Madrid.

Gouanve, F., Marais, S., Bessadok, A., Langevin, D., Morvan, C., and Metayer, M. (2006). Study of water sorption in modified flax fibers. *Journal of Applied Polymer Science*, 101:4281–4289.

Griffiths, D. and Hall, G. (1993). Biosensors - what real progress is being made. *Trends in Biotechnology*, 11:122–130.

Gu, T. and Rupprecht, H. (1990). Hemimicelle shape and size. *Colloid & Polymer Science*, 268:1148–1150.

Guan, J.-G., Miao, Y.-Q., and Zhang, Q.-J. (2004). Impedimetric biosensors. *Journal of Bioscience and Bioengineering*, 97:219–226.

Gupta, R. K. (1998). Aluminum compounds as vaccine adjuvants. *Advanced Drug Delivery Reviews*, 32:155–172.

Gutierrez, M. C., Ferrer, M. L., Tartaj, P., and del Monte, F. (2009). Biomedical applications of organic-inorganic hybrid nanoparticles. In Merhari, L., editor, *Hybrid Nanocomposites for Nanotechnology*, chapter 15, pages 707–768. Springer Science.

Hamilton, B. K., Stockmeyer, L. J., and Colton, C. K. (1973). Comments on diffusive and electrostatic effects with immobilized enzymes. *Journal of Theoretical Biology*, 41:547–560.

Heathcote, J. G. and Hibbert, J. R. (1978). *Aflatoxins: Chemical and Biological Aspects*. Elsevier Scientific: Amsterdam.

Heegaard, P., Dedieu, L., Johnson, N., Le Potier, M.-F., Mockey, M., Mutinelli, F., Vahlenkamp, T., Vascellari, M., and Sörensen, N. (2010). Adjuvants and delivery systems in veterinary vaccinology: Current state and future developments. *Archives of Virology*, 156:183–202.

Hernandez-Moreno, M. J., Ulibarri, M. A., Rendon, J. L., and Serna, C. J. (1985). IR characteristics of hydrotalcite-like compounds. *Physics and Chemistry of Minerals*, 12:34–38.

Hirayama, C., Sugimura, M., Saito, H., and Nakamura, M. (2000). Purification and properties of urease from the leaf of mulberry, morus alba. *Phytochemistry*, 53:325–330.

Hobson, D. C. A., Beare, A., and Ward-Gardner, A. (1973). Hemagglutination inhibition antibody titers as a measure of protection against influenza in man. *Developments in Biological Standardization*, 20(164-168).

Hoffman, A. S. (2002). Hydrogels for biomedical applications. *Advanced Drug Delivery Reviews*, 54:3–12.

Hope, M. J., Bally, M. B., Webb, G., and Cullis, P. R. (1985). Production of large unilamellar vesicles by a rapid extrusion procedure. Characterization of size distribution, trafiped volume and ability to maintain a membrane potential. *Biochimica et Biophysica Acta*, 812:55–65.

Hou, Y. X., Jaffrezic-Renault, N., Zhang, A. D., Wan, J. L., Errachid, A., and Chovelon, J. M. (2002). Study of pure urease Langmuir-Blodgett film and application for biosensor development. *Sensors and Actuators B-Chemical*, 86:143–149.

Huang, Q., Opitz, R., Knapp, E.-W., and Herrmann, A. (2002). Protonation and stability of the globular domain of influenza virus hemagglutinin. *Biophysical Journal*, 82:1050–1058.

Hubbard, J. B., Silin, V., and Plant, A. L. (1998a). Self assembly driven by hydrophobic interactions at alkanethiol monolayers: Mechanism of formation of hybrid bilayer membranes. *Biophysical Chemistry*, 75:163–176.

Hubbard, J. B., Silin, V., and Plant, A. L. (1998b). Self assembly driven by hydrophobic interactions at alkanethiol monolayers: Mechanism of formation of hybrid bilayer membranes. *Biophysical Chemistry*, 75:163–176.

Huleatt, J. W., Jacobs, A. R., Tang, J., Desai, P., Kopp, E. B., Huang, Y., Song, L., Nakaar, V., and Powell, T. J. (2007). Vaccination with recombinant fusion proteins incorporating toll-like receptor ligands induces rapid cellular and humoral immunity. *Vaccine*, 25:763–775.

Ichijo, H., Nagasawa, J., and Yamauchi, A. (1990). Immobilization of biocatalysts with poly(vinyl alcohol) supports. *Journal of Biotechnology*, 14:169–178.

Illanes, A., editor (2008). *Enzyme Biocatalysis: Principles and Applications*. Springer, Netherlands.

Itoh, T., Yano, K., Inada, Y., and Fukushima, Y. (2002). Photostabilized chlorophyll a in mesoporous silica: Adsorption properties and photoreduction activity of chlorophyll a. *Journal of the American Chemical Society*, 24:13437–13441.

Jaynes, W. F., Zartman, R. E., and Hudnall, W. H. (2007). Aflatoxin B1 adsorption by clays from water and corn meal. *Applied Clay Science*, 36:197–205.

Jenkins, R. and Snyder, R. L. (1996). *Introduction to X-ray Powder Diffractometry*. Wiley-Interscience, 1 edition.

Johansson, B. E. and Brett, I. C. (2007). Changing perspective on immunization against influenza. *Vaccine*, 25:3062–3065.

Jönsson, B., Lindman, B., Holmberg, R., and Kronberg, B., editors (1997). *Surfactants and Polymers in Aqueous Solution*. John Wiley & Sons Ldt., Chichester, 1 edition.

Jurak, M. and Chibowski, E. (2007). Wettability and topography of phospholipid DPPC multilayers deposited by spin-coating on glass, silicon, and mica slides. *Langmuir*, 23:10156–10163.

Kam, L. and Boxer, S. G. (2003). Spatially selective manipulation of supported lipid bilayers by laminar flow: Steps toward biomembrane microfluidics. *Langmuir*, 19:1624–1631.

Kannewischer, I., Arvide, M. G. T., White, G. N., and Dixon, J. B. (2006). Smectite clays as adsorbents of aflatoxin B1: Initial steps. *Clay Science Japan*, 12:199–204.

Karlovska, J., Uhrikova, D., Kucerka, N., Teixeira, J., Devinsky, F., Lacko, I., and Balgavy, P. (2006). Influence of N-dodecyl-N,N-dimethylamine N-oxide on the activity of sarcoplasmic reticulum Ca^{2+}-transporting ATPase reconstituted into diacylphosphatidylcholine vesicles: Effects of bilayer physical parameters. *Biophysical Chemistry*, 119:69–77.

Kato, K., Walde, P., Mitsui, H., and Higashi, N. (2003). Enzymatic activity and stability of d-fructose dehydrogenase and sarcosine dehydrogenase immobilized onto giant vesicles. *Biotechnology and Bioengineering*, 84:415–423.

Kawasaki, H., Ban, K., and Maeda, H. (2004). Investigation of the stability of graphite particle dispersion and the hemimicelle formation process at graphite/solution interfaces using atomic force microscopy. *The Journal of Physical Chemistry B*, 108:16746–16752.

Knapp, C., Gil-Llambias, F. J., Gulppi-Cabra, M., Avila, P., and Blanco, J. (1997). Phase distribution in titania-sepiolite catalyst supports prepared by different methods. *Journal of Materials Chemistry*, 7:1641–1645.

Korn, M. and Killmann, E. (1980). Infrared and microcalorimetric studies of the adsorption of polymers with ester groups, in the main or side chain, at the silica/carbon tetrachloride interface. *Journal of Colloid and Interface Science*, 76:19–31.

Kosaric, N., editor (1993). *Biosurfactants: Production, properties, applications*. Surfactant Science Series. CRC Press, Boca Raton, 1 edition.

Kouassi, G., Irudayaraj, J., and McCarty, G. (2005). Examination of cholesterol oxidase attachment to magnetic nanoparticles. *Journal of Nanobiotechnology*, 3:1.

Krajewska, B. (2009). Ureases I. Functional, catalytic and kinetic properties: A review. *Journal of Molecular Catalysis B-Enzymatic*, 59:9–21.

Kreit, J. and Sampson, N. S. (2009). Cholesterol oxidase: Physiological functions. *Febs Journal*, 276:6844–6856.

Kruger, N. J. (2002). The bradford method for protein quantification. In Walker, J. M., editor, *The Protein Protocols Handbook*. Humana Press Inc, Totowa, NJ, 2 edition.

Kuang, W., Facey, G. A., Detellier, C., Casal, B., Serratosa, J. M., and Ruiz-Hitzky, E. (2003). Nanostructured hybrid materials formed by sequestration of pyridine molecules in the tunnels of sepiolite. *Chemistry of Materials*, 15:4956–4967.

Kumar, N., Garoff, S., and Tilton, R. D. (2004). Experimental observations on the scaling of adsorption isotherms for nonionic surfactants at a hydrophobic solid-water interface. *Langmuir*, 20:4446–4451.

Kurganov, B. I., Lobanov, A. V., Borisov, I. A., and Reshetilov, A. N. (2001). Criterion for Hill equation validity for description of biosensor calibration curves. *Analytica Chimica Acta*, 427:11–19.

Kurien, B. T. and Scofield, R. H., editors (2009). *Protein Blotting and Detection*, volume 536 of *Methods in Molecular Biology*. Humana Press, 1 edition.

Labajos, F. M., Rives, V., and Ulibarri, M. A. (1992). Effect of hydrothermal and thermal treatments on the physicochemical properties of Mg-Al hydrotalcite-like materials. *Journal of Materials Science*, 27:1546–1552.

Lagaly, G. (1986). Interaction of alkylamines with different types of layered compounds. *Solid State Ionics*, 22(1):43–51.

Lang, S. (2002). Biological amphiphiles (microbial biosurfactants). *Current Opinion in Colloid Interface Science*, 7:12–20.

Lehn, J. M. (1978). Cryptates: The chemistry of macropolycyclic inclusion complexes. *Accounts of Chemical Research*, 11:49–57.

Lemke, S. L. (2000). PhD thesis, Texas A&M University.

Lemke, S. L., Mayura, K., Reeves, W. R., Wang, N., Fickey, C., and Phillips, T. D. (2001). Investigation of organophilic montmorillonite clay inclusion in zearalenone-contaminated diets using the mouse uterine weight bioassay. *Journal of Toxicology and Environmental Health, Part A*, 62:243–258.

Lide, D. R. (2009). *CRC Handbook of Chemistry and Physics*. CRC Press: Boca Raton, 86 edition.

Liu, Z. H. and Brown, N. M. D. (1998). XPS characterization of mica surfaces processed using a radio-frequency argon plasma. *Journal of Physics D: Applied Physics*, 31:1771–1781.

Livage, J. (1977). Vers une chimie écologique. Quand l'air et l'eau remplacent le pétrole. Le Monde. October 27th, 1977.

Lu, J. R., Zhao, X. B., and Yaseen, M. (2007). Biomimetic amphiphiles: Biosurfactants. *Current Opinion in Colloid & Interface Science*, 12:60–67.

Madaras, M. B. and Buck, R. P. (1996). Miniaturized biosensors employing electropolymerized permselective films and their use for creatinine assays in human serum. *Analytical Chemistry*, 68:3832–3839.

Magana-Plaza, I., Montes, C., and Ruiz-Herrera, J. (1971). Purfication and biochemical characteristics of urease from proteus-rettgeri. *Biochimica et Biophysica Acta*, 242:230–237.

Malvern (2011). Dynamic light scattering: An introduction in 30 minutes. Technical report, Malvern Instruments Ltd. Technical note.

Mann, S. (1989). Crystallochemical strategies in biomineralization. In Mann, S., Werbb, J., and Williams, R., editors, *Biomineralization, Chemical and Biological Perspectives*, chapter 2, pages 35–62. VCH, Weinheim.

Marzadori, C., Miletti, S., Gessa, C., and Ciurli, S. (1998). Immobilization of jack bean urease on hydroxyapatite: Urease immobilization in alkaline soils. *Soil Biology and Biochemistry*, 30:1485–1490.

Maslova, M. V., Gerasimova, L. G., and Forsling, W. (2004). Surface properties of cleaved mica. *Colloid Journal*, 66:322–328.

Matsumura, S., Imai, K., Yoshikawa, S., Kawada, K., and Uchibor, T. (1990). Surface activities, biodegradability and antimicrobial properties of n-alkyl glucosides, mannosides and galactosides. *Journal of the American Oil Chemists' Society*, 67:996–1001.

Maxwell, D. J., Taylor, J. R., and Nie, S. (2002). Self-assembled nanoparticle probes for recognition and detection of biomolecules. *Journal of the American Chemical Society*, 124:9606–9612.

Mayer, L. D., Hope, M. J., and Cullis, P. R. (1986). Vesicles of variable sizes produced by a rapid extrusion procedure. *Biochimica et Biophysica Acta*, 858:161–168.

McConnell, H. M., Watts, T. H., Weis, R. M., and Brian, A. A. (1986). Supported planar membranes in studies of cell-cell recognition in the immune-system. *Biochimica et Biophysica Acta*, 864:95–106.

McCulloch, W. S. (1962). In Bernard, E. E. and Kare, M. R., editors, *Biological Prototypes and Synthetic Systems*, volume 1, pages 393–397. Plenum Press, New York.

Mechler, A., Praporski, S., Piantavigna, S., Heaton, S. M., Hall, K. N., Aguilar, M. I., and Martin, L. L. (2009). Structure and homogeneity of pseudo-physiological phospholipid bilayers and their deposition characteristics on carboxylic acid terminated self-assembled monolayers. *Biomaterials*, 30:682–689.

Mendes, R. K., Freire, R. S., Fonseca, C. P., Neves, S., and Kubota, L. T. (2004). Characterization of self-assembled thiols monolayers on gold surface by electrochemical impedance spectroscopy. *Journal of the Brazilian Chemical Society*, 15:849–855.

Menger, F. M., Chlebowski, M. E., Galloway, A. L., Lu, H., Seredyuk, V. A., Sorrells, J. L., and Zhang, H. (2005). A tribute to the phospholipid. *Langmuir*, 21:10336–10341.

Meyn, M., Beneke, K., and Lagaly, G. (1990). Anion-exchange reactions of layered double hydroxides. *Inorganic Chemistry*, 29:5201–5207.

Miller, R., Fainerman, V. B., and Möhwald, H. (2002). Adsorption behavior of oxyethylated surfactants at the air/water interface. *Journal of Colloid and Interface Science*, 247:193–199.

Mittal, A. (2006). Adsorption kinetics of removal of a toxic dye, malachite green, from wastewater by using hen feathers. *Journal of Hazardous Materials*, B133:196202.

Mizutani, F., Sato, Y., Sawaguchi, T., Yabuki, S., and Iijima, S. (1998). Rapid measurement of transaminase activities using an amperometric l-glutamate-sensing electrode based on a glutamate oxidase-polyion complex-bilayer membrane. *Sensors and Actuators B-Chemical*, 52:23–29.

Mizutani, F., Yabuki, S., and Sato, Y. (1997). Voltammetric enzyme sensor for urea using mercaptohydroquinone-modified gold electrode as the base transducer. *Biosensors Bioelectronics*, 12:321–328.

Molina-Bolivar, J. A. and Carnero Ruiz, C. (2009). Self-assembly and micellar structures of sugar-based surfactants: Effect of temperature and salt addition. In Carnero Ruiz, C., editor, *Sugar-based Surfactants*, Surfactant Science Series, chapter 3, pages 61–104. CRC Press, Boca Raton.

Moujahid, E. M., Besse, J. P., and Leroux, F. (2002). Synthesis and characterization of a polystyrene sulfonate layered double hydroxide nanocomposite. In-situ polymerization vs. polymer incorporation. *Journal of Materials Chemistry*, 12:3324–3330.

Murray, D. K., Harrison, J. C., and Wallace, W. E. (2005). A ^{13}C CP/MAS and ^{31}P NMR study of the interactions of dipalmitoylphosphatidylcholine with respirable silica and kaolin. *Journal of Colloid and Interface Science*, 288:166–170.

Nagata, H., Shimoda, S., and Toshio, S. (1974). Dehydration of bound water of sepiolite. *Clays and Clay Minerals*, 22:285–293.

Nauck, M., Marz, W., and Wieland, H. (2000). Is lipoprotein (a) cholesterol a significant indicator of cardiovascular risk? *Clinical Chemistry*, 46:436–437.

Naumann, C., Brumm, T., and Bayerl, T. M. (1992). Phase-transition behavior of single phosphatidylcholine bilayers on a solid spherical support studied by DSC, NMR and FT-IR. *Biophysical Journal*, 63:1314–1319.

Nayak, D. P., Hui, E. K. W., and Barman, S. (2004). Assembly and budding of influenza virus. *Virus Research*, 106:147–165.

Nikolelis, D. P., Hianik, T., and Krull, U. J. (1999). Biosensors based on thin lipid films and liposomes. *Electroanalysis*, 11:7–15.

Nikolelis, D. P., Hianik, T., and Nikoleli, G.-P. (2010). Stabilized lipid films in electrochemical biosensors. *Electroanalysis*, 22:2747–2763.

Nir, S., Undabeytia, T., Yaron-Marcovich, D., El-Nahhal, Y., Polubesova, T., Serban, C., Rytwo, G., Lagaly, G., and Rubin, B. (2000). Optimization of adsorption of hydrophobic herbicides on montmorillonite preadsorbed by monovalent organic cations: Interaction between phenyl rings. *Environmental Science & Technology*, 34:1269–.

Niyo, K., editor (1989). *Mycotoxins: Economic and Health Risks*. CAST, Task force Report No 116. Ames, IA. Council for Agricultural Science and Technology.

Nuzzo, R. G., Fusco, F. A., and Allara, D. L. (1987). Spontaneously organized molecular assemblies. 3. Preparation and properties of solution adsorbed monolayers of organic disulfides on gold surfaces. *Journal of the American Chemical Society*, 109:2358–2368.

Oberts, B. P. and Blanchard, G. J. (2009). Formation of air-stable supported lipid monolayers and bilayers. *Langmuir*, 25:2962–2970.

Oda, I., Hirata, K., Watanabe, S., Shibata, Y., Kajino, T., Fukushima, Y., Iwai, S., and Itoh, S. (2006). Function of membrane protein in silica nanopores: Incorporation of photosynthetic light-harvesting protein LH2 into FSM. *Journal of Physical Chemistry B*, 110:1114–1120.

Ogura, K., Nakaoka, K., Nakayama, M., Kobayashi, M., and Fujii, A. (1999). Thermogravimetry/mass spectrometry of urease-immobilized sol-gel silica and the application of such a urease-modified electrode to the potentiometric determination of urea. *Analytica Chimica Acta*, 384:219–225.

Pack, D. W., Ng, K., Maloney, K. M., and Arnold, F. H. (1997). Ligand-induced reorganization and assembly in synthetic lipid membranes. *Supramolecular Science*, 4:3–10.

Pacwa-Plociniczak, M., Plaza, G. A., Piotrowska-Seget, Z., and Cameotra, S. S. (2011). Environmental applications of biosurfactants: Recent advances. *International Journal of Molecular Sciences*, 12:633–654.

Pajares, J. A. (1984). Personal Communication.

Park, G. S. (1986). Transport principles solution, diffusion and permeation in polymer membranes. In Bungay, P. M., Lonsdale, H. K., and de Pinto, M. N., editors, *Synthetic Membranes: Science, Engineering and Applications*, page 57107. Reidel, Holland.

Paul, S. O. and Ford, T. A. (1986). Infrared spectroscopic studies of hydrogen-bonded complexes of water with oxygen bases. III. The HOH-bending region of the spectra of water-molecules dissolved in some ketones and ethers. *Journal of Crystallographic and Spectroscopic Research*, 16:811–821.

Peetla, C., Stine, A., and Labhasetwar, V. (2009). Biophysical interactions with model lipid membranes: Applications in drug discovery and drug delivery. *Molecular Pharmaceutics*, 6:1264–1276.

Persson, C. M., Claesson, P. M., and Lunkenheimer, K. (2002). Interfacial behavior of n-decyl-beta-D-maltopyranoside on hydrophobic interfaces and the effect of small amounts of surface-active impurities. *Journal of Colloid and Interface Science*, 251:182–192.

Petelska, A. D. and Figaszewski, Z. A. (2000). Effect of pH on the interfacial tension of lipid bilayer membrane. *Biophysical Journal*, 78:812–817.

Petty, M. A. (1996). *Langmuir-Blodgett Films. An Introduction.* Cambridge University Press.

Phang, T.-L. and Franses, E. I. (2006). Physically self-assembled monolayers (PSAMs) of lecithin lipids at hydrophilic silicon oxide interfaces. *Langmuir*, 24:1609–1618.

Phillips, T. D. (1999). Dietary clay in the chemoprevention of aflatoxin-induced disease. *Toxicological Sciences*, 52:118–126.

Phillips, T. D., Lemke, S. L., and Grant, P. G. (2002). Characterization of clay-based enterosorbents for the prevention of aflatoxicosis. *Advances in Experimental Medicine and Biology*, 504:157–171.

Pimentel, G. C. and McClellan, A. L. (1960). *The Hydrogen Bond*. W.H. Freeman, San Francisco.

Plant, A. L. (1999). Supported hybrid bilayer membranes as rugged cell membrane mimics. *Langmuir*, 15:5128–5135.

Poon, L. L. M., Chan, K. H., Smith, G. J., Leung, C. S. W., Guan, Y., Yuen, K. Y., and Peiris, J. S. M. (2009). Molecular detection of a novel human influenza (H1N1) of pandemic potential by conventional and real-time quantitative RT-PCR assays. *Clinical Chemistry*, 55:1555–1558.

Pugh, R. J. and Bergström, L., editors (1994). *Surface and Colloid Chemistry in Advanced Ceramics Processing*, volume 51 of *surfactant science series*. Marcel Dekker, Inc, New York, 1 edition.

Pulendran, B. and Ahmed, R. (2011). Immunological mechanisms of vaccination. *Nature Immunology*, 12:509–517.

Puri, A., Loomis, K., Smith, B., Lee, J. H., Yavlovich, A., Heldman, E., and Blumenthal, R. (2009). Lipid-based nanoparticles as pharmaceutical drug carriers: From concepts to clinic. *Critical Reviews in Therapeutic Drug Carrier Systems*, 26.

Radler, J., Strey, H., and Sackmann, E. (1995). Phenomenology and kinetics of lipid bilayer spreading on hydrophilic surfaces. *Langmuir*, 11:4539–4548.

Ramsden, J. J. (1998). Biomimetic protein immobilization using lipid bilayers. *Biosensors & Bioelectronics*, 13:593–598.

Rapuano, R. and Carmona-Ribeiro, A. M. (1997). Physical adsorption of bilayer membranes on silica. *Journal of Colloid and Interface Science*, 193:104–111.

Rapuano, R. and Carmona-Ribeiro, A. M. (2000). Supported bilayers on silica. *Journal of Colloid and Interface Science*, 226:299–307.

Reimhult, E. (2010). Advances in nanopatterned and nanostructured supported lipid membranes and their applications. *Biotechnology genetic engineering reviews*, 27:185–216.

Reimhult, E., Baumann, M. K., Kaufmann, S., Kumar, K., and Spycher, P. R. (2008). Membrane biosensor platforms using nano- and microporous supports. *Trends in Biotechnology*, 26:82–89.

Remaut, H., Safarov, N., Ciurli, S., and Van Beeumen, J. (2001). Structural basis for Ni^{2+} transport and assembly of the urease active site by the metallochaperone uree from bacillus pasteurii. *Journal of Biological Chemistry*, 276:49365–49370.

Richard, C., Balavoine, F., Schultz, P., Ebbesen, T. W., and Mioskowski, C. (2003). Supramolecular self-assembly of lipid derivatives on carbon nanotubes. *Science*, 300:775–778.

Richter, R. P., Bérat, R., and Brisson, A. R. (2006). Formation of solid-supported lipid bilayers: An integrated view. *Langmuir*, 22:3497–3505.

Rodríguez, J. R. (2011). Personal Communication.

Rossow, K. D. (1998). Porcine reproductive and respiratory syndrome. *Veterinary Pathology Online*, 35:1–20.

Ruiz-Hitzky, E. (1974). *Contribution a l'etude des reactions de greffage des groupements organiques sur les surfaces minerales. Greffage de la sepiolite.* PhD thesis, University of Louvain, Belgium.

Ruiz-Hitzky, E. (2001). Molecular access to intracrystalline tunnels of sepiolite. *Journal of Materials Chemistry*, 11:86–91.

Ruiz-Hitzky, E. (2004). Organic-inorganic materials: From intercalation chemistry to devices. In Gómez-Romero, P. and Sanchez, C., editors, *Functional Hybrid Materials*, chapter 2. Wiley-VCH: Weinheim.

Ruiz-Hitzky, E., Aranda, P., and Darder, M.and Rytwo, G. (2010a). Hybrid materials based on clays for environmental and biomedical applications. *Journal of Materials Chemistry*, 20:9306–9321.

Ruiz-Hitzky, E., Aranda, P., and Darder, M. (2007). Polymer- and biopolymer-layered solid nanocomposites: Organic-inorganic assembling in two-dimensional hybrid systems. In Ariga, K. and Nalwa, H. S., editors, *Bottom-up Nanofabrication: Supramolecules, Self-assemblies, and Organized Films*, chapter 73, pages 1–38. American Scientific Publisher, Stevenson Ranch, CA.

Ruiz-Hitzky, E., Aranda, P., and Darder, M. (2008a). Bionanocomposites. In *Kirk-Othmer Encyclopedia of Chemical Technology*, pages 1–28. John Wiley Sons, Inc., Hoboken, NJ.

Ruiz-Hitzky, E., Aranda, P., Darder, M., and Ogawa, M. (2011). Hybrid and biohybrid silicate based materials: Molecular vs. block-assembling bottom-up processes. *Chemical Society Reviews*, 40:801–828.

Ruiz-Hitzky, E., Aranda, P., and Serratosa, J. M. (2004). Clay-organic interactions: Organoclay complexes and polymer-clay nanocomposites. In Auerbach, S. M., Carrado, K. A., and Dutta, P., editors, *Handbook of Layered Materials*, chapter 3, pages 91–154. Marcel Dekker: New York.

Ruiz-Hitzky, E., Darder, M., and Aranda, P. (2005). Functional biopolymer nanocomposites based on layered solids. *Journal of Materials Chemistry*, 15:3650–3662.

Ruiz-Hitzky, E., Darder, M., and Aranda, P. (2008b). An introduction to bio-nanohybrid materials. In Ruiz-Hitzky, E., Ariga, K., and Lvov, Y. M., editors, *Bio-inorganic Hybrid Nanomaterials - Strategies, Syntheses, Characterization and Application*, chapter 2, pages 1–40. Wiley-VCH,, Weinheim, 1 edition.

Ruiz-Hitzky, E., Darder, M., Aranda, P., and Ariga, K. (2010b). Advances in biomimetic and nanostructured biohybrid materials. *Advanced Materials*, 22:323–336.

Ruiz-Hitzky, E., Darder, M., Aranda, P., del Burgo, M. A. M., and del Real, G. (2009). Bionanocomposites as new carriers for influenza vaccines. *Advanced Materials*, 21:4167–4171.

Ruiz-Hitzky, E. and Van Meerbeeck, A. (2006). Clay mineral and organoclay-polymer nanocomposites. In Bergaya, F., Theng, B. K. G., and Lagaly, G., editors, *Handbook of Clay Science*, chapter 10. Elsevier Science Ltd.: Amsterdam.

Sackmann, E. (1996). Supported membranes: Scientific and practical applications. *Science*, 271:43–48.

Sahai, N. (2002). Biomembrane phospholipidoxide surface interactions: Crystal chemical and thermodynamic basis. *Journal of Colloid and Interface Science*, 252:309–319.

Sanchez, C., Arribart, H., and Guille, M. M. G. (2005). Biomimetism and bioinspiration as tools for the design of innovative materials and systems. *Nature Materials*, 4:277–288.

Sánchez-Verdejo, T., Undabeytia, T., Nir, S., Maqueda, C., and Morillo, E. (2008). Environmentally friendly slow release formulations of alachlor based on clay-phosphatidylcholine. *Environmental Science & Technology*, 42:5779–5784.

Santarén, J., Sanz, J., and Ruiz-Hitzky, E. (1990). Structural fluorine in sepiolite. *Clay Minerals*, 38:63–68.

Sanz, J. (1990). Distribution of ions in phyllosilicates by NMR spectroscopy. In A., M. and Burragato, F., editors, *Absorption Spectroscopy in Mineralogy*, pages 103–144. Elsevier Sci. Publ.: Amsterdam.

Savarala, S., Ahmed, S., Ilies, M. A., and Wunder, S. L. (2010). Formation and colloidal stability of DMPC supported lipid bilayers on SiO_2 nanobeads. *Langmuir*, 26:12081–12088.

Schauer, R. (2000). Achievements and challenges of sialic acid research. *Glycoconjugate Journal*, 17:485–499.

Scherrer, P. (1918). Bestimmung der Grösse und der inneren Struktur von Kolloidteilchen mittels Röntgenstrahlen. *Nachrichten von der Gesellschaft der Wissenschaften zu Göttingen*, 26:98100.

Schultz, L. G. (1969). Lithium and potassium absorption, dehydroxylation temperature, and structural water content of aluminous smectites. *Clays and Clay Minerals*, 17:115–149.

Seelig, J. (1978). ^{31}P nuclear magnetic resonance and head group structure of phospholipids in membranes. *Biochimica et Biophysica Acta*, 515:105–140.

Serna, C. and Vanscoyoc, G. E. (1978). Infrared study of sepiolite and palygorskite surfaces. In Mortland, M. M. and Farmer, V. C., editors, *International Clay Conference*, pages 197–206, Oxford. Elsevier, Amsterdam.

Serna, J. C. (1973). PhD thesis, University of Madrid.

Sethi, R. S. (1994). Transducer aspects of biosensors. *Biosensors & Bioelectronics*, 9:243–264.

Shervedani, R. K., Mehrjardi, A. H., and Zamiri, N. (2006). A novel method for glucose determination based on electrochemical impedance spectroscopy using glucose oxidase self-assembled biosensor. *Bioelectrochemistry*, 69:201–208.

Shijiazhuang (2011). Sepiolite fibers used as thermal insulation materials. Technical report, Shijiazhuang Mining Imp & Exp Trade Co., Ldt. Product details.

Shinoda, K., Yamaguchi, T., and Hori, R. (1961). The surface tension and the critical micelle concentration in aqueous solution of beta-d-alkyl glucosides and their mixtures. *Bulletin of the Chemical Society of Japan*, 34:237–241.

Simonsen, A. C. and Bagatolli, L. A. (2004). Structure of spin-coated lipid films and domain formation in supported membranes formed by hydration. *Langmuir*, 20:9720–9728.

Singleton, W., Gray, M., Brown, M., and White, J. (1965). Chromatographically homogeneous lecithin from egg phospholipids. *Journal of the American Oil Chemists' Society*, 42:53–56.

Small, D. (1967). Phase equilibria and structure of dry and hydrated egg lecithin. *Journal of Lipid Research*, 8:551–557.

Snyder, J. A. and Madura, J. D. (2008). Interaction of the phospholipid head group with representative quartz and aluminosilicate structures: An ab initio study. *Journal of Physical Chemistry B*, 112:7095–7103.

Steinem, C. and Janshoff, A. (2010). Multicomponent membranes on solid substrates: Interfaces for protein binding. *Current Opinion in Colloid Interface Science*, 15:479–488.

Stenesh, J. (1998). *Biochemistry - Part II: Biomolecules*. Plenum Press, 1 edition.

Stephenson, I., Wood, J. M., Nicholson, K. G., and Zambon, M. C. (2003). Sialic acid receptor specificity on erythrocytes affects detection of antibody to avian influenza haemagglutinin. *Journal of Medical Virology*, 70:391–398.

Streeter, I., Leventis, H. C., Wildgoose, G. G., Pandurangappa, M., Lawrence, N. S., Jiang, L., Jones, T. G. J., and Compton, R. G. (2004). A sensitive reagentless pH probe with a ca. 120 mV/pH unit response. *Journal of Solid State Electrochemistry*, 8:718–721.

Stubbs, G. W., Smith, H. G., and Litman, B. J. (1976). Alkyl glucosides as effective solubilizing agents for bovine rhodopsin - comparison with several commonly used detergents. *Biochimica et Biophysica Acta*, 426:46–56.

Sumner, J. B. (1926). The isolation and crystallization of the enzyme urease. Preliminary paper. *Journal of Biological Chemistry*, 69:435–441.

Sun, T., Qing, G., Su, B., and Jiang, L. (2011). Functional biointerface materials inspired from nature. *Chemical Society Reviews*, 40:2909–2921.

Szabo, T., Mitea, R., Leeman, H., Premachandra, G. S., Johnston, C. T., Szekeres, M., Dékány, I., and Schoonheydt, R. A. (2008). Adsorption of protamine and papain proteins on saponite. *Clays Clay Minerals*, 56:494–504.

Tamm, L. K. and McConnell, H. M. (1985). Supported phospholipid-bilayers. *Biophysical Journal*, 47:105–113.

Traving, C. and Schauer, R. (1998). Structure, function and metabolism of sialic acids. *Cellular and Molecular Life Sciences*, 54:1330–1349.

Trojanowicz, M. (2001). Miniaturized biochemical sensing devices based on planar bilayer lipid membranes. *Fresenius Journal of Analytical Chemistry*, 371:246–260.

Tsai, Y.-S., Ma, S.-M., Kamaya, H., and Ueda, I. (1987). Fourier transform infrared studies on phospholipid hydration: Phosphate-oriented hydrogen bonding and its attenuation by volatile anesthetics. *Molecular Pharmacology*, 31:623–630.

Turner, A. P. F., Karube, I., and Wilson, G. S., editors (1987). *Biosensors: Fundamentals & Applications*. Oxford University Press, Oxford, UK.

Tyagi, B., Chudasama, C. D., and Jasra, R. V. (2006). Determination of structural modification in acid activated montmorillonite clay by FT-IR spectroscopy. *Spectrochimica Acta Part A: Molecular and Biomolecular Spectroscopy*, 64(2):273–278.

Undabeytia, T., Mishael, Y. G., Nir, S., Papahadjopoulos-Sternberg, B., Rubin, B., Morillo, E., and Maqueda, C. (2003). A novel system for reducing leaching from formulations of anionic herbicides: Clay-liposomes. *Environmental Science & Technology*, 37:4475–4480.

Vaidya, R. and Wilkins, E. (1994). Effect of interference on amperometric glucose biosensors with cellulose-acetate membranes. *Electroanalysis*, 6:677–682.

van Meer, G., Voelker, D. R., and Feigenson, G. W. (2008). Membrane lipids: Where they are and how they behave. *Nature Reviews Molecular Cell Biology*, 9:112–124.

van Olphen, H. (1977). *An introduction to clay colloid chemistry*. John Wiley Sons, New York, 2 edition.

Vemula, P. K. and John, G. (2008). Soft materials from renewable resources. *Accounts of Chemical Research*, 41:769–782.

Vial, S., Prevot, V., Leroux, F., and Forano, C. (2008). Immobilization of urease in Zn/Al layered double hydroxides by soft chemistry routes. *Microporous and Mesoporous Materials*, 107:190–201.

Voller, A., Bartlett, A., Bidwell, D. E., Clark, M. F., and Adams, A. N. (1976). The detection of viruses by enzyme-linked immunosorbent assay (ELISA). *Journal of General Virology*, 33:165–167.

Waltermo, A., Claesson, P. M., and Johansson, I. (1996). Alkyl glucosides on hydrophobic surfaces studied by surface force and wetting measurements. *Journal of Colloid and Interface Science*, 183:506–514.

Wang, B., Zhang, H., Evans, D. G., and Duan, X. (2005). Surface modification of layered double hydroxides and incorporation of hydrophobic organic compounds. *Materials Chemistry and Physics*, 92:190–196.

Wang, C., Ye, F., Valardez, G. F., Peters, G. H., and Westh, P. (2011). Affinity of four polar neurotransmitters for lipid bilayer membranes. *The Journal of Physical Chemistry B*, 115:196–203.

Wang, J. (2000). Fundamental concepts. In *Analytical Electrochemistry*, pages 1–27. Wiley-VCH, 2 edition.

Wang, R., Wang, Y., Lassiter, K., Li, Y., Hargis, B., Tung, S., Berghman, L., and Bottje, W. (2009). Interdigitated array microelectrode based impedance immunosensor for detection of avian influenza virus H5N1. *Talanta*, 79:159–164.

Warren, H. S., Vogel, F. R., and Chedid, L. A. (1986). Current status of immunological adjuvants. *Annual Review of Immunology*, 4:369–388.

Wicklein, B., Darder, M., Aranda, P., and Ruiz-Hitzky, E. (2010). Bio-organoclays based on phospholipids as immobilization hosts for biological species. *Langmuir*, 26:5217–5225.

Widrig, C. A., Chung, C., and Porter, M. D. (1991). The electrochemical desorption of n-alkanethiol monolayers from polycrystalline Au and Ag electrodes. *Journal of Electroanalytical Chemistry and Interfacial Electrochemistry*, 310:335–359.

Wiegart, L., Struth, B., Tolan, M., and Terech, P. (2005). Thermodynamic and structural properties of phospholipid Langmuir monolayers on hydrosol surfaces. *Langmuir*, 21:7349–7357.

Wildgoose, G. G., Pandurangappa, M., Lawrence, N. S., Jiang, L., Jones, T. G. J., and Compton, R. G. (2003). Anthraquinone-derivatised carbon powder: Reagentless voltammetric pH electrodes. *Talanta*, 60:887–893.

Wiley, D. C. and Skehel, J. J. (1987). The structure and function of the hemagglutinin membrane glycoprotein of influenza virus. *Annual Review of Biochemistry*, 56:365–394.

Willaert, R. G. and Baron, G. V. (1996). Gel entrapment and micro-encapsulation: Methods, applications and engineering principles. *Reviews in Chemical Engineering*, 12:5–205.

Willard, H. H., Merritt, J. L. L., Dean, J. A., and Settle, J. F. A., editors (1988). *Instrumental Methods of Analysis*. Wadsworth Publishing Company: Belmont, 7 edition.

Wu, Z.-S., Zhou, G.-Z., Jiang, J.-H., Shen, G.-L., and Yu, R.-Q. (2006). Gold colloid-bienzyme conjugates for glucose detection utilizing surface-enhanced raman scattering. *Talanta*, 70:533–539.

Xu, C., Taylor, P., Ersoz, M., Fletcher, P. D. I., and Paunov, V. N. (2003). Microcontact printing of DNA-surfactant arrays on solid substrates. *Journal of Materials Chemistry*, 13:3044–3048.

Xu, R., Pang, W., Yu, J., and Huo, Q. (2007a). *Chemistry of zeolites and related porous materials: Synthesis and structure*. John Wiley Sons, Singapore, 1 edition.

Xu, W. Z., Johnston, C. T., Parker, P., and Agnew, S. F. (2000). Infrared study of water sorption on Na-, Li-, Ca-, and Mg-exchanged (SWy-1 and SAz-1) montmorillonite. *Clays and Clay Minerals*, 48:120–131.

Xu, Z. P., Stevenson, G., Lu, C. Q., and Lu, G. Q. (2006). Dispersion and size control of layered double hydroxide nanoparticles in aqueous solutions. *Journal of Physical Chemistry B*, 110:16923–16929.

Xu, Z. P., Walker, T. L., Liu, K. L., Cooper, H. M., Lu, G. Q. M., and Bartlett, P. F. (2007b). Layered double hydroxide nanoparticles as cellular delivery vectors of supercoiled plasmid dna. *International Journal of Nanomedicine*, 2:163–174.

Yao, H.-B., Tan, Z.-H., Fang, H.-Y., and Yu, S.-H. (2010). Artificial nacre-like bionanocomposite films from the self-assembly of chitosan/montmorillonite hybrid building blocks. *Angewandte Chemie International Edition*, 49:10127–10131.

Zhang, L., Somasundaran, P., and Maltesh, C. (1997). Adsorption of n-dodecyl-(beta)-maltoside on solids. *Journal of Colloid and Interface Science*, 191:202–208.

Zhang, S., Zhao, Y., Zhao, B., and Wang, B. (2010). Hybrids of nonviral vectors for gene delivery. *Bioconjugate Chemistry*, 21:1003–1009.

Zhao, Y., Li, F., Zhang, R., Evans, D. G., and Duan, X. (2002). Preparation of layered double-hydroxide nanomaterials with a uniform crystallite size using a new method involving separate nucleation and aging steps. *Chemistry of Materials*, 14:4286–4291.

Zhou, Q. and Somasundaran, P. (2009). Synergistic adsorption of mixtures of cationic gemini and nonionic sugar-based surfactant on silica. *Journal of Colloid and Interface Science*, 331:288–294.

Zimmermann, R., Kuttner, D., Renner, L., Kaufmann, M., Zitzmann, J., Muller, M., and Werner, C. (2009). Charging and structure of zwitterionic supported bilayer lipid membranes studied by streaming current measurements, fluorescence microscopy, and attenuated total reflection fourier transform infrared spectroscopy. *Biointerphases*, 4:1–6.